UNIVERSIDAD AUTÓNOMA DE MADRID

DOCTORADO EN BIOCIENCIAS MOLECULARES

Transcription factor NRF2 regulates the expression of autophagy genes

Marta Pajares Cabetas

Madrid, 2018

UNIVERSIDAD AUTÓNOMA DE MADRID
DEPARTAMENTO DE BIOQUÍMICA
FACULTAD DE MEDICINA

Transcription factor NRF2 regulates the expression of autophagy genes

Memoria de la Tesis para optar al grado de Doctor
Presentada por la Licenciada en Bioquímica

MARTA PAJARES CABETAS

Directores de tesis:
Prof. ANTONIO CUADRADO PASTOR
Catedrático de Bioquímica y Biología Molecular
Dra. ANA ISABEL ROJO SANCHÍS
Prof. Ayudante Doctor en Bioquímica y Biología Molecular

Departamento de Bioquímica, Facultad de Medicina
Instituto de Investigaciones Biomédicas "Albertos Sols"
UAM-CSIC

Antonio Cuadrado Pastor, Doctor en Ciencias Biológicas y Catedrático del Departamento de Bioquímica, Facultad de Medicina, Universidad Autónoma de Madrid,

CERTIFICA:

Que el trabajo presentado por Marta Pajares Cabetas, Licenciada en Bioquímica por la Universidad Autónoma de Madrid, para optar al grado de Doctor, bajo el título: "Transcription factor NRF2 regulates the expression of autophagy genes", se ha realizado bajo mi dirección en el Departamento de Bioquímica e Instituto de Investigaciones Biomédicas "Alberto Sols".

Considero que este estudio experimental es satisfactorio y apto para ser presentado como Tesis Doctoral en el Departamento de Bioquímica de la Facultad de Medicina de la Universidad Autónoma de Madrid.

Y para que conste, expido el presente certificado en Madrid, a 23 de julio de 2018,

Fdo: Antonio Cuadrado Pastor
Catedrático de Universidad
Departamento de Bioquímica e
Instituto de Investigaciones Biomédicas "Alberto Sols"
Facultad de Medicina
Universidad Autónoma de Madrid.

Ana Isabel Rojo Sanchís, Doctora en Bioquímica por el Departamento de Bioquímica, Facultad de Medicina, Universidad Autónoma de Madrid,

CERTIFICA:

Que el trabajo presentado por Marta Pajares Cabetas, Licenciada en Bioquímica por la Universidad Autónoma de Madrid, para optar al grado de Doctor, bajo el título: "Transcription factor NRF2 regulates the expression of autophagy genes", se ha realizado bajo mi dirección en el Departamento de Bioquímica e Instituto de Investigaciones Biomédicas "Alberto Sols".

Considero que este estudio experimental es satisfactorio y apto para ser presentado como Tesis Doctoral en el Departamento de Bioquímica de la Facultad de Medicina de la Universidad Autónoma de Madrid.

Y para que conste, expido el presente certificado en Madrid, a 23 de julio de 2018,

Fdo: Ana Isabel Rojo Sanchís
Prof. Ayudante Doctor
Departamento de Bioquímica
Universidad Autónoma de Madrid.

Este trabajo ha sido realizado en el Departamento de Bioquímica de la Facultad de Medicina e Instituto de Investigaciones Biomédicas “Alberto Sols” (UAM-CSIC) gracias a una beca predoctoral para Formación de Personal Investigador concedida por la Universidad Autónoma de Madrid y con subvención del Ministerio de Ciencia e Innovación (SAF2013-43271-R y SAF2016-76520-R) así como financiación internacional (Organización: Centres of Excellence in Neurodegeneration (JPND); Call: 2013 COEN initiative on international research “pathfinder” projects).

‘Education is not the learning of facts,
it’s rather the training of the mind to think.’
Albert Einstein

‘If you can make one heap of all your winnings
And risk it on one turn of pitch-and-toss,
And lose, and start again at your beginnings
And never breathe a word about your loss;
If you can force your heart and nerve and sinew
To serve your turn long after they are gone,
And so hold on when there is nothing in you
Except the Will which says to them: "Hold on"
...
Yours is the Earth and everything that's in it’.
Rudyard Kipling

Acknowledgements

Y después de unos cuantos años, parece que llegó el final de esta etapa…Un camino lleno de buenos y malos momentos, pero en el que siempre he estado acompañada. Y, por ello, me siento tremendamente agradecida.

En primer lugar, me gustaría agradecer al Prof. Antonio Cuadrado la oportunidad de incorporarme en su grupo allá por 2012, cuando ni siquiera estaba en la lista para hacer la Bioquímica Experimental Avanzada. Aún recuerdo aquella entrevista en la que me transmitió una seguridad y determinación que a mí en ese momento me faltaban. Gracias por creer en mí estos años, por la paciencia y, sobre todo, por cultivar en mí el pensamiento crítico y la curiosidad tan necesarios para un científico.

Por supuesto, tengo muchísimo que agradecer a la Dra. Ana I. Rojo, por ser una excelente co-directora y estar siempre ahí, tanto en lo científico como en lo personal. Gracias por esas discusiones científicas a través de '*Moneypenny*', por resolver siempre mis dudas y enseñarme a no dudar de mí y, sobre todo, ¡por pararme los pies cuando era necesario! Pero, sobre todo, gracias por convertirte en una amiga. Por las mil risas compartidas, por vencer a *Rita* juntas o dejarme a tu *patronum* cuando lo necesitaba. Eres todo un ejemplo a seguir y lo que me has enseñado no puedo resumirlo en palabras. ¡Te quiero mucho!

No puedo dejar de agradecer a la gente del labo, que ha estado ahí siempre apoyándome. Gracias al *pato mayor* por enseñarme a hacer *maxis* aquel verano cuando llegué. Por todos los marujeos y las risas, aquel viaje a Spetses o el día que casi morimos de frío hablando sin parar fuera del coche al volver del GENN… Gracias por ser siempre el ejemplo más "cercano" de la científica en la que me quiero convertir. Gracias a Isa por preguntarme siempre cómo estoy y escuchar mis logros y penas por los pasillos del IIB. Por animarme y ofrecerme siempre un huequito en su *nuevo labo* para mí. Quiero agradecer también a Ángel, no sólo por su apoyo técnico todos estos años, sino también por su risa contagiosa y su buen humor. ¡Todo un superviviente entre tanta mujer! A la Mari, que llegó más tarde pero se ha convertido en un apoyo fundamental en el 1.7. Tanto por sus maravillosos lentivirus o su buffer *Abdala*, como por su buena disposición siempre para ayudar a los demás. ¡Gracias por todos tus consejos de Doctora a Doctoranda! Gracias también a la Robledinos, mi *tocaya* en el sufrimiento pre-doctoral (pero… esto se acaba ya, ¿no?). Por las miles de tardes (o noches) hablando (o quejándonos) hasta las mil! Por ese congreso al que aún no hemos ido juntas, ¡pero sé que será inolvidable! Gracias también a Raquel, porque a pesar de llevar tan poquito, transmites cariño y alegría por donde vas. ¡Te va a ir muy bien, lo sé!

Me gustaría agradecer también a nuestros colaboradores, especialmente al *Cuervo lab*. A Ana María Cuervo y Esperanza Arias por enseñarme el maravilloso mundo de la CMA,

acogerme en mi primera estancia en NY (¡tan buena que al final repetí!) y la inestimable ayuda científica sin la que buena parte de esta tesis no hubiera sido posible.

Un apoyo fundamental estos años han sido mis amigos. En primer lugar, quiero agradecer a *mis bioquis*. Porque le han dado a la Bioquímica un valor añadido para mí: el poder conocerlas y haber compartido tantos años de agobios, repasos de última hora, trabajos en grupo y, sobre todo, muchas risas y complicidad. Y ahora que nos vemos menos, ¡cada reencuentro es único! Gracias a mis *cinco*, sobre todo a mi *Lapit*. Por ser una extremidad más. Incluso acompañándome más de un finde al labo y alucinando con cada tontería que hacía. Porque llevamos toda una vida juntas y esta es otra etapa que hemos tenido la suerte de compartir.

Por último, me gustaría agradecer a los que más debo: mi familia. Me gustaría hacer una mención especial a mi *yayo*, que es todo un ejemplo de perseverancia, responsabilidad y superación. Porque aunque no te hiciera mucha gracia que dejara Medicina, al final has sabido ver lo que me apasiona la Bioquímica y valorar todo lo que he hecho. Gracias a Carlos por emocionarse con cada uno de mis logros como si fueran suyos. A Pau por ser la mayor constante en mi vida. Por dejarme hacer de su *maestra* de pequeñas, y haberme enseñado tantísimo ella a mí todos estos años. ¡Vales millones!

A mis padres directamente les debo todo… Ellos se han dejado la piel para que tuviéramos siempre la mejor formación posible. Por habernos educado, sobre todo, en valores. Infinitas gracias por creer en mí siempre y por el apoyo cada vez que me he sentido perdida. Por no dejarme sola nunca. Papi, me encantan nuestras conversaciones científicas en las que nadie más nos entiende, ¡algún día trabajaremos juntos, lo sé! No te imaginas lo que me halaga que te sientas tan orgulloso de mí. Mami, no puedo dejar de agradecerte que me sentaras aquel día y me ayudaras a ver que tenía que estudiar lo que realmente me gustaba. Me animaste a dar el paso y por eso estoy hoy aquí. Gracias por ser mi mayor consejera y mi ejemplo a seguir. ¡Os quiero muchísimo!

Y por último, quiero dar las gracias a mi compañero de vida. No tengo palabras para expresar lo tremendamente afortunada que me siento porque estés a mi lado. Porque me digas "*tranquila, al final todo va a ir bien*" cuando estoy agobiada. Por haberme sufrido como nadie estos años y por la ilusión con la que siempre hemos enfrentado y sé que enfrentaremos todo lo que se nos ponga por delante. ¡Por hacerme feliz cada día!

Me dejo a mucha gente que también me ha acompañado en esta etapa, pero os tengo a todos muy presentes. ¡Millones de gracias!

Summary/Resumen

Cells control the quality of the proteome through an integrative network of mechanisms that include protein degradation by autophagy. The regulation of this process by signaling pathways has been intensively studied but less is known about its transcriptional control. Because this degradative pathway has an essential cytoprotective role, especially under stress conditions, in this thesis we have analyzed the regulation of autophagy by the transcription factor Nuclear factor (erythroid-derived 2)-like 2 (NRF2), which is considered a master regulator of cellular homeostastis. NRF2 controls the expression of a wide battery of cytoprotective genes that have a tremendous impact on physiological responses such as inflammation, senescence or metabolism. However, its relevance in proteostasis is just starting to be unveiled.

Therefore, we focused our study on the transcriptional regulation of two types of autophagy, i.e. macroautophagy and chaperone mediated autophagy (CMA). We have identified NRF2 enhancer sequences, termed antioxidant response elements (AREs), in the promoter region of 9 genes involved in different steps of macroautophagy and CMA. Consequently, we show that genetic and pharmacological manipulation of NRF2 results in the modulation of autophagy gene expression and activity.

The role of NRF2 in the regulation of macroautophagy may have a significant relevance upon stressful conditions, including proteotoxic stress. To address the functional relevance of NRF2 in proteinopathy, we have generated a new mouse model of Alzheimer's disease (AD) that reproduces the amyloid and TAU pathology in the presence or absence of NRF2 expression. NRF2 deficiency worsens some of the main hallmarks of AD, including low-grade chronic oxidative and inflammatory stress as well as exacerbated proteinopathy due, at least in part, to impaired macroautophagy. Moreover, our results reflect a positive correlation between the expression of NRF2 and macroautophagy in AD patients.

We have also established the role of NRF2 in the basal and inducible regulation of CMA, based on the transcriptional regulation of the lysosomal receptor LAMP2A. This novel NRF2/LAMP2A axis may have important implications in the physiological response to stress and, consequently, be of interest for human pathology. In fact, data mining of The Cancer Genome Atlas showed a positive correlation between *NRF2* an *LAMP2* expression in gliomas and glioblastomas.

Overall, this thesis describes a novel role of NRF2 in the regulation of macroautophagy and CMA, suggesting a new strategy to combat proteinopathies.

Las células controlan la calidad del proteoma mediante una compleja red que integra diversos mecanismos, incluida la degradación de proteínas mediante autofagia. La regulación de este proceso a través de vías de señalización ha sido ampliamente estudiada, pero su control transcripcional es aún poco conocido. Debido a que esta vía de degradación tiene un papel citoprotector fundamental, especialmente en condiciones de estrés, en esta tesis hemos analizado la regulación de la autofagia por el factor de transcripción NRF2 (Nuclear factor (erythroid-derived 2)-like 2), considerado un regulador maestro de la homeostasis celular. NRF2 controla la expresión de una extensa batería de genes citoprotectores con un importante impacto en respuestas fisiológicas como la inflamación, la senescencia o el metabolismo. Sin embargo, su papel en proteostasis está aún comenzando a comprenderse.

Por todo ello, hemos centrado nuestro estudio en la regulación transcripcional de dos tipos de autofagia, la macroautofagia y la autofagia mediada por chaperonas (CMA). Hemos identificado elementos de respuesta a NRF2, llamados elementos de respuesta antioxidante (ARE), en la región promotora de 9 genes involucrados en diferentes pasos de la macroautofagia y la CMA. En consecuencia, mostramos que la manipulación genética y farmacológica de NRF2 resulta en la modulación de la expresión génica y la actividad de la autofagia.

El papel del factor de transcripción NRF2 en la regulación de la macroautofagia podría ser importante en condiciones de estrés, incluido el estrés proteotóxico. Para analizar la relevancia funcional de NRF2 en proteinopatía, hemos generado un nuevo modelo animal de la Enfermedad de Alzheimer (EA) que reproduce la amiloidopatía y tauopatía en presencia o ausencia de NRF2. La deficiencia en NRF2 agrava algunos eventos característicos de la EA, como el estrés oxidativo e inflamatorio crónico de bajo grado, así como la proteinopatía debido, al menos en parte, a una desregulación de la macroautofagia. Además, nuestros resultados reflejan una correlación positiva entre NRF2 y marcadores de macroautofagia en muestras de EA.

Hemos establecido también un papel de NRF2 en la regulación basal e inducible de la CMA, basado en la regulación transcripcional del receptor lisosomal LAMP2A. Este nuevo eje NRF2/LAMP2A podría tener implicaciones relevantes para patologías humanas. De hecho, el análisis de datos obtenidos de *The Cancer Genome Atlas* mostró una correlación positiva en la expresión de *NRF2* y *LAMP2* en gliomas y glioblastomas.

Con todo ello, esta tesis describe un nuevo papel de NRF2 en la regulación de la macroautofagia y la CMA, sugiriendo una nueva diana para combatir proteinopatías.

Table of contents

Abbreviations

Aβ	Amyloid beta
ACTB	Actin beta
ACTB	Human gene encoding ACTB
Actb	Murine gene encoding ACTB
AD	Alzheimer's disease
AMPK	AMP-activated protein kinase
Aox1	Murine gene encoding Aldehyde oxidase 1
APP	Amyloid beta precursor protein
ARE	Antioxidant response element
ATG5	Autophagy related 5
ATG5	Human gene encoding ATG5
Atg5	Murine gene encoding ATG5
ATG7	Autophagy related 7
ATG7	Human gene encoding ATG7
Atg7	Murine gene encoding ATG7
AT-*Nrf2*-WT	Mouse expressing APP(V717I) and TAU(P301L) in a *Nrf2*-wild type background
AT-*Nrf2*-KO	Mouse expressing APP(V717I) and TAU(P301L) in a *Nrf2*-knockout background
BACH1	BTB domain and CNC homolog 1
β-TrCP	β-transducin repeat-containing protein
bZIP	Basic leucine zipper
CALCOCO2	Human gene encoding NDP52
Calcoco2	Murine gene encoding NDP52
cDNA	Complementary deoxyribonucleic acid
CD11b	Cluster of Differentiation molecule 11B
ChIP	Chromatin immunoprecipitation
CNC	Cap 'n' collar
CMA	Chaperone mediated autophagy
CUL1	Cullin 1
CUL3	Cullin 3
Cys	Cysteine
DAPI	4',6-diamidino-2-phenylindole
DHE	Dihydroethidium

DMEM	Dulbecco's modified Eagle medium
DMF	Dimethyl fumarate
DNA	Deoxyribonucleic acid
ECL	Enhanced chemiluminiscence
EDTA	Ethylenediaminetetraacetic acid
EGTA	Ethylene glycol tetraacetic acid
ENCODE	Enciclopedia of DNA elements at the University of California, Santa Cruz
FBS	Fetal bovine serum
FoxO	Forkhead box protein O
GABARAPL1	GABA type A receptor associated protein like 1
GABARAPL1	Human gene encoding GABARAPL1
Gabarapl1	Murine gene encoding GABARAPL1
GAPDH	Glyceraldehyde-3-phosphate dehydrogenase
GBA	β-Glucocerebrosidase
GBMLGG	Cohort of patients of Low Grade Glioma and Glioblastoma from The Cancer Genome Atlas
GCLC	Glutamate-cysteine ligase catalytic subunit
GCLM	Glutamate-cysteine ligase modulatory subunit
GFP	Green fluorescent protein
GFAP	Glial fibrilar acidic protein
GSK3	Glycogen synthase kinase 3
GSH	Reduced glutathione
GSSG	Oxidized glutathione
HEPES	N-2-hydroxyethylpiperazine-N'-2-ethanesulfonic acid
HMOX1	Heme oxygenase 1 (also termed HO1)
HMOX1	Human gene encoding HMOX1
Hmox1	Murine gene encoding HMOX1
H_2O_2	Hydrogen peroxide
HSC70	Heat shock protein family A (Hsp70) member 8
IBA1	Ionized calcium binding adaptor molecule 1
KEAP1	Kelch like ECH associated protein 1
KO	Knock-out
LAMP2A	Lysosome-associated membrane protein 2 isoform A

LAMP2A	Human gene encoding LAMP2A
Lamp2a	Murine gene encoding LAMP2A
LAMP2B	Lysosome-associated membrane protein 2 isoform B
LAMP2B	Human gene encoding LAMP2B
LAMP2C	Lysosome-associated membrane protein 2 isoform C
LAMP2C	Human gene encoding LAMP2C
LAMP1	Lysosome-associated membrane protein 1
LC3B	Microtubule-associated proteins 1A/1B light chain 3
LC3B-I	Non-lipidated LC3B form
LC3B-II	Phosphatidyl ethanolamine-lipidated LC3B form
LTP	Long term potentiation
MAFF	Avian Musculoaponeurotic Fibrosarcoma Oncogene Homolog F
MAFK	Avian Musculoaponeurotic Fibrosarcoma Oncogene Homolog K
MAPK	Mitogen activated protein kinases
MEFs	Mouse embryo fibroblasts
MHCII	Major Histocompatibility Complex class II molecule
mRNA	Messenger ribonucleic acid
mTOR	Mammalian target of rapamycin
NDP52	Calcium binding and coiled-coil domain 2 protein (also called CALCOCO2)
Neh	NRF2-ECH homology domain
NL	Ammonium chloride (NH_4Cl) and leupeptin
NFE2L2	Human gene encoding NRF2
Nfe2l2	Murine gene encoding NRF2
NQO1	NAD(P)H quinone dehydrogenase 1
NQO1	Human gene encoding NQO1
Nqo1	Murine gene encoding NQO1
NRF2	Nuclear factor (erythroid-derived 2)-like 2
p62	Sequestosome 1
PBS	Phosphate saline buffer
PE	Phosphatidyl ethanolamine
PFA	Paraformaldehyde
PI	Protease inhibitors
PI3P	Phosphatidylinositol(3,4,5)triphosphate

PI3K	Phosphatidylinositol 3 kinase
PMSF	Phenylmethylsulfonyl fluoride
PQ	Paraquat
PSSM	Position-specific scoring matrix
Rapa	Rapamycin
RBX1	RING-box protein 1
qRT-PCR	Quantitative real-time polymerase chain reaction
RNAse A	Ribonuclease A
ROS	Reactive oxygen species
SEM	Standard error of the mean
SD	Serum-deprived
SDS	Sodium dodecyl sulfate
SDS-PAGE	Sodium dodecyl sulfate polyacrilamide gel electrophoresis
SFN	Sulforaphane
SQSTM1	Human gene encoding p62
Sqstm1	Murine gene encoding p62
SS	Sarkosyl-soluble
SI	Sarkosyl-insoluble
shRNA	Short hairpin RNA
TAU	Microtubule-associated protein TAU
TBP	TATA box binding protein
TFEB	Transcription factor EB
ULK1	Unc-51 like autophagy activating kinase 1
ULK1	Human gene encoding ULK1
Ulk1	Murine gene encoding ULK1
VEH	Vehicle
WT	Wild type

Introduction

1. The transcription factor NRF2

Nuclear factor (erythroid-derived 2)-like 2 (NRF2) is a basic-leucine-zipper (bZIP) protein that belongs to the cap 'n' collar (CNC) family of transcription factors and is considered nowadays the master regulator of cellular homeostasis.

NRF2 was first identified in 1994 by Moi and co-workers using a tandem repeat of the consensus sequence for the transcription factors AP1 (activator protein 1) and NF-E2 (nuclear factor-erythroid 2) in the *β-globin* gene [1]. This sequence was similar to the *cis*-acting elements originally recognized in the promoter regions of the murine and rat genes coding for GSTYa (glutathione S-transferase) and NQO1 (NAD(P)H:quinone oxidoreductase) and is responsible for the induction of these genes by electrophiles [2, 3]. The consensus sequence 5'-TGA$^{G}/_{C}$NNNGC-3' was then confirmed to be conserved in a number of antioxidant genes, including *Hmox1* (heme oxygenase 1), *Gclc* (glutamate-cysteine ligase catalytic subunit), *Gclm* (glutamate-cysteine ligase modifier subunit) or *Gpx1* (glutathione peroxidase), and received the name of electrophilic/stress response element (EpRE/StRE), now widely known as antioxidant response element (ARE) [4]. Venugopal *et al* connected NRF2 to ARE-driven gene expression *in vitro* [5], and subsequent studies in *Nrf2*-knockout mice confirmed NRF2-dependent regulation of ARE-containing genes *in vivo* [6-8].

NRF2 binds the ARE motif as a heterodimer with sMAF (small musculoaponeurotic fibrosarcoma) proteins (MAFF, MAFG, and MAFK). These proteins contain a bZIP domain but lack a transactivation domain, making heterodimerization with CNC transcription factors essential to regulate gene expression [9]. It is believed that sMAF are responsible for the high-affinity binding of the heterodimer to the ARE by preferentially recognizing the conserved GC residues [10-12]. The bZIP transcription factor BACH1 (BTB and CNC homolog 1) can also bind sMAF, competing with NRF2 and repressing *Hmox1* expression [13].

1.1. Structure of the transcription factor NRF2

NRF2 contains between 586 and 695 aminoacids depending on the species. This modular protein is composed by seven NRF2-ECH homology (Neh) domains. As shown in Fig. 1, the Neh1 domain comprises the CNC-bZIP region that dimerizes with sMAF proteins and binds DNA[14]. The Neh2 domain negatively controls NRF2 because, through its DLG and ETGE motifs, allows binding to the repressor KEAP1 (Kelch-like ECH associated protein 1) [15, 16]. The C-terminal Neh3 region of NRF2 binds the transcriptional co-activator CHD6

(Chromo-ATPase/helicase DNA-binding protein 6) [17]. The Neh4 and Neh5 regions represent transactivation domains that bind to CBP (cAMP response element-binding protein -CREB-binding protein) and/or RAC3 (Receptor-associated coactivator 3) [18, 19]. The Neh6 domain negatively controls NRF2 because it is recognized, through the phosphorylated DSGIS and DSAPGS motifs, by the E3-ligase adaptor β-TrCP (β-transducin repeat-containing protein) [20-22]. Finally, the Neh7 domain mediates repression of NRF2 by the RXRα (retinoid X receptor alpha) through a physical association between these two proteins [23].

1.2. NRF2 regulation

1.2.1. KEAP1 regulation

The activity of the transcription factor NRF2 is tightly controlled. Under homeostatic conditions, NRF2 is maintained at low levels due to continuous proteasomal degradation.

The view that the E3-ligase adaptor KEAP1 is a major repressor of NRF2 is supported by the observation that disruption of *Keap1* in the mouse [24] or knockdown in human cells [25] is sufficient to increase the levels and activity of this transcription factor. The mechanism of KEAP1 regulation elegantly explains how NRF2 levels adjust to oxidant fluctuations (Fig. 2). KEAP1 is a dimeric BTB-Kelch protein, and each of its two subunits contains a binding site for NRF2. The proposed 'hinge-and-latch' [26], also called 'two tethering site'[16], model proposes that under basal conditions newly synthesized NRF2 binds first one KEAP1 subunit

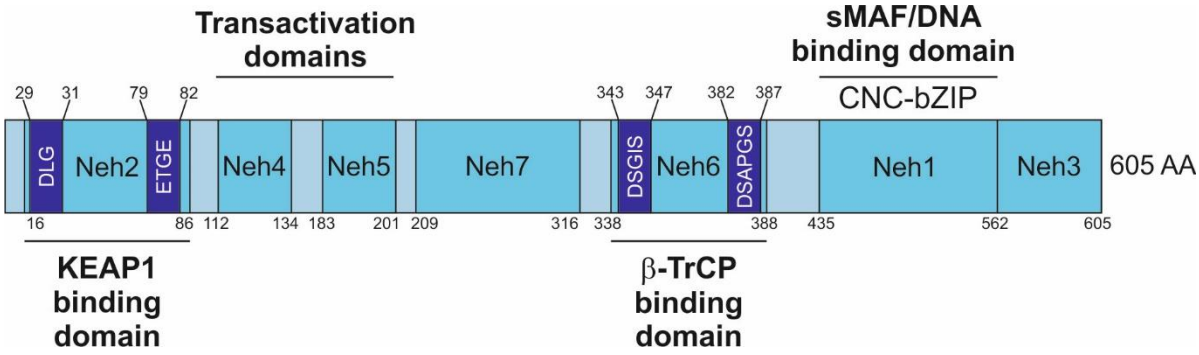

Figure 1. Protein structure of the transcription factor NRF2. NRF2 contains seven conserved domains called Neh1-Neh7. Neh1 serves as the DNA binding and heterodimerization domain with sMAF proteins. Neh2 and Neh6 target NRF2 to degradation by the proteasome. The transactivation activity of NRF2 lies in Neh4 and Neh5. Neh3 was reported to interact with the co-activator CHD6 and Neh7 to repress NRF2 activity through the RXRα. Aminoacid numbers are indicated and correspond to the human protein.

through the high-affinity 79-ETGE-82 motif to form an 'open' conformation that allows association between the other KEAP1 monomer and the low-affinity 29-DLG-31 motif in NRF2 to form the 'closed' conformation. KEAP1 then functions as a bridge between NRF2 and the E3 ligase complex formed by CUL3 (Cullin 3) and RBX1 (RING-box protein 1). This complex is responsible for NRF2 ubiquitination in a series of conserved Lys residues located between the 79-ETGE-82 and 29-DLG-31 motifs, allowing NRF2 proteasomal degradation. However, reactive oxygen species (ROS), electrophiles or xenobiotics can promote the formation of adducts or oxidation of sulfhydryl groups in some of the 25 Cys residues of KEAP1 (Cys-151, Cys-273 and Cys-288 are the most sensitive to thiol reactivity), promoting a conformational change that prevents NRF2 ubiquitination and subsequent proteasomal degradation. It was first proposed that this structural perturbation in KEAP1 would impair binding to the DLG sequence, necessary for maintaining NRF2 in a constrained position to be properly ubiquitinated. More recently, single-cell imaging showed that some inducers favor the 'closed' conformation of the KEAP1-NRF2 complex instead, but alter the stable positioning of the KEAP1 domains and thus induce an improper geometry for ubiquitination. In both cases, the unproductive KEAP1/NRF2 complex allows newly synthetized NRF2 to escape KEAP1-dependent degradation, accumulate in the nucleus and activate ARE-containing genes [15, 16, 26-30].

1.2.2. NRF2 regulation by GSK3/β-TrCP

Our group described an alternative mechanism of regulation of NRF2 stability mediated by the phosphorylation by the Ser/Thr kinase GSK3β (glycogen synthase kinase 3β). This kinase phosphorylates Ser-344 and Ser-347 in the 343-DSGIS-347 motif located in the Neh6 domain of NRF2. This phosphorylation creates a degron for the E3-ligase adaptor β-TrCP that presents NRF2 to a CUL1 (Cullin 1)/RBX1 complex, leading to an alternative pathway for ubiquitin-dependent proteasomal degradation of NRF2.

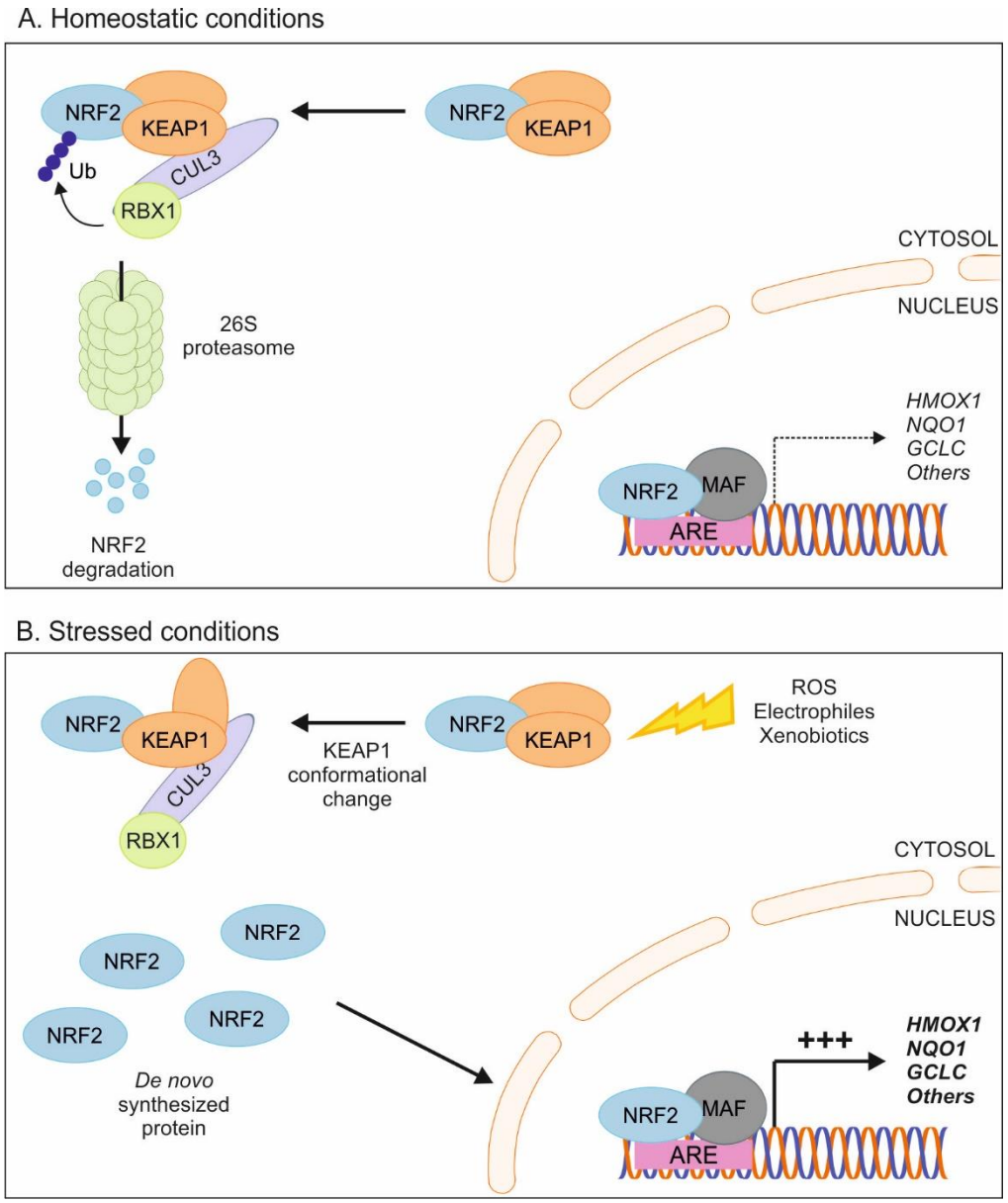

Figure 2. KEAP1 is a major repressor of NRF2. A, In homeostatic conditions, KEAP1 targets NRF2 to ubiquitination through the CUL3-RBX1 ubiquitin ligase complex. As a consequence, NRF2 is directed to proteasomal degradation and, hence, maintained at low levels. B, Upon exposure to ROS, electrophiles or xenobiotics, Cys sensors in KEAP1 promote a conformational change that prevents NRF2 ubiquitination and proteasomal degradation. In this context, newly synthesized NRF2 accumulates, translocates into the nucleus and leads to the transcriptional activation of ARE-driven genes.

The GSK3β/β-TrCP axis contributes to NRF2 repression under homeostatic conditions, as inhibition of GSK3β by highly selective drugs or siRNAs against GSK3 isoforms results in increased NRF2 protein levels. Moreover, stabilization of NRF2 following GSK3β inhibition occurred in KEAP1-deficient mouse embryo fibroblasts and in an ectopically expressed NRF2 deletion mutant lacking the critical 79-ETGE-82 residues for high-affinity binding to KEAP1 (NRF2-ΔETGE), suggesting that GSK3β/β-TrCP regulation of NRF2 is independent on KEAP1 [20, 21]. Another β-TrCP recognition site was described

within the Neh6 domain (382-DSAPGS-387). Deletion of either binding sites in NRF2 decreased β-TrCP-mediated ubiquitination of this transcription factor. However, while phosphorylation of the 343-DSGIS-347 site resulted in increased binding affinity, this was not the case for the 382-DSAPGS-387 motif, suggesting the absence of a functional GSK3β phosphorylation site [22]. While the KEAP1-mediated regulation explains how NRF2 levels adjust to oxidant fluctuations, GSK3β/β-TrCP regulation connects NRF2 with signaling responses.

1.2.3. Other layers of regulation

NRF2 is a highly acidic protein because of abundant Asp and Glu residues (pI 4.6). Moreover, 17% of its aminoacids are phosphorylable residues (Ser, Tyr and Thr). Indeed, different kinases besides GSK3β have been shown to phosphorylate and regulate NRF2. Several studies have shown that ROS or xenobiotics can activate the signaling pathways involving MAPKs (mitogen activated protein kinases), namely JNK (c-Jun N-terminal kinase), ERK1/2 (extracellular signal–regulated kinase) and p38, which are Ser/Thr kinases directed to Pro. Although NRF2 contains six conserved Ser-Pro pairs that may be phosphorylated by MAPKs, its contribution to NRF2 activity remains unclear and is most likely indirect [31-35]. NRF2 can be phosphorylated by PERK (double-stranded RNA-activated protein kinase-like ER kinase), one of the three arms of the unfolded protein response (UPR). When unfolded proteins accumulate in the ER, PERK phosphorylates Ser-40 in NRF2, which was reported to allow NRF2 dissociation from KEAP1 and translocation to the nucleus [36]. PKC (protein kinase C) [37], CK2 (casein kinase 2) [38], Fyn (tyrosine-protein kinase Fyn) [39] or HIPK2 (homeodomain-interacting protein kinase 2) [40] have also been reported to modulate NRF2 stability through phosphorylation. However, the relevance of these phosphorylation events has not been fully established and, in some cases, like Fyn-mediated NRF2 phosphorylation, has been questioned [41].

NRF2 is submitted to other layers of regulation. These include inhibition by microRNAs (miRNAs), such as miR153, miR27a, miR142-5p, and miR144[42]. Abundant miRNAs in aged tissues may be in part responsible for impaired NRF2 activity with age[43]. Activation by CBP/p300-induced acetylation [44] and repressive methylation of cytosine-guanine (CG) islands within the *NRF2* promoter [45] constitute additional mechanisms of NRF2 regulation.

1.2.4. NRF2 inducers and pharmacological modulators

The majority of known physiological or pharmacological NRF2 inducers are electrophilic molecules that covalently modify by oxidation or alkylation critical Cys residues present in the thiol-rich KEAP1 protein [46, 47]. The list of endogenous and exogenous NRF2 inducers is continuously growing.

In this study, we have used the pro-oxidants paraquat (PQ) and hydrogen peroxide (H_2O_2) to increase NRF2 activity (Fig. 3). PQ (1,1-dimethyl-4,4-bipyrimidyl chloride), widely used as an herbicide, belongs to a broad class of redox cycling compounds and inhibits complex I of the mitochondrial respiratory chain, leading to the generation of O_2^- and subsequently H_2O_2 [48]. H_2O_2 was shown to increase intramolecular and intermolecular disulfide linking in KEAP1 [49].

Pharmacological activation of NRF2 was addressed with sulforaphane (SFN) and dimethyl fumarate (DMF) (Fig. 3). SFN is an isothiocyanate produced from enzymatic cleavage of glucoraphanin, which is present in sprouts of broccoli, cabbage and other *Brassicacea* plants. Isothiocyanates are characterized by the –N=C=S group, in which the central electrophilic C reacts rapidly but reversibly with the thiol group of Cys-151 in KEAP1 to give rise to an inactive dithiocarbamate [29, 50, 51]. DMF, and its metabolite monomethyl fumarate (MMF), are Michael acceptors that also react with Cys-151 in KEAP1 [52]. DMF is to date the only Food and Drug Administration– and European Medicines Agency–approved drug registered as NRF2 activator and is employed to treat psoriasis and remitting relapsing multiple sclerosis. Although the main mechanism of NRF2 activation in all these cases is oxidative modification of KEAP1, other pathways may be involved as well, since redox sensitive proteins others than KEAP1 may be targeted. For instance, DMF activates the PI3K/AKT pathway, thereby inhibiting GSK3 [53]. Considering the lack of selectivity of electrophiles, a new strategy is now based on the development of small molecules that inhibit the interaction of KEAP1 with NRF2. At the time of working on this thesis, these inhibitors are still under development and have not been used.

Despite the high abundance of NRF2 inducers, no specific NRF2 inhibitors are currently available. As shown in Fig. 3, we have used trigonelline for NRF2 pharmacological inhibition. This alkaloid present in coffee and fenugreek seed, has different pharmacological activities [54], including the improvement of chemotherapy in different models via NRF2

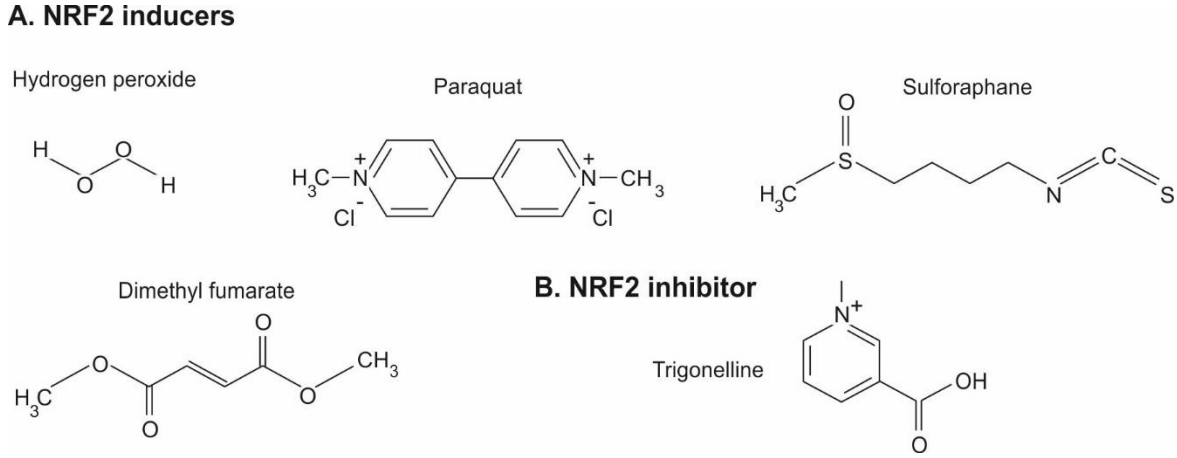

Figure 3. Chemical structure of NRF2 inducers and pharmacological inhibitors used in this study.

inhibition [55-58]. Although the exact mechanisms of NRF2 inhibition by trigonelline are still unknown, prevention of NRF2 nuclear import has been proposed [55].

1.3. Physiological function of NRF2

For many years, NRF2 has been considered the master regulator of biotransformation and the cellular antioxidant response, as it controls the expression of genes that participate in phase I, II and III detoxification reactions (*NQO1*, *GSTA1*, *ABCC1*, etc.), glutathion (*GCLC*, *GCLM*, *GPX1*, etc.) and peroxiredoxin/thioredoxin metabolism (*PRDX1*, *TXN1*, *TXNRD*, etc.)[59]. However, nowadays we know that NRF2 controls the basal and stress-inducible expression of over 250 ARE-containing genes and the current view is that it represents a master regulator of cellular homeostasis (Fig. 4).

The NRF2-directed transcriptional program allows the cell to adapt and survive under various stress conditions, not only oxidative stress. Cellular protection also requires alterations in metabolism and bioenergetics. In fact, it is becoming increasingly clear that NRF2 has a profound effect on mitochondrial function and intermediary metabolism, regulating the expression of genes implicated in NADPH production through the pentose phosphate pathway and malic enzyme as well as enzymes involved in fatty acid oxidation and iron metabolism (*G6PD*, *ME1*, *HMOX1*, *FTH1*, etc.)[59].

Moreover, the NRF2 transcriptional response acts as a brake for inflammation. On one hand, the antioxidant activity of many NRF2-regulated genes counteracts several pro-inflammatory signals (i.e., NFκB pathway or migration and infiltration of immune cells) [60]. On the other hand, NRF2 directly up-regulates the expression of some immunomodulatory genes, such as those coding for MARCO (macrophage receptor MARCO), CD36 (platelet

glycoprotein 4), IL17D (interleukin 17D) and LTB4DH (leukotriene B4 dehydrogenase)[60, 61]. More recently, NRF2 was shown to directly inhibit the expression of the pro-inflammatory cytokines IL6 (interleukin 6) and IL1β (interleukin 1 beta)[62, 63].

Finally, NRF2 activation may have an impact on proteostasis. Thus, NRF2 regulates the expression of genes involved in the metabolism of glutathione, critical for an adequate folding of proteins in the endoplasmic reticulum (ER) and specifically *GPX8* (glutathione peroxidase 8), involved in the unfolded protein response (UPR). Moreover, NRF2 activation has been shown to induce a transient increase in the expression and activity of specific proteasome subunits, which may have an important role in the degradation of oxidized proteins[64-66]. More recently, NRF2 has been reported to control the expression of the autophagy cargo receptors p62/SQSTM1 (sequestosome 1) and NDP52/CALCOCO2 (calcium-binding and coiled-coil domain-containing protein 2)[67, 68], which will be further addressed in the following sections.

2. Autophagy

Protein homeostasis, proteostasis, necessarily depends on the continuous maintenance and renewal of the whole proteome. For this purpose, cells have developed a wide quality check network that assures adequate protein synthesis, folding, conformational maintenance and degradation of disused or defective proteins. Two main cellular degradation systems are found in mammals: the ubiquitin-proteasome system (UPS), which degrades individual short-lived proteins, and the autophagy-lysosomal system, which is able to degrade single long-lived proteins, aggregates and whole organelles[69].

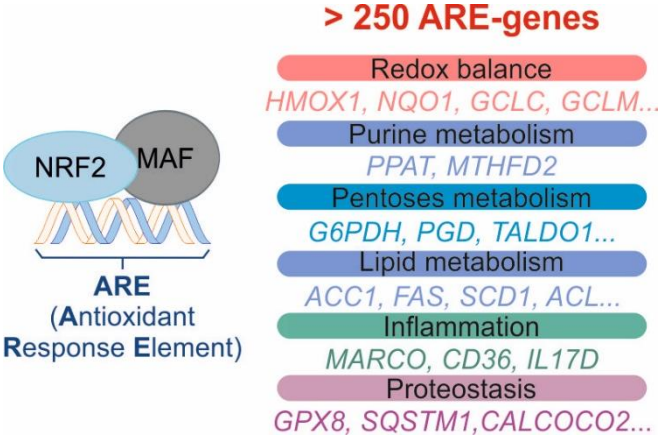

Figure 4. NRF2 as a master regulator of cell homeostasis. NRF2/MAF heterodimers bind the enhancer sequence termed antioxidant response element (ARE) in the regulatory regions of over 250 genes implicated in different homeostatic processes.

The term "autophagy", derived from the Greek term for "self-eating", embraces all the processes by which cellular components (proteins, organelles, aggregates and intracellular pathogens) are delivered to lysosomes for degradation. Lysosomes contain more than 60 acid hydrolases which degrade almost every type of macromolecule: nucleases, proteases, lipases, glycosidases[70]. The resulting products are re-cycled into the cytoplasm by specific transporters located at the lysosomal membrane[71, 72].

2.1. Types of autophagy in mammals

Several distinctive types of autophagy co-exist in mammals according to the way in which cargoes are delivered to lysosomes: a) macroautophagy, in which portions of the cytosol are engulfed by a growing double membrane that originates a vesicle that eventually fuses with the lysosome; b) chaperone mediated autophagy (CMA), which allows proteins bearing a certain motif to specifically be delivered to lysosomes or c) microautophagy, a process whereby the lysosome itself swallows up small components of the cytoplasm by inward invagination of the lysosomal membrane. Macroautophagy and CMA are the best described types of autophagy in mammals and constitute the focus of this study.

2.1.1. Macroautophagy

Macroautophagy (often referred to as simply 'autophagy') was first described in the late 60s by Christian De Duve, who identified intracellular organelles with a double membrane and a lumen similar to the cytoplasm[73]. In fact, macroautophagy is a process whereby portions of the cytoplasm are sequestered by the expansion and closure of membranous cisterna (termed "phagophores"), to produce double- or multiple-membraned vesicles called "autophagosomes," which eventually fuse with lysosomes for degradation of the sequestered content.

a. Steps in macroautophagy

It was not until the identification of the *Atg* genes in yeast that the molecular players implicated in macroautophagy have started to be unveiled [74]. Indeed, this process is evolutionarily conserved in eukaryotes [75] and many autophagy-related proteins (ATGs) orthologues have also been identified in mammals [76].

Macroautophagy can be non-selective, implying *in bulk* sequestration of random portions of the cytosol; or selective, when specific substrates are recognized and degraded. According to the specific material to be degraded, macroautophagy can be named as xenophagy (when cargoes for degradation are pathogens), mitophagy (mitochondria), lipophagy (lipid droplets), etc. Although cell-specific or context-dependent regulatory mechanisms may direct the process, there are some common players involved in the autophagosome formation, which are represented in Fig.5.

Initiation relies on the ULK complex (ULK1/ULK2-ATG13-FIP200-ATG10l), which is activated by different signals, enabling phagophore nucleation and assembly. The exact origin of the nucleation membrane is still a matter of debate, but some reports suggest that it derives from the plasma membrane, the outer mitochondrial membrane or the ER membrane [77]. ULK1/2 kinase is capable of auto-phosphorylating itself and also ATG13 and FIP200. The activated ULK complex recruits a class III phosphatidylinositol-3 kinase complex (PI3K-III/VPS34-BECLIN1-VPS15-ATG14 or UVRAG) which locally produces phosphatidylinositol-3-phosphate (PI3P) in the phagophore membrane in order to recruit other proteins to the nucleation site, including WIPIs (WD repeat protein interacting with phosphoinositides) or ATG2. The phagophore expansion step is associated with two ubiquitination-like reactions. First, ATG7 acts as an E1 ubiquitin-activating enzyme and ATG10 as an E2 ubiquitin conjugating enzyme, enabling ATG12 conjugation to ATG5. Second, ATG12-ATG5 complexes interact non-covalently with ATG16L. This complex acts as an E3-ligase, facilitating the second ubiquitin-like reaction, where LC3 (microtubule-associated protein 1A/1B light chain 3) and GABARAP (γ-aminobutyric acid receptor-associated protein) are conjugated to phosphatidylethanolamine (PE) by ATG7 (E1-like) and ATG3 (E2-like) to form LC3-II and GABARAPs-II anchored to the phagophore membrane. In selective autophagy, different autophagy cargo receptors, such as p62 and NDP52, interact with ubiquitin-labelled proteins as well as with LC3s and GABARAPs, enabling specific substrates to be engulfed by autophagosomes. ATG12-ATG5 complexes dissociate from the autophagosomal membrane once autophagosome formation is complete, while ATG4 is necessary for the de-lipidation and recycling of LC3-II and GABARAPs-II, as well as for the initial proteolytic activation of newly expressed pro-LC3 and pro-GABARAP proteins. Autophagosomes are delivered, along microtubules, to lysosomes, where fusion subsequently occurs mediated by SNARE (soluble NSF attachment protein receptor) and ESCRT (endosomal sorting complex required for transport) complexes. Once inside lysosomes, the

material is degraded by acid hydrolases and the resulting breakdown products are released through permeases for recycling at the cytosol [78, 79].

b. Regulation of macroautophagy

Provided that it is a catabolic process, macroautophagy must be tightly regulated so that it is induced only when necessary. One of the most evolutionarily conserved functions of macroautophagy is adaptation to starvation through the degradation of proteins and other macromolecules [80-82] and subsequent release of their primary constituents to the cytosol, which can be used for the synthesis of specific proteins needed under these conditions or employed for energy production. As shown in Fig. 5, two main regulators participate in the up-regulation of macroautophagy upon nutritional stress: mechanistic target of rapamycin kinase (mTOR) and AMP-activated protein kinase (AMPK) [83].

mTOR is a highly conserved Ser/Thr kinase that integrates signals from different stimuli, including aminoacids, energy levels, oxygen or growth factors. During nutrient-rich conditions, mTOR phosphorylates and inhibits ULK1/2 and ATG13, thereby repressing autophagy initiation. mTOR inhibition (upon starvation or rapamycin treatment, for instance) results in mTOR removal from the ULK complex, allowing ULK1/2 to autophosphorylate and phosphorylate subsequent substrates [84, 85]. AMPK directly senses increased levels of ADP/AMP, indicative of energetic stress. This Ser/Thr kinase is an essential activator of autophagy by, at least, three different mechanisms: mTOR inhibition [86, 87], direct phosphorylation and activation of ULK1[85] and activation of VPS34 complexes [88, 89].

Additional stress conditions, such as hypoxia, mitochondrial dysfunction, genomic damage, ER stress or oxidative stress also activate macroautophagy via different signaling pathways in order to eliminate damaged proteins or organelles[90]. Thus, ROS have been shown to affect upstream regulators and macroautophagy core components, generally resulting in its up-regulation [91, 92]. An elegant example of the essential role of redox signaling in macroautophagy is provided by the generation of ROS upon nutrient starvation. ROS can oxidize key Cys residues in AMPK, generating S-glutathionylated derivatives with increased kinase activity [93, 94]. Mitochondria-generated ROS were reported to induce autophagy via

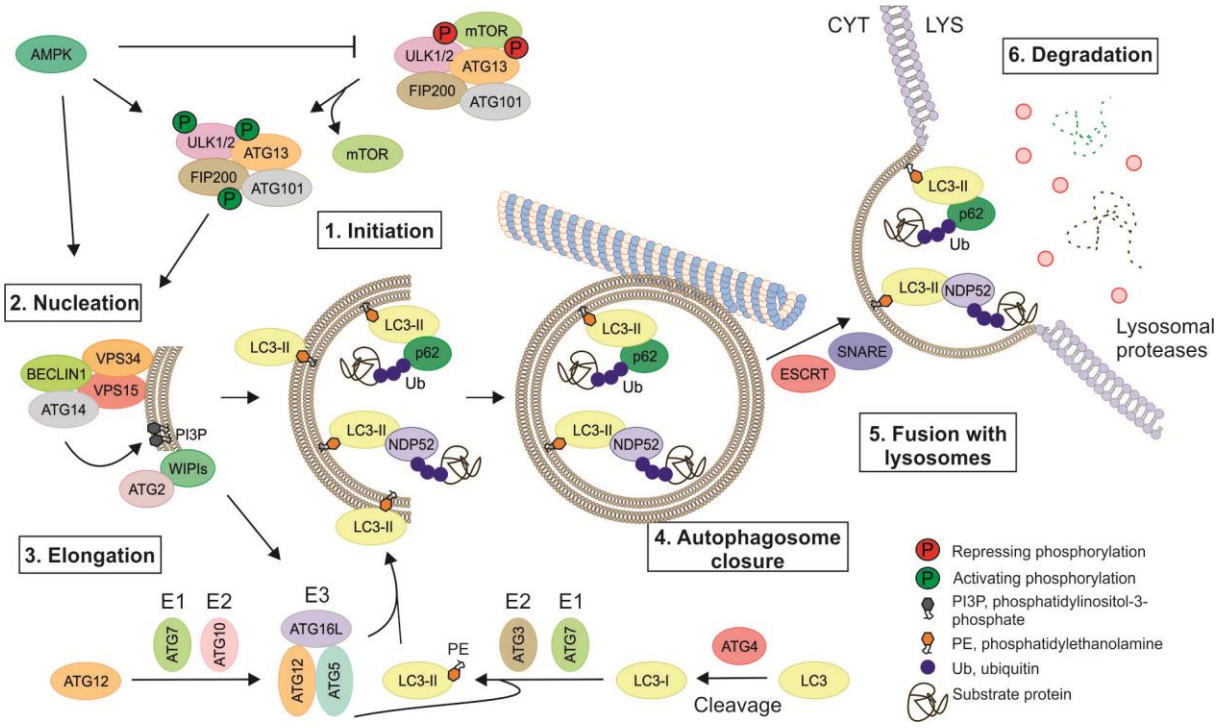

Figure 5. Schematic representation of the different steps in macroautophagy and main protein complexes implicated: 1) initiation (ULK initiation complex); 2) membrane nucleation and phagophore formation (PI3K complex); 3) autophagosome elongation and 4) autophagosome closure (ATG5-ATG12 and LC3 conjugation systems); 5) lysosome fusion, and 6) degradation.

AMPK, and this was prevented by overexpression of the antioxidant enzyme manganese-superoxide dismutase 2, pre-treatment with a ROS scavenger or AMPK inhibition[95]. Moreover, the protease ATG4 contains reactive cysteines prone to oxidation that transiently inhibit its de-lipidation activity. As explained before, ATG4 has the dual role of; first, cleaving pro-LC3 and pro-GABARAPs at the C-terminus so that they can be conjugated to PE and, second, de-lipidating LC3 and GABARAPs to be re-cycled once the process is completed. It was proposed that starvation-induced H_2O_2 in the vicinity of the place of autophagosome formation would locally inactivate the de-lipidation activity of ATG4 maintaining its protease activity and allowing autophagosome formation. As the autophagosome is trafficked to lysosomes, low H_2O_2 concentrations would allow ATG4 reactivation to de-lipidate LC3 and GABARAPs [96]. On the other hand, oxidation of catalytic thiols in ATG3 and ATG7 was shown to prevent LC3 lipidation, inhibiting starvation-induced autophagy [97]. Therefore, the impact of redox signaling in macroautophagy may depend on the type, localization and levels of ROS.

Recent studies have directly connected autophagy with the KEAP1/NRF2 axis (Fig. 6). A KEAP1 interacting region (KIR) was identified in the autophagy cargo receptor p62, which allowed binding to KEAP1 in the same basic surface pocket and with a binding affinity

similar to the 79-ETGE-82 motif in NRF2, suggesting competition between p62 and NRF2 [67, 98-101]. In fact, p62 overexpression led to reduced NRF2 ubiquitination and subsequent stabilization as well as induction of its target genes[98], whereas silencing of p62 increased KEAP1 stability in parallel with a decrease in NRF2 levels [101]. The phosphorylation of Ser-351 in the KIR motif in p62 (349-DP**S**TGE-354) was shown to increase its affinity for KEAP1, competing with NRF2 binding and allowing its accumulation and transcriptional activation of its target genes [102]. The kinases mTORC1 (mammalian target of rapamycin complex 1) and TAK1 (TGF-β-activated kinase 1) involved in nutrient sensing and inflammation, respectively, were suggested to participate in this phosphorylation [102, 103]. The observations that the levels of KEAP1 were increased in *Atg7*-knockout mice and reduced upon starvation [104], led to the suggestion that KEAP1 is targeted for degradation by autophagy. Therefore, p62 accumulation (due to, for instance, autophagy impairment) and/or phosphorylation would result in KEAP1 sequestration and degradation, favoring NRF2 transactivation of its target genes. Importantly, p62 contains a functional ARE in its gene promoter [67], creating a positive feedback loop. It is possible that this non-canonical mechanism of NRF2 induction would result in prolonged NRF2 signaling relative to the canonical KEAP1 pathway, activating the NRF2 transcriptional network in order to restore cell homeostasis.

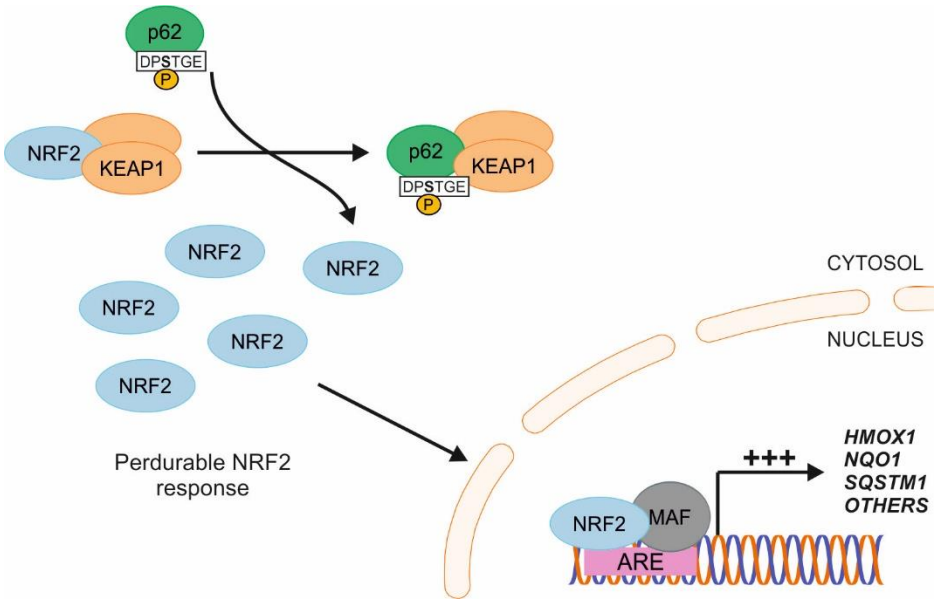

Figure 6. NRF2 levels are regulated by the autophagy adaptor protein p62. p62 competes with NRF2 for binding to KEAP1 through its STGE motif. Phosphorylation of the Ser in this KEAP1 interacting region (KIR) of p62 increases its binding affinity for KEAP1. Therefore, increased and/or phosphorylated p62 displaces NRF2 and enables the transcriptional activation of its target genes, including *SQSTM1* (coding for p62) in a positive feedback loop.

In addition to p62, NRF2 also controls the expression of the cargo recognition adaptor NDP52. Five putative AREs were found in the gene coding for NDP52, called *CALCOCO2*, and three of them were identified with different mutant constructs and ChIP assays as indispensable for NRF2-mediated transcription [68].

Transcriptional control of macroautophagy gene expression is increasingly emerging as a fundamental regulatory mechanism. In fact, whereas most studies on macroautophagy regulation have focused on post-translational modifications and protein-protein interactions, transcriptional control of autophagy may represent an enduring regulation essential for cell type- and stimulus-dependent responses. In this regard, the transcription factor TFEB (transcription factor EB) is considered the master regulator of lysosomal biogenesis and has an essential role in the transcriptional response to starvation [105]. When nutrients are present, mTOR inhibits TFEB at the lysosomal membrane. However, upon starvation or other types of lysosomal stress, mTOR is released from the lysosome, being unable to inhibit TFEB, which progressively accumulates in the nucleus [106]. TFEB controls the expression of genes such as *Lamp1*, *Atg9b* or *Sqstm1* [107, 108]. Members of the FOXO family of transcription factors have also been reported to control the expression of several autophagy-related genes, including *Atg4*, *Atg12* or *Ulk1* in muscle [109-111].

Considering the recent advances in understanding the impact of NRF2 in macroautophagy as well as the important roles of both processes in the response to oxidative stress, one of the main goals of this work was to analyze a mechanistic link between NRF2 and macroautophagy gene expression.

2.1.2. Chaperone mediated autophagy

Chaperone mediated autophagy (CMA) is a selective degradative process that contributes to the maintenance of proteostasis in mammals. In this case, proteins with a specific motif are recognized in the cytosol, delivered to lysosomes and individually translocated through a lysosomal receptor for degradation.

a. Steps in CMA

The concept of selectivity for lysosomal degradation first came from the observation that starvation in animals or serum removal in cultured cells for more than 8-10 h accelerated the lysosomal degradation of specific proteins. This led to the identification of a common

targeting motif and a chaperone recognizing it [112, 113]. Thus, soluble cytosolic proteins bearing a KFERQ-like motif are recognized by HSC70 (heat shock cognate protein of 70 kDa)[114, 115]. The genuine KFERQ motif is present in ribonuclease A (RNAse A), the first protein identified as a CMA substrate [112, 116]. However, HSC70 can recognize KFERQ-like sequences as far as they follow this rule: flanking Q (either at the beginning or at the end of the sequence); up to two of the allowed hydrophobic residues (I, F, L or V) or two of the allowed positive residues (R or K), and only one negative charge provided either by E or D.

HSC70 delivers cargoes to the lysosomal surface, where they interact with LAMP2A (lysosomal associated membrane protein type 2A)[117] (Fig. 7). In contrast to the highly abundant cytosolic HSC70, levels of LAMP2A at the lysosomal membrane are limiting for CMA and, hence, subject to tight regulation [118]. Binding of substrates to the cytosolic tail of LAMP2A induces the organization of this single span membrane protein into a multimeric complex that facilitates substrate translocation in an unfolded conformation [119]. Protein unfolding is thought to occur after binding to LAMP2A, but prior to translocation [120]. Then, proteins are pulled inside lysosomes by an intra-luminal HSC70 form [121] and eventually degraded by lysosomal proteases. Once the substrate protein crosses the lysosomal membrane, the translocation complex disassembles into monomeric forms of LAMP2A to allow a new cycle of substrate binding and translocation [119].

b. Regulation of CMA

Although basal CMA activity can be detected in most cell types [122], this process is maximally activated in response to stressors such as starvation [123], oxidative stress [124], hypoxia [125] or genotoxic stress [126]. Activation of CMA is associated with increased levels of LAMP2A and its multimerization to form membrane translocation complexes, lysosomal enrichment in HSC70 and relocation of lysosomes to the perinuclear region [123, 124, 127].

LAMP2A is one of the three proteins that originate from alternative splicing of the *LAMP2* gene. All LAMP2A, LAMP2B and LAMP2C isoforms share identical luminal regions but differ in their cytosolic and transmembrane tails [128]. Moreover, they are expressed in a tissue-specific manner, pointing to different cellular functions and a cell-specific yet unknown regulation of differential splicing [129-131]. Nevertheless, LAMP2A is the only LAMP2 variant required for CMA [117, 132]. In fact, the availability of LAMP2A at the lysosomal membrane is the limiting step of CMA, as knockdown or overexpression of LAMP2A results in a proportional decrease or increase in CMA, respectively [117, 132].

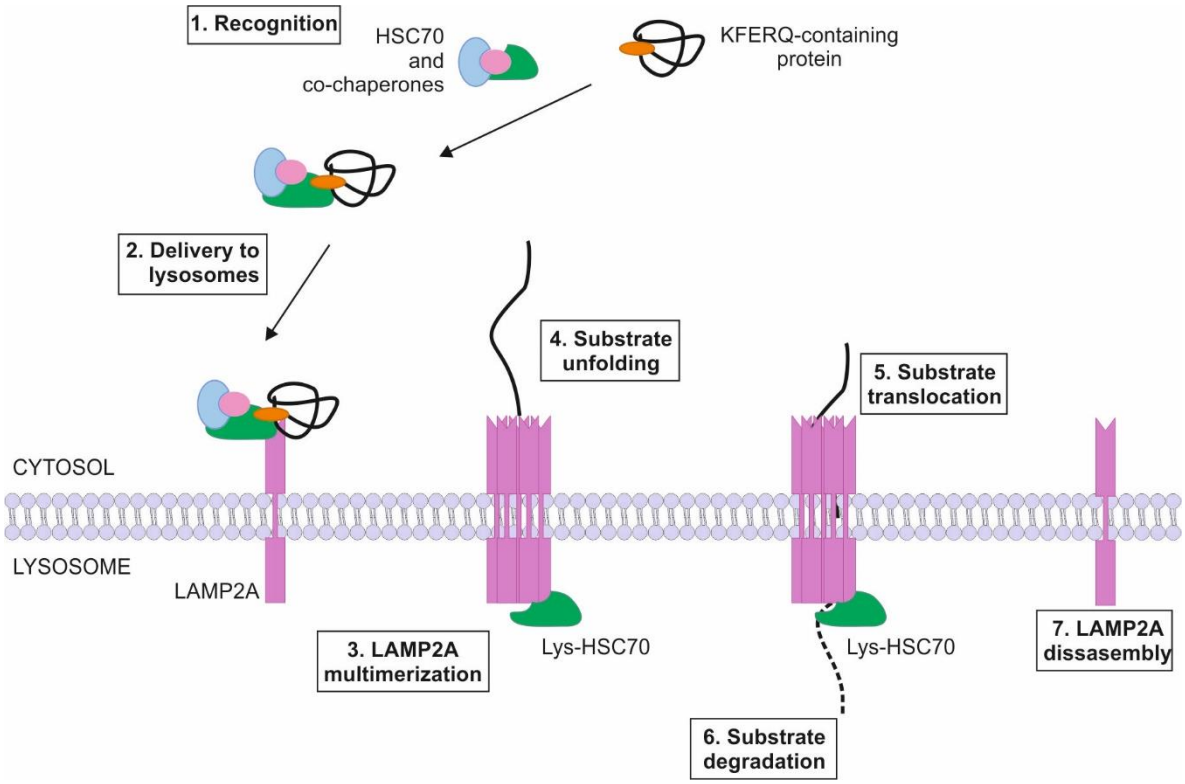

Figure 7. Schematic representation of the different steps in CMA. Proteins bearing a KFERQ-like motif are recognized by HSC70 and delivered to lysosomes, where they interact with the lysosomal receptor LAMP2A. LAMP2A multimerizes and the unfolded protein is translocated inside lysosomes assisted by luminal HSC70. The substrate protein is degraded inside lysosomes and LAMP2A multimer is disassembled.

Levels of LAMP2A at the lysosomal membrane are tightly regulated by lysosomal degradation of this receptor and a dynamic equilibrium between the matrix and the membrane of the lysosome. Therefore, activation of CMA during starvation implies reduced LAMP2A degradation as well as re-location of internalized LAMP2A to the lysosomal membrane [118]. Furthermore, LAMP2A organizes inside and outside lipid-enriched microdomains in the lysosomal membrane, being active outside them and susceptible to proteolytic cleavage and degradation while located inside [133].

More recently, a signaling mechanism involving GFAP (glial fibrilar acidic protein), mTORC2 (mammalian target of rapamycin complex 2) and PHLPP1 (PH domain leucine-rich repeat-containing protein phosphatase 1) was described to regulate CMA. GFAP favors the stabilization of the LAMP2A multimeric complex at the lysosomal membrane, allowing substrate translocation and degradation. Under basal conditions, however, mTORC2 phosphorylated- lysosome-associated AKT1 (RAC-alpha serine/threonine-protein kinase) phosphorylates GFAP. Phosphorylated GFAP displays reduced binding affinity for LAMP2A, not contributing to its stabilization. However, starvation leads to the recruitment of the phosphatase PHLPP1 to lysosomes. This phosphatase inactivates AKT1 and the resulting de-

phosphorylated GFAP can now contribute to the stabilization of the LAMP2A multimer under these conditions [134].

Macroautophagy is early activated upon starvation, reaches its maximum at about 6 h and then gradually declines [132]. Meanwhile, CMA increases after 8-10 h of starvation and remains activated even for days [123]. This might represent a switch to a more selective proteolytic mechanism in order to avoid degrading proteins and structures essential for cell survival, while at the same time degrading proteins of lesser importance in such conditions (such as glycolytic enzymes [135] or catalytic subunits of the 20S proteasome [136]).

CMA is also induced by several pro-oxidant factors [132, 137], indicating its essential role in the cellular response to stress. Oxidized proteins are more easily degraded by CMA [124], although the exact mechanisms have not been fully clarified. This supports the possibility of regulating CMA at the level of the KFERQ-like motifs. On one hand, these motifs can be hidden and become accessible for HSC70 at some point: motifs in the core of the protein will only be exposed when unfolding (caused by oxidation for instance); motifs placed in regions of protein/protein interaction will become accessible when the protein is no longer part of a complex; motifs close to an enzyme catalytic site can only become accessible in the absence of substrate [138]. On the other hand, post-translational modifications can complete or create a KFERQ-like motif.

In contrast to nutritional stress, CMA induction upon oxidative stress may result from transcriptional up-regulation of *Lamp2a* [124]. In the case of T cell activation, the generation of ROS results in NFAT (nuclear factor of activated T-cells)-mediated *Lamp2a* transcription [139]. However, a generic mechanism that might regulate the expression of *Lamp2a* under these and other circumstances remains unknown. Consequently, one aim of the present study was to analyze a potential connection between the transcription factor NRF2 and CMA.

3. Dysfunctional redoxtasis and proteostasis in chronic diseases

NRF2 and autophagy play a crucial role in cell homeostasis, as already described. Consequently, dysregulation of these pathways is intimately related to many chronic diseases, including neurodegenerative diseases such as Alzheimer's Disease or cancer.

3.1. Alzheimer's disease

Alzheimer's disease (AD) is a proteinopathy characterized by the accumulation of insoluble aggregates of amyloid β (Aβ) peptides along with other components in senile plaques, as well as the presence of neurofibrillary tangles of hyperphosphorylated TAU (microtubule-associated protein TAU). At the molecular level, AD is characterized by mitochondrial dysfunction, oxidative stress, low-grade chronic neuroinflammation and a loss of proteostasis. However, the causal relationship between these molecular events remains elusive.

The brain is highly susceptible to oxidative stress due to reliance in oxidative metabolism for energy and lower levels of antioxidant systems compared to other organs [140]. In fact, oxidative damage has been shown to increase in the brain with age [92], and even further in subjects with conditions ranging from mild cognitive impairment to advanced AD [141, 142]. This imbalance in the brain redox state likely represents an early marker of AD prior to the appearance of the histopathological hallmarks [143, 144] and probably contributes to mitochondrial dysfunction [145, 146], neuroinflammation [147] and the aggregation of damaged and misfolded proteins [148-150].

The Aβ peptides that build up senile plaques are originated from APP (amyloid precursor protein). Under physiological conditions, APP is mostly cleaved by α- and γ-secretases, resulting in a secreted form of APP and C-terminal fragments. Although the exact physiological role of APP and its products remains unknown, APP appears to be important for neuronal and synaptic function [151]. In AD, an imbalance towards cleavage of APP by β- and γ-secretases results in the generation of Aβ peptides, which vary in length and are considered toxic [152].

TAU normally binds to and stabilizes the microtubules. In AD, however, different post-translational modifications of TAU, including hyperphosphorylation, alter TAU binding to microtubules [153]. In this regard, hyperactivation of GSK3β has been proposed to participate in the abnormal phosphorylation of TAU in AD, resulting in its aggregation, formation of neurofibrillary tangles and interruption of axonal transport [154].

Autophagy impairment is intimately connected to the loss of proteostasis in AD. In fact, autophagy ablation in mice is sufficient to produce neurodegeneration [155-157]. Overall reduced rates of protein degradation with age were first observed almost three decades ago [158] and the levels of core macroautophagy and CMA proteins in various tissues were reported to be reduced with age in distinct organisms [159-162]. Thus, excessive accumulation of

autophagosomes and autophagic vacuoles (AVs), together with p62 and ubiquitinated proteins, has been shown in the brains of AD patients [163, 164]. This is likely due to incomplete autophagosome-lysosome fusion and digestion, which may favor the accumulation of aggregated proteins and damaged organelles, and lead to the abnormal production of ROS.

Overall, AD is considered a multifactorial process in which genetic and environmental factors along with increased susceptibility to stress with age influence each other, resulting in the loss of neuronal and brain homeostasis. Given NRF2 wide cytoprotective functions, it is possible that a single pharmacological hit in NRF2 might mitigate the effect of the main culprits of AD, including oxidative, inflammatory and proteotoxic stress. In fact, some evidence support a key role of NRF2 in AD. On the one hand, NRF2 activity declines with age [165, 166] and GSK3β hyperactivation in AD would presumably decrease NRF2 levels. Moreover, NRF2 deficiency has been shown to aggravate and, conversely, NRF2 activation to ameliorate the phenotype of mouse models of AD [66]. Interestingly, one haplotype allele in the *NFE2L2* gene promoter, encoding NRF2, was associated with an earlier onset of AD, implying that common variants of the *NFE2L2* gene might affect AD progression [167]. A better understanding of the impact of NRF2 in AD is necessary in order to eventually take advantage of its therapeutic potential.

3.2. Cancer

The term ‘cancer’ refers to a group of disorders caused by genetic alterations that affect cellular signaling pathways and lead to abnormal cell proliferation and tumor generation. The evolution of a normal cell to a malignant one involves the activation of genes stimulating proliferation or protection against cell death (called oncogenes) and the inactivation of genes which would normally inhibit proliferation (called tumor suppressor genes).

NRF2 seems to have context-dependent and even opposing effects on tumor behavior. Under normal conditions, NRF2 has a protective role and it inhibits tumor initiation and metastasis by eliminating carcinogens, ROS and other DNA-damaging agents. However, persistently activated NRF2 may be advantageous to cancer cells for survival to ROS, chemotherapy, radiotherapy or adaptation to the tissue microenvironment. In fact, missense mutations in *KEAP1* and *NFE2L2* genes that disrupt its interaction and result in constitutive NRF2 activation have been identified in many human cancers [168, 169]. However, it is believed

that the increase in NRF2 activity results from selection during tumor development rather than being a cancer initiating event [170].

Autophagy plays a dual and complex role in cancer as well. Defects in autophagy result in p62 accumulation, oxidative stress, DNA damage and cell death, leading to chronic tissue damage and creating an ideal environment for tumor initiation. However, once cells have undergone transformation, they upregulate macroautophagy and CMA probably because of inherent deficiencies in the microenvironment and to the increased metabolic and biosynthetic demands imposed by deregulated proliferation. In this scenario, activating autophagy may increase resistance to cytotoxic stressors and sustain the specific metabolic needs of tumor cells [171, 172]. Therefore, it is thought that autophagy prevents cancer development, but, once cancer is established, increased autophagic flux enables tumor cell survival and growth [171]. This is supported by several studies showing improved outcomes in models of cancer when autophagy is inhibited. For instance, increased CMA activity was reported in several types of cancer [173-175], and LAMP2A blockage in different cancer cell lines reduced its tumorigenic activity [173]. Moreover, clinical interventions to manipulate autophagy in cancer therapy are already under way and usually directed towards autophagy inhibition [171].

In this study, we have employed gliomas as a model of cancer, as they constitute the most common brain malignancies. Gliomas are neuroepithelial tumors originating from the supporting glial cells of the central nervous system. Therefore, gliomas can be classified according to the presumed cell of origin into astrocytomas, oligodendrogliomas, ependymomas, and mixed gliomas. Glioblastomas are the most malignant and frequently occurring type of primary astrocytoma. Therefore, all glioblastomas are gliomas, but not all gliomas are glioblastomas [176]. Because of the poor prognosis of these patients, it is imperative that novel avenues for therapy are explored.

AD and cancer are analyzed in this work as two examples of the deleterious effects of reduced and enhanced autophagy and NRF2 activity on physiology, respectively.

Objectives

Both autophagy as well as NRF2 transcriptional activity are essential for maintaining cell homeostasis, especially upon stressful conditions such as oxidative stress. Therefore, our aim in this work is to analyze the role of the transcription factor NRF2 in the regulation of the best characterized forms of autophagy in mammals, namely macroautophagy and chaperone mediated autophagy (CMA). Our specific objectives are the following:

1. **Analysis of the regulation of macroautophagy genes by NRF2**

    1.1. *In silico* identification and further validation of putative antioxidant response elements (AREs) in the promoter regions of macroautophagy-related genes
    1.2. Analysis of the regulation of macroautophagy by NRF2
    1.3. Generation and characterization of a new mouse model of Alzheimer's disease (AD) in a wild type or an *Nrf2*-knockout background
    1.4. Relevance of NRF2 in controlling macroautophagy in the new AD model of proteinopathy
    1.5. Translation of our observations to AD pathology in human brain samples

2. **Analysis of the regulation of CMA by NRF2**

    2.1. *In silico* identification and further validation of putative antioxidant response elements (AREs) in the *LAMP2* gene
    2.2. Analysis of the regulation of LAMP2A expression by NRF2
    2.3. Role of NRF2 in CMA activation by oxidative stress
    2.4. Relevance of the regulation of CMA by NRF2
    2.5. Pathophysiological significance of the NRF2/LAMP2A axis in cancer

Materials and Methods

1. Materials

1.1. Reagents

Cell culture: DMEM (*Dulbecco's Modified Eagle Medium*) and PBS (*Phosphate Buffered Saline*) were prepared by the *Culture Media Preparation Facility* at the *Instituto de Investigaciones Biomédicas "Alberto Sols" (UAM-CSIC)*; minimum essential medium (MEM), phenol red-free neurobasal, horse serum, fetal bovine serum, B27 supplement, glutamine, sodium pyruvate and trypsin (Gibco-Invitrogen); gentamicin (Genta Gobens); glucose, rapamycin, heparin, polybrene, puromycin (Sigma-Aldrich); human fibroblast growth factor and epidermal growth factor (hFGF-2 and hEGF (Peprotech); metrizamide (AK Scientific); plastic material (Nunc, Falcon y Sarstedt).

Pharmacological activators, inhibitors and other compounds: Paraquat, hydrogen peroxide, trigonelline, dimethylfumarate and leupeptin hemisulfate salt (>95%) (Sigma-Aldrich). R,S-sulforaphane (SFN) (LKT Laboratories).

DNA manipulation and extraction: Antibiotics: ampicillin **(**Sigma-Aldrich). Plasmid DNA preparation: *Genopure Plasmid Maxi Kit* (Roche Applied Science) and *"Miniprep Kit"* (Qiagen). Plasmid digestions: restriction enzymes (Thermo Fisher Scientific, Invitrogen and New England Biolabs). DNA cloning: alkaline phosphatase (Roche), T4 polynucleotide kinase and T4 DNA ligase (Promega). DNA electrophoresis: agarose (CONDA laboratories) and low melting temperature agarose (Nusieve®, agarose, Lonza). DNA molecular weight markers: DNAλ *Hin*dIII (Thermo Fisher Scientific). DNA purification from band in agarose gel: "*Geneclean® Kit"* (MP Biomedicals).

Protein electrophoresis, transfer and immunoblotting: Protein quantification (Pierce™ BCA Protein Assay Kit). Molecular weight markers *"Bench protein ladder"* (Invitrogen), TEMED, ammonium persulfate, acrylamide/bys-acrylamide (BioRad), Immobilon-P membranes (Millipore), enhanced chemiluminescence substrate (Amersham™ ECL™ Select Western Blotting Detection Reagent, GE Healthcare).

RNA extraction and qRT-PCR: TRIzol® Plus RNA Purification Kit (Invitrogen). Retrotranscriptase (High Capacity RNA-to-cDNA Kit, Applied Biosystems). SYBR green, PCR plates (Applied Biosystems), chloroform, isopropanol (Merck).

Luciferase activity: Dual-Luciferase® Reporter Assay System (Promega).

NADP/NADPH measurement: NADP/NADPH Assay Kit (Abcam).

Immunofluorescence and immunohistochemistry: Normal goat serum (Millipore), paraformaldehyde, formic acid, triton X-100 and 3´-3´-diaminobenzidine tetrahydrochloride (DAB) (Sigma-Aldrich), gelatin and cupric sulfate (Panreac), DePeX (Thermo Fisher Scientific), ProLong (Life Technologies).

1.2. Antibodies

1.2.1. Primary antibodies

Primary antibodies used in this study have been listed in Table 1.

1.2.2. Secondary antibodies

The corresponding secondary antibodies conjugated to horseradish peroxidase (HRP) were supplied by Life Technologies (anti-goat), Amersham (anti-rabbit and anti-mouse) and Chemicon (anti-rat). The secondary antibodies for immunofluorescence and immunohistochemistry were acquired from Molecular Probes and Chemicon, respectively.

Antibody	Source	Catalog number	Clonality	Isotype	Dilution
ACTB	Santa Cruz Biotechnology	sc-1616	Polyclonal	G	1/5000 (WB)
APP/Aβ (4G8)	Covance	SIG-39220-200	Monoclonal	M	1/2000 (WB) 1/1000 (IHC-f/p)
APP/Aβ (6E10)	Covance	SIG-39320-200	Monoclonal	M	1/2000 (WB)
APP/Aβ (22C11)	EMD Millipore	MAB348	Monoclonal	M	1/2000 (WB)
ATG5	Abcam	ab108327	Monoclonal	R	1/2000 (WB) 1/200 (IHC-f)
ATG7	Abcam	ab53255	Polyclonal	R	1/2000 (WB)
NDP52/CALCOCO2	ProteinTech	12229-1-AP	Polyclonal	R	1/1000 (WB)
CD11B	Abcam	ab53187	Polyclonal	R	1:100 (IHC-f)
GABARAPL1	Abcam	ab86497	Polyclonal	R	1/2000 (WB) 1/200 (IHC-f)
GAPDH	Calbiochem	CB1001	Monoclonal	M	1/5000 (WB)
GFAP	Sigma Aldrich	G3893	Monoclonal	M	1:500 (IHC-f)
GCLC	Dr. Terrance Kavanagh		Polyclonal	R	1/2000 (WB)
HMOX1	Enzo life sciences	OSA110	Monoclonal	M	1/2000 (WB)
HSC70 (13D3)	Novus Biologicals	NB1202788	Monoclonal	M	1/5000 (WB) 1/500 (ICF)
IBA1	Wako	019-19741	Polyclonal	R	1:500 (IHC-f/p)

Table 1. Antibodies used in immunoblots, immunofluorescence and ChIP. IHC-f, immunohistochemistry on floating slices; IHC-p, immunohistochemistry on paraffin slices; WB, western blot; ChIP, chromatin immunoprecipitation; R, rabbit; M, mouse; G, goat;

IgG2a	Abcam	ab18413	Monoclonal	M	1/250 (ChIP)
LAMIN B	Santa Cruz Biotechnology	sc-6217	Polyclonal	G	1/5000 (WB)
mLAMP2A (Igp96)	Zymed/Invitrogen	51-2200	Polyclonal	R	1/1000 (WB) 1/100 (ICF)
hLAMP2A	Abcam	ab18528	Polyclonal	R	1/1000 (WB)
LAMP2B	Cuervo lab		Polyclonal	R	1/1000 (WB)
LAMP2C	Cuervo lab		Polyclonal	R	1/1000 (WB)
LAMP1 (1D4B)	Hybridoma Bank	1D4B	Monoclonal	Rat	1/1000 (WB) 1/250 (ICF)
LC3B	Cell signaling	2775	Polyclonal	R	1/2000 (WB) 1/250 (IHC-f/p)
NQO1	Abcam	ab2346	Polyclonal	G	1/2000 (WB)
NRF2	Cuadrado lab		Polyclonal	R	1/2500 (WB)
hNRF2	Abyntek	AJ1555a	Monoclonal	R	1/2000 (WB)
hNRF2	Thermo Scientific	PA138312	Polyclonal	R	1/200 (IHC)
p62/SQSTM1	Sigma Aldrich	P0067	Polyclonal	R	1/2000 (WB) 1/250 (IHC-f/p)
TAU (HT7)	Thermo Scientific	MN1000B	Monoclonal	M	1/2000 (WB) 1/250 (IHC-f/p)
TAU (TAU46)	Sigma Aldrich	T9450	Monoclonal	M	1/4000 (WB)
p-TAU (PHF1)	Dr. M Pérez gift		Polyclonal	R	1/1000 (WB)

Table 1 (*continued*). Antibodies used in immunoblots, immunofluorescence and ChIP. IHC-f, immunohistochemistry on floating slices; IHC-p, immunohistochemistry on paraffin slices; WB, western blot; ChIP, chromatin immunoprecipitation; R, rabbit; M, mouse; G, goat;

p-TAU (AT8)	Thermo Scientific	MN1020	Monoclonal	M	1/1000 (IHC-f)
ULK1	Abcam	ab128859	Monoclonal	R	1/2000 (WB) 1/200 (IHC-f)
V5	Life Technologies	37-7500	Monoclonal	M	1/250 (ChIP)

Table 1 (*continued*). Antibodies used in immunoblots, immunofluorescence and ChIP. IHC-f, immunohistochemistry on floating slices; IHC-p, immunohistochemistry on paraffin slices; WB, western blot; ChIP, chromatin immunoprecipitation; R, rabbit; M, mouse; G, goat;

1.3. Plasmids

pcDNA3.1-m*Nrf2*-V5/HisB: plasmid that contains the wild type sequence of murine *Nrf2*, with a V5 tag (GKPIPNPLLGLDST) in the C-terminus. This plasmid was originally provided by Dr. J. D. Hayes.

pcDNA3.1-mNrf2-$^{\Delta ETGE}$-V5/HisB: plasmid that contains the KEAP1-insensitive version of murine NRF2, with a V5 tag in the C-terminus. This construct lacks residues 79-ETGE-82, responsible for the high affinity binding to KEAP1. This plasmid was originally provided by Dr. J. D. Hayes.

pTK-Renilla: plasmid employed as an internal control in the luciferase assays. It contains the sea pansy (*Renilla reniformis*) luciferase gene under the control of the thymidine kinase promoter from *Herpes Simplex Virus* for its constitutive expression in mammalian cells.

***LAMP2* ARE-LUC and ARE*-LUC reporters:** artificial oligonucleotides with three tandem repetitions of the putative AREs identified in the *LAMP2* gene or its mutated versions* (underlined sequences) separated with a *BamHI* site (bold green colored) and a random separating-sequence (bold orange colored), as well as the oligonucleotides that contain an aleatory sequence used as negative control are shown below. These oligonucleotides were subcloned into the *Nhe*I and *Xho*I sites of a pGL3bv vector (Promega) with the 29 bp-long minimal promoter from the human *SOD1* gene described in [177] controlling the expression of the firefly (*Photinus pyralis*) luciferase. Cloning of the insert eliminated the *NheI* site to facilitate re-ligated vectors exclusion with *NheI* digestion prior to transformation. Scramble-LUC included also a *SalI* site (bold purple colored) instead of the random separating-sequence to facilitate differentiation between constructs.

Lamp2 ARE1-LUC:

5’- CTAGTATGACACTGCA**GGATCC**ATGACACTGCA**ACGTGA**ATGACACTGCAC -3’

3’- ATACTGTGACGT**CCTAGG**TACTGTGACGT**TGCACT**TACTGTGACGTGAGCT-5’

Lamp2 ARE2-LUC:

5’- CTAGTTTGACTCAGCG**GGATCC**TTGACTCAGCG**ACGTGA**TTGACTCAGCGC -3’

3’- AAACTGAGTCGC**CCTAGG**AACTGAGTCGC**TGCACT**AACTGAGTCGCGAGCT-5’

Lamp2 ARE3-LUC:

5’- CTAGTATGACAAACCAGGATCCATGACAAACCAACGTGAATGACAAACCAC -3’

3’- ATACTGTTTGGTCCTAGGTACTGTTTGGTTGCACTTACTGTTTGGTGAGCT-5’

Lamp2 ARE1*-LUC:

5’- CTAGTATGACACTACAGGATCCATGACACTACAACGTGAATGACACTACAC -3’

3’- ATACTGTGATGTCCTAGGTACTGTGATGTTGCACTTACTGTGATGTGAGCT-5’

Lamp2 ARE2*-LUC:

5’- CTAGTTTGACTCAACGGGATCCTTGACTCAACGACGTGATTGACTCAACGC -3’

3’- AAACTGAGTTGCCCTAGGAACTGAGTTGCTGCACTAACTGAGTTGCGAGCT-5’

Scramble-LUC:

5’- CTAGTTCAGATTCACGGGATCCTCAGATTCACGGTCGACTCAGATTCACGC -3’

3’- AAGTCTAAGTGCCCTAGGAGTCTAAGTGCCAGCTGAGTCTAAGTGCGAGCT-5’

pMD2.G: plasmid that encodes the G protein from the envelope of the *Vesicular Stomatitis Virus* used for lentiviral production (Addgene, #12259).

pSPAX2: packaging plasmid that encodes the Gag and Pol proteins from the *Human Immunodeficiency Virus* necessary for lentiviral production (Addgene, #12260).

pLKO.1-TRC control: plasmid used for the generation of lentiviral particles with the sequence CCGCAGGTATGCACGCGT to be used as a non-hairpin control (Addgene, #10879).

pLKO.1-puro shNRF2 (mouse): plasmid used for the generation of lentiviral particles with the sequence CCAAAGCTAGTATAGCAATAA transcribed into a short hairpin RNA (shRNA) sequence against murine *Nfe2l2* gene (MISSION shRNA, Sigma-Aldrich).

pLKO.1-puro shNRF2 (human): plasmid used for the generation of lentiviral particles with the sequence AGTTTGGGAGGAGCTATTATC transcribed into a shRNA sequence against human *NFE2L2* gene (MISSION shRNA, Sigma-Aldrich).

pWPXL-GFP: plasmid for the generation of lentiviral particles expressing the green fluorescence protein (GFP) under the control of the Elongation Factor 1α promoter. This plasmid was originally provided by Dr. D. Trono.

pWPXL-mNrf2-$^{\Delta ETGE}$-V5/HisB: plasmid for the generation of lentiviral particles expressing the murine version of NRF2 lacking residues 79-ETGE-82 and with a V5 tag in the C-terminus. The m*Nrf2*-$^{\Delta ETGE}$-V5/HisB insert from pcDNA3.1-mNrf2-$^{\Delta ETGE}$-V5/HisB was subcloned into the *BsteII* and *SmaI/PmeI* restriction sites of the pWPXL-GFP vector.

1.4. Buffers and solutions

General buffers: Luria-Bertani medium (LB) for the growth of bacteria, LB agar plates, phosphate saline buffer (PBS), 1 M Tris-HCl pH 7.5, 1 M Tris-HCl pH 8.8, 1 M Tris-HCl pH 6.6, 1 M HEPES pH 7.5, 10% SDS, 0.5 M EDTA pH 8.0 and 0.5 M EGTA pH 7.5 were provided by the *Culture Media Preparation Facility* at the *Instituto de Investigaciones Biomédicas "Alberto Sols" (UAM-CSIC).*

Cellular lysis buffer: 1% NP-40, 10% glycerol, 137 mM NaCl, 20 mM Tris-HCl pH 7.5, 1 mM sodium pyrophosphate, 1 mM sodium orthovanadate, 20 mM sodium phosphate, 1μg/ml leupeptin and 1 mM PMSF.

Animal tissue lysis buffer (RIPA buffer): 1% NP-40, 150 mM NaCl, 25 mM Tris-HCl, pH 7.5, 1% sodium deoxycholate, 0.1% SDS, 1 mM EGTA, 1 mM sodium orthovanadate, 1 mM sodium phosphate, 1μg/ml leupeptin and 1 mM PMSF.

Protein loading buffer for SDS-PAGE: 50 mM Tris-HCl pH 6.8, 2% SDS, 0.1% bromophenol blue, 10% glycerol, 150 mM β-mercaptoethanol.

Electrophoresis running buffer: 0.37% EDTA, 1.44% glycine, 0.1% SDS and 0.3% Tris.

Transfer buffer: 25 mM Tris, 190 mM Glycine and 20% Methanol.

Tris buffered saline with Tween 20 (TTBS): 50 mM Tris-HCl pH 7.5, 150 mM NaCl and 0.1% Tween-20.

DNA loading buffer: DNA Gel Loading Dye (6X) (Thermo Scientific), consisting on 10 mM Tris-HCl (pH 7.6), 0.03% bromophenol blue, 0.03% xylene cyanol FF, 60% glycerol and 60 mM EDTA.

Tris buffered saline (TBS): 100 mM Tris and 225 mM NaCl.

Tris-EDTA buffer (TE): 10 mM Tris-HCl and 1 mM EDTA.

Tris base, acetic acid and EDTA buffer (TAE): 40 mM Tris, 20 mM acetic acid and 1mM EDTA.

1.5. Bacterial stocks

The DH5-α *E.coli* bacterial strain competent for transformation was provided by the *Culture Media Preparation Facility* from the *Instituto de Investigaciones Biomédicas "Alberto Sols" (UAM-CSIC).*

1.6. Cell lines

A549: human lung adenocarcinoma epithelial cell line initiated in 1972 by Dr. D.J. Giard through explant culture of lung carcinomatous tissue from a 58-year-old Caucasian male. A549 harbour KEAP1 protein with a Gly to Cys change at amino acid 333 [178] and exhibit hypermethylation of the *KEAP1* promoter [179], leading to constitutive NRF2 activation.

HEK293T: cell line derived from human embryonic kidney cells, generated in 1987 in Dr. Michele P. Calos (Standford University, USA) by stable insertion of the simian virus 40 (SV40) large T antigen in the HEK293 cell line. This allows a very efficient replication of vectors carrying the SV40 region of replication, achieving remarkable expression levels.

HEK293T/17: specific clone (clone 17) from HEK293T cells that was selected for its high transfectability (Rockefeller University, USA), which makes them especially suitable for lentiviral and retroviral production.

Hippocampal/cortical neurons from *Nrf2*-KO and wild type mice: primary hippocampal/cortical neurons from *Nrf2*-KO and their wild-type counterparts were stablished in Dr. Cuadrado Laboratory by Dr. Ana I Rojo and Marta Pajares with the method described in section 2.2.

HT22: immortalized mouse hippocampal neuronal cell line subcloned from the HT4 cell line by Dr. David Schubert (Salk Institute for Biological Research, USA). The parental HT4 cell line was originally immortalized from primary mouse hippocampal neuronal cells with a temperature sensitive SV40 T-antigen.

Immortalized hepatocytes from *Nrf2*-KO and wild-type mice: primary hepatocytes from *Nrf2*-KO and their wild-type counterparts were stablished in Dr. Cuadrado Laboratory by Dr. Patricia Rada and immortalized with the SV40 large T antigen.

Mouse embryo fibroblasts (MEFs) from *Nrf2*-KO and wild-type mice: primary embryo fibroblasts from *Nrf2*-KO and their wild-type counterparts were stablished in Dr. Cuadrado Laboratory by Dr. Isabel Lastres-Becker.

N2A (Neuro-2a): mouse neuroblastoma cells established by R.J. Klebe and F.H. Ruddle from a spontaneous tumor of a strain A albino mouse. This tumor line was obtained from the Jackson Laboratory (USA).

1.7. Animals

Animals were housed under a 12 h light-dark cycle. Food and water were provided *ad libitum* and mice were cared according to protocols approved by the Ethics Committee for Research of the Universidad Autónoma de Madrid following institutional, Spanish and European guidelines (Boletín Oficial del Estado of 18 March 1988; and 86/609/EEC, 2003/65/EC European Council Directives).

C57/BL6J-*Nrf2*$^{-/-}$ (*Nrf2*-KO) mice and their wild type counterparts were kindly provided by Dr. M. Yamamoto (Tohoku University, Sendai, Japan). C57/BL6J-*Nrf2*$^{-/-}$ mice bear a lacZ-neo *cassette* replacing a 1.2 kb long segment from the fifth exon of *Nrf2*. Where indicated, food was removed for 24 h but water was still provided *ad libitum*. Where stated, mice received intraperitoneal injections of vehicle (0.9 % saline buffer) or leupeptin (2 mg/100 g body weight) 16 h and 2 h before sacrifice.

APP(V717I) mice expressing in heterozygosis the human APP695 isoform with the V717I mutation under the control of the neuron-specific elements of the mouse *Thy1* promoter [180], were backcrossed with C57/BL6J-*Nrf2*$^{+/+}$ or C57/BL6J-*Nrf2*$^{-/-}$ mice for over 5 generations. Similarly, TAU(P301L) mice, expressing in homozygosis the longest isoform of human TAU with the P301L mutation (Tau.4R/2N-P301L) under control of the mouse *Thy1* gene promoter, were backcrossed with C57/BL6J-*Nrf2*$^{+/+}$ or C57/BL6J-*Nrf2*$^{-/-}$ mice for over 5 generations. APP-TAU-*Nrf2*$^{+/+}$ (AT-*Nrf2*-WT) and APP-TAU-*Nrf2*$^{-/-}$ (AT-*Nrf2*-KO) mice were obtained by crossing the proper founder mice from above. Genotypic characterization of the AT-*Nrf2*-WT transgenic mice was described previously [181-183]).

1.8. Human material

Frozen post-mortem brain tissues were obtained from five control subjects (age range from 59 to 78 years) and five patients with AD (age range from 73 to 94 years) within a 5 h post-mortem interval, according to the standardized procedures of the Tissue Bank of Fundación CIEN. Information on patient samples is provided in Table 2. Brain samples used for AD analysis belong to patients with a clinical history with no familiar cases of AD. Control subjects had no background of neuropsychiatric disease and relevant brain pathology was excluded by a full neuropathological examination. AD diagnosis was confirmed by HT100 staining on frozen tissue sections from the same cases used in the immunofluorescence studies. All procedures were approved by the Ethics Committee of the Tissue Bank of Fundación CIEN (Madrid, Spain).

Human glioblastomas were derived from brain surgery biopsies in the Hospital Ramón y Cajal (Madrid, Spain) and were kindly supplied by Dr. Marta Izquierdo (Centro de Biología Molecular “Severo Ochoa” - UAM), with the approval of the Ethics Committees.

Patient	Disease	Sex	Age	ApoE
BCPA56	Control	M	75	E3/E3
BCM65	Control	M	78	E3/E3
BCM537	Control	F	74	ND
BCM 98	Control	F	62	ND
BCM121	Control	F	59	ND
BCM64	AD (Braak II)	M	73	E3/E3
BCM67	AD (Braak III)	M	84	E3/E3
BCM74	AD (Braak IV)	F	90	E3/E3
BCPA234	AD (Braak V)	F	94	E3/E3
BCPA399	AD (Braak V)	F	79	ND

Table 2. Information about human samples from control and AD patients used in this study. M, male; F, female; ND, not determined.

2. Methods

2.1. *In silico* analysis of putative AREs in autophagy genes

Putative antioxidant response elements (AREs) in autophagy-related gene promoters were identified in The Encyclopedia of DNA Elements at UCSC (ENCODE) (https://genome.ucsc.edu/encode/) for human genome (Feb. 2009), taking as reference the available chromatin immunoprecipitation (ChIP) information of the ARE-binding factors MAFF, MAFK and BACH1. These sequences were localized in 200-400 pb long DNase-sensitive and H3K27Ac-enriched regions, i.e. most likely regulatory promoter regions. On the other hand, a frequency matrix of the consensus human ARE sequence based on the JASPAR database was converted to a PSSM (Position Specific Scoring Matrix) (see Table 6 in the 'Results' section) by turning the frequencies into scores through the $\log_2$(odd-ratio) (odd ratio: observed frequency/expected frequency). One unit was added to each frequency to avoid log(0). Then, a script was generated with Python 3.4 (Appendix I) to scan the promoter sequences with candidate AREs retrieved from the ENCODE with the PSSM. The max score was calculated by adding the independent scores for each of the 11 bp of the consensus

human ARE sequence with the PSSM. The relative score (score $_{relative}$) was calculated from this max score (score of the sequence $_{max}$) as: score $_{relative}$ = (score of the sequence $_{max}$ − score $_{min\ possible}$)/ (score $_{max\ possible}$ − score $_{min\ possible}$). The min possible score (score $_{min\ possible}$) is calculated as the lowest possible number obtained for a sequence from the PSSM and the max possible score (score $_{max\ possible}$) is the highest possible score that can be obtained. The PSSM and the script were courtesy of Natalia Jiménez-Moreno (present address: University of Bristol, UK). We considered putative ARE sequences those with a score $_{relative}$ higher than 80%, which is a commonly used threshold for the TFBS (computational framework for transcription factor binding site) analysis using PSSM.

2.2. Cell culture

Adenocarcinoma human alveolar A549 cells, mouse embryo fibroblasts (MEFs), mouse hippocampus-derived HT22 cells, neuroblastoma N2A, human embryonic kidney HEK293T and HEK237T/17 cells were grown in DMEM supplemented with 10% FBS and 80 μg/ml gentamicin. HT22 medium was further supplemented with 2 mM glutamine. Immortalized mouse hepatocytes were grown in the same medium supplemented with 2 mM glutamine, 1 mM sodium pyruvate and 5 mM HEPES pH 7.4.

Hippocampal/cortical neurons were obtained from E17-18 mouse embryos. Briefly, embryonic hippocampi were incubated in 0.25% papain (Sigma-Aldrich) plus 1 mg/ml DNAse-I (Roche) at 37 °C for 20 min. After mechanical dissociation and centrifugation (900 g, 5 min) cells were plated in minimum essential medium supplemented with 0.1 mM glutamine, 20% glucose, 5% horse serum, 5% fetal bovine serum and 80 μg/ml gentamicin, and incubated for 24h. After plating, the medium was changed to phenol red-free neurobasal medium supplemented with B27. Neurons were selected with cytosine β-D-arabinofuranoside (Ara-C, Sigma-Aldrich), an anti-mitotic reagent that intercalates into the DNA, inhibits replication and results in DNA fragmentation. Thus, Ara-C removes proliferating cells (glial cells) and allows neuronal selection. Neurons were maintained under these conditions for 10 days in vitro.

Glioblastoma cells obtained from patient explants were maintained in stem cell culture conditions with DMEM:F12 (1:1) supplemented with 2 mM glutamine, 5 mg/ml Albumax I, 6 mg/ml glucose, B27 supplement (without Vitamin A), 15 ng/ml hFGF-2, 20 ng/ml hEGF, 2 μg/ml heparine and 80 μg/ml gentamicin.

All cell cultures were maintained under a controlled atmosphere of 95% relative humidity, 5% CO_2 concentration and 37ºC.

2.3. Transient transfections

Transient transfections in HEK293T were performed with TransFectin™ Lipid Reagent (Bio-Rad) according to the manufacturer's instructions. Transient transfections in MEFs were done with GenJet™ In Vitro DNA Transfection Reagent (SignaGen Laboratories) following the manufacturer's instructions.

2.4. Production of lentiviral stocks and infection

Recombinant lentiviral stocks were produced in HEK293T/17 cells. These cells were plated on 10-cm plates until they reached 85% confluence and co-transfected with 10 μg of transfer vector (the one that encodes the DNA of interest), 6 μg of envelope pMD2.G and 6 μg of packaging plasmid pSPAX2, using *Lipofectamine*® 2000 Reagent (Invitrogen by Life Technologies). After 12 h at 37°C the medium was replaced with fresh DMEM containing 10% FBS and viral particles were harvested 24 h and 48 h post-transfection.

For viral infection, cells were incubated with the lentivirus in the presence of 4 μg/ml polybrene during 24 h and cell extracts were collected 3 and/or 10 days after lentiviral transduction, unless otherwise indicated. Selection of infected cells was done with 1 μg/ml puromycin. In the case of cells originated from glioblastomas, they were first disgregated and plated with OptiMEM supplemented with 10% FBS. 24 h after adhesion, cells were incubated with the lentivirus in the presence of 4 μg/ml polybrene. The next day, cells were again grown in stem cell culture conditions and selected with 1 μg/ml puromycin.

2.5. Chromatin immunoprecipitation assays

HEK293T cells were grown on 10-cm plates until they reached 85% confluence and transfected with an NRF2 expression plasmid that lacks the high affinity binding site for KEAP1 and contains a V5 tag (pcDNA3.1-mNrf2-$^{\Delta ETGE}$-V5/HisB). For chromatin immunoprecipitation (ChIP), a protocol modified from the Upstate protocol was applied.

Gene product	Forward primer (5'-3')	Reverse primer (5'-3')	ARE sequence
HMOX1	CCCTGCTGAGTAATCCTTTCCCGA	ATGTCCCGACTCCAGACTCCA	GTGACTCAGCA
NQO1	TGCACCCAGGGAAGTGTGTTGTAT	CCCTTTTAGCCTTGGCACGAAA	GTGACTCAGCA
***SQSTM1* (1)**	CTCCTGATATGGGGGCTGT	CATTGCTGACCCCTCTCTTC	ATGACTCAGCA
SQSTM1* (2)	CTCTCAGGCGCCTGGGCTGCTGAG	CGGCGGTGGAGAGTGGAAAATGCC	GTGACTCAGCA
***SQSTM1* (3)**	AGGATGCCATGCGCTGTAAGAGG	TGGGCCTGGCCATGACTCAGCAAT	GCGACCTAGCA
***SQSTM1* (4)**	AGCCACTCCCCAGCCCAGCCT	GAGGCCTCCCGGAGGTAAACAAG	GTGAGTCAGCG
CALCOCO2*	ACTTGTCCCTGCAGACCGAGTTTA	CCAAAGTGCTGGGATTACAGGCAT	ATGAGTAAGCC
ULK1	GACCAGCTGGCTTTCGTG	TGGGCTCAGTAAACAGGTCA	ATTAGTCAGCA
ULK2	TGGATAGGAGGTTGGCTCTG	GCAGAGATTGCAGTGAGCTG	GTGACAGAGCA
ATG2B	GATGCTGGCCTTGCAATTTGCTCCA	GTTTTAACCTTACTAATCAGTGAAT	CTGCCTAAGCA
ATG3	GGAGAAGCGGCTTATCCCGC	GTCCTCGCTTTGCTTCACTCGCGC	None
ATG4C	TTAGATCGCTCCTGGAAAGC	TTGGGCATAGAAACGTAACAAA	ATGAAATAGCA
ATG4D	TTCCTGCCCAGAGGTGAGCCATAGG	GGCATGAGCCACCGTTTCCAACC	ATGACAATGCA
ATG5	GCTGAGATGGGGAGTGATGT	CTCCCAAAGTGCTGGGATTA	CTGACCTTGCA
ATG7	GCTTTCTTTGCCTTCCCTCT	GCTAGCTTTCAATGGCCAGA	ATGAGTCAGCA
GABARAPL1	GCTTTTAAAACCCCGTATGC	CTAACCAGTCTCGCCCACAG	GTGACTCAGCA
ATG9B	TGGGAAGCACAGTGTCCATA	CAGGGAGGAGCTGAACTGAG	CTGACTCAGCC
ATG10	AAAAATTCAGCCTGGTGTGG	TCAGCGCTCCTCATGTCATA	CTGACTCAGCA
ATG16L1	CAGCTGGAAGCCATATCACC	TACTGCCCATCAGGAAAACC	ATGATTCAGCA
WIPI2	GCCTACATAGGAGGGCAGGT	CAACGCGGGAAAATAAATTG	ATGACTGAGCA
LAMP1	ATCCGTCTGCCCTTTCTCC	ACCCTGGACCCACGTGAC	GTGACCCGGCC
AMBRA1	GGCATTTTCTCCTCATCAGCA	ACTGATGGGAAGAAGTCAGAGG	TTGACTTAGCT
***LAMP2* (1)**	TATTGCTAGCATTATGTTCTTC	TGGGGGAATGGAACAAGACCCTGTCA	ATGACACTGCA
***LAMP2* (2)**	AGGGAAACCGAAGGATTGAT	TAAATTCAAGGAGGCCGTTT	TTGACTCAGCG
***LAMP2* (3)**	AAACGGCCTCCTTGAATTT	ATGAATTTGGCTAAATGAATTGAC	ATGACAAACCA
ACBT	CACCCAGCACATTTAGCTAGCTGA	TTCAGAGCAACTGCCCTGAAAGCA	None
NQO1*	TCTCAGTTTTTGCCCTTATTTAATC	TAAAAAGTAGAGTGGTTGGAGTGATGAC	None

Table 3. Primers used for chromatin immunoprecipitation (ChIP) analysis indicating the specific ARE amplified in each gene.

Briefly, cells were cross-linked with 1% formaldehyde (Fluka) for 12 min and the reaction was stopped with 125 mM glycine (Bio-Rad). Cells were then washed twice with cold PBS, lysed and sonicated in order to obtain adequate fragment sizes of DNA (200-800

bp). Supernatant was diluted 10-fold with ChIP dilution buffer (0.01% sodium dodecyl sulfate, 1.1% Triton X100, 1.2 mM ethylenediaminetetraacetic acid, 16.7 mM Tris-HCl pH 8.1, 167 mM NaCl, 1 mM phenylmethylsulfonyl fluoride, 1 µg/ml leupeptin) and pre-cleared with Protein G Sepharose (GE Healthcare). Transfected NRF2 was immunoprecipitated with anti-V5 antibody and an anti-IgG antibody was used as a negative control. DNA was eluted and purified, analyzing the presence of previously identified putative AREs by quantitative real-time polymerase chain reaction (qRT-PCR) with specific primers (Table 3). Samples from at least three independent immunoprecipitations were analyzed.

2.6. Cellular and tissue lysis

Cells were washed twice with cold PBS and lysed in the adequate volume of lysis buffer with a cell scraper. Mice were sacrificed by cervical dislocation and organs of interest were anatomically dissected on ice. Tissues were lysed with RIPA buffer and mechanically homogenized with a Potter-Elveihem. Protein quantification in cell and tissue samples was done with the BCA method (Pierce ^{TM} BCA Protein Assay Kit) and protein loading buffer was added. Samples were sonicated, boiled at 95ºC for 5 min and cellular debris was eliminated by centrifugation at 13,000 rpm for 5 minutes.

2.7. Electrophoresis and immunoblotting

Protein electrophoresis was performed as previously described by Laemmli [184]. Proteins were separated in SDS-PAGE and transferred to 0.45 µm pore size Immobilon-P membranes.

For immunoblotting, membranes were hydrated in methanol for 1 min, washed with TTBS buffer for 3 min and blocked with either 4% bovine serum albumin (BSA) or 5% non-fat dry milk in TTBS. Membranes were incubated with the appropriate dilution of the primary antibodies in 0.4% TTBS for 2 h. After washing the membranes three times with TTBS (10 min each), membranes were incubated with 1:10.000 secondary antibodies coupled to HRP in 0.4% TTBS for 1 h. Proteins were detected by enhanced chemiluminescence (GE Healthcare) after washing the membranes three times with TTBS (10 min each wash).

2.8. Messenger RNA analysis by quantitative real time PCR (qRT-PCR)

Total RNA extraction was done with TRIzol according to the manufacturer's instructions. One µg of RNA, quantified with a NanoDrop™ spectrophotometer (Thermo Fisher Scientific), was used to synthesize cDNA in a 20 µl volume with the *High Capacity RNA-to-cDNA* kit (Applied Biosystems). The quantitative real time polymerase chain reaction (qRT-PCR) was done in a volume of 10 µl with the S*ybr Green Master Mix* (Applied Biosystems) and 5 pmol of each specific oligonucleotide (Table 4 and 5). The reaction took place in a *StepOne* thermocycler (Applied Biosystems). After an initial 10 min denaturation at 95°C, 40 cycles with the following conditions were applied: 15 s at 95°C (denaturation), 30 s at 60 °C (annealing) and 30 s at 60 °C (elongation). The melting curve analysis enabled us to assess the specificity of the amplification with each pair of oligonucleotides. The threshold cycle (Ct), inversely related to the amount of amplified DNA, was measured as the cycle at which fluorescence emission exponentially exceeded the background fluorescence. Messenger RNA (mRNA) levels were estimated with the ΔΔCt method, using *Actb*, *Gapdh* and/or *Tbp* house-keeping genes as reference. Samples were analyzed in quatriplicates.

Gene product	Forward primer (5'-3')	Reverse primer (5'-3')
SQSTM1/P62	CTGGGACTGAGAAGGCTCAC	GCAGCTGATGGTTTGGAAAT
CALCOCO2/NDP52	ACCATGGAGGAGACCATCAA	TTCTGGACGGAATTGGAAAG
ULK1	TCATCTTCAGCCACGCTGT	CACGGTGCTGGAACATCTC
ATG2B	AACTCACAAACAGAATGGTTCAAA	AAGGGTACCAGGAAGACACCA
ATG3	CATGCAGGCATGCTGAGGTG	CGTTAACAGCCATTTTGCCACT
ATG4D	CACATCCTCAGGAAAGCCGT	GACCACAGACTTCCACTCGG
ATG5	GGGAAGCAGAACCATACTATTG	AAATGTACTGTGATGTTCCAAGG
ATG7	AGGAGATTCAACCAGAGACC	GCACAAGCCCAAGAGAGG
GABARAPL1	ACCATGGGCCAACTGTATGA	TGGGCTTCCAACCACTCATTT
HMOX1	TGCTCAACATCCAGCTCTTTGA	GCAGAATCTTGCACTTTGTTGC
ACBT	TCCTTCCTGGGCATGGAG	AGGAGGAGCAATGATCTTGATCTT
LAMP2A	GTGCAACAAAGAGCAGACTGT	GGCACAAGGAAGTTGTCGTC
TBP	TGCACAGGAGCCAAGAGTGAA	CACATCACAGCTCCCCACCA

Table 4 . Human primers used for quantitative real time polymerase chain reaction (RT-PCR).

Gene product	Forward primer (5'-3')	Reverse primer (5'-3')
Sqstm1/p62	GGCGCACTACCGCGATGAGGA	TGTTCCCGCCGGCACTCCTT
Calcoco2/NDP52	TGGCAACTTCTCTCAGGTCCTGTT	TCCTTGCGTCGAGGGATGAACTTT
Ulk1	TGCCCTTGATGAGATGTTCC	AGTCTCCTCTCAATGCACAGC
Atg2b	TGATCCCAACTATCGTTCCCG	CGGATCTCCATTCTCTTGCTTC
Atg3	CCATTGAAAACCATCCTCATCTC	GCCTTCTGCAACTGTCTCAATAATT
Atg4d	ACGTCAAGTATGGTTGGGCA	ATGTCACCCTCTCCCTCGAA
Atg5	ATATCAGACCACGACGGAGC	TTGGCTCTATCCCGTGAATC
Atg7	GGCCTTTGAGGAATTTTTTGG	ACGTCTCTAGCTCCCTGCATG
Gabarapl1	GACCTCACTGTTGGCCAGTTC	GTGGGAGGGATGGTGTTGTT
Lamp2a	AGGTGCTTTCTGTGTCTAGAGCGT	AGAATAAGTACTCCTCCCAGAGCTGC
Lamp2b	ATGTGCTGCTGACTCTGACCTCAA	TGGAAGCACGAGACTGGCTTGATT
Lamp2c	GGTGCTGGTCTTTCAGGCTTGATT	ACCACCCAATCTAAGAGCAGGACT
Hmox1	CACAGATGGCGTCACTTCGTC	GTGAGGACCCACTGGAGGAG
Aox1	CTTTTGACCAAAGCATCAGTCTC	CCCTTTCTCCCAGTCTATATTCGA
Nqo1	GGTAGCGGCTCCATGTACTC	CATCCTTCCAGGATCTGCAT
Nrf2	CCCGAAGCACGCTGAAGGCA	CCAGGCGGTGGGTCTCCGTA
Cd11b	CCTTGTTCTCTTTGATGCAG	GTGATGACAACTAGGATCTT
Gfap	TCCTGGAACAGCAAAACAAG	CAGCCTCAGGTTGGTTTCAT
Il6	CCTACCCCAATTTCCAATGCT	TATTTTCTGACCACAGTGAGGAATG
Nos2	CCTCCTTTGCCTCTCACTCTTC	AGTATTAGAGCGGTGGCATGGT
Adam10	CGCACAACTCTGGCTGAAAG	CCGGAGAAGTCTGTAGTCTG
Adam17	CAGAAGAAGTGCCAGCAGGCTA	GTTGTCAGTGTCAACGCATGC
Bace1	GGGCTGGCCTATGCTGAGATTGC	GCACCACAAAGCTGCAGGGAGAA
Psen1	TGGCCACCATCAAATCAG	TCATGATGGCCGCATTCAG
Actb	TCCTTCCTGGGCATGGAG	AGGAGGAGCAATGATCTTGATCTT
Tbp	TGCACAGGAGCCAAGAGTGAA	CACATCACAGCTCCCCACCA
Gapdh	CGACTTCAACAGCAACTCCCACTCTTCC	TGGGTGGTCCAGGGTTTCTTACTCCTT

Table 5 .Mouse primers used for quantitative real time polymerase chain reaction (RT-PCR).

2.9. Measurement of luciferase activity

Nrf2-KO MEFs were seeded in 24-well (75,000 cells per well) plates and transiently transfected with GenJET according to the manufacturer's instructions. 48 h after transfection, cells were lysed in 100 µl lysis buffer (Promega) and 40 µl of this lysate was employed for the luciferase assay, performed according to the manufacturer's instructions. Luciferase expression was quantified as luminol oxidation with a *GloMax 96 microplate luminometer with dual injectors (*Promega). Each sample was measured in triplicate and normalized to Renilla levels.

2.10. Morris water maze

After a 1-day habituation trial (day 0), in which preferences between quadrants in the different experimental groups were ruled out, the animals were placed in the swimming pool during 4 trials/day, 60 s each trial plus 20 s in the platform for 5 consecutive days, so that they learned to find the hidden platform. If an animal failed to reach the platform, it was placed on it by the experimenter. Subsequently, the animals were subjected to two trials on the 7th day, the first without the platform to assess possible differences in swimming speed and preference for the platform quadrant. And in the second, a cued version protocol using a visible platform was conducted to determine sensorimotor and motivational status of the animals. The animal behavior was recorded through an automated tracking system (Smart video tracking system, version 2.0.14, Panlab; Harvard Apparatus).

2.11. Electrophysiological recordings

Electrophysiological recordings were obtained from six urethane-anaesthetized (1.6g/kg i.p.) adult mice per group as described in [185]. Briefly, field potentials were recorded through tungsten macroelectrodes (1 MΩ; World Precision Instruments) stereotaxically implanted in the dentate gyrus (A:-2,3; L: 2; H: 3.5 mm from Bregma according to the Paxinos and Watson Atlas). Twisted bipolar electrodes for electrical stimulation were placed at the perforant path (A: -2.5; L: 0.5; H: 3.5 mm from Bregma). Baseline recordings were taken with test stimuli (10-50 µA, 0.3 ms, 0.5 Hz) for 15 min before tetanic stimulation consisting of three pulse trains of 10-50 µA, lasting each pulse 0.3 ms and at 50 Hz. Trains lasted 500 ms and the inter-train interval was 2 s. Recording was maintained for 30 min after

tetanic stimulation. Field potentials were 0.1 Hz–1 kHz band-pass filtered, amplified (P15 Amplifier, Grass Co., USA), and digitalized at 10 kHz (CED 1401; Cambridge Electronic Design). Signal analysis was carried out with Spike 2 software (Cambridge Electronic Design, Cambridge, UK). Field potential segments of 5 min were analyzed to obtain the response average. The mean average response during the 15 min period before the tetanic stimulation was considered as 100%. Recordings were accepted for analysis when baseline variability was less than 10%.

2.12. Animal perfusion and brain sectioning with the microtome

Animals were anesthetized with 8 mg/kg ketamine and 1.2 mg/kg xylazine and perfused through the left heart ventricle with PBS. Brains were sectioned along the sagittal axis. Left hemispheres were rapidly dissected and frozen for biochemical analysis. Right hemispheres were post-fixed in 4% paraformaldehyde during 16 h and cryoprotected by soaking in 30% sucrose solution in PB until they sank. A frozen-tissue-sectioning manual microtome (Hyrax) was used to obtain 30 µm thick sagittal or coronal slices, which were collected in PB for the immediate use or preserved in anti-freeze solution (33.3 % glycerol, 33.3 % ethylene glycol, 20 mM PB).

2.13. Immunofluorescence

Cells were seeded on sterile coverslips in 24-well plates (75,000 cells per well), cultured for 16 h and treated as indicated. Cells were washed with cold PBS and fixed in 4% paraformaldehyde for 15 min at room temperature or with cold methanol for 2 min at room temperature. After three 5-min washes with PBS, cells were incubated with blocking solution (0.2% powdered milk, 2% normal goat serum, 0.1 M glycine, 1% bovine serum albumin and 0.01% Triton X-100) for 30 minutes at room temperature. After briefly washing twice with PBS, slides were incubated with the indicated primary antibodies (Table 1) for 90 minutes at room temperature in a humidified chamber. Then cells were washed three times with PBS and incubated with secondary antibodies for 45 minutes under the same conditions. To visualize the nuclei, cells were stained with DAPI (4,6-diamidino-2-phenylindole). After washing with PBS and sterile water, coverslips were mounted on slides with a drop of ProLong.

Mouse brain free-floating 30 µm-thick sections were washed three times with PBS for 5 min. When necessary, antigen retrieval was performed by incubation with 10 mM citrate

buffer pH 6 at 90 ºC for 20 min. Antigen retrieval for APP and Aβ detection was performed by incubating the sections in formic acid for 5 min. Sections were then incubated with blocking solution (5% normal goat serum and 0.3 % Triton X-100 in PBS). Sections were incubated with primary antibodies diluted in 0.5% normal goat serum and 0.3 % Triton X-100 in PBS (Table 1) for 24 h at 4ºC. After washing twice with PBS (5 min each), sections were incubated with secondary antibodies coupled to Alexa fluorophores diluted in 0.5% normal goat serum and 0.3 % Triton X-100 in PBS for 1 h at room temperature. To visualize the nuclei, cells were stained with DAPI and the surplus antibody was removed with two additional 5 min-washes with PBS. Brain sections were mounted on gelatin-coated slides with a drop of ProLong.

Fluorescence images were captured using appropriate filters in a Leica SP5 confocal microscope (*Confocal Microscopy Facility* from the Facultad de Medicina, UAM).

2.14. Immunohistochemistry

Free-floating sections were incubated with 10% methanol and 3% H_2O_2 in TBS for 30 min at room temperature to inactivate endogenous peroxidase. Antigen retrieval was performed with 10 mM citrate buffer pH 6 for 20 min at 90ºC (or formic acid for 5 min at room temperature for APP/Aβ). Slices were incubated with blocking solution (10% normal goat serum and 0.4% Triton X-100 in TBS) for 2 h. Incubation with the appropriate dilutions of the primary antibodies was done for 24 h at room temperature in an humidified chamber Detection was enhanced with biotinylated secondary antibodies and the avidin/biotin system with the Vectastain^R ABC Kit (Vector Laboratories) according to manufacturer's instructions. Sections were then developed with 0.003% H_2O_2, 0.05% 3-3'diaminobenzidine tetrahydrochloride (DAB) in TB pH 8 until the appearance of the desired intensity. Staining development was stopped with consecutive washes with TBS in all sections at the same time. Sections were mounted on gelatin-coated slides, de-hydrated by consecutive immersions in 70%, 96%, 100% ethanol and xylol. Eventually, sliced were covered with DePeX (Serva) and a slide cover.

Four µm-thick paraffin fixed consecutive human brain sections were incubated at 65ºC in a heater overnight. The following day, slides were hydrated by consecutive incubations in xylol, 100%, 96%, 70% ethanol and sterile water. Endogenous peroxidase was inhibited with 3% H_2O_2 and antigen retrieval was performed with 10 mM citrate buffer pH 6 for 3 min in the microwave (or formic acid for 15 min at room temperature for APP/Aβ). Sections were

immunostained with the Histostain-SP Kits Invitrogen LAB-SA Detection System (Invitrogen) following the manufacturer's instructions**.**

2.15. Determination of reduced and oxidized glutathione, protein carbonyls and lipid peroxidation

Reduced glutathione (GSH) levels were determined with the following fluorometric protocol. Mouse brains were homogenized in 1 ml of EDTA-phosphate pH 8.0 buffer supplemented with 300 µl HPO_3 (25 %). Proteins were eliminated by centrifugation at 3,000 g for 15 min. We next separated 500 µl of the supernatant and added 500 µl of EDTA-phosphate buffer supplemented with 100 µl o-phthalaldehyde (OPA). Samples were dark-incubated for 15 min at room temperature. Fluorescence was detected in a Synergy HT (Bio-Tek) with excitation at 350 nm and emission at 420 nm. Values were interpolated from a standard GSH curve, corrected upon total protein content and expressed as µg of GSH per mg of protein. Oxidized glutathione (GSSG) was determined in the remaining 500 µl of supernatant with 100 µl dithiothreitol (DTT) (25 mM) to reduce disulfur bonds and obtain total GSH content. Samples were incubated for 30 min at 4ºC and centrifuged at 5,000 g for 10 min. Supernatants were then used to measure GSH as described above and GSSG concentration was obtained by substracting GSH values to total GSH values. Values were expressed as µg of GSH per mg of protein.

To determine protein carbonyl quantity, mouse brains were homogenized in EDTA-phosphate buffer, incubated with streptomycin sulfate for 1 h and centrifuged at 6,000 g in order to eliminate nucleic acids. Supernatants were then treated with 2,4-dinitrophenylhydrazine (DNPH) (10 mM) in phosphate-HCl buffer (2N) and incubated under dark and shaking-conditions for 1 h at room temperature. Afterwards, proteins were precipitated with 20 % trichloroacetic acid (TCA) and centrifuged at 3,000 g for 10 min. The pellet was resuspended in guanidine hydrochloride (1M). Carbonyl content was estimated as the generation of hydrazones after the reaction of DNPH with protein aldehydes, which absorb at 370 nm. Protein carbonylation content was expressed as nm of carbonyl per mg of protein (molar extinction coefficient = 22.000 M^{-1} cm^{-1}).

Lipid peroxidation can be determined as the generation of malondialdehyde (MDA). 200 µL of mouse brain homogenates were mixed with 300 µl of TBA solution (0.375 g thiobarbituric acid, 7.5 g trichloroacetic acid, 2.5 ml HCl) and incubated for 30 min at 100ºC. Samples were kept for 5 min on ice and then centrifuged at 3,000 g for 15 min. The presence

of peroxidized lipids results in the appearance of a pink pigment that can be measured at 490 nm. Values in our samples were interpolated from a tetramethoxypropane (TMPO) standard curve and presented as nmol of MDA per mg of protein.

2.16. Aβ determination by ELISA

Aβ measurements were performed with two ELISA kits, one for each fragment (Aβ1-40 and Aβ1-42) (Novex®, Thermo Fisher Scientific) following the manufacturer's instructions. Samples were sonicated (5 s) in 10 volumes of protein lysis buffer (20 mM (4-(2-hydroxyethyl)-1-piperazineethanesulfonic acid pH 7.9, 100 mM NaCl, 1 mM ethylene glycol tetraacetic acid, 1 mM ethylenediaminetetraacetic acid, 1% Triton-X100, 5 mM dithiothreitol, 2.5 mM sodium pyrophosphate, 1 mM sodium orthovanadate, and complete protease inhibitor cocktail). The lysate was centrifuged (18,000 g for 10 min at 4°C). The supernatant was considered soluble and the pellets were further extracted in formic acid by sonication, and centrifuged. Results were expressed as pg/mg of protein measured by the BCA method, using BSA as standard.

2.17. Aβ oligomers detection

Hippocampal samples were fractionated by a four step extraction method previously described [186]. Briefly, mouse hippocampi were lysed in NP-40 buffer (50 mM Tris–HCl, pH 7.6, 0.01% NP-40, 150 mM NaCl, 2 mM EDTA, 0.1% SDS). After centrifugation, the supernatant was sequentially centrifuged allowing the recovery of the extracellular enriched fraction and the original pellet was resuspended in TNT-lysis buffer (50 mM Tris–HCl, pH 7.4, 150 mM NaCl, 0.1% Triton X-100). After centrifugation, the supernatant was centrifuged different times to collect the intracellular enriched fraction, whereas the pellet was lysed with RIPA buffer to extract membrane-bound proteins. After centrifugation, the supernatant will correspond to membrane-bound proteins and the pellet is further processed with 70% formic acid. After elimination of endogenous immunoglobulins with protein G-sepharose beads, one hundred micrograms of protein per sample was electrophoresed on 10-20% SDS-polyacrylamide Tristricine gels (Bio-Rad). Proteins were transferred to PVDF and membranes were boiled in PBS for 5 min after immunoblotting.

2.18. TAU extraction

Mouse brain tissue was homogenized in 0.2 ml of ice-cold buffer (0.1 M 3-(N-morpholino)propanesulfonic acid, pH 7.0, 1 mM ethylenediaminetetraacetic acid, 0.5 mM $MgSO_4$, 1 M sucrose containing 1 mM NaF, 1 mM Na_3VO_4, 1 mM phenylmethylsulfonyl fluoride, 10 μg/ml aprotinin and 1μg/ml leupeptin). The homogenates were cleared by centrifugation at 50,000 g for 20 min at 4°C, and the supernatants were collected as soluble fractions. To prepare the sarkosyl-insoluble fractions, pellets were resuspended in lysis buffer (0.1 M 3-(N-morpholino)propanesulfonic acid, pH 7.0, 10% sucrose, 2 mM (ethylene glycol tetraacetic acid, 0.5 mM $MgSO_4$, 500 mM NaCl, 1 mM $MgCl_2$, 10 mM NaH_2PO_4, 20 mM NaF) containing 1% N-lauroylsarcosine (sarkosyl) (Sigma-Aldrich) with protease inhibitors, vortexed for 1 min at room temperature, incubated at 4°C for 16 h and then centrifuged at 200,000 g for 30 min at room temperature. The supernatants were collected as sarkosyl-soluble fractions, while the pellets were resuspended in sodium dodecyl sulfate protein loading buffer and incubated at 95°C for 5 min (sarkosyl-insoluble fractions).

2.19. NADP/NADPH measurement

NADP and NADPH levels were measured with the NADP/NADPH Assay Kit (Abcam) following the manufacturer's instructions.

2.20. ROS measurement with dihydroethidium

The probe dihydroethidium (DHE), also called hydroethidine, is a cell-permeable fluorescent dye used as a redox indicator. It exhibits a weak blue-fluorescence in the cytosol but it is highly sensitive to reactive oxygen species (ROS), especially superoxide, which oxidizes it to ethidine, exhibiting a bright red fluorescence and intercalating within the cellular DNA. In our experiments, cells were stained with 5 μM DHE for 1 h at 37ºC and then visualized in a Leica DMIL fluorescence microscope (*Confocal Microscopy Facility* from the Facultad de Medicina, UAM). The probe was excited at 488 nm and emitted between 557 nm and 740 nm.

2.21. Lysosomal isolation

For *in vivo* analysis, lysosomal enriched fractions or CMA active lysosomes from *Nfe2l2*-WT and *Nfe2l2*-KO mouse livers were obtained as previously described [187]. Briefly, livers were mechanically homogenized in 0.25M sucrose with a Potter-Elvehjem. Samples were then filtered through double gauze and centrifuged at 6,800 g. The supernatant was centrifuged at 17,000 g and the pellet was resuspended with a 'cold finger' (dry glass test tube filled with ice). This step was repeated twice to wash the lysosomal enriched fraction. Lysosomes active for CMA were isolated by further centrifugation of the lysosomal enriched fraction (light mitochondria and lysosomes) in a discontinuous metrizamide density gradient. The fraction of broken lysosomes at the moment of isolation was measured with the β-hexosaminidase latency assay, as this enzyme is released when the lysosomal membrane is disrupted [188].

In some experiments, a crude lysosomal fraction was prepared from hepatocytes derived from wild type and *Nfe2l2*-KO mice using the *Lysosome Isolation Kit* (BioVision) according to the manufacturer's instructions.

2.22. Measurement of chaperone mediated autophagy in intact cells

To measure CMA activity in intact cells the photoswitchable KFERQ-PS-Dendra2 reporter was transduced into cells using lentiviral delivery [189]. As represented in Fig. 8, cells were first photoactivated with a 405 nm light emitting diode (LED: Norlux) for 4 min with a 3.5 mA (constant current) intensity. After 16 h, cells were fixed with 4% PFA and slides prepared using mounting medium containing DAPI to highlight the cell nucleus. CMA activation was detected as changes in the fluorescence pattern from diffuse/cytosolic to punctate/lysosomal and quantified as the average number of fluorescent puncta per cell or as the cellular area positive for KFERQ-Dendra puncta. All images were acquired with an Axiovert 200 fluorescence microscope (Albert Einstein College of Medicine, NY, USA) with a 100X objective and 1.4 numerical aperture, mounted with an ApoTome.2 slider. Where indicated, high content microscopy was used instead to better determine dose-dependence effects in a larger number of cells. Briefly, cells were plated in glass-bottom 96-well plates, treated for the indicated times and after fixation images were acquired using a high-content microscope (Operetta, Perkin Elmer, Albert Einstein College of Medicine, NY, USA).

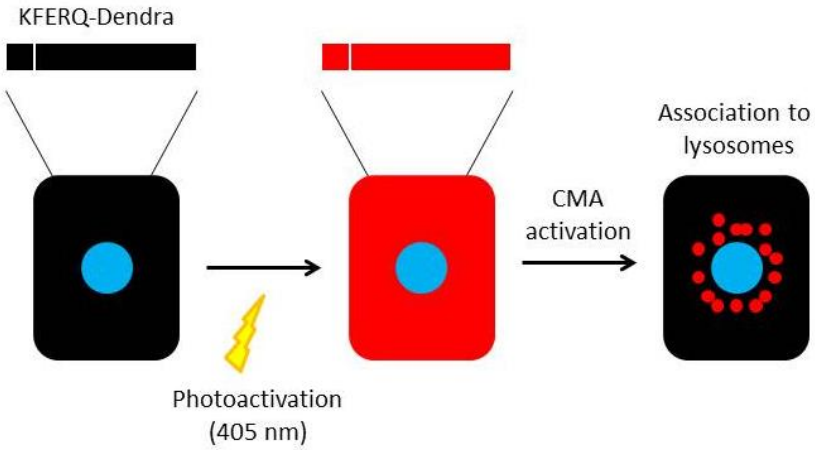

Figure 8. Scheme showing how the KFERQ-PS-Dendra2 reporter allows monitoring CMA activity in cultured cells. Photoactivation allows tracking the already existing protein over the newly synthesized. Because the reporter contains a KFERQ motif, it is delivered to lysosomes upon CMA activation, displaying a characteristic punctate pattern.

2.23. Measurement of chaperone mediated autophagy *in vitro*

CMA activity *in vitro* was measured using isolated intact lysosomes incubated with purified recombinant proteins and subjected to immunoblot [187]. Binding was calculated as the amount of substrate protein bound to the lysosomal membrane in the absence of protease inhibitors and uptake by subtracting the amount of protein associated with lysosomes in the presence (protein bound to the lysosomal membrane and taken up by lysosomes) and absence (protein bound to the lysosomal membrane) of protease inhibitors (Fig. 9A).

Proteolytic activity was determined by incubating lysosomes with a cocktail of long-lived radiolabeled proteins (^{3}H-pool) previously demonstrated to be enriched in CMA substrates [187, 190] in the presence of 0.1% Triton-X100 to disrupt the lysosomal membrane. Samples were incubated in 20mM MOPS, 1mM DTT, 5.4 µM cysteine pH 7.3, and 0.25 M sucrose for 20 min at 37 º C. At the end of the incubation, 10% TCA was added to all the samples and they were subjected to filtration through 0.2□m filter. Proteolysis was calculated as the percentage of acid precipitable radioactivity (protein) at the begging of the incubation that became acid soluble (amino acids) at the end of the incubation (Fig. 9B).

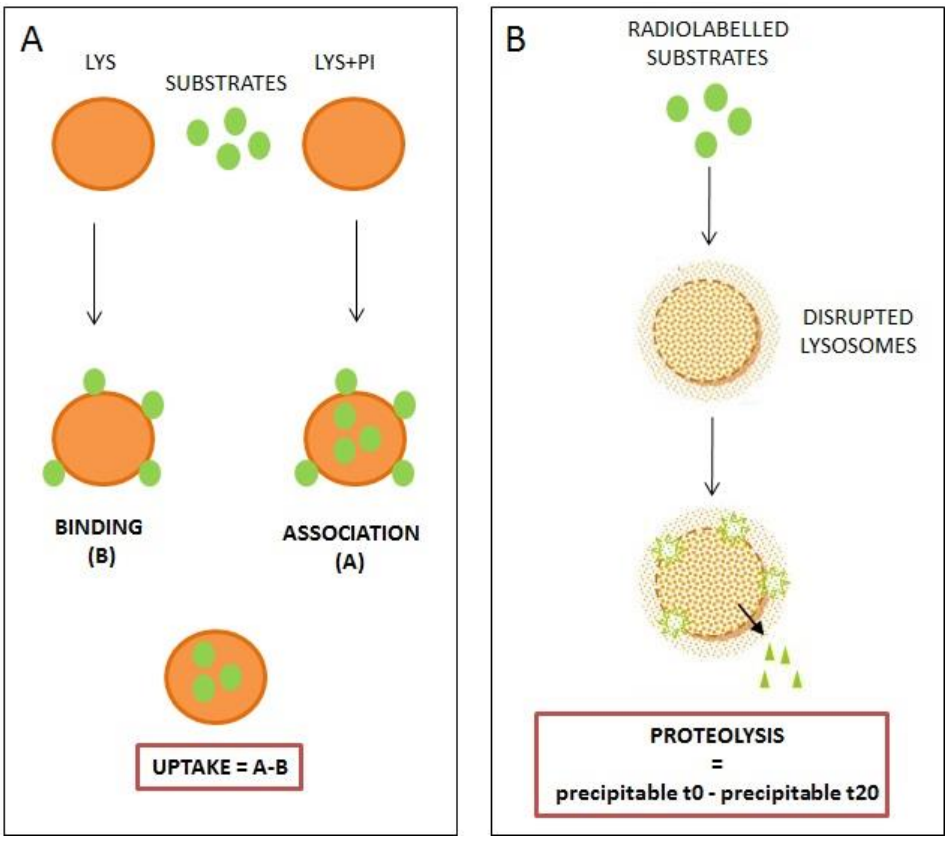

Figure 9. Scheme showing the experimental design for the uptake assays (A) and proteolysis measurement (B). A, Incubation of CMA substrates with intact lysosomes treated or not with protease inhibitors (PI) allows determination of the amount of substrate bound to the lysosomal membrane (without PI) or associated with lysosomes both in the membrane and the lumen (+PI). Total uptake can be calculated by subtracting the amount of "bound" substrate from the total amount of substrate associated with the protease-inhibited lysosomes. B, Proteolysis was calculated after incubating a pool of radiolabeled substrates with broken lysosomes as the percentage of acid precipitable radioactivity (protein) at the begging of the incubation that became acid soluble (amino acids) at the end of the incubation. Figure modified from Patel *et al*, 2015.

2.24. Image analysis

Different band intensities corresponding to immunoblot detection of protein samples were quantified using ImageJ software (NIH). Fluorescence intensity and M1 and M2 colocalization coefficients were measured by Mander's analysis using the ImageJ JACoP plugging. The number of puncta per cell was analyzed with the 'Analyze particles' plugin of ImageJ after thresholding in non-saturated images. In the case of high content microscopy, images of 9 different fields per well were captured, resulting in an average of 2,500-3,000 cells per condition. Nuclei and puncta were identified using the manufacturer's software. The number of particles/puncta per cell was quantified using the `particle identifier' function in the cytosolic region after thresholding in non-saturated images. DHE fluorescence intensity was quantified with ImageJ and is presented as the corrected total cell fluorescence (CTCF;

CTCF = integrated density - (area of selected cell x mean fluorescence of background readings)). Perinuclear LAMP2A fluorescence was measured with the 'Radial profile angle' plugin of ImageJ after properly calibrating the image. A circular mask with a radius of 100 pixels (25 µm, approximately) was used to analyze fluorescence intensity per cell. For each cell, the algorithm measured the mean signal intensity in a series of concentric circles drawn along the established radius, starting from the nucleus and towards the cell periphery. Quantifications were performed in 50-75 cells per condition in three independent experiments.

2.25. Data mining of gene expression in cancer and statistical analysis

The expression levels of *NFE2L2* and *LAMP2* genes in tumors determined by RNAseq compiled at The Cancer Genome Atlas (TCGA) was downloaded with the Xena Browser database (https://xenabrowser.net/). We then calculated the Pearson correlation coefficient (R). The statistical significance of the R was calculated as a function of the t distribution. Kaplan-Meier curves and logrank test statistical analysis were also obtained from Xena Browser database.

For other analysis, unless otherwise indicated, all experiments were performed at least three times and all data presented in the graphs are the mean of at least three independent samples ± standard error of the mean (SEM). Student's t-test was used to assess differences between groups with Graph Pad Prism 5.0. and $p<0.05$ was considered significant.

Results

I. The transcription factor NRF2 is a regulator of macroautophagy gene expression

1. Identification of putative AREs in macroautophagy genes.

We first performed a bioinformatics analysis in search for putative AREs in the promoter region of macroautophagy-related genes. For this purpose, we searched the Encyclopedia of DNA Elements at UCSC (ENCODE) of the human genome (Feb. 2009) (https://genome.ucsc.edu/encode/). This database gathers extensive information about the human genome, including experimental data from chromatin immunoprecipitation (ChIP) studies of several transcription factors. Although NRF2 is not included, we analyzed the presence of binding sequences for three other ARE-binding factors MAFF, MAFK and BACH1, for which information is available. We found evidence of MAFF, MAFK or BACH1 binding in many genes involved directly or indirectly in autophagy. These sequences were usually located in DNAse sensitive regions (indicative of open chromatin conformation) [191, 192] and enriched in H3K27Ac (acetylation in the 27th Lys of histone H3, which correlates with active transcription) [193]. Then, we developed a position specific scoring matrix (PSSM), based on the nucleotide frequencies from the human consensus ARE of the JASPAR database (Table 6).

In order to scan the putative AREs retrieved from the ENCODE with the PSSM, a Python 3.4-script was generated (Appendix I) that provides a relative score for each sequence analyzed. The *relative score* represents the probability of a certain sequence of being a real ARE. As summarized in Table 7, this bioinformatics approach enabled the detection of 30 putative AREs with a relative score over 80% (a commonly used threshold for TFBS -computational framework for transcription factor binding site- analysis using PSSM) in 17 macroautophagy genes. As internal controls, the algorithm also retrieved the already known AREs in the NRF2 *bona fide* target genes *NQO1* and *HMOX1*. AREs in the autophagy genes *SQSTM1* [67] or *CALCOCO2* [68], coding for p62 and NDP52, respectively, had been previously described. In addition to these sequences, our analysis detected new potential AREs in these and in other macroautophagy-related genes.

2. Validation of putative AREs by ChIP analysis.

The newly identified ARE sequences were subsequently validated by ChIP. Because of the lack of adequate antibodies to immunoprecipitate endogenous NRF2 efficiently, we used HEK293T cells transfected with an expression vector for V5-tagged NRF2. Moreover, this construct lacked the KEAP1 regulatory domain ETGE (NRF2-$^{\Delta EGTE}$-V5), facilitating

	1	2	3	4	5	6	7	8	9	10	11
A	1.13750	–2.3219	–2.3219	2.07038	–2.3219	0.48542	0.26303	1.76553	–2.3219	–2.3219	1.67807
C	–1.3219	–2.3219	–2.3219	–2.3219	1.84799	–0.7369	1.13750	–2.3219	–2.3219	2.07038	–0.7369
G	1.00000	–2.32192	2.00000	–2.3219	–1.3219	–1.3219	–1.3219	–0.7369	2.07038	–2.3219	–0.7369
T	–2.3219	2.07038	–1.3219	–2.3219	–0.7369	1.26303	0.00000	–0.7369	–2.3219	–2.3219	–1.3219

Table 6. Position specific scoring matrix (PSSM). A score is given for each nucleotide in each position based on the nucleotide frequencies matrix from the human consensus ARE of the JASPAR database (depicted below the table).

NRF2 stabilization, translocation to the nucleus and binding to its target genes. Thus, ChIPs were performed with anti-V5 antibody and also with anti-IgG as a negative control. Immunoprecipitated DNA was analyzed by quantitative real time PCR (qRT-PCR) with specific primers surrounding the putative AREs.

Among the 30 putative AREs detected in macroautophagy genes, we found consistent enrichment of 11 ARE regions in V5- over IgG-immunoprecipitated chromatin, indicating that NRF2 binds these promoter regions (Fig. 10A and 10B). Our study also detected enrichment of the two positive controls from the *bona fide* NRF2 targets *NQO1* and *HMOX1*. No enrichment was detected with specific primers for *ACTB*, for an upstream region of *NQO1* that does not contain AREs [194] or for *ATG3*, in which MAFF, MAFK and/or BACH1 binding sequences yielded low *relative scores*. In the *SQSTM1* gene, we identified a previously reported ARE [67] plus three more (Fig. 10B).

3. Pharmacological activation of NRF2 with sulforaphane induces macroautophagy gene expression in human and murine cells.

To examine the potential regulation of the selected macroautophagy genes by NRF2, we next analyzed its expression levels upon NRF2 pharmacological activation. We treated human HEK293T cells with 15 μM of the NRF2 activator sulforaphane (SFN) for 12 h. SFN makes adducts with, at least, Cys-151 of KEAP1, preventing NRF2 proteasomal degradation and allowing newly synthesized protein to accumulate, translocate to the nucleus and exert its transcriptional function [51]. As observed in Fig. 11A, the transcript levels of the selected macroautophagy genes were analyzed by qRT-PCR, demonstrating increased expression of human *SQSTM1*, *CALCOCO2*, *ULK1*, *ATG2B*, *ATG4D*, *ATG5* and *GABARAPL1* upon SFN

Gene		Localization in the human genome	Max Score	Relative score	ARE putative binding sequence
SQSTM1	**(1)**	chr5:179247562-179247551	19.11	1.0	A**TGA**CTCA**GC**A
	(2)	chr5:179246594-179246583	18.97	0.997	G**TGA**CTCA**GC**A*
	(3)	chr5:179247479-179247490	11.44	0.816	GC**GA**CCTA**GC**A
	(4)	chr5:179246116-179246105	13.39	0.863	G**TGA**GTCA**GC**G
CALCOCO2	**(1)**	chr17:46906385-46906374	12.65	0.845	A**TGA**GTAA**GC**C*
	(2)	chr17:46906430-46906441	12.34	0.838	G**TGA**GGAA**GC**A
ULK1		chr12:132381043-132381032	12.62	0.844	ATT**A**GTCA**GC**A
ULK2		chr17:19783789-19783800	15.74	0.919	G**TGA**CAGA**GC**A
ATG2B		chr14:96849918 -96849929	11.38	0.815	C**TG**CCTAA**GC**A
ATG4C		chr1:63212369-63212380	13.03	0.854	A**TGA**AATA**GC**A
ATG4D	**(1)**	chr19:10652326-10652315	14.96	0.9	A**TGA**CAAT**GC**A
	(2)	chr19:10655902-10655891	10.94	0.804	G**TGA**CTTT**G**AA
ATG5		chr6:106873861-106873872	11.01	0.806	C**TGA**CCTT**GC**A
ATG7	**(1)**	chr3:11347170-11347159	15.94	0.924	A**TGA**GTCA**GC**A
	(2)	chr3:11320731-11320720	13.65	0.869	C**TGA**CTCA**GC**T
	(3)	chr3:11347216-11347227	11.08	0.807	AG**GA**CTTG**GC**A
	(4)	chr3:11320599-11320610	11.07	0.807	A**TGA**TTGA**GC**T
MAP1LC3B2	**(1)**	chr6:41681230-41681219	13.39	0.863	G**TGA**GTCA**GC**G
	(2)	chr6:41680999-41681010	11.55	0.818	A**TGA**GTCAC**C**A
	(3)	chr6:41706984-41706973	14.65	0.893	G**T**C**A**CTCA**GC**A
GABARAPL1	**(1)**	chr12:10364974-10364963	14.58	0.891	G**TGA**CTCA**G**GA
	(2)	chr12:10366072-10366083	18.97	0.997	G**TGA**CTCA**GC**A
ATG9B		chr7:150723213-150723224	14.24	0.883	C**TGA**CTCA**GC**C
ATG10		chr5:81278192-81278181	16.65	0.941	C**TGA**CTCA**GC**A
ATG16L1	**(1)**	chr2:234134609-234134598	16.53	0.938	A**TGA**TTCA**GC**A
	(2)	chr2:234134578-234134589	13.56	0.867	A**TGA**CCTA**GC**C
WIPI2		chr7:5239766-5239755	16.65	0.941	A**TGA**CTGA**GC**A
LAMP1		chr13:113951364-113951353	12.06	0.831	G**TGA**CCCG**GC**C
AMBRA1	**(1)**	chr11:46576251-46576240	11.51	0.818	T**TGA**CTTA**GC**T
	(2)	chr11:46572300-46572311	10.84	0.802	A**TGA**CTAAT**C**T
NQO1		chr16:69760919-69760908	18.97	0.997	G**TGA**CTCA**GC**A*
HMOX1	**(1)**	chr22:35768205-35768216	12.3	0.837	A**TG**CCTCA**GC**C
	(2)	chr22:35768021-35768010	18.97	0.997	G**TGA**CTCA**GC**A*
	(3)	chr22:35768127-35768116	18.97	0.997	G**TGA**CTCA**GC**A*
	(4)	chr22:35747111-35747100	13.24	0.859	GTTACTCA**GC**C

Table 7. Putative Antioxidant Response Elements (AREs) in the promoter regions of autophagy genes with a *relative score* higher than 80%. The table also shows the *max score* and the localization in the human genome. Asterisks denote AREs that have been described previously and were retrieved with our script as positive controls.

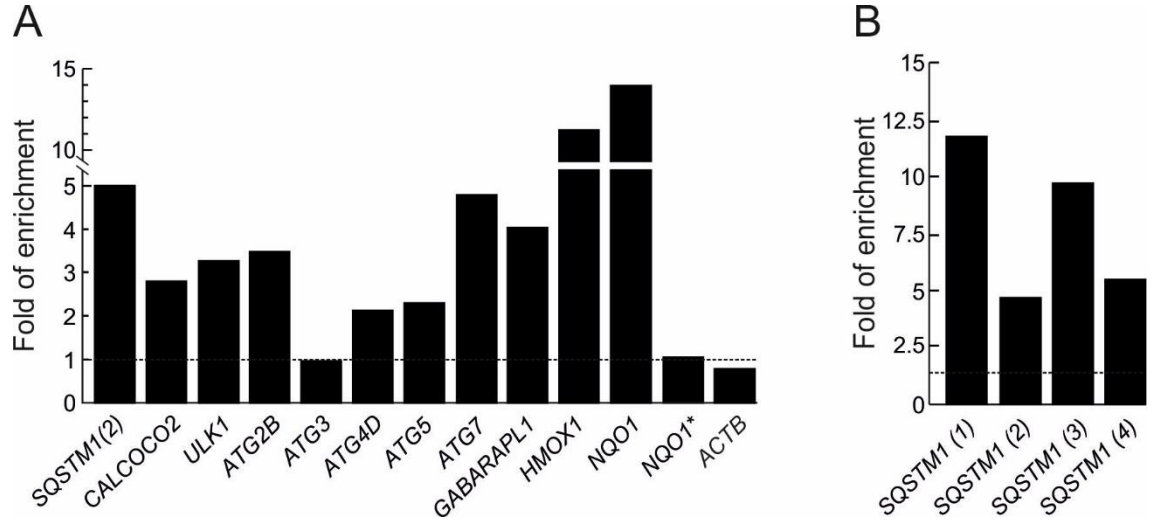

Figure 10. Validation of NRF2 binding to putative AREs in autophagy genes. A, HEK293T cells were transfected with an expression vector for NRF2-$^{\Delta ETGE}$-V5. ChIP analysis was performed with anti-IgG or anti-V5 antibodies and the potential AREs with the highest score were analyzed by qRT-PCR. *ATG3*, *ACTB* and an upstream region of *NQO1* that does not contain any ARE (NQO1*) were analyzed as negative controls. Previously described AREs in *HMOX1*, *NQO1*, *SQSTM1(2)* and *CALCOCO2* were analyzed as positive controls. B, Same ChIP analysis of putative AREs in the promoter region of *SQSTM1*. The figures show representative data normalized as the fold of enrichment with the anti-V5 antibody vs. the IgG antibody (dashed line). These experiments were repeated three times with similar results. Numbers in brackets indicate the AREs from Table 7 specifically amplified.

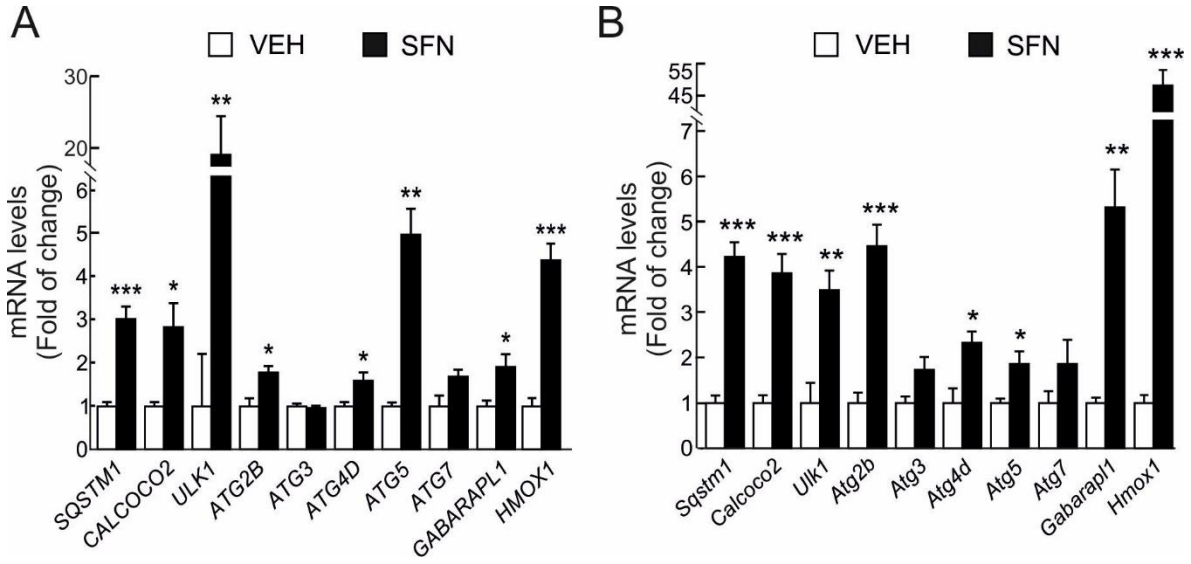

Figure 11. Sulforaphane (SFN) enhances autophagy gene expression. HEK293T (A) and HT22 (B) cells were submitted to 15 µM SFN for 12 h and 6 h, respectively. Messenger RNA levels of the indicated genes were determined by qRT-PCR and normalized to *Actb* levels. Data are mean ± SEM (n = 3). Statistical analysis was performed with Student's t test. *p<0.05, ** p<0.01 and *** p<0.001 vs. vehicle-treated conditions.

4. Reduced expression of autophagy-related genes in the absence of NRF2.

Initially, we tested the effect of pharmacological inhibition of NRF2 in HT22 cells with the alkaloid trigonelline, which, although not specific for NRF2 inhibition, was reported to inhibit NRF2 nuclear translocation [55]. Fig. 12A shows that treatment of HT22 cells with 0.1 μM trigonelline for 12 h resulted in reduced expression of *Hmox1* as a positive control and had no effect on *Atg3*, as expected. With the exception of *Ulk1*, the other genes exhibited a significant reduction in expression.

Considering the lack of specificity of trigonelline or other NRF2 inhibitors, we addressed the impact of NRF2 deficiency on macroautophagy gene expression in mouse embryo fibroblasts (MEFs) from *Nrf2*-WT and *Nrf2*-KO mice by qRT-PCR (Fig. 12B). Impaired expression of *Sqstm1, Calcoco2, Ulk1, Atg2b, Atg4d, Atg5, Atg7* and *Gabarapl1* was observed in *Nrf2*-KO MEFs. Moreover, reduced expression of *Sqstm1, Calcoco2* and *Atg7* products in the absence of NRF2 was also confirmed at the protein level with available antibodies (Fig. 12C and 12D). These results point to a critical role of NRF2 on the basal expression of macroautophagy genes.

We next combined chemical and genetic manipulation of this transcription factor. We treated wild type and *Nrf2*-KO MEFs with SFN (15 μM, 6 h) and analyzed mRNA levels of macroautophagy genes by qRT-PCR. As shown in Fig. 12E, SFN consistently increased the expression of the macroautophagy related genes. However, *Nrf2*-KO MEFs exhibited impaired induction of autophagy genes, indicating that the effect of SFN is mediated at least in part by NRF2.

Finally, we conducted rescue experiments in which *Nrf2*-KO MEFs were infected with a lentivirus expressing NRF2-$^{\Delta EGTE}$-V5 and maintained *in vitro* during 3 or 10 days. We first analyzed the expression levels of *Hmox1* and *Nfe2l2* (because the gene coding for NRF2 has an ARE itself [195] by qRT-PCR, and confirmed effective NRF2 overexpression and induction of target genes (Fig. 12F). Moreover, overexpression of NRF2-$^{\Delta EGTE}$-V5 in *Nrf2*-KO MEFs resulted in increased expression of macroautophagy genes when compared to *Nrf2*-KO MEFs infected with a control GFP-expressing lentivirus (Fig. 12F).

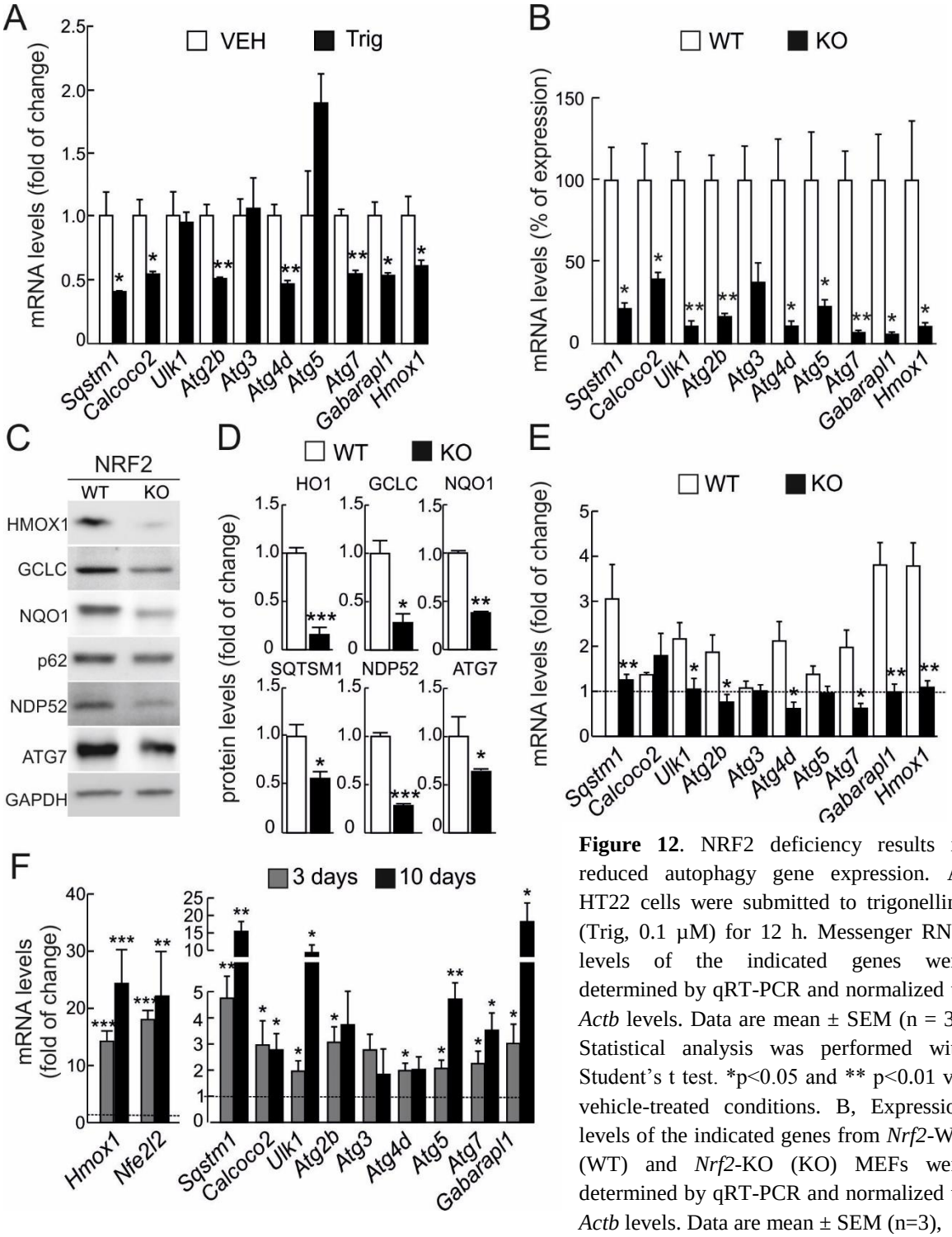

Figure 12. NRF2 deficiency results in reduced autophagy gene expression. A, HT22 cells were submitted to trigonelline (Trig, 0.1 µM) for 12 h. Messenger RNA levels of the indicated genes were determined by qRT-PCR and normalized to *Actb* levels. Data are mean ± SEM (n = 3). Statistical analysis was performed with Student's t test. *p<0.05 and ** p<0.01 vs. vehicle-treated conditions. B, Expression levels of the indicated genes from *Nrf2*-WT (WT) and *Nrf2*-KO (KO) MEFs were determined by qRT-PCR and normalized to *Actb* levels. Data are mean ± SEM (n=3), represented as percentage of expression vs. *Nrf2*-WT MEFs. Statistical analysis was performed with Student's t test. *p<0.05, ** p<0.01 and *** p<0.001 vs. *Nrf2*-WT MEFs. C, Representative immunoblots for the indicated proteins of *Nrf2*-WT and *Nrf2*-KO MEFs. D, Densitometric quantification of representative blots from C relative to GAPDH levels. Data are mean ± SEM (n = 3). Statistical analysis was performed using Student's t test. *p<0.05, ** p<0.01 and ***p < 0.001 vs. *Nrf2*-WT MEFs. E, *Nrf2*-WT and *Nrf2*-KO MEFs were submitted to SFN (15 µM, 6 h). Messenger RNA levels of the indicated genes were determined by qRT-PCR and normalized to *Actb* levels. Data are mean ± SEM (n=3), represented as the fold of change vs. vehicle-treated cells (dashed line). Statistical analysis was performed with Student's t test. *p<0.05 and ** p<0.01 vs. vehicle-treated cells. F, *Nrf2*-KO MEFs were transduced with NRF2-$^{\Delta ETGE}$-V5 or GFP-expressing lentivirus and mRNA levels of the indicated genes were analyzed by qRT-PCR following 3 and 10 days after transduction. Bars represent the fold of change normalized to GFP-lentivirus infected cells, depicted with the dashed line. Data are mean ± SEM (n = 3). Statistical analysis was performed with Student's t test. * p<0.05 and ** p<0.01 vs. GFP-infected cells.

Altogether, these data indicate that NRF2 controls the expression of at least murine *Sqstm1*, *Calcoco2*, *Ulk1*, *Atg2B*, *Atg4D*, *Atg5*, *Atg7* and *Gabarapl1* genes involved in macroautophagy.

5. Analysis of autophagy flux in NRF2-deficient cells.

In order to evaluate the functional impact of NRF2-dependent macroautophagy gene regulation, we first analyzed the conversion of protein LC3B-I (non-lipidated and slower migrating form) to LC3B-II (phosphatidylethanolamine-lipidated and faster migrating form) as an indicator of autophagosome formation. This was combined or not with inhibition of lysosomal degradation by ammonium chloride (NH_4Cl, 20 mM), which impairs lysosomal acidification, and leupeptin (Leup, 100 µM), which is an inhibitor of proteases [196]. As shown in Fig. 13A and 13B, treatment with NH_4Cl and leupeptin (NL, 4 h) increased LC3B-II levels, reflecting the accumulation of autophagosomes that are not being degraded. Activation of autophagy with serum-deprivation, led to a slight increase in LC3B-II levels due to enhanced formation of autophagosomes. Nevertheless, we could not detect significant differences in the levels of LC3B-II between *Nrf2*-WT and *Nrf2*-KO MEFs under basal or induced autophagy with short term lysosomal inhibition. When we examined the accumulation of autophagosomes with time in *Nrf2*-WT and *Nrf2*-KO MEFs, we observed a subtle reduction in LC3B-II levels in the absence of NRF2 at longer time points, that may reflect the existence of slight differences in the dynamics of autophagosomes formation between *Nrf2*-WT and *Nrf2*-KO MEFs (Fig. 13C and 13D).

We then analyzed the role of NRF2 in controlling the autophagy flux under oxidative stress conditions. For this purpose, wild type and *Nrf2*-KO MEFs were treated with increasing concentrations of H_2O_2 for 6 h as indicated in Fig. 13E and 13F. H_2O_2 increased LC3B-II levels in both cell types, but to a lesser extent in *Nrf2-KO* MEFs, suggesting that NRF2 is necessary for a proper autophagy induction under oxidative stress conditions.

Altogether, these results suggest that basal expression of autophagy genes in *Nrf2*-KO MEFs may be sufficient to sustain basal or SD-induced autophagy, but transcriptional input from NRF2 is necessary for a proper induction of autophagy under oxidative or stress conditions.

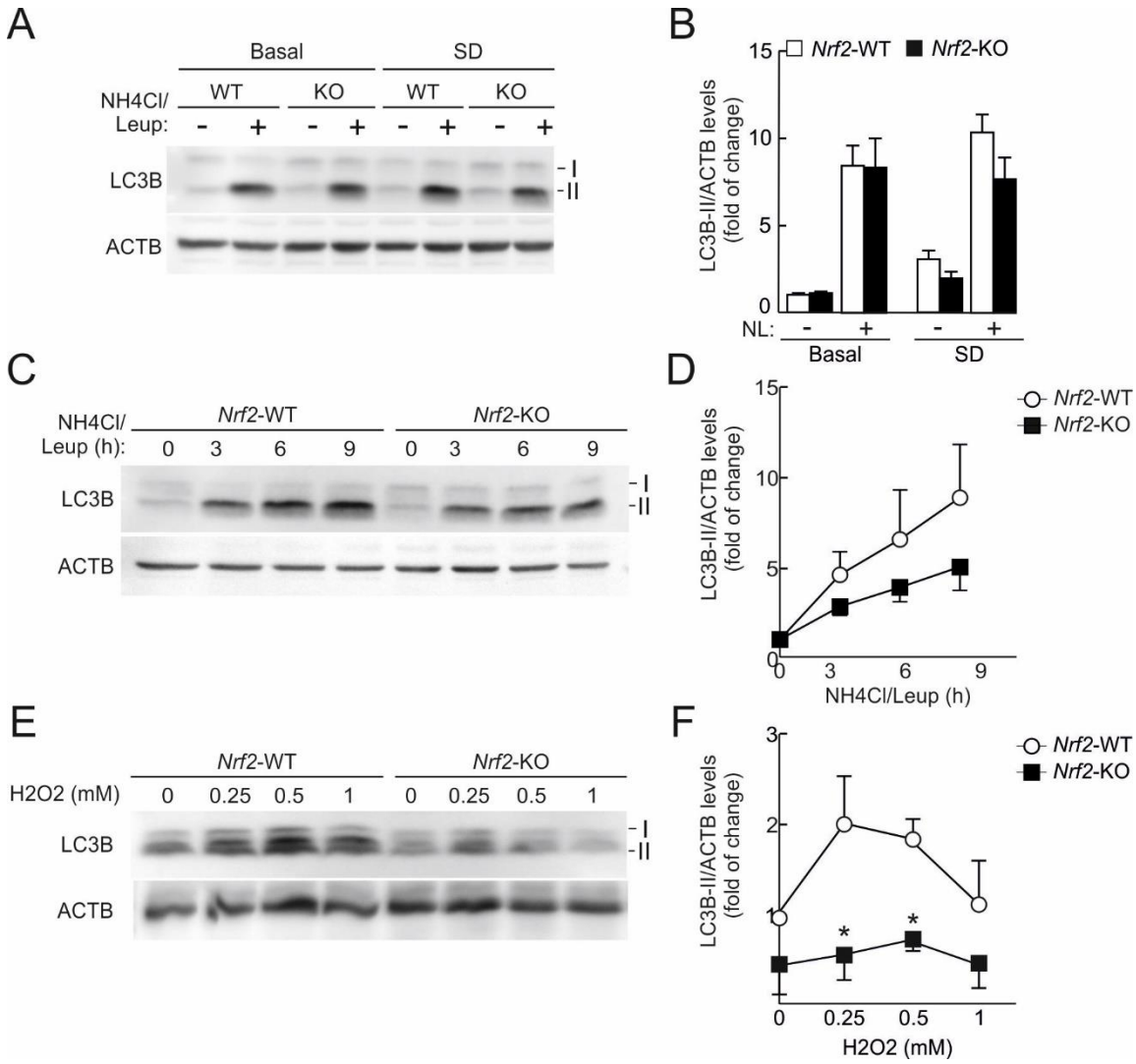

Figure 13. NRF2 deficiency impairs autophagy flux in response to stress. A, Representative immunoblots for the indicated proteins of *Nrf2*-WT (WT) or *Nrf2*-KO (KO) MEFs under basal conditions or deprived from serum (SD) during 6 h in the absence or presence of NH_4Cl/Leupeptin (NL) for the last 4 h. B, Densitometric quantification of representative blots from A relative to ACTB levels. Data are mean ± SEM (n = 4). Statistical analysis was performed using Student's t test vs. *Nrf2*-WT MEFs. C, Representative immunoblots for the indicated proteins of *Nrf2*-WT or *Nrf2*-KO MEFs treated with NL for the indicated times. D, Densitometric quantification of representative blots from C relative to ACTB levels. Data are mean ± SEM (n = 3). Statistical analysis was performed using Student's t test. E, Representative immunoblots for the indicated proteins of *Nrf2*-WT or *Nrf2*-KO MEFs treated with the indicated concentrations of H_2O_2 for 6 h. F, Densitometric quantification of representative blots from E relative to ACTB levels. Data are mean ± SEM (n = 3). Statistical analysis was performed using Student's t test. *p<0.05 vs. *Nrf2*-WT MEFs.

6. Generation of a new mouse model of proteinopathy.

To understand the loss of homeostasis recapitulated by NRF2 deficiency and its impact on proteostasis, we generated a new mouse model of AD based on the expression of human mutant APP(V717I) and TAU(P301L) under the neuronal *Thy1* promoter in a C57BL/6 wild type (denoted as AT-*Nrf2*-WT mice) or *Nrf2*-KO (named AT-*Nrf2*-KO mice)

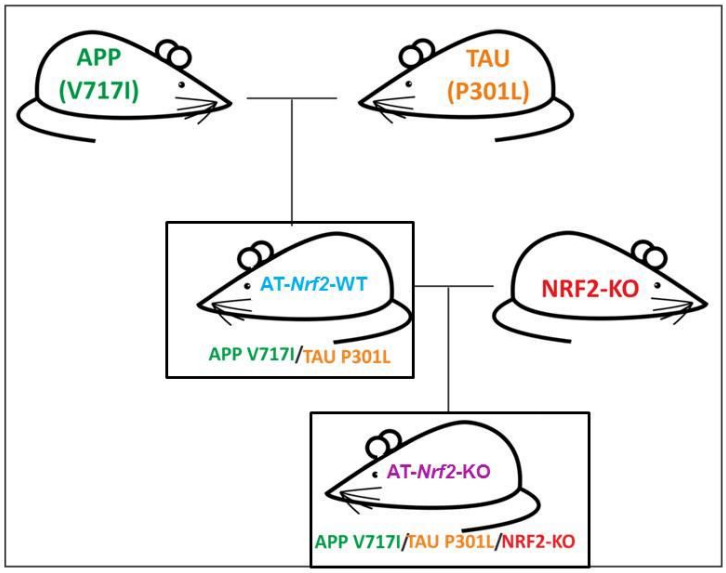

Figure 14. Generation of a new mouse model of AD. Scheme showing the generation of a new mouse model of AD based on the expression of human APP(V717I) and TAU(P301L) under the control of the neuronal *Thy1* promoter on an *Nrf2*-wild type (AT-*Nrf2*-WT mice) or *Nrf2*-knockout (AT-*Nrf2*-KO) genetic background.

genetic background (Fig. 14). The APP(V717I) mutation, called the "London mutation", is one of the most common APP mutations identified in familial cases of AD. This mutation is located very close to the γ-secretase cleavage site, inducing the amyloidogenic cleavage of APP to Aβ42 as well as subsequent TAU phosphorylation [197, 198]. On the other hand, TAU(P301L) affects the microtubule binding region of TAU, being the most common mutation found in frontotemporal dementia of chromosome 17 and accelerating the formation of aggregates and NFTs [199].

6.1. Characterization of TAU and Aβ/APP expression in brains from AT-*Nrf2*-WT and AT-*Nrf2*-KO mice.

The tissue distribution of human TAU(P301L) and APP(V717I) in AT-*Nrf2*-WT and AT-*Nrf2*-KO mice was analyzed by immunohistochemistry of sagittal brain sections with anti-TAU (clon HT7) and anti-APP/Aβ (clon 4G8) antibodies. Fig. 15A-C and Fig. 16A-C show representative images of TAU and APP/Aβ positive neurons located in different brain regions, including cortex (mainly in the entorhinal cortex and M1 and M2 motor cortex), hippocampus (CA1, CA2, subiculum and hilum), brainstem (being more abundant in the reticular formation of the bulb and the pons) or cerebellum (deep cerebellum nuclei and granular layer). We also detected positive neurons and fibers in the spinal cord.

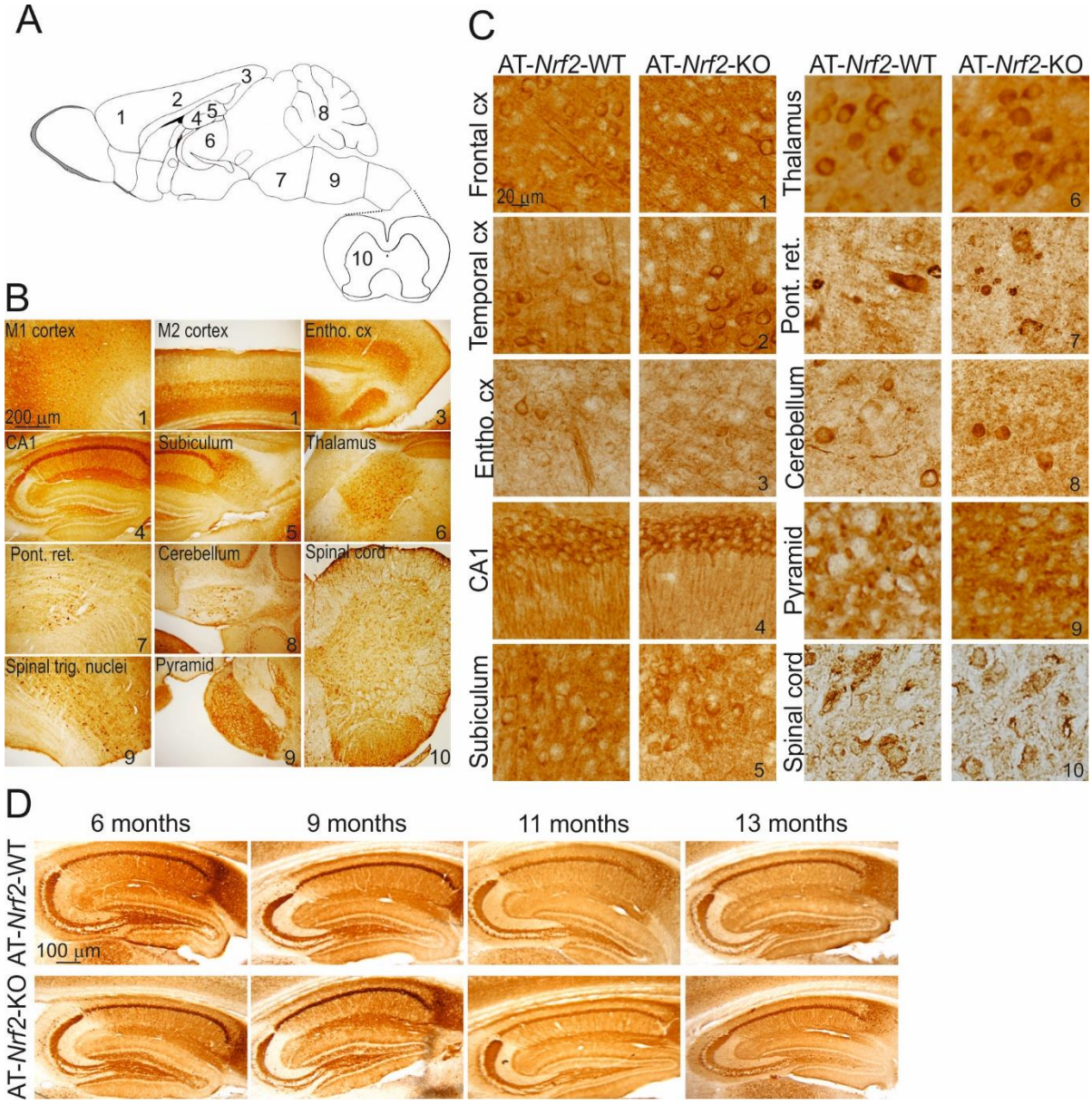

Figure 15. Analysis of tissue distribution of human TAU positive neurons in the brain of the indicated genotypes. A, Scheme showing different brain regions were human TAU positive neurons were detected. 1, Frontal cortex; 2, Temporal cortex; 3, Entorhinal cortex; 4, CA1; 5, Subiculum; 6, Thalamus; 7, Pons; 8, Cerebellum; 9, Medulla, 10, Spinal cord. B, Representative images of TAU (HT7 clon) positive neurons in the brain regions depicted in A. C, Higher magnification of TAU positive neurons from the indicated genotypes in the brain regions from A. D, Representative immunohistochemistry images of human TAU (HT7) staining in the hippocampus of AT-*Nrf2*-WT and AT-*Nrf2*-KO mice at the indicated ages.

We further characterized TAU expression as well as development of amyloid plaques in AT-*Nrf2*-WT and AT-*Nrf2*-KO as a function of ageing. For this purpose, we performed immunohistochemistry analysis employing anti-TAU (clon HT7) or anti-APP/Aβ (clon 4G8) antibodies in sagittal brain sections of the hippocampus from 6, 9, 11 and 13-months old mice. As shown in Fig. 15D, TAU expression was detectable at all the different ages analyzed

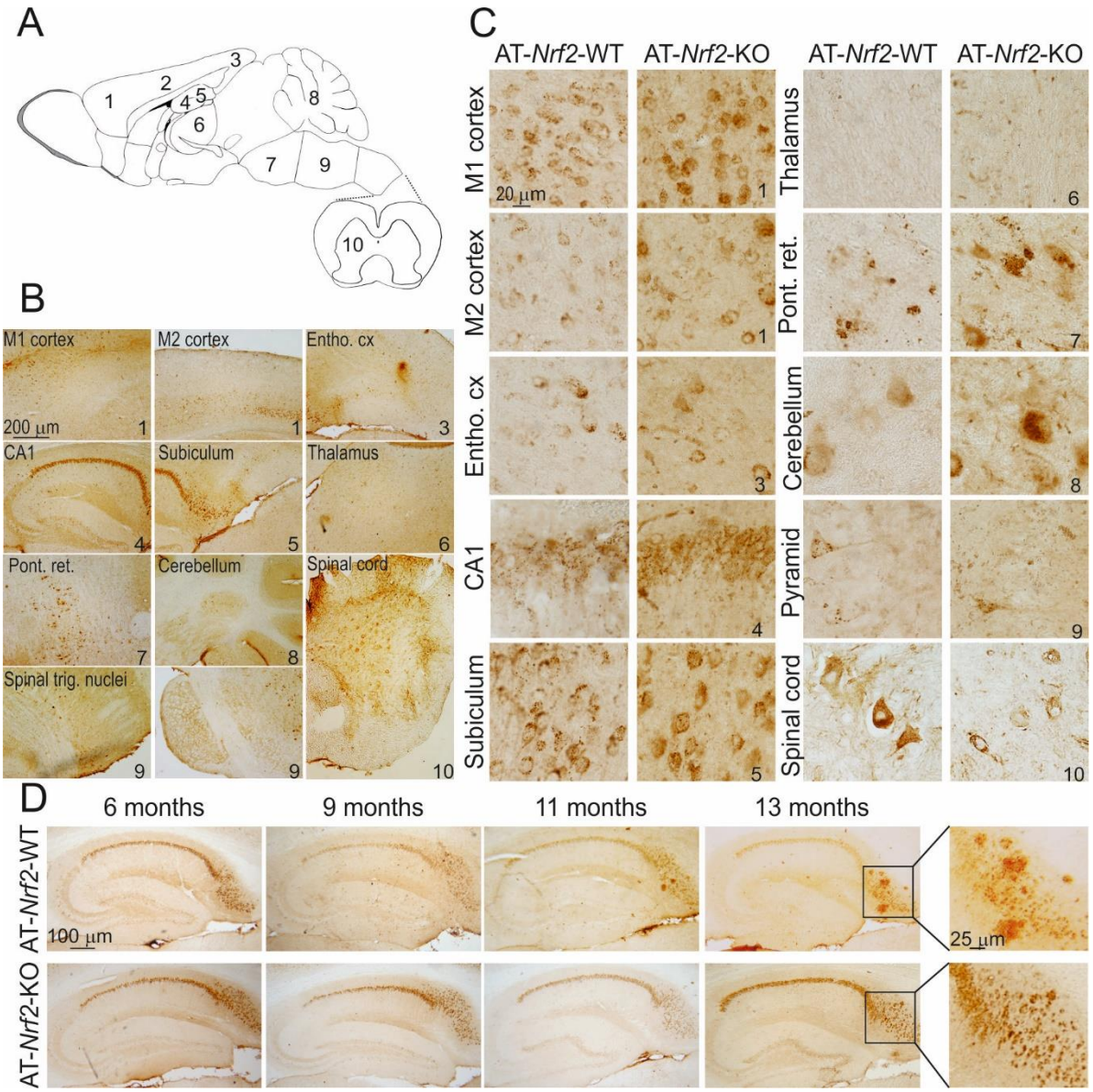

Figure 16. Analysis of tissue distribution of human APP/Aβ positive neurons in the brain of the indicated genotypes. A, Scheme showing different brain regions were human APP/Aβ positive neurons were detected. 1, Frontal cortex; 2, Temporal cortex; 3, Entorhinal cortex; 4, CA1; 5, Subiculum; 6, Thalamus; 7, Pons; 8, Cerebellum; 9, Medulla, 10, Spinal cord. B, Representative images of APP/Aβ (4G8 clon) positive neurons in the brain regions depicted in A. C, Higher magnification of APP/Aβ positive neurons from the indicated genotypes in the brain regions from A. D, Representative immunohistochemistry images of human APP/Aβ staining in the hippocampus of AT-*Nrf2*-WT and AT-*Nrf2*-KO mice at the indicated ages. Higher magnification images showing big compact amyloid plaques in AT-*Nrf2*-WT vs. small diffuse or even intracellular amyloid in AT-*Nrf2*-KO mice.

and displayed no major changes with age or between genotypes. As observed in Fig. 16D, amyloid plaques started to appear at 11-13 months of age and were mainly present in the subiculum. Surprisingly, we detected fewer plaques in the subiculum of AT-*Nrf2*-KO than in the wild type counterparts. A more detailed analysis of Aβ/APP and TAU pathological specimens will be described in the next section.

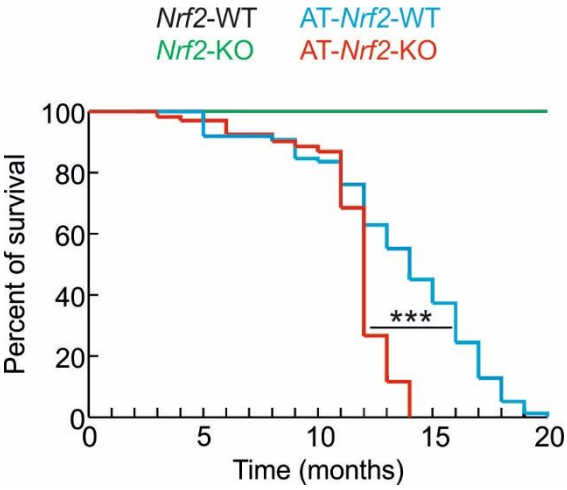

Figure 17. Early death of the AT-mice is accelerated in the absence of NRF2. Kaplan-Meier curves of *Nrf2*-WT (n=250), *Nrf2*-KO (n=217), AT-*Nrf2*-WT (n=269) and AT-*Nrf2*-KO (n=209) mice over 3 years of observation. A p value of ***p<0.001 was obtained comparing AT-*Nrf2*-WT and AT-*Nrf2*-KO curves.

6.2. NRF2 deficiency accelerates premature death due to APP(V717I) and TAU(P301L) expression.

We first evaluated the lifespan of *Nrf2*-WT, *Nrf2*-KO, AT-*Nrf2*-WT and AT-*Nrf2*-KO animals. As observed in the Kaplan-Meier survival curves depicted in Fig. 17, *Nrf2*-WT and *Nrf2*-KO mice lived longer than 20 months and AT-*Nrf2*-WT mice lived for an average of 14 months. Approximately 50% of the AT-*Nrf2*-KO mice died before the age of 12 months, with hardly any survivor reaching the 14 months of age (Fig. 17). This observation highlights the importance of NRF2 in a stressful environment, such as the one generated by proteinopathy in the APP/TAU-expressing mice.

6.3. Cognitive and long term potentiation impairment is aggravated by NRF2 deficiency.

In order to address memory capabilities, we subjected 6-months-old *Nrf2*-WT, *Nrf2*-KO, AT-*Nrf2*-WT and AT-*Nrf2*-KO to the Morris water maze test. This test consists in daily training of mice in an open swimming pool where they must find a submerged platform. As the mice learn, the time to reach the platform (acquisition time) decreases. Prior to the test, we observed that all genotypes showed similar swimming speed at this age, indicating uncompromised motor abilities. As observed in Fig. 18A, after 5 days of trials, all mice found the platform in approximately 20 s except for the AT-*Nrf2*-KO mice, who took significantly longer (almost 40 s). Spatial memory was assessed at the seventh day by removing the platform. As shown in Fig. 18B, *Nrf2*-WT, *Nrf2*-KO and AT-*Nrf2*-WT mice exhibited a tendency to swim around the area were the platform used to be located. AT-*Nrf2*-KO mice,

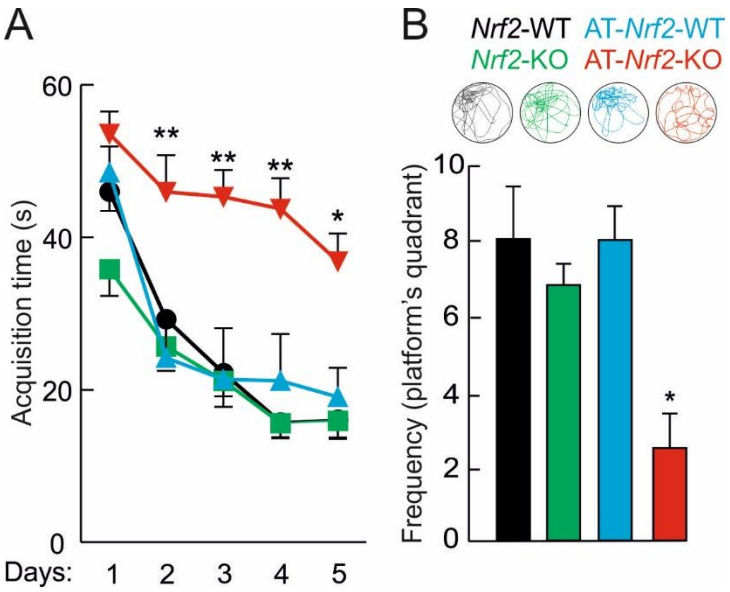

Figure 18. Spatial learning and memory are impaired in AT-*Nrf2*-KO mice. A, Acquisition time to reach the hidden platform in each of the five trials during Morris Water Maze test performed to 6 months-old mice of the indicated genotypes. Data are mean ± SEM (n = 10). Statistical analysis was performed with Two way ANOVA followed by Bonferroni post-hoc test. *p<0.05 and **p < 0.01 vs. *Nrf2*-WT mice. B, Upper circles are representative swimming tracks of the indicated genotypes during the probe phase in which the platform was removed. Lower graph shows the frequency spent at the platform quadrant. Data are mean ± SEM (n = 10). Statistical analysis was performed with One way ANOVA followed by Bonferroni post-hoc test. *p<0.05 vs. *Nrf2*-WT mice.

however, displayed random swimming-tracks all over the pool, reflecting their inability to remember the original platform location. These results demonstrate impaired cognition in AT-*Nrf2*-KO mice already at 6 months of age.

To further analyze synaptic function in AT-*Nrf2*-KO mice and its wild type counterparts, we measured long term potentiation (LTP). This mechanism of synaptic plasticity, involving a long-lasting increase in the strength of synaptic transmission after prolonged high frequency input, is known to participate in memory formation [200]. We recorded synaptic transmission in the dentate gyrus upon electrophysiological stimulation of the performant path (Fig. 19). High frequency stimulation increased the field excitatory post-synaptic potential (fEPSP) in control *Nrf2*-WT mice, but to a lesser extent in both *Nrf2*-KO and AT-*Nrf2*-WT mice, indicating that NRF2 deficiency or proteinopathy alone are sufficient to impair LTP. Moreover, the combination of proteinopathy and NRF2 deficiency in the AT-*Nrf2*-KO mice resulted in a more profound effect, drastically reducing the fEPSP (Fig. 19).

6.4. Increased oxidative markers in AT-*Nrf2*-KO mice.

We next evaluated the presence of oxidative markers in the brains of 12-14 months-old *Nrf2*-WT, *Nrf2*-KO, AT-*Nrf2*-WT and AT-*Nrf2*-KO mice. As observed in Fig. 20A, NRF2 deficiency or proteinopathy did not significantly modify the ratio of GSH/GSSG as compared to wild type animals. However, the AT-*Nrf2*-KO mice showed a decreased GSH/GSSG ratio, indicating diminished availability of reduced glutathione and,

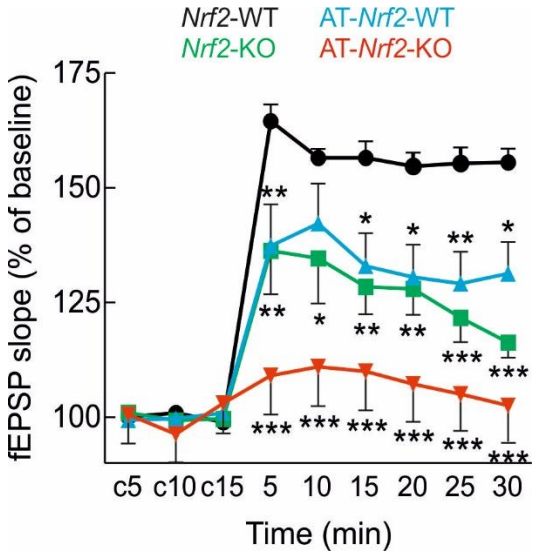

Figure 19. Long term potentiation is drastically reduced by NRF2 deficiency. Field excitatory post-synaptic potential (fEPSP) in 6 months-old animals of the indicated genotypes before and after tetanic stimulation of the perforant pathway. c5, c10, c15: baseline recordings before tetanic stimulation. Data are mean ± SEM (n = 6). Statistical analysis was performed with two-way ANOVA followed by Bonferroni post-hoc test. *p<0.05, **p<0.01 and ***p<0.001 vs. *Nrf2*-WT mice.

consequently, less antioxidant capacity. Next, we evaluated the oxidative damage to macromolecules, including protein carbonylation, which reflects oxidation of specific aminoacids (preferentially Lys, Arg or Pro). Protein carbonylation was measured with 2,4-dinitrophenylhydrazine (DNPH). This method revealed similar levels of protein carbonylation between genotypes, except for the AT-*Nrf2*-KO mice, which exhibited increased levels of carbonylated proteins (Fig. 20B). Lipid peroxidation, indicative of direct oxidation of polyunsaturated fatty acids mainly, due to oxidation of methylene groups, was quantified according to the generation of malondialdehyde (MDA). As observed in Fig. 20C, *Nrf2*-WT, *Nrf2*-KO and AT-*Nrf2*-WT mice all had similar levels of peroxidized lipids, whereas AT-*Nrf2*-KO mice displayed a significant increase.

Altogether, these results suggest that only the combination of proteinopathy and NRF2 deficiency renders subtle but significant alterations in redox homeostasis towards a more oxidized environment.

6.5. Low-grade chronic inflammation in APP(V717I) and TAU(P301L)-expressing mice that lack NRF2.

We examined astrogliosis and microgliosis in 12-14 months-old *Nrf2*-WT, *Nrf2*-KO, AT-*Nrf2*-WT and AT-*Nrf2*-KO mice. Astrogliosis was determined with Glial Fibrillar Acidic Protein (GFAP) immunostaining of CA1 and subiculum. As observed in Fig. 21A-21C, no significant changes in the number of GFAP positive cells between *Nrf2*-WT and *Nrf2*-KO mice either in the hippocampal CA1 or subiculum regions were detected. The expression of APP(V717I) and TAU(P301L) led to a slight increase in the number of GFAP positive cells

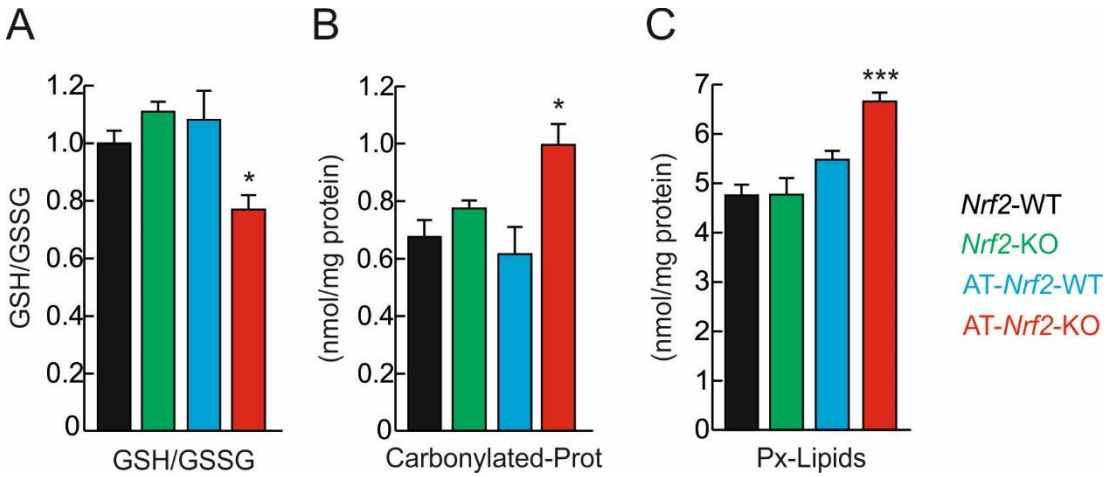

Figure 20. Increased oxidative markers in the brains of AT-*Nrf2*-KO mice. A, Ratio of reduced glutathione (GSH) and oxidized glutathione (GSSG) in the brains of 12-14 months old mice of the indicated genotypes. B, Protein carbonyl content in the brains of the indicated genotypes determined by 2,4-dinitrophenylhydrazine levels and normalized to total protein levels. C, Peroxidized lipids (Px-lipids) determined by malondialdehyde levels normalized to total protein levels. Data are mean ± SEM (n = 4). Statistical analysis was performed with One way ANOVA followed by Newman-Keuls post-hoc test. *p<0.05 and ***p<0.001 vs. *Nrf2*-WT mice.

in the subiculum, which display activated-specific morphology with thick cell bodies and small cytoplasmic branches (Fig. 21B). Nevertheless, abolishment of NRF2 expression did not change the number of GFAP positive cells in either of these brain regions.

We then analyzed microgliosis in the hippocampus of these mice with Cluster of Differentiation molecule 11B (CD11b) immunostaining. No evident changes were observed between *Nrf2*-WT and *Nrf2*-KO mice (Fig. 21D-21F). The APP/TAU-expressing mice showed a trend to have increased microgliosis and the absence of NRF2 in these mice resulted in a significant larger number of CD11b positive microglia in both CA1 and subiculum (Fig. 21D-21F).

To delve into the differences observed in the microglial population between the AT-*Nrf2*-KO vs. the AT-*Nrf2*-WT mice, we analyzed the expression of the Major Histocompatibility Complex class II molecule (MHCII) as a marker of microglial activation in the hippocampus. As observed in Fig. 22A, MHCII immunostaining yielded very low specific signal in the AT-*Nrf2*-WT mice while the lack of NRF2 resulted in increased MHCII immunostaining in the hippocampus of APP/TAU-expressing mice. Importantly, MHCII co-localized with Ionized calcium binding adaptor molecule 1 (IBA1) microglial marker, resulting in abundant yellow dots indicative of increased microglial activation (Fig. 22A).

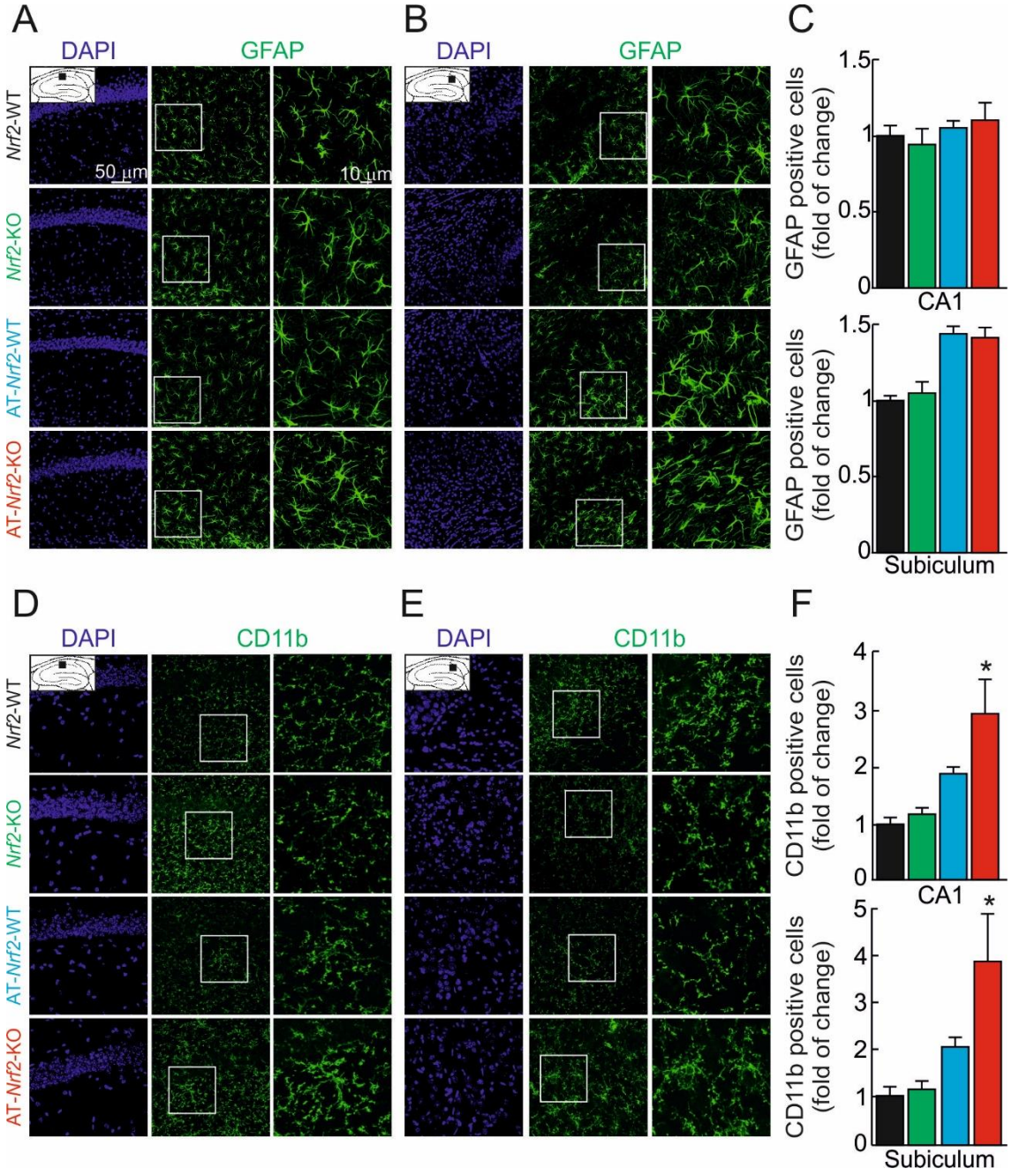

Figure 21. Neuroinflammation in the hippocampus of AT-*Nrf2*-WT and AT-*Nrf2*-KO mice. A and B, Representative immunofluorescence images of GFAP staining in CA1 (A) and subiculum (B) regions of the hippocampus of 12-14 months old mice of the indicated genotypes. The area inside the boxes is shown at a higher magnification. C, Quantification of the number of GFAP positive cells relative to the total number of cells in CA1 and subiculum. Data are mean ± SEM (n = 3). Statistical analysis was performed with Student's t test. *p<0.05 vs. AT-*Nrf2*-WT mice. D and E, Representative immunofluorescence images of CD11b staining in CA1 (D) and subiculum (E) regions of the hippocampus of 12-14 months old mice of the indicated genotypes. The area inside the boxes is shown at a higher magnification. F, Quantification of the number of CD11b positive cells relative to the total number of cells in CA1 and subiculum. Data are mean ± SEM (n = 3). Statistical analysis was performed with Student's t test. *p<0.05 vs. AT-*Nrf2*-WT mice.

The expression levels of some inflammatory genes were analyzed by qRT-PCR (Fig. 22B). In line with our previous results, no significant changes in the expression of *Gfap* were detected between AT-*Nrf2*-KO and AT-*Nrf2*-WT mice. However, AT-*Nrf2*-KO mice

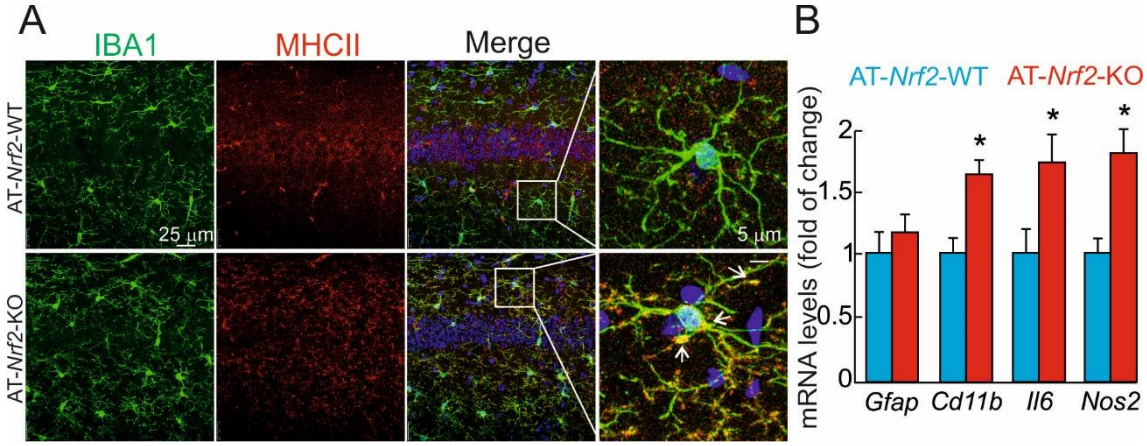

Figure 22. NRF2 deficiency increases microglial activation and pro-inflammatory gene expression. A, Representative immunofluorescence images of IBA1 and MHCII staining in the hippocampus of 12-14 months old mice of the indicated genotypes. The area inside the boxes is shown at a higher magnification. B, Expression levels of the indicated genes from hippocampus of AT-*Nrf2*-WT and AT-*Nrf2*-KO mice were determined by qRT-PCR and normalized to *ActB* levels. Data are mean ± SEM (n=4). Statistical analysis was performed with Student's t test. *p<0.05, vs. AT-*Nrf2*-WT mice.

exhibited a modest but significant increase in the expression levels of the pro-inflammatory *Cd11b*, *Il6* and *Nos2* genes when compared to age-matched AT-*Nrf2*-WT mice.

Altogether, these results indicate that the proteinopathy induced by APP(V717I) and TAU(P301L) induces a modest gliosis and neuroinflammation that is detectable at 12-14 months of age.

7. NRF2 deficiency impairs autophagy *in vivo*.

7.1. NRF2 deficiency results in reduced levels of macroautophagy markers in neurons.

First of all, we analyzed macroautophagy gene expression in hippocampal/cortical primary neurons by qRT-PCR (Fig. 23). In line with our previous results in MEFs, *Nrf2*-KO cells exhibited impaired expression of *Sqstm1*, *Calcoco2*, *Ulk1*, *Atg2b*, *Atg5*, *Atg7 and Gabarapl1*. These results confirm the role of NRF2 in the modulation of autophagy-related genes in neurons.

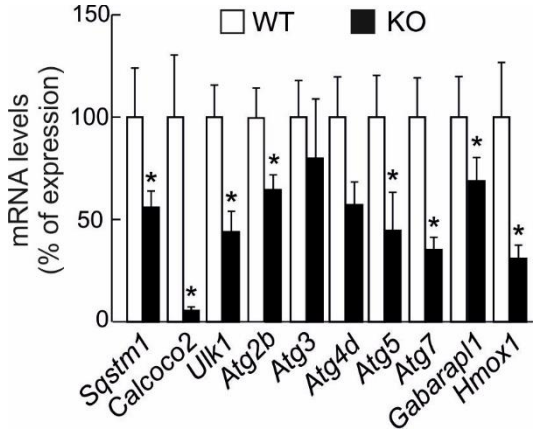

Figure 23. NRF2 deficiency impairs autophagy gene expression in neurons. Expression levels of the indicated genes from *Nrf2*-WT and *Nrf2*-KO primary hippocampal/cortical neurons were determined by qRT-PCR and normalized to *Actb* levels. Data are mean ± SEM (n=3). Statistical analysis was performed with Student's t test. *p<0.05, vs. *Nrf2*-WT neurons.

Autophagy gene expression was then evaluated in the hippocampus of *Nrf2*-WT, *Nrf2*-KO, AT-*Nrf2*-WT and AT-*Nrf2*-KO mice by qRT-PCR. In agreement with previous studies [201], 11-13 months old *Nrf2*-KO mice had minimal changes in the expression levels of *bona fide* NRF2-dependent genes compared to *Nrf2*-WT mice, *Aox1* (coding aldehyde oxidase 1) being the most significant. Comparison of AT-*Nrf2*-WT vs. AT-*Nrf2*-KO hippocampus also showed a small but significant change in the expression of *Sqstm1*, *Atg2b*, and *Gabarapl1* (Table 8).

Due to the small changes found in whole brain tissue, we reasoned that the effect of NRF2 on autophagy might be more evident in the neurons that express human mutant APP and TAU proteins. Therefore, we performed immunofluorescence analysis of autophagy

Gene	*Nrf2*-WT	*Nrf2*-KO	AT-*Nrf2*-WT	AT-*Nrf2*-KO	p-value (*Nrf2*-WT vs *Nrf2*-KO)	p-value (AT-*Nrf2*-WT vs AT-*Nrf2*-KO)
Sqstm1	1,0±0,15	0,63±0,14	0,67±0,03	0,55±0,04	0.12	*0.05
Calcoco2	1,00±0,02	1,56±0,27	1,24±0,15	1,12±0,23	0.08	0.67
Ulk1	1,00±0,07	0,98±0,15	0,85±0,04	0,70±0,09	0.9	0.17
Atg2b	1,00±0,05	1,06±0,12	0,69±0,04	0,48±0,02	0.66	**0.003
Atg3	1,00±0,15	1,2±0,15	1,13±0,11	1,12±0,10	0.38	0.95
Atg4d	1,00±0,11	1,17±0,09	1,09±0,19	1,06±0,13	0.27	0.9
Atg5	1,00±0,27	1,32±0,05	1,51±0,14	1,35±0,09	0.28	0.37
Atg7	1,00±0,11	1,05±0,09	0,84±0,18	0,73±0,13	0.73	0.63
Gabarapl1	1,00±0,06	1,21±0,22	1,45±0,07	0,83±0,16	0.39	*0.021
Hmox1	1,00±0,03	1,11±0,05	1,27±0,17	1,23±0,10	0.1	0.84
Aox1	1,00±0,17	0,44±0,08	0,90±0,07	0,56±0,11	*0.02	*0.04

Table 8. Analysis of NRF2-dependent genes in the hippocampus of *Nrf2*-WT, *Nrf2*-KO, AT-*Nrf2*-WT and AT-*Nrf2*-KO 11-13 months old mice. Expression levels of the indicated genes were determined by qRT-PCR and normalized to *Actb* levels. Data are mean ± SEM (n=4). Statistical analysis was performed with Student's t test. *p<0.05 and **p<0.01 vs. the indicated genotype.

proteins in APP- or TAU-expressing neurons in sagittal brain sections of AT-*Nrf2*-WT and AT-*Nrf2*-KO mice. As shown in Fig. 24, the protein levels of p62, NDP52, ULK1, ATG5 and GABARAPL1 were reduced in neurons of the AT-*Nrf2*-KO mice expressing APP, compared to those of AT-*Nrf2*-WT mice. The same approach was followed with TAU-expressing neurons, obtaining similar results (Fig. 25). Moreover, we analyzed LC3B staining in the hippocampus as an estimate of overall autophagy. We found that LC3B protein levels were also reduced in neurons of AT-*Nrf2*-KO vs. AT-*Nrf2*-WT mice expressing APP (Fig. 24F) or TAU (Fig. 25F). Together, these results indicate the relevance of NRF2 in the regulation of macroautophagy under proteotoxic stress *in vivo*.

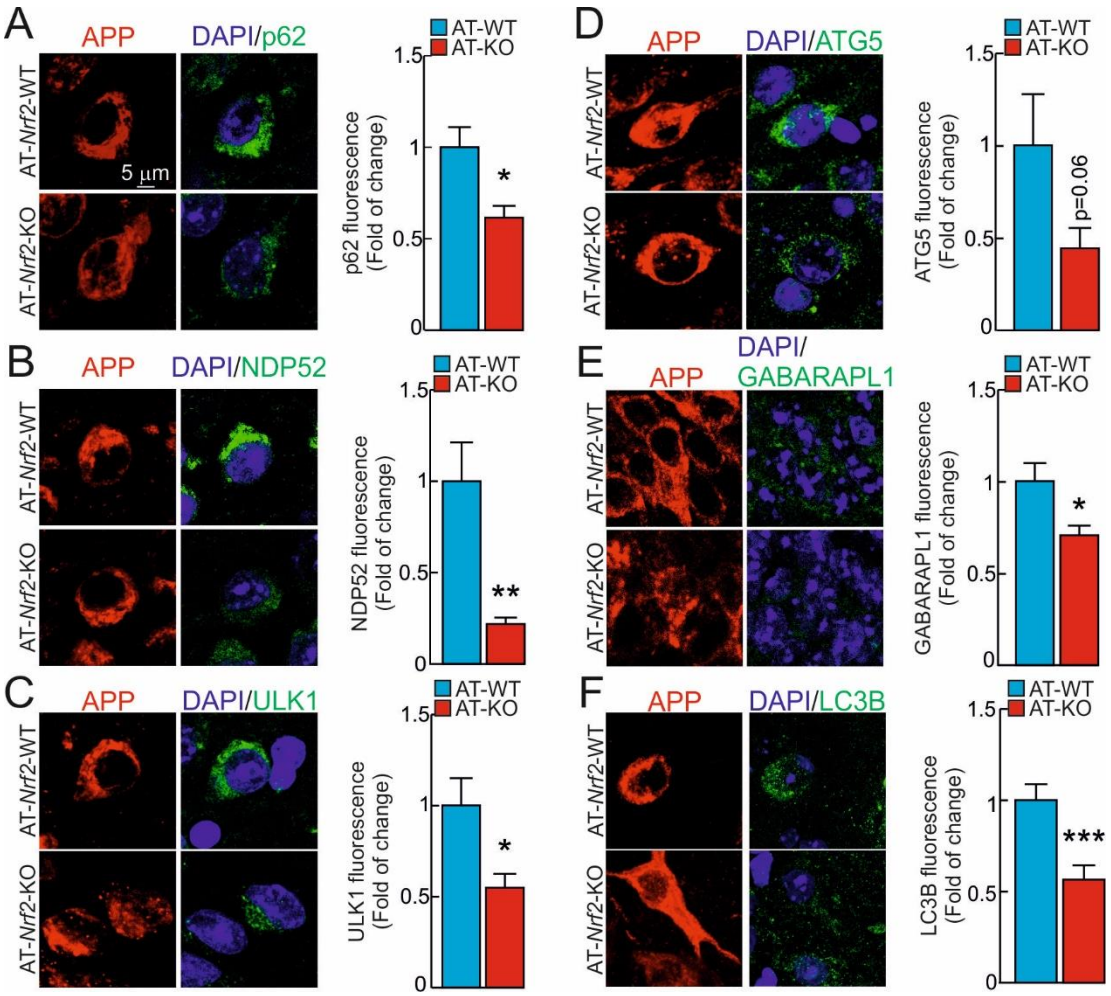

Figure 24. Reduced autophagy markers in APP/Aβ-expressing neurons from AT-*Nrf2*-KO mice. A-F, Confocal analysis of double immunofluorescence with anti-APP/Aβ (4G8, red) and anti-p62, NDP52, ULK1, ATG5, GABARAPL1 or LC3B (green) antibodies in the brains of AT-*Nrf2*-WT and AT-*Nrf2*-KO mice. Fluorescence intensity was analyzed in the cytosol of 100 randomly chosen APP/Aβ-positive neurons of each genotype. Quantification was derived from 3 independent experiments with 2 fields per experiment. Fluorescence intensity was quantified in 1.5-µm-thick stacks using ImageJ software. Data are mean ± SEM (n=3). Statistical analysis was performed with Student's t test. *p<0.05, **p<0.01, ***p<0.001, vs. AT-*Nrf2*-WT mice.

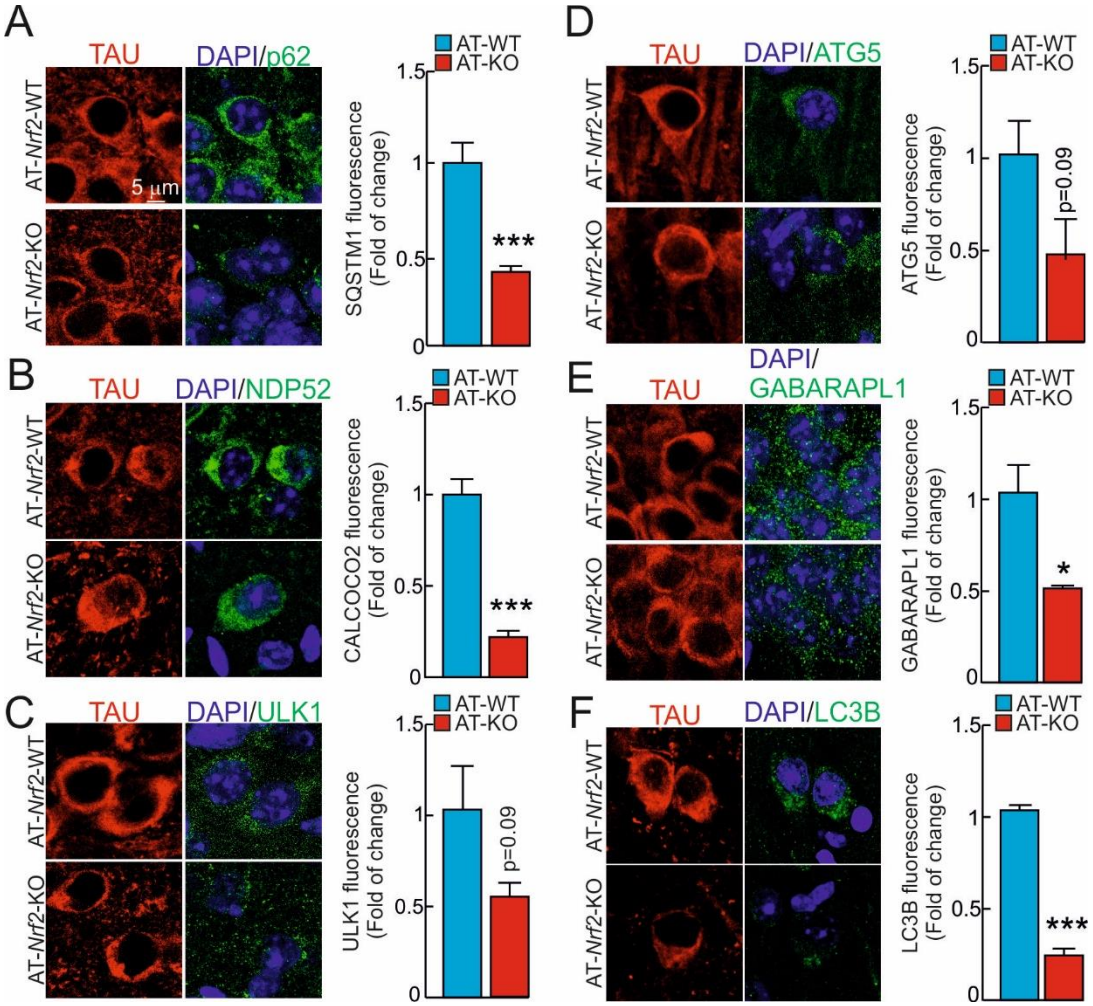

Figure 25. Reduced autophagy markers in TAU-expressing neurons from AT-*Nrf2*-KO mice. A-F, Confocal analysis of double immunofluorescence with anti-TAU (HT7, red) and anti-p62, NDP52, ULK1, ATG5, GABARAPL1 or LC3B (green) antibodies in the brains of AT-*Nrf2*-WT and AT-*Nrf2*-KO mice. Fluorescence intensity was analyzed in the cytosol of 100 randomly chosen APP/Aβ-positive neurons of each genotype. Quantification was derived from 3 independent experiments with 2 fields per experiment. Fluorescence intensity was quantified in 1.5-µm-thick stacks using ImageJ software. Data are mean ± SEM (n=3). Statistical analysis was performed with Student's t test. *p<0.05, **p<0.01 and ***p<0.001, vs. AT-*Nrf2*-WT mice.

7.2. Higher oligomeric Aβ*56 levels and intracellular APP/Aβ aggregates in AT-*Nrf2*-KO mice.

To better understand the impact of reduced macroautophagy markers in neurons from AT-*Nrf2*-KO mice, we subsequently analyzed the toxic and aggregated forms of APP/Aβ and TAU. We first determined the expression levels of *Adam10*, *Adam17*, *Bace1* and *Psen1*, encoding enzymes involved in APP processing. As shown in Fig. 26A, the mRNAs of these genes were not significantly altered by the lack of NRF2 in the APP/TAU-expressing mice. We then analyzed the levels of Aβ-oligomeric species that have been proposed to correlate with cognitive impairment in humans [202]. Hippocampi from AT-*Nrf2*-WT and AT-*Nrf2*-KO

mice were separated into extracellular (EC) (Fig. 26B and 26C) and membrane-bound (MB) fractions (Fig. 26B and 26D), and subjected to immunoblot with antibodies specific for certain APP and Aβ domains (Fig. 26B). We did not detect significant differences in the levels of full-length APP (holoAPP), the soluble form released by α-secretase cleavage (sAPPα), the soluble form released by β-secretase cleavage (sAPPβ), or the oligomers Aβ (3-mer), Aβ (6-mer) or Aβ (2-mer). However, NRF2 deficiency significantly increased the levels of the toxic Aβ*56 oligomer in both the extracellular and the membrane-bound fractions (Fig. 26C-E).

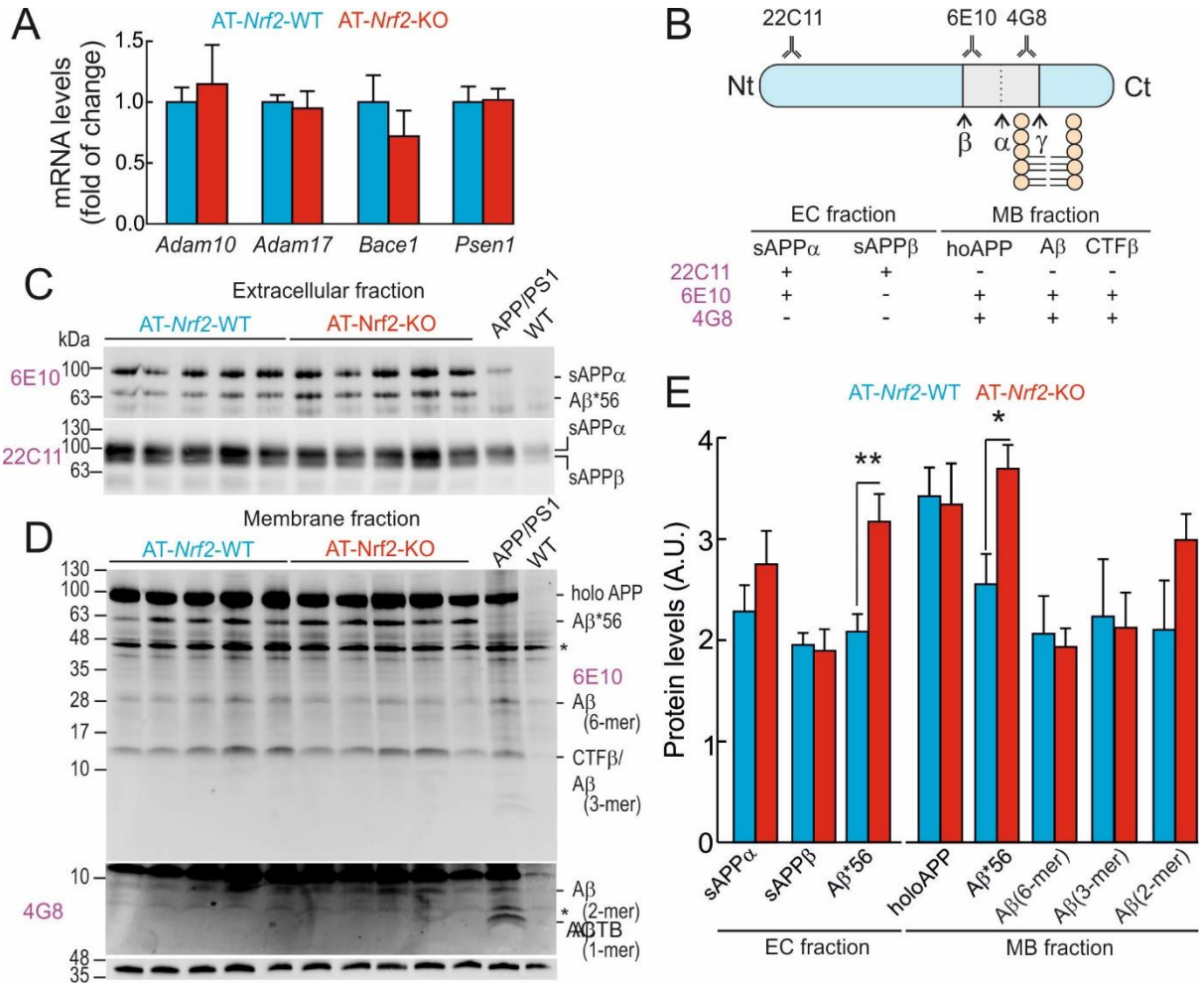

Figure 26. NRF2 deficiency leads to Aβ*56 accumulation. A, Scheme showing APP processing by α-, β- and γ-secretases and the location of the epitopes recognized by the different antibodies employed. B and C, Hippocampal homogenates of 12-14 months old AT-*Nrf2*-WT and AT-*Nrf2*-KO mice were separated into extracellular (EC) and membrane-bound (MB) fractions and immunoblotted with the indicated antibodies. Samples from APP/PS1 and wild type mice were used as positive and negative controls, respectively. The asterisks indicate non-specific bands. D, Densitometric quantification of immunoblots from B and C. Data are mean ± SEM (n=5). Statistical analysis was performed with Student's t test. *p<0.05 and **p<0.01 vs. AT-*Nrf2*-WT mice. E, Expression levels of the indicated genes determined by qRT-PCR and normalized to *ActB* levels. Data are mean ± SEM (n=4). Statistical analysis was performed with Student's t test. *p<0.05, vs. AT-*Nrf2*-WT mice.

Increased Aβ*56 levels might be related to either oxidative alterations of the amyloidogenic pathway or impaired clearance of the oligomers. To gain a better understanding on the formation of Aβ peptides in these mice, the soluble and insoluble levels of the amyloidogenic Aβ40 and Aβ42 peptides were determined by ELISA. Similar levels of soluble Aβ40 and Aβ42 peptides were detected in AT-*Nrf2*-WT and AT-*Nrf2*-KO mice (Fig. 27A and 27B). However, NRF2 deficiency resulted in reduced insoluble Aβ40 (Fig. 27A) and Aβ42 (Fig. 27B) in the hippocampus. These results are consistent with the fewer number of amyloid plaques that we had observed in the AT-*Nrf2*-KO mice (Fig. 16D), where most of the insoluble Aβ accumulates. Because macroautophagy has been shown to be necessary for Aβ secretion [157], we performed immunohistochemical staining of hippocampal sections of AT-*Nrf2*-WT and AT-*Nrf2*-KO mice to determine APP/Aβ localization. As observed in Fig. 27D and 27E, we found more intracellular vesicles in neurons from AT-*Nrf2*-KO mice when compared to AT-*Nrf2*-WT sections. This was most notorious in the subiculum, which was the first brain region to develop amyloidopathy. Taken together, these results suggest that NRF2 deficiency impairs proteostasis of APP/Aβ leading to the accumulation of this protein inside neurons.

7.3. AT-*Nrf2*-KO mice have increased levels of insoluble hyperphosphorylated TAU.

Different post-translationally modified forms of TAU, including hyperphosphorylation, can abnormally aggregate into paired helical filaments (PHFs) and neurofibrillary tangles (NFTs) in AD. This insoluble TAU fraction can be extracted with sarkosyl detergent. Despite not observing major differences in TAU immunostaining in the hippocampus of AT-*Nrf2*-KO vs. their wild type counterparts (Fig. 28A), we detected with anti-total TAU antibody (clon TAU46) a modest but significant increase in the levels of both murine endogenous and human transgenic TAU in the sarkosyl-insoluble fractions from AT-*Nrf2*-KO when compared to AT-*Nrf2*-WT hippocampal homogenates (Fig. 28B and 28C). These results reflected that both transgenic and endogenous TAU are prone to accumulate in the insoluble fraction in the absence of NRF2.

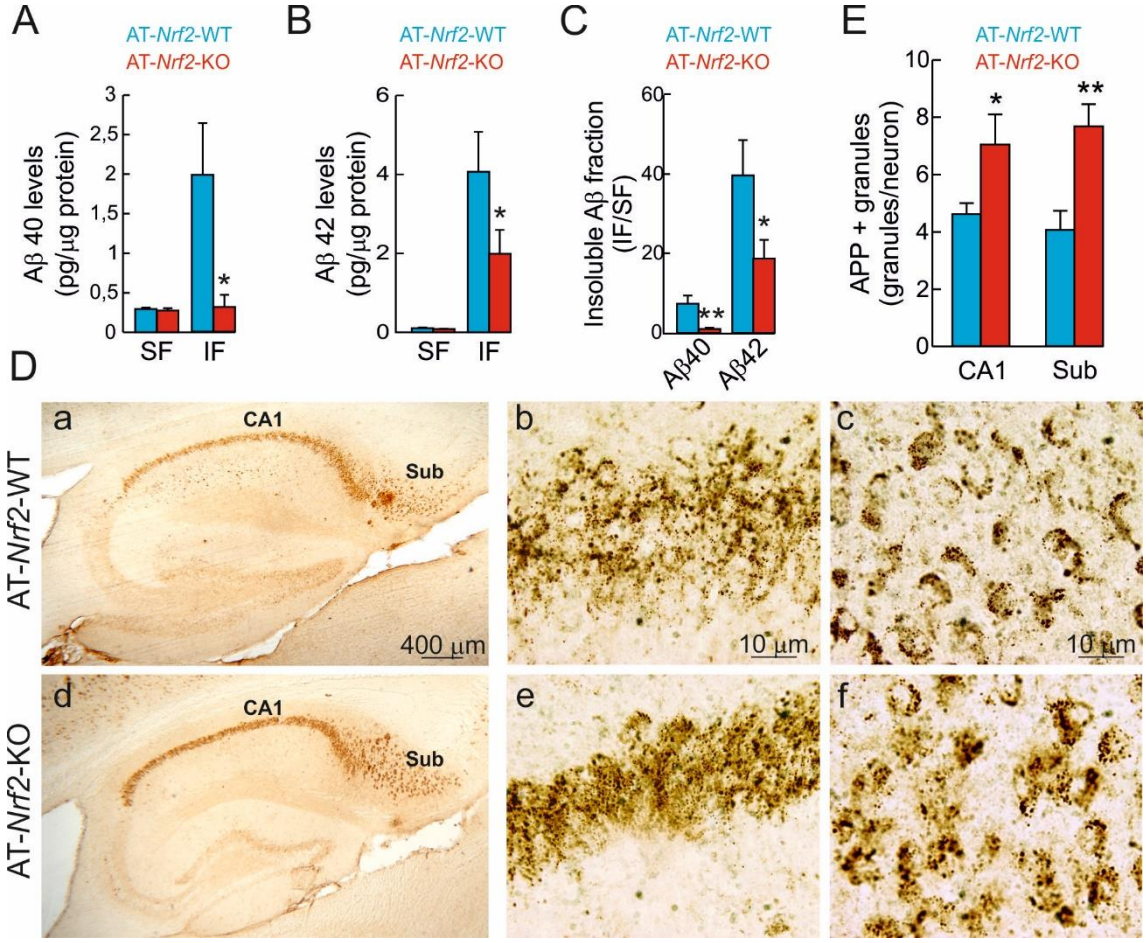

Figure 27. NRF2 deficiency leads to intracellular APP/Aβ accumulation. A-B, Determination of Aβ levels by ELISA in hippocampal brain homogenates of 12-14 months old AT-*Nrf2*-WT and AT-*Nrf2*-KO mice. Aβ40 (A) and Aβ42 (B) levels were measured in the soluble (SF) and insoluble (IF) fractions (formic acid extracted) and normalized by total protein amount. C, Ratio of IF/SF of Aβ40 and Aβ42 peptides. Data are mean ± SEM (n = 10). Statistical analysis was performed with Student's t test. * $p<0.05$ and ** $p < 0.01$ vs. AT-*Nrf2*-WT mice. D, Representative immunohistochemistry images of APP/Aβ (4G8) in the hippocampus of 13 months old AT-*Nrf2*-WT (a, b, c) and AT-*Nrf2*-KO (d, e, f) mice; a and d, low magnification of the hippocampus; b and e, details of the CA1 layer ; c and f, details of subiculum. E, Quantification of the number of APP/Aβ positive granules in CA1 and subiculum from 12-14 months old AT-*Nrf2*-WT and AT-*Nrf2*-KO mice. Data are mean ± SEM (n = 8). Statistical analysis was performed with Student's t test. *$p<0.05$ and **$p < 0.01$ vs. AT-*Nrf2*-WT mice.

To gain more insight on how NRF2 deficiency can affect TAU phosphorylation, we analyzed the hippocampus by immunohistochemistry with the anti-pTAU antibody (clon AT8) specific for phosphorylated hTAU at residues Ser-202 and Thr-205 (Fig. 29A). As shown in Fig. 29B, no clear differences in phospho-TAU pattern were observed in either CA1 or subiculum regions of the hippocampus between AT-*Nrf2*-WT and AT-*Nrf2*-KO mice. We next analyzed phospho-TAU in the soluble and insoluble fractions employing anti-pTAU antibody (PHF1) specific for phosphorylated hTAU at residues Ser-396 and Thr-404. As

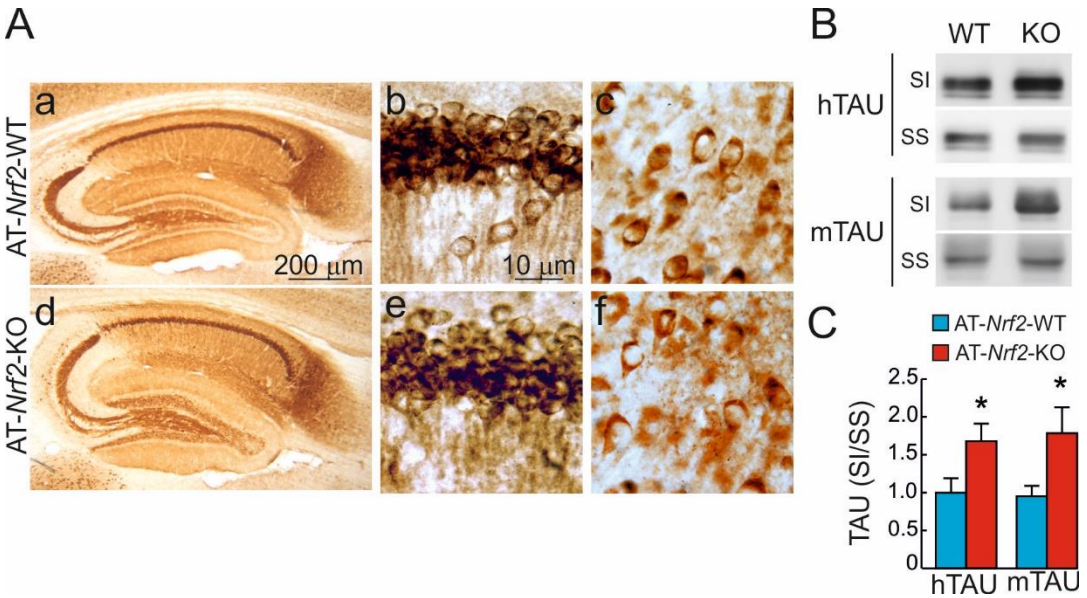

Figure 28. NRF2 deficiency leads to the accumulation of insoluble TAU. A, Representative immunohistochemistry images of human TAU (HT7) staining in the hippocampus (CA1 -b and e- and subiculum- c and f-) of 12-14 months old mice of the indicated genotypes. B, Hippocampal tissue lysates from AT-*Nrf2*-WT (WT) and AT-*Nrf2*-KO (KO) mice were separated into sarkosyl-soluble (SS) and sarkosyl-insoluble (SI) fractions. Total human and murine TAU levels were determined by immunoblot with anti-TAU (TAU46) antibody. C, Densitometric quantification of representative immunoblots from B. Data are mean ± SEM (n=6). Statistical analysis was performed with Student's t test. *p<0.05, vs. AT-*Nrf2*-WT mice.

shown in Fig. 29C, three forms of phospho-TAU, termed hP1, hP2 and hP3, were detected with the PHF1 antibody when separated by SDS-PAGE, which represent various degrees of phosphorylation. AT-*Nrf2*-KO mice exhibited higher levels of phosphorylated TAU in both fractions, and increased insoluble to soluble ratio of the hP2 TAU form was found in comparison to the AT-*Nrf2*-WT mice (Fig. 29C and 29D).

These results strongly suggest that the loss of NRF2 impairs TAU proteostasis, leading to its abnormal hyperphosphorylation and accumulation into insoluble aggregates.

7.4. Decreased co-localization of APP/Aβ and TAU with p62 in the absence of NRF2.

To discern if the accumulation of intracellular APP/Aβ and TAU in the AT-*Nrf2*-KO mice was due to impaired macroautophagy, we analyzed the localization of human APP/Aβ and TAU proteins in connection to the macroautophagy receptor p62 by double immunofluorescence staining. As observed in Fig. 30A and 30B, in AT-*Nrf2*-WT mice most APP/Aβ vesicles were decorated with the NRF2-regulated autophagy gene product p62, resulting in multiple yellow dots. In contrast, AT-*Nrf2*-KO mice showed less co-localization of APP/Aβ with p62, as reflected by fewer yellow dots and reduced Mander's co-localization

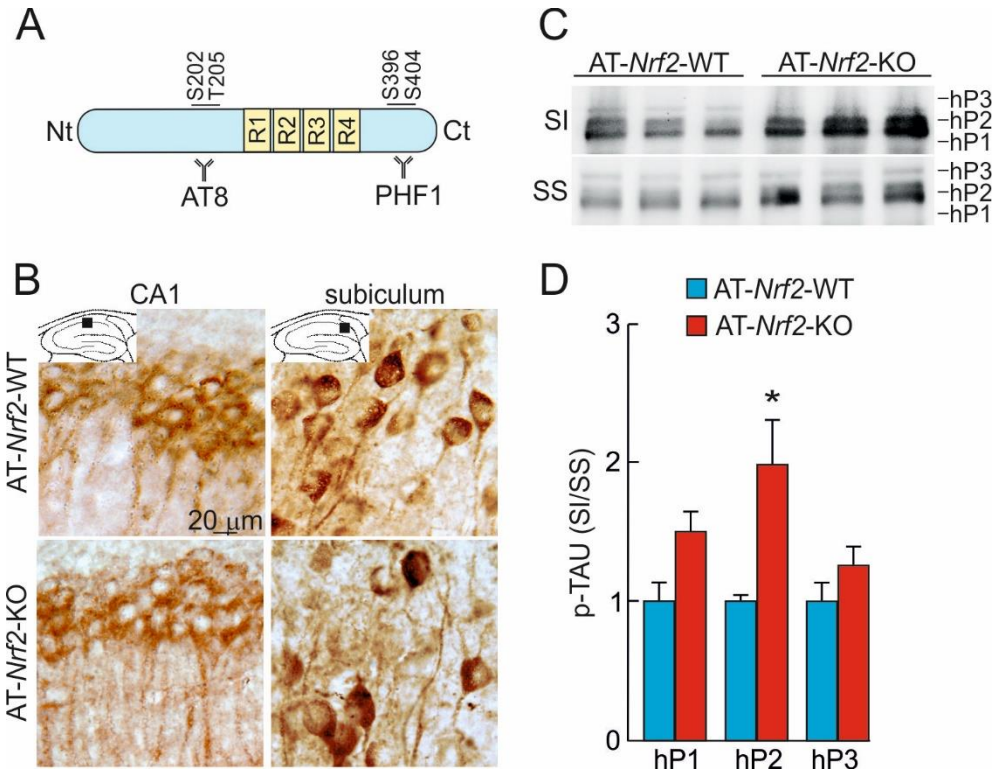

Figure 29. Increased insoluble phospho-TAU in the absence of NRF2. A, Scheme of 4R TAU showing the phosphorylated residues recognized by the AT8 and PHF1 antibodies. B, Representative immunohistochemistry images of human phospho-TAU (AT8) staining in CA1 and subiculum zones of the hippocampus from 12-14 months old AT-*Nrf2*-WT and AT-*Nrf2*-KO mice. C, Immunoblot analysis of sarkosyl-insoluble (SI) and sarkosyl-soluble (SS) phospho-TAU fractions with the PHF1 antibody. D, Densitometric quantification of representative immunoblots from C. Data are mean ± SEM (n=6). Statistical analysis was performed with Student's t test. *p<0.05, vs. AT-*Nrf2*-WT mice.

coefficients. Moreover, we could detect larger and apparently swollen APP/Aβ positive vesicles compared to those in the AT-*Nrf2*-WT mice (Fig. 30A). TAU showed a more diffuse pattern than APP/Aβ, but again AT-*Nrf2*-KO mice exhibited less co-localization between TAU and p62 (Fig. 30C and 30D). Overall, these results suggest that the expression of human mutant APP and TAU proteins increase the need for macroautophagy, which cannot be fulfilled efficiently in NRF2-deficient mice due to the reduced expression of macroautophagy genes.

8. Evidence of altered NRF2 and macroautophagy in AD patients.

In order to determine if this new functional axis has an impact on the AD brain, we examined the levels of NRF2 and several macroautophagy products in lysates from brain hippocampus of asymptomatic control individuals and AD donors (Fig. 31A and 31B). The levels of NRF2 and one of its downstream targets, HMOX1, were increased in AD patients

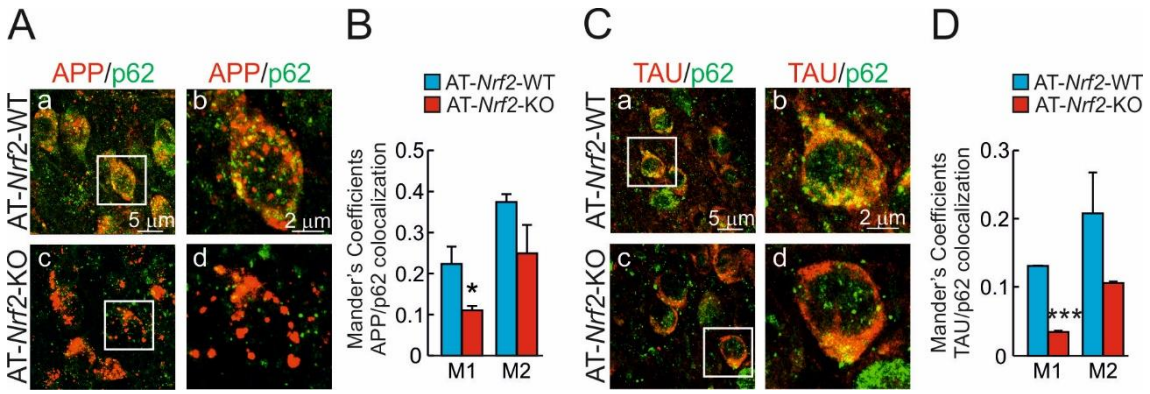

Figure 30. NRF2 modulates neuronal autophagy. A, Confocal analysis of double immunofluorescence with anti-APP/Aβ (4G8, red) and anti-p62 (green) antibodies in subiculum of AT-*Nrf2*-WT and AT-*Nrf2*-KO mice. B, Quantification of co-localization between APP/Aβ and p62 staining expressed as Mander's coefficients. C, Confocal analysis of double immunofluorescence with anti-TAU (HT7, red) and anti-p62 (green) in subiculum of AT-*Nrf2*-WT and AT-*Nrf2*-KO mice. D, Quantification of co-localization between TAU and p62 expressed as Mander's coefficients. For B and D, Mander's coefficients were derived from 3 independent experiments with 2 fields per experiment. Fluorescence was quantified in 1.5-µm-thick stacks using the JACoP plugin of ImageJ software. Data are mean ± SEM (n=6). Statistical analysis was performed with Student's t test. *p<0.05 and ***p<0.001 vs. AT-*Nrf2*-WT mice.

vs. controls. The levels of at least the macroautophagy proteins p62, NDP52 and ATG7 were also increased. A slower migrating band, which could represent phosphorylated p62, was increased in AD samples. These results show a positive correlation between NRF2 levels and macroautophagy proteins in AD samples when compared to controls.

Then, we analyzed more specifically the NRF2/p62 pathway in neurons from AD patients by immunohistochemistry. Because it was technically not possible to perform triple labeling due to the different retrieval requirements for each of the antigens, we analyzed 3 adjacent sections (each 4 µm-thick) containing the same cells. We observed intracellular APP/Aβ in dense vesicles, similar to the ones observed in AT-*Nrf2*-WT and AT-*Nrf2*-KO mice (Fig. 31C). Neurons in the AD brains with the highest abundance of vesicular APP/Aβ were found in the entorhinal cortex, and also expressed high levels of NRF2 and p62 (Fig. 31C a-c). Similarly, some scattered neurons were found in the cortex that presented TAU-positive neurofibrillary tangles, stained with anti-TAU (clon HT7). Such neurons that were intensely stained for TAU were also expressing high levels of nuclear NRF2 and p62 (Fig. 31C d-f). These results confirm in human brain that NRF2 and its target p62 are up-regulated in neurons suffering from proteotoxic APP/Aβ or TAU insults.

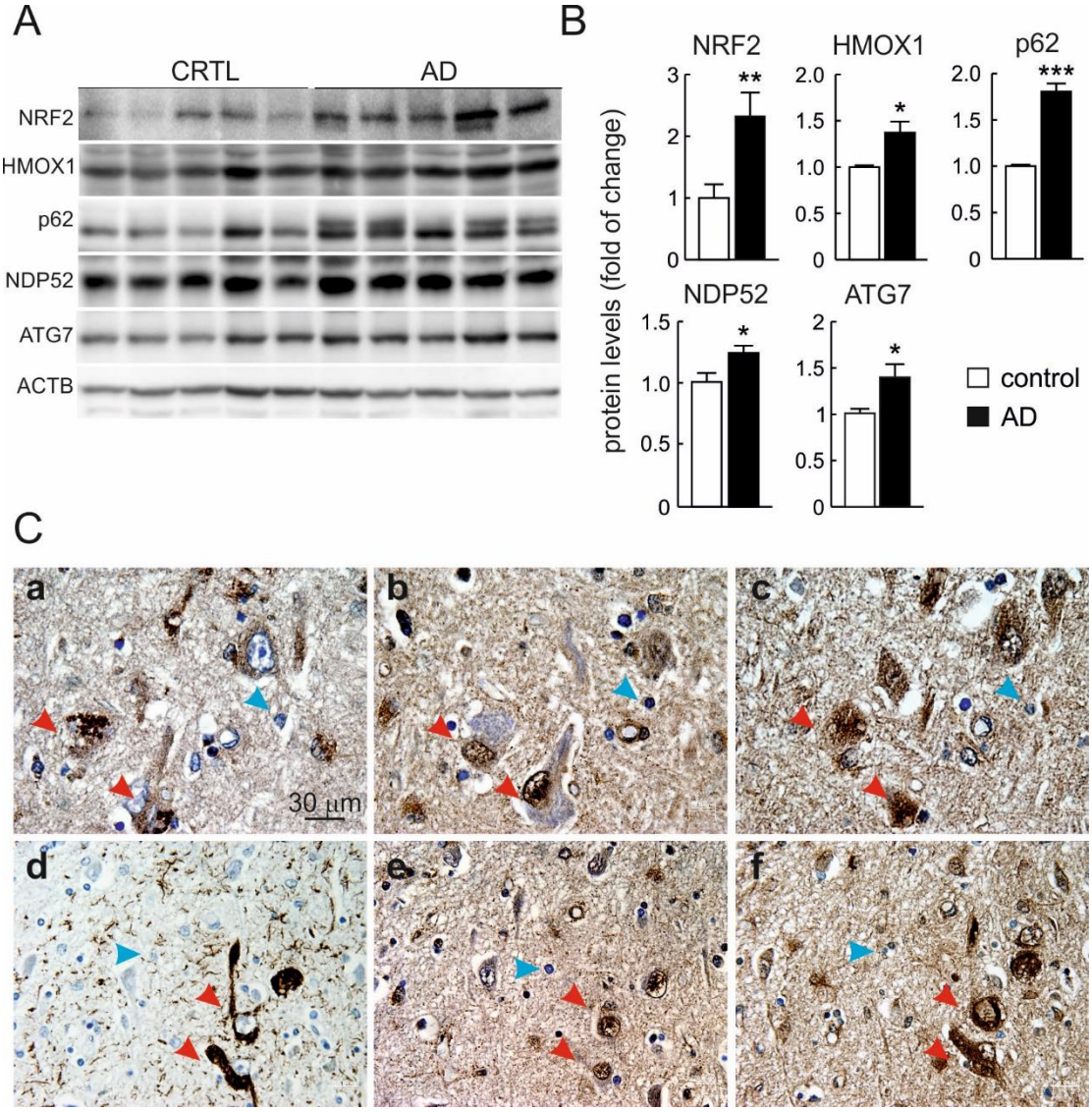

Figure 31. Evidence of NRF2 up-regulation in neurons of AD subjects expressing high levels of APP/Aβ and TAU. A, Immunoblot analysis of NRF2, HMOX1, p62, NDP52, and ATG7 in hippocampus of asymptomatic controls and patients with diagnosed AD with combined amyloidopathy and tauopathy. B, Densitometric quantification of protein levels from representative immunoblots of A relative to ACTB. Data are mean ± SEM (n=5 controls and n=5 AD subjects). Statistical analysis was performed with Student's t test. *p<0.05, *p<0.01 and ***p<0.001 vs. comparing control vs. AD groups. C, Adjacent 4-µm-thick brain sections from AD subjects were immunostained with anti-APP/Aβ (4G8) (a), anti-TAU (HT7) (d), anti-NRF2 (b and e) and anti-p62 (c and f) antibodies. Red arrows point to the same neuron expressing APP/Aβ or TAU, NRF2 and p62; blue arrows depict internal negative controls for cells that do not express APP/Aβ or TAU and present basal staining for NRF2 and p62.

II. NRF2 controls chaperone mediated autophagy through the regulation of *Lamp2a*

1. Identification of putative AREs in the *LAMP2* gene.

Following the same approach as with macroautophagy genes, we first searched the ENCODE database of the human genome for putative AREs in the *LAMP2* gene. Although there are other important players for CMA, the levels of LAMP2A are considered the limiting step for this process [127].

As shown in Fig. 32A, the human *LAMP2* gene contains several MAFF, MAFK and BACH1 binding sites located in H3K27-histone acetylated and DNAse-sensitive regions, both factors being typical of active enhancers. We scanned these binding regions with the script described in the previous section seeking for putative AREs. We detected 8 putative AREs (Table 9) and 3 of them showed a relative score higher than the 80%, which is considered an adequate threshold for significance as previously mentioned.

2. NRF2 binds to functional AREs in the *LAMP2* gene.

To validate the AREs with the highest score (ARE1, ARE2 and ARE3), we analyzed NRF2 binding to these sequences by ChIP analysis. HEK293T cells were transfected with an expression vector for V5-tagged NRF2-$^{\Delta EGTE}$ to facilitate NRF2 stabilization and binding to its target genes. NRF2 was immunoprecipitated with an anti-V5 antibody and an anti-IgG antibody was used as a negative control. NRF2 binding was analyzed by qRT-PCR employing as template the immunoprecipitated DNA and primers designed to specifically amplify ARE1, ARE2 or ARE3. We detected NRF2 binding to the well-known positive control AREs in *HMOX1*, *NQO1* and *SQSTM1*, whereas NRF2 did not bind to *ACTB* or to a region of *NQO1* that does not contain any ARE (*NQO1*).* Immunoprecipitation with V5 showed enrichment

Gene		Localization of the potential ARE	Max Score	Relative score	Putative binding sequence
LAMP2	**(1)**	chrX:119596430-119596441	15.83	0.921	ATGACACTGCA
	(2)	chrX:119 619599-119619610	13.24	0.859	TTGACTCAGCG
	(3)	chrX:119619560-119619571	13.07	0.855	ATGACAAACCA
	(4)	chrX:119562034-119562045	10.62	0.796	ATTACACATCA
	(5)	chrX:119603247-119603258	10.25	0.787	GTGATGTAGCG
	(6)	chrX:119603427-119603416	10.0	0.781	GTAACAAAGCT
	(7)	chrX:119562112-119562101	9.05	0.758	GTGGCTTAGAA
	(8)	chrX:119596457-119596446	4.84	0.657	AAAACCTAGCC

Table 9. Putative Antioxidant Response Elements (AREs) in the *LAMP2* gene. The table also shows the localization in the human genome, the *max score* and the *relative score*.

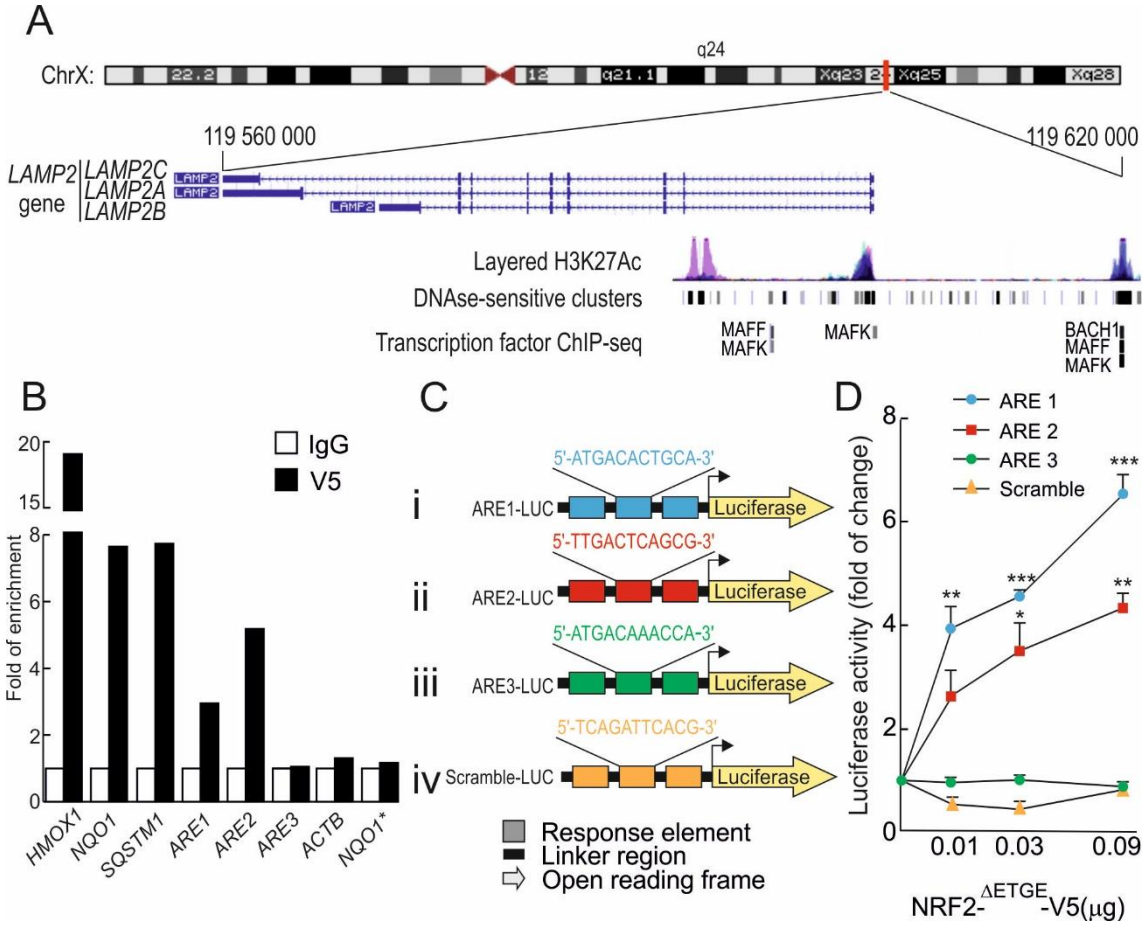

Figure 32. NRF2 binds to 2 functional antioxidant response elements (AREs) in the *LAMP2* gene. A, Scheme of the *LAMP2* gene from The Encyclopedia of DNA Elements at UCSC (ENCODE) for human genome, showing the 3 splice variants: *LAMP2A*, *LAMP2B* and *LAMP2C*. Putative AREs in the *LAMP2* gene were identified taking as reference the available information from ChIP of ARE-binding factors MAFK, MAFF and BACH1. These regions were localized in 200-400 base-pair-long DNAse-sensitive and H3K27Ac-rich regions, i.e. most likely regulatory promoter regions. B, HEK293T cells were transfected with an expression vector for NRF2-$^{\Delta ETGE}$-V5 (lacking the KEAP1 regulatory domain). ChIP analysis was performed with anti-IgG or anti-V5 antibodies and the potential AREs with the highest score, termed ARE1, ARE2 and ARE3 (Table 9), were analyzed by qRT-PCR. The figure shows representative data normalized as the fold of enrichment with the anti-V5 antibody vs. the IgG antibody. The presence of already known AREs in *HMOX1*, *NQO1* and *SQSTM1* was analyzed as positive control and *ACTB*, and a region of *NQO1* that does not contain an ARE (NQO1*) were amplified as negative controls. C, Luciferase reporter constructs carrying 3 tandem putative ARE sequences from the *LAMP2* gene (i-iii) or a scramble sequence as negative control (iv) controlling the expression of luciferase. D, *Nrf2*-KO mouse embryo fibroblasts were co-transfected with the reporters represented in C and increasing amounts of NRF2-$^{\Delta ETGE}$-V5 construct. Values were normalized to pTK-Renilla activity and presented as fold of change. Data are mean ± SEM (n = 3). Statistical analysis was performed using Student's t test. *p< 0.05, ** p<0.01 and *** p<0.001 vs. basal levels.

in ARE1 and ARE2 in *LAMP2* but not in ARE3 (Fig. 32B). Therefore, NRF2 binds to at least two regulatory regions of *LAMP2* gene denoted here as ARE1 and ARE2.

3. AREs found in *LAMP2* are transcriptionally activated by NRF2.

To address the functionality of the putative AREs found in the *LAMP2* gene, we next generated luciferase reporters. Three tandem nucleotide sequences of each ARE1, ARE2 or ARE3, as well as a control aleatory sequence, were cloned in the promoter region of a luciferase reporter (pGL3bv) as shown in Fig. 32C. *Nrf2*-deficient cells were transiently co-transfected with each of these constructs plus a *Renilla* expression vector (pTK-Renilla) used for normalization and increasing amounts of NRF2-$^{\Delta ETGE}$-V5, measuring luciferase expression 48 h after. We found that NRF2 expression induced luciferase activity in a concentration-dependent manner in reporters carrying ARE1 and ARE2 but not ARE3 or the negative control (Fig. 32D).

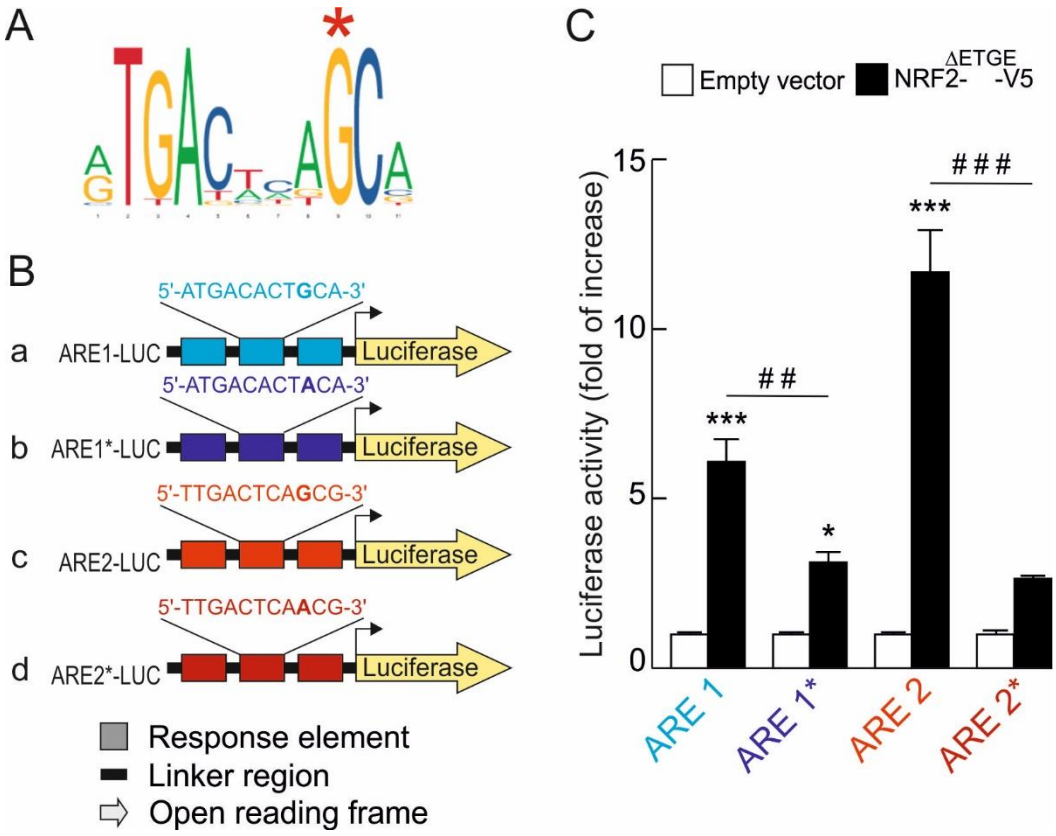

Figure 33. Importance of conserved residues for transcriptional activity of AREs in *LAMP2*. A, Consensus antioxidant response element (ARE) from the JASPAR database. The bigger a letter is, the more conserved is the nucleotide in that position among different already-known AREs. The asterisk shows the conserved G substituted to A. B, Luciferase reporter constructs carrying the 2 functional ARE sequences from the *LAMP2* gene (i-ii) and the same sequences with a substitution G>A in the 9th position (iii-iv) controlling the expression of luciferase. C, *Nrf2*-KO mouse embryo fibroblasts were co-transfected with the control and mutated reporters in B and 0.1 µg of NRF2-$^{\Delta ETGE}$-V5 construct. Values were normalized to pTK-Renilla activity and presented as fold of change. Data are mean ± SEM (n = 3). Statistical analysis was performed using Student's t test. * p< 0.05, ** p<0.01 and *** p<0.001 vs. empty vectors. ## p<0.01 and ### p<0.001 vs. not mutated vectors.

According to the JASPAR consensus ARE shown in Fig. 33A, the most conserved nucleotides are a T, a G and an A in the 2nd, 3rd and 4th positions, respectively, together with a G and a C in the 9th and 10th positions. ARE1 and ARE2 (Fig. 33B a and c) contain all these conserved nucleotides, while ARE3 has a C instead of a G in the 9th position. Therefore, we replaced the highly conserved G to A in ARE1 and ARE2, generating two new reporters shown in Fig. 33B b and d and analyzed luciferase/Renilla activity after co-transfection with 0.1 µg NRF2-$^{\Delta ETGE}$-V5. As shown in Fig. 33C, replacement of this single nucleotide reduced NRF2-induced luciferase expression in both ARE1 and ARE2.

Altogether, these results confirm that ARE1 and ARE2 are transcriptionally activated by NRF2 and point to the importance of the conserved G in the 9th position for their activity, probably explaining why ARE3 is not functional.

4. Genetic manipulation of NRF2 results in alteration of LAMP2A levels.

We analyzed the relevance of NRF2 on LAMP2A expression in HEK293T cells infected with a lentiviral vector expressing NRF2-$^{\Delta ETGE}$-V5 or GFP as a negative control. At 3 days post-infection, we analyzed mRNA expression and protein levels of the *bona fide* NRF2-targets HMOX1 and p62, as well as LAMP2A. As shown in Fig. 34A-C, NRF2 overexpression led to a modest but consistent increase in both the mRNA and protein levels of LAMP2A, as well as in the positive controls HMOX1 and p62.

In addition, we used a knockdown strategy to reduce NRF2 activity in the lung carcinoma cell line A549, characterized by constitutive NRF2 activation [178, 179]. A549 cells were infected with a lentiviral vector expressing a short hairpin RNA against human *NFE2L2* (shNRF2) or a random sequence used as a negative control (shCTRL). We analyzed mRNA and protein levels after 3 days of infection, observing that NRF2-knockdown reduced both mRNA and protein levels of HMOX1, p62 and also LAMP2A (Fig. 34D-F). We did not observe consistent differences in the expression levels of the LAMP2B or LAMP2C isoforms upon NRF2 overexpression (Fig. 34A-C) or silencing (Fig. 34D-F) (see Discussion).

Our combined results in both human cell lines support a NRF2-dependent basal regulation of LAMP2A levels. Because CMA has been well characterized in liver, we focused most of the functional study on the regulation of LAMP2A by NRF2 in mouse hepatocytes. First, we determined mRNA levels of *Lamp2a* in *Nrf2*-WT vs. *Nrf2*-KO immortalized hepatocytes. In line with our results in human cells, NRF2 deficiency resulted in reduced *Hmox1*, *Sqstm1* and *Lamp2a* expression levels (Fig. 35A).

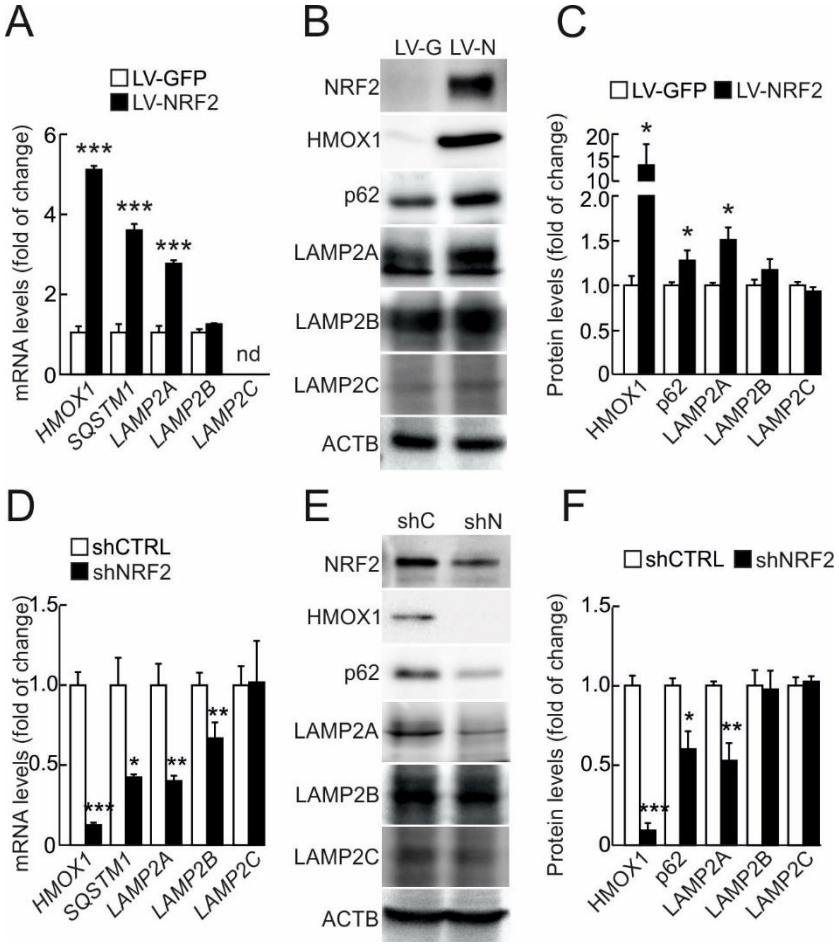

Figure 34. LAMP2A levels are modified upon genetic manipulation of NRF2. A, HEK293T cells were transduced with GFP- or NRF2-$^{\Delta ETGE}$-V5-expressing lentivirus (LV-GFP or LV-NRF2, respectively). Expression levels of the indicated genes were determined 3 days post-infection by qRT-PCR and normalized to *ACTB* levels. Data are mean ± SEM (n = 4). Statistical analysis was performed with Student's t test. ***p<0.001 vs. LV-GFP-infected cells. B, Representative immunoblots for the indicated proteins in cells transduced in A. C, Densitometric quantification of representative immunoblots from B relative to ACTB protein levels. Data are mean ± SEM (n=4). Statistical analysis was performed using Student's t test. *p<0.05 vs. LV-GFP-infected cells. D, A549 cells were transduced with a lentivirus carrying shRNA against a scramble sequence (shCTRL) or against NRF2 (shNRF2). Expression levels of the indicated genes were determined 3 days post-infection by qRT-PCR and normalized to *ACTB* levels. Data are mean ± SEM (n = 4). Statistical analysis was performed with Student's t test. *p<0.05, **p<0.01 and ***p<0.001 vs. shCTRL infected cells. E, Representative immunoblots for the indicated proteins in cell lysates from cells transduced as in D. F, Densitometric quantification of representative immunoblots from E relative to ACTB protein levels. Data are mean ± SEM (n=4). Statistical analysis was performed using Student's t test. . *p<0.05; **p<0.01 and ***p<0.001 vs. shCTRL infected cells.

We next performed a rescue experiment, in which lentivirally-induced overexpression of NRF2-$^{\Delta ETGE}$-V5 partially rescued the mRNA expression of these 3 genes in *Nrf2*-KO hepatocytes (Fig. 35B). Accordingly, a modest reduction in LAMP2A protein levels was detected in whole cell lysates of *Nrf2*-KO hepatocytes when compared to *Nrf2*-WT lysates (Fig. 35C and 35D). We then isolated lysosomes and immunoblotted them for LAMP2A, taking LAMP1 as a control lysosomal protein that is not involved in CMA. Very relevant,

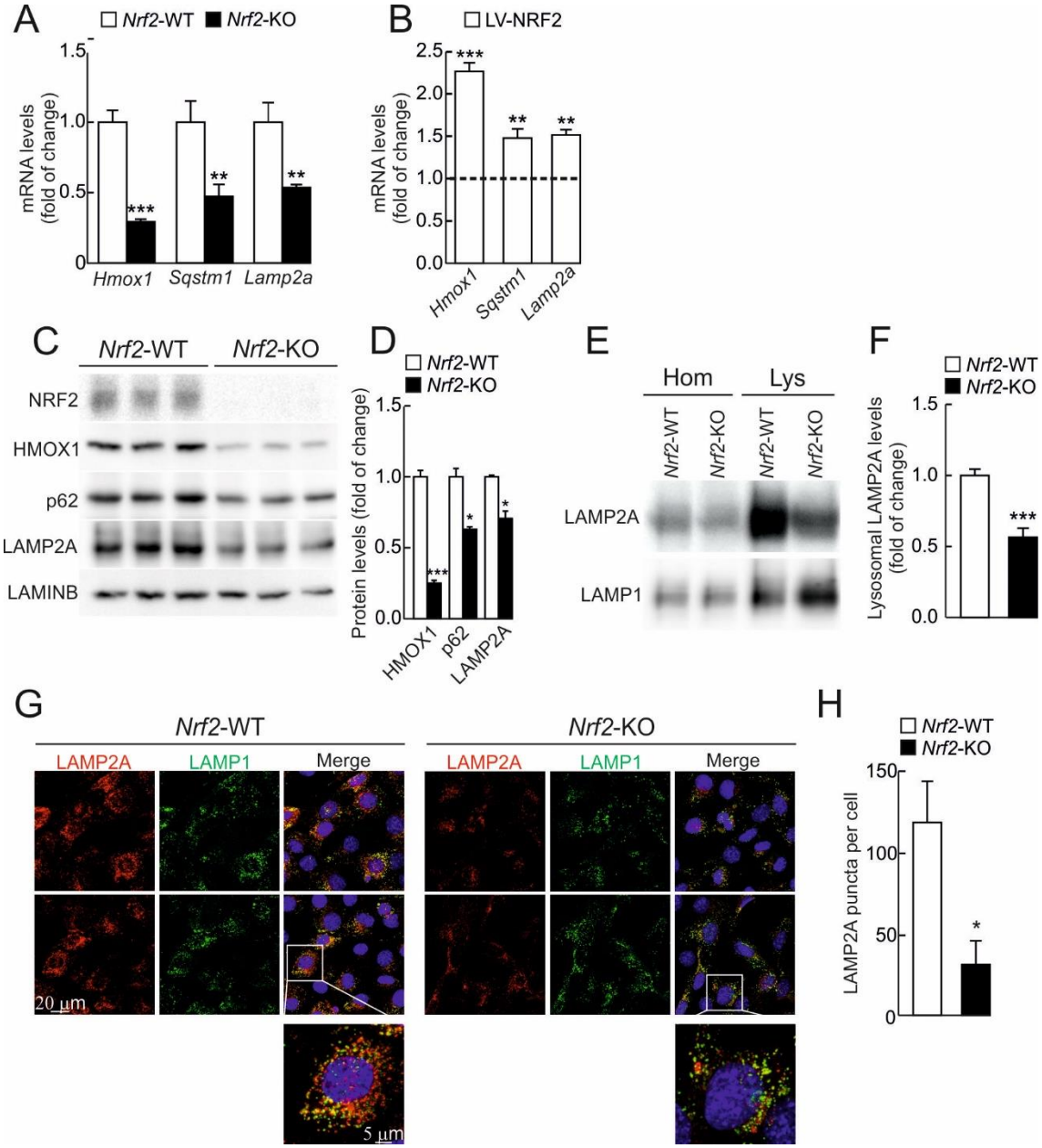

Figure 35. LAMP2A levels are reduced in the absence of NRF2. A, Expression levels of *Hmox1*, *Sqstm1* and *Lamp2a* from *Nrf2*-WT and *Nrf2*-KO immortalized hepatocytes were determined by qRT-PCR and normalized to *Actb* levels. Data are mean ± SEM (n = 4). Statistical analysis was performed with Student's t test. **p<0.01 and ***p<0.001 vs. *Nrf2*-WT cells. B, *Nrf2*-KO immortalized hepatocytes were rescued with an NRF2-$^{\Delta ETGE}$-V5-expressing lentivirus (LV-NRF2). Expression levels of *Hmox1*, *Sqstm1* and *Lamp2a* were analyzed 3 days post-infection by qRT-PCR and normalized to *Tbp* levels. The dotted line represents expression levels of cells transduced with a control lentivirus (LV-GFP). Data are mean ± SEM (n=4). Statistical analysis was performed with Student's t test. **p<0.01 and ***p<0.001 vs. LV-GFP infected cells. C, Representative immunoblots for the indicated proteins in *Nrf2*-WT and *Nrf2*-KO hepatocytes. D, Densitometric quantification of representative immunoblots from C relative to LAMIN B levels. Data are mean ± SEM (n=3). Statistical analysis was performed using Student's t test. **p<0.01 and ***p<0.001 vs. *Nrf2*-WT cells. E, Representative immunoblots of LAMP2A and LAMP1 in homogenates (Hom) and isolated lysosomes (Lys) from *Nrf2*-WT and *Nrf2*-KO hepatocytes. F, Densitometric quantification of representative immunoblots from E relative to LAMP1 levels. Data are mean ± SEM (n=6). Statistical analysis was performed using Student's t test. ***p<0.001 vs. *Nrf2*-WT levels. G, Confocal analysis of double immunofluorescence with anti-LAMP2A (red) and anti-LAMP1 (green) antibodies in *Nrf2*-WT and *Nrf2*-KO hepatocytes. The inset shows a higher magnification of the indicated cell. H, Quantification of the total number of LAMP2A-positive puncta per cell. Values are mean ± SEM (n=3, with >50 cells counted per experiment). Statistical analysis was performed using Student's t test. *p<0.05 vs. *Nrf2*-WT cells.

there was a dramatic reduction in lysosomal LAMP2A levels in the absence of NRF2, whereas no changes or even a slight increase in LAMP1 could be observed (Fig. 35E and 35F). Finally, we analyzed LAMP2A levels in lysosomes by immunofluorescence and, as shown in Fig. 35G and 35H, the overall intensity and the number of puncta per cell of LAMP2A (red), which co-localized with LAMP1 (green), were dramatically reduced in *Nrf2*-KO compared with *Nrf2*-WT hepatocytes. From these results we conclude that the absence of NRF2 correlates with a reduction in mRNA and protein levels of LAMP2A, especially in the lysosomal fraction.

5. NRF2 induces LAMP2A upon oxidative stress.

The physiological significance of this novel regulation was evaluated in the context of oxidative stress. First, we characterized the redox status of immortalized hepatocytes derived from *Nrf2*-WT or *Nrf2*-KO mice. We employed the fluorescent dye dihydroethidium (DHE), which can be oxidized to ethidine by ROS (especially superoxide), exhibiting bright red fluorescence. As shown in Fig. 36A and 36B, DHE staining did not reflect major differences in ROS levels between *Nrf2*-WT or *Nrf2*-KO hepatocytes under basal conditions. However, upon treatment with the oxidative stress-inducing drug paraquat (PQ, 200 μM, 16 h), *Nrf2*-KO hepatocytes exhibited increased DHE fluorescence compared to *Nrf2*-WT cells.

Considering that NRF2 controls the production of the universal reducing agent NADPH, we analyzed the ratio between oxidized $NADP^+$ and reduced NADPH in these cells by a colorimetric method. As expected, *Nrf2*-KO hepatocytes showed an augmented $NADP^+$/NADPH ratio, indicative of increased oxidative status (Fig. 36C). Altogether, these results suggest that the NADPH levels in *Nrf2*-KO hepatocytes may be sufficient to handle ROS under basal conditions (similar DHE staining), but not in the presence of oxidants such as PQ (increased ROS in *Nrf2*-KO cells as reflected by DHE staining). In the context of CMA, a more oxidant environment should result in increased *Lamp2a* levels. Nevertheless, treatment with increasing concentrations of PQ (Fig. 36D and 36E) and H_2O_2 (Fig. 36F and 36G) for 16 h, led to increased NRF2, HMOX1, p62 and LAMP2A levels in *Nrf2*-WT but not in *Nrf2*-KO hepatocytes.

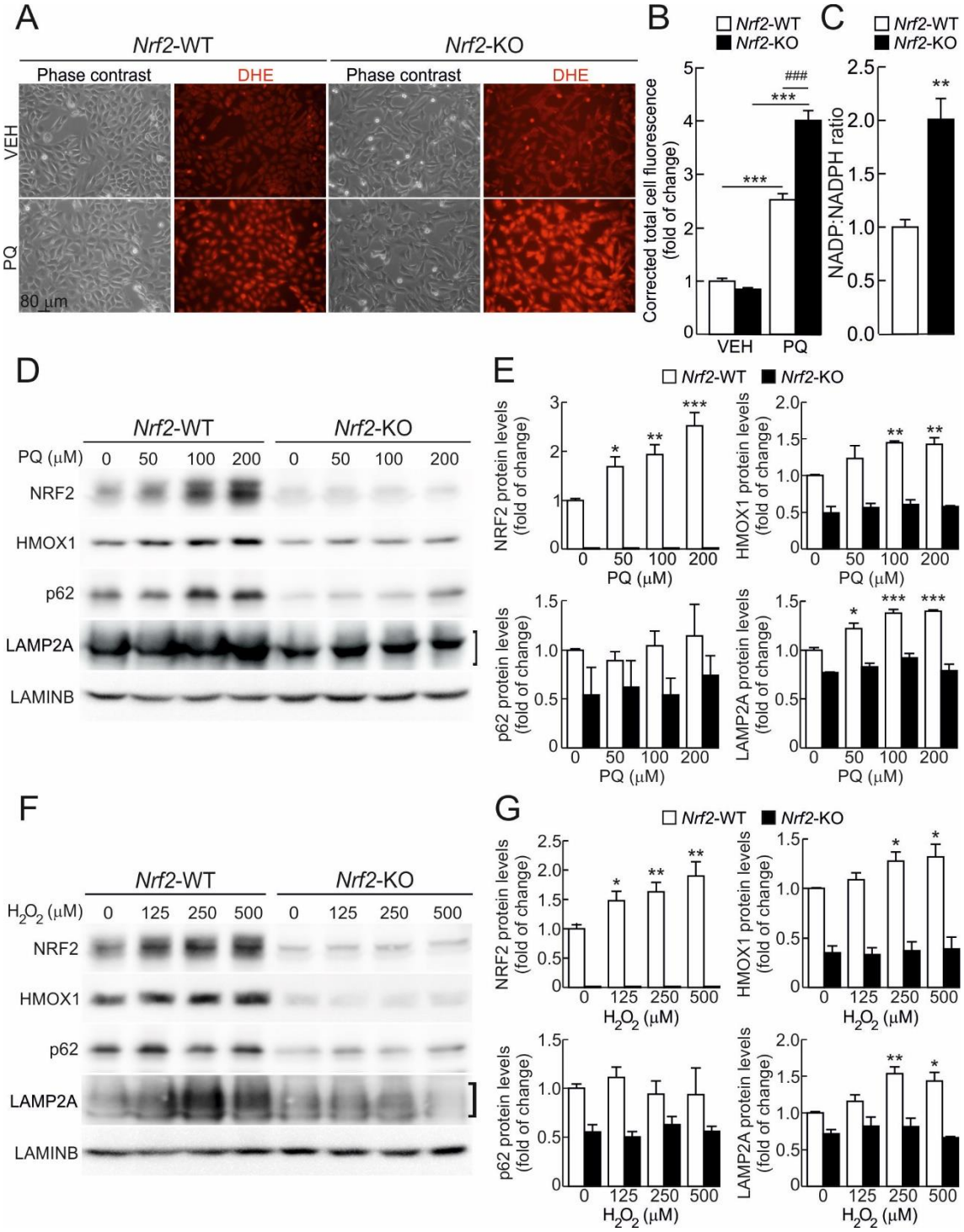

Figure 36. Oxidants induce LAMP2A in a NRF2-dependent manner. A, Representative images of ROS levels determined with dihydroethidium (DHE) in immortalized *Nrf2*-WT and *Nrf2*-KO hepatocytes under basal conditions (VEH) or after treatment with paraquat (PQ, 200 μM, 16 h). The probe was added to a final concentration of 5 μM 1 h before *in vivo* imaging of the cells. B, Corrected total cell fluorescence of representative images from A. Values are mean ± SEM (n=100 cells, derived from at least 3 different fields). Statistical analysis was performed using Student's t test. ***p<0.001 vs. untreated conditions; ###p<0.001 vs. *Nrf2*-WT cells. C, NADP:NADPH ratio in *Nrf2*-WT and *Nrf2*-KO hepatocytes. Data are mean ± SEM (n=4). Statistical analysis was performed using Student's t test. **p<0.01 vs. *Nrf2*-WT cells. D-G, Immortalized hepatocytes from *Nrf2*-WT and *Nrf2*-KO mice were submitted to the indicated concentrations of PQ (D-E) or hydrogen peroxide (H_2O_2) (F-G) for 16 h. Representative immunoblots for the indicated proteins in cell lysates. E and G, Densitometric quantification of representative immunoblots from D and F, respectively, relative to LAMIN B protein levels. Data are mean ± SEM (n=3). Statistical analysis was performed using Student's t test. *p<0.05, **p<0.01 and ***p<0.001 vs. untreated conditions

6. NRF2 controls CMA activity under basal and oxidant conditions.

We analyzed CMA activity in *Nrf2*-WT vs. *Nrf2*-KO hepatocytes by using a lentivirus expressing the photoactivable CMA-specific fluorescent substrate KFERQ-PS-Dendra (modified from [189]). Upon 405 nm light exposure, Dendra protein is modified to emit red fluorescence. This tool allows tracking the subcellular localization of this protein without the interference of newly synthesized protein. CMA activity is then detected as a change from diffuse (cytosolic) fluorescence to a punctate (lysosomal) pattern, as the fluorescence substrate is delivered to CMA-active lysosomes (see Fig. 8 in 'Materials and Methods'). As shown in Fig. 37A and 37C, *Nrf2*-WT cells exhibited a low cytosolic signal and some Dendra-positive fluorescent puncta, reflecting basal CMA activity. However, a more intense and diffuse fluorescent pattern throughout the cytoplasm, together with an extremely reduced number of Dendra-positive puncta per cell, were observed in *Nrf2*-KO cells, consistent with impaired basal CMA activity. This observation indicates that the KFERQ-PS-Dendra reporter is not being properly degraded by CMA and accumulates in the cytosol. Besides, when cells were treated with PQ, a well-characterized activator of CMA [124], we found a significant increase in Dendra-positive puncta per cell in *Nrf2*-WT but not in *Nrf2*-KO hepatocytes, indicating impaired induction of CMA by PQ in the absence of NRF2 (Fig. 37B and 37C).

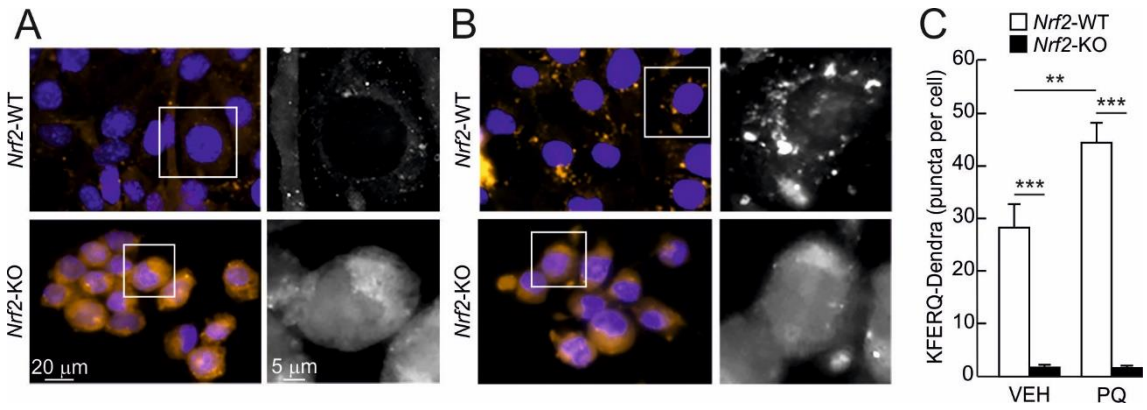

Figure 37. The oxidant agent paraquat (PQ) induces CMA in a NRF2-dependent manner. A and B, *Nrf2*-WT and *Nrf2*-KO hepatocytes were transduced with a lentivirus carrying the CMA reporter KFERQ-PS-Dendra and, after photoswitching, were cultured without additions (A) or in the presence of 100 μM paraquat (PQ) (B) for 16 h. CMA was analyzed as the number of fluorescent puncta per cell at the end of the incubation time. Representative full-field images and inset showing black and white high magnification of the boxed regions in the Dendra channel. C, Quantification of the number of puncta per cell after the indicated treatment. Values are mean ± SEM (n=3, with >75 cells per experiment). Statistical analysis was performed using Student's t test. **p<0.01 and ***p<0.001 vs. *Nrf2*-WT cells or untreated conditions.

7. Pharmacological activation of NRF2 induces LAMP2A and CMA.

We next used two well-established activators of NRF2, sulforaphane (SFN) and dimethylfumarate (DMF), to test if pharmacological activation of NRF2 could lead to augmented LAMP2A levels. As observed in Fig. 38A to 38D, treatment of *Nrf2*-WT hepatocytes with increasing concentrations of SFN (Fig. 38A-B) or DMF (Fig. 38C-D) for 16 h led to increased protein levels of NRF2, HMOX1, p62 and also LAMP2A, and this response was abolished in *Nrf2*-KO cells.

As shown in Fig. 38E and 38F, immunofluorescence analysis of LAMP2A (red) and LAMP1 (green) revealed that SFN-treated cells displayed mobilization of lysosomes (labeled either with LAMP2A or LAMP1) toward the perinuclear region, a typical characteristic of CMA activation [124]. Nevertheless, perinuclear LAMP2A fluorescence was much lower in the absence of NRF2.

To confirm CMA activation, we transduced cells with the KFERQ-PS-Dendra reporter (Fig. 39A and 39B). Under basal conditions, we found some Dendra positive puncta in *Nrf2*-WT vs. a much more diffuse pattern with almost no puncta in *Nrf2*-KO hepatocytes. SFN treatment induced a significant dose-dependent increase in Dendra-positive puncta per cell in *Nrf2*-WT cells (note that because perinuclear relocation made individual puncta indiscernible, data are presented as punctate KFERQ-Dendra positive area per cell). By contrast, SFN treatment failed to upregulate CMA in the absence of NRF2.

All in all, NRF2 pharmacological up-regulation induces LAMP2A expression and, consequently, CMA activation.

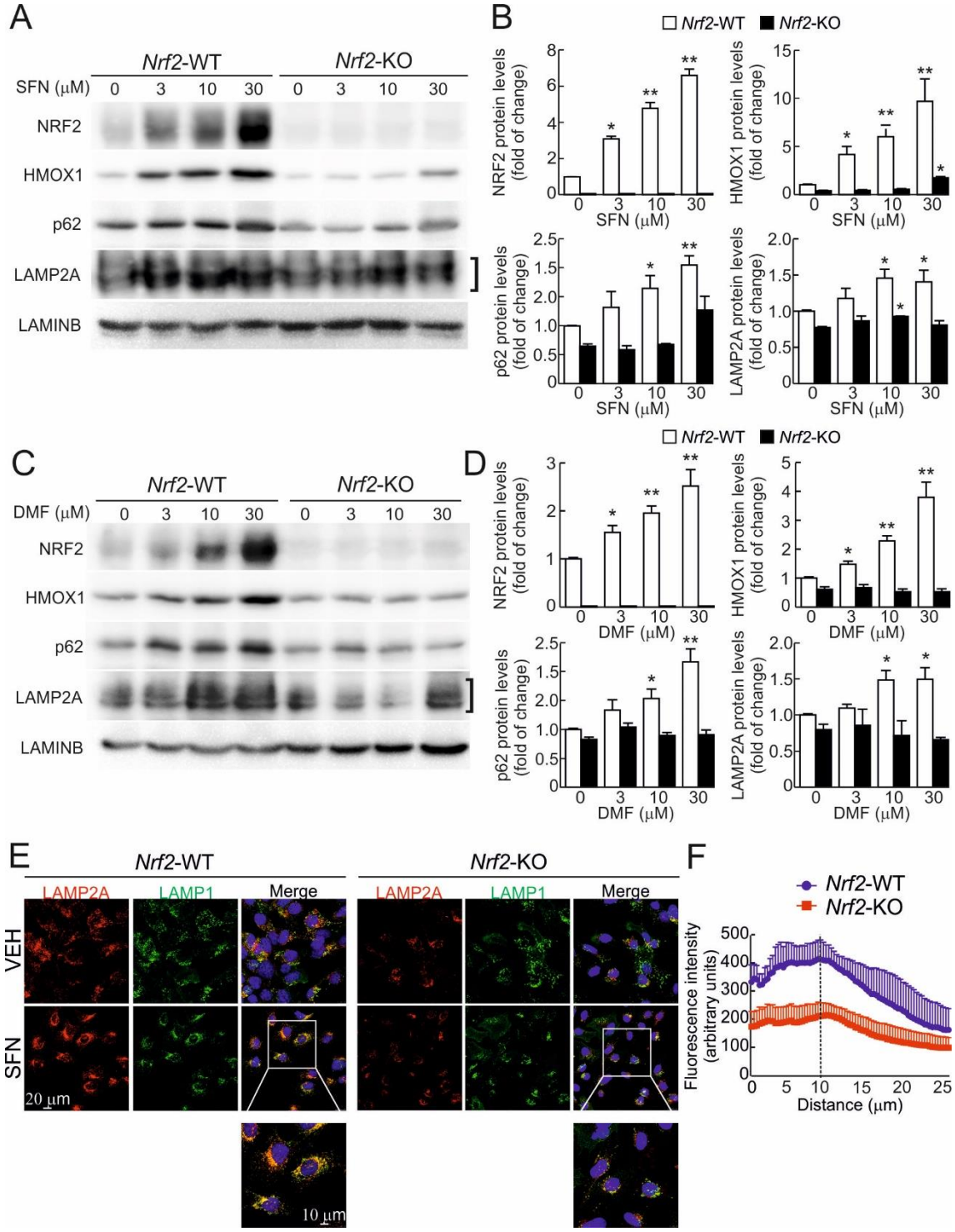

Figure 38. Pharmacological activation of NRF2 induces LAMP2A. A-D, Immortalized hepatocytes from *Nrf2*-WT and *Nrf2*-KO mice were submitted to the indicated concentrations of sulforaphane (SFN) or dimethyl fumarate (DMF) for 16 h. Representative immunoblots for the indicated proteins in cell lysates. B and D, Densitometric quantification of representative immunoblots from A and C, respectively, relative to LAMIN B protein levels. Data are mean ± SEM (n=3). Statistical analysis was performed using Student's t test. *p<0.05 and **p<0.01 vs. untreated conditions. E, Confocal analysis of double immunofluorescence with anti-LAMP2A (red) and anti-LAMP1 (green) antibodies in immortalized *Nrf2*-WT and *Nrf2*-KO hepatocytes treated with vehicle (VEH) or sulforaphane (SFN, 15 μM, 16 h). The inset shows a higher magnification of the indicated cells. F, Radial profile of LAMP2A fluorescence in cells treated with SFN in E. The graph shows the total mean fluorescence as a function of radial distance to the center of the cell. The dashed line represents the nuclear limits. Quantification was done with *Z*-stack. Values are mean ± SEM (n=3, with >50 cells counted per experiment).

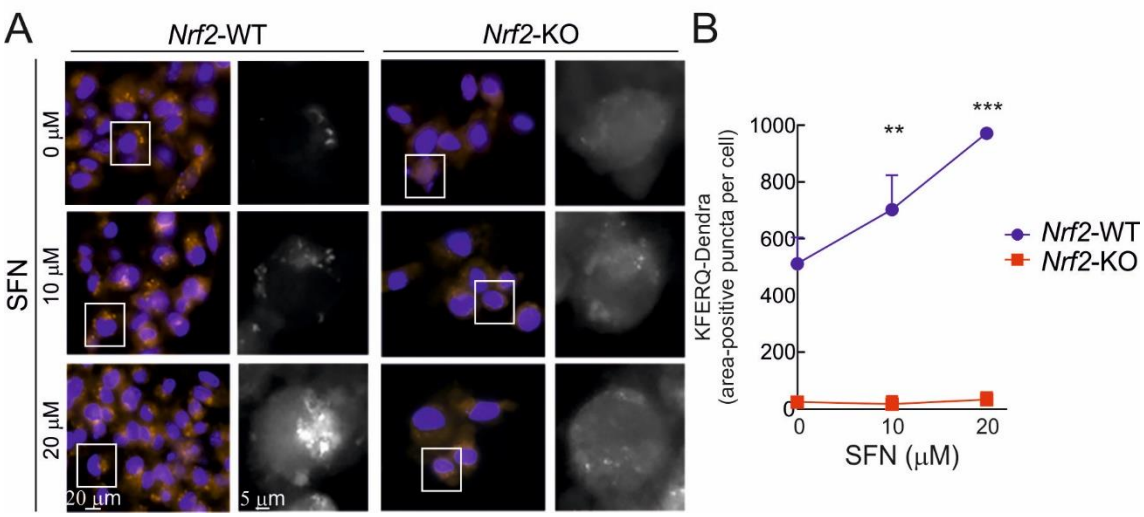

Figure 39. *Nrf2*-WT and *Nrf2*-KO hepatocytes were transduced with a lentivirus carrying the CMA reporter KFERQ-PS-Dendra and, after photoswitching, were cultured without additions or in the presence of 10 μM or 20 μM SFN for 16 h. CMA was analyzed as the area positive for fluorescent puncta per cell at the end of the incubation time. Representative full-field images and inset showing black and white high magnification of the boxed regions in the Dendra channel. B, Quantification of the KFERQ-Dendra-positive area per cell. Values are mean ± SEM (n=3, with >75 cells per experiment). Statistical analysis was performed using Student t test. **p<0.01 and ***p<0.001 vs. untreated conditions.

8. CMA activation by NRF2 is independent on macroautophagy.

Previous studies have shown multiple levels of cross-talk between CMA and macroautophagy [132, 137, 203]. Because we have shown that NRF2 regulates macroautophagy, we investigated if CMA activation by NRF2 was a direct effect or a consequence of changes in macroautophagy. We employed *Atg5*-KO MEFs since ATG5 is a non-redundant and essential protein in macroautophagy, enabling LC3 conjugation to phosphatidylethanolamine, as demonstrated by the fact that *Atg5*-KO cells are unable to construct autophagosomes properly [204]. We treated *Atg5*-KO MEFs with increasing concentrations of SFN for 16 h, and still observed induction of LAMP2A (Fig. 40A and 40B). We also evaluated CMA in *Atg5*-WT and *Atg5*-KO MEFs transduced with the KFERQ-PS-Dendra reporter. As presented in Fig. 40C and 40D, basal CMA activity was slightly higher in *Atg5*-KO cells, consistent with CMA up-regulation due to impairment of macroautophagy. However, SFN resulted in a similar increase in the area positive of puncta per cell independent on the genotype. These findings indicate that the regulation of CMA by NRF2 occurs, for the most part, independently of changes in macroautophagy.

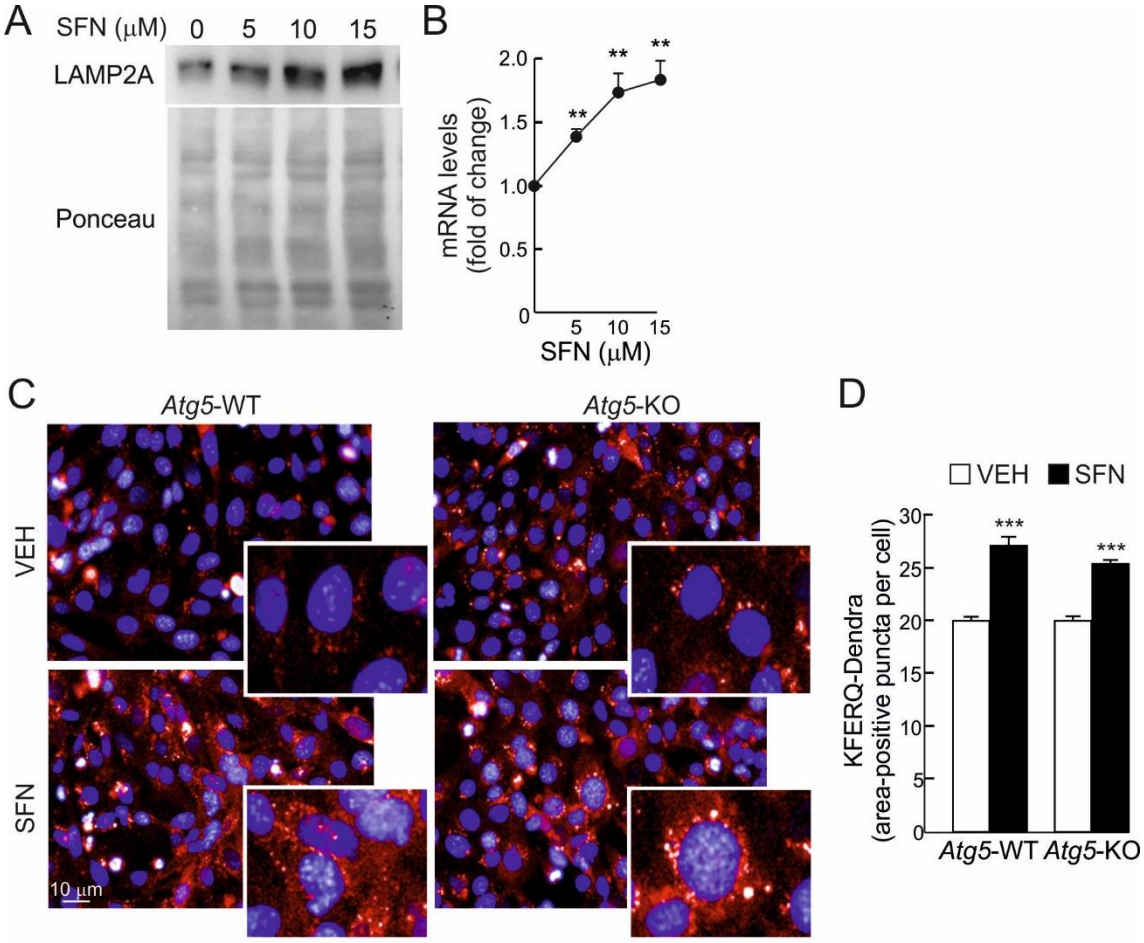

Figure 40. Pharmacological activation of NRF2 with sulforaphane (SFN) modulates LAMP2A and CMA independently of macroautophagy. A and B, MEFs from *Atg5*-KO mice were submitted to the indicated concentrations of SFN for 16 h. Representative immunoblot of LAMP2A levels (A) and expression levels of *Lamp2a* determined by qRT-PCR and normalized to *Actb* levels (B). Data are mean ± SEM (n = 3). Statistical analysis was performed using Student's t test. **p<0.01 untreated conditions. C, *Atg5*-WT and *Atg5*-KO MEFs were transduced with a lentivirus carrying the CMA reporter KFERQ-PS-Dendra and, after photoswitching, were cultured in 96-well glass-bottom plates without additions or in the presence of sulforaphane (SFN, 30 μM, 16 h). Cells were imaged using high-content microscopy and CMA was analyzed as the number of fluorescent puncta per cell at the end of the incubation time. Representative full-field images and inset at higher magnification. D, Quantification of the number of puncta per cell after the indicated treatment. Values are mean ± SEM (n=3, with >25000 cells per experiment). Statistical analysis was performed using Student's t test. ***p<0.001 vs. untreated conditions.

9. Conservation of the NRF2/LAMP2A axis among different cell types.

We analyzed the regulation of LAMP2A by NRF2 in different cell types upon genetic and pharmacological NRF2 manipulation. In addition to human A549 and murine hepatocytes, reduction of *LAMP2A/Lamp2a* levels in the absence of NRF2 was also confirmed in human astrocytes and mouse HT22 cells with NRF2-knockdown, as well as MEFs and cortical neurons derived from *Nrf2*-WT *vs Nrf2*-KO mice (Fig.41A and 41B).

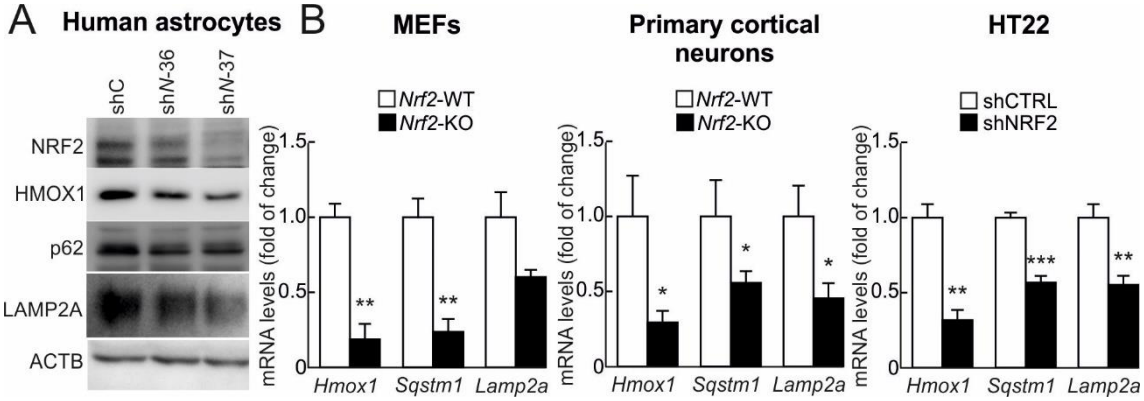

Figure 41. NRF2-LAMP2A axis is functional in different cell types. A, Immunoblot of the indicated proteins in human primary astrocytes transduced with lentivirus carrying shRNA against a scramble sequence (shCTRL) or 2 different shRNA against *Nrf2* (shN-36 and shN-37). B, Expression levels of *Hmox1*, *Sqstm1* and *Lamp2a* in primary mouse embryonic fibroblasts (MEFs) and primary cortical neurons obtained from *Nrf2*-WT and *Nrf2*-KO mice, as well as hippocampal murine HT22 cells transduced with lentivirus carrying shRNA against a scramble sequence (shCTRL) or *Nrf2* (sh*Nrf2*), were determined by qRT-PCR and normalized to *Actb* levels. Data are mean ± SEM (n = 3). Statistical analysis was performed using Student's t test. *p<0.05 and **p<0.01 vs. *Nrf2*-WT or shCTRL cells.

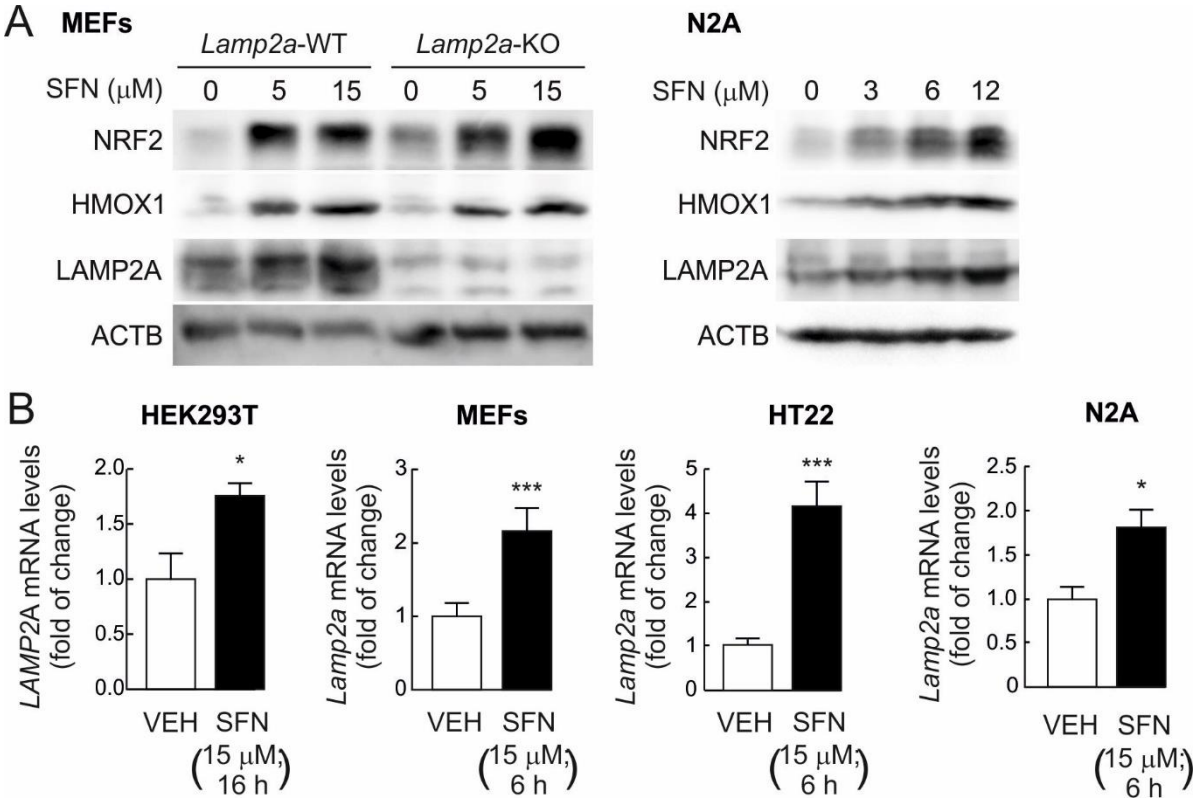

Figure 42. NRF2-LAMP2A axis is functional in different cell types. A, Mouse embryonic fibroblasts (MEFs) and neuroblastoma N2A cells were submitted to the indicated concentrations of SFN (16 h). Representative immunoblots of the indicated proteins. B, Different cell types were submitted to the indicated concentrations of SFN for the indicated periods of time. Expression levels of *Hmox1* and *Lamp2a* were determined by qRT-PCR and normalized to *Actb* levels. Data are mean ± SEM (n = 3). Statistical analysis was performed using Student's t test. *p<0.05 and ***p<0.001 vs. untreated conditions.

Moreover, pharmacological activation of NRF2 with SFN also led to increased LAMP2A/*Lamp2a* mRNA and protein levels in human HEK293T, mouse HT22, MEFs and N2A cells (Fig. 42A and 42B). Altogether, these results point to the conservation of this NRF2/LAMP2A axis among different cell types in humans and mice.

10. Impaired CMA in lysosomes from livers of *Nrf2*-KO mice.

To analyze the functional role of NRF2 in the modulation of CMA *in vivo*, we analyzed the expression levels of *Hmox1*, *Sqstm1* and *Lamp2a* in livers of *Nrf2*-WT and *Nrf2*-KO mice by qRT-PCR. Consistent with our results with cultured hepatocytes, mRNA levels of these three genes were reduced in the absence of NRF2 (Fig. 43A). Analysis of lysosomes isolated from these livers revealed a discrete decrease in LAMP2A levels in the *Nrf2*-KO group (Fig. 43B and 43C). The discrete differences in lysosomal LAMP2A levels might be the consequence of an overall increase in the ratio between lysosomal components and cargo in the *Nrf2*-KO mice because of their lower CMA activity. In fact, contrary to the decrease in LAMP2A, the levels of other lysosomal resident proteins such as HSC70 or β-Glucocerebrosidase (GBA) were relatively higher in the lysosomes of *Nrf2*-KO mice when compared to their wild type counterparts (Fig. 43B and 43C).

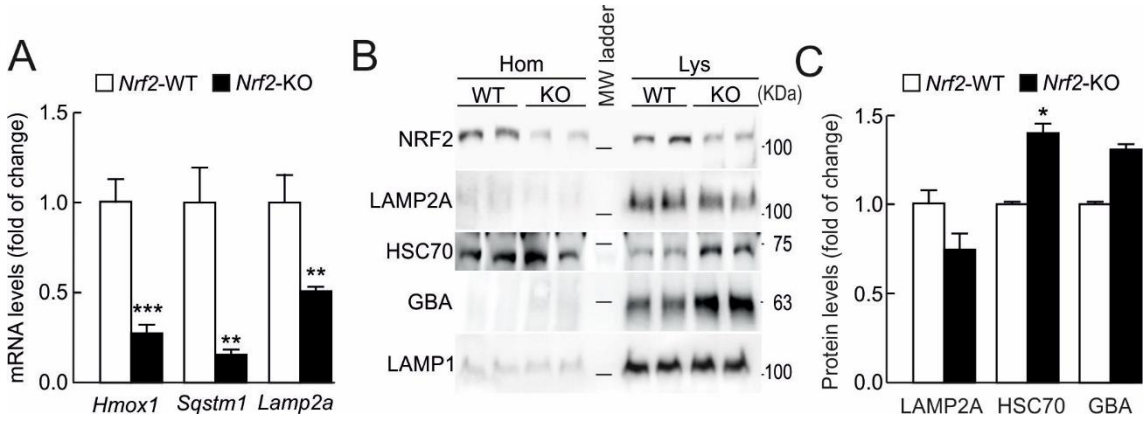

Figure 43. Role of NRF2 in the modulation of CMA *in vivo*. A, Expression levels of *Hmox1*, *Sqstm1* and *Lamp2a* in livers from *Nrf2*-WT and *Nrf2*-KO mice were determined by qRT-PCR and normalized by the geometric mean between *Actb*, *Gapdh* and *Tbp* levels. Data are mean ± SEM (n=4). Statistical analysis was performed using Student's t test. **p<0.01 and ***p<0.001 vs. *Nrf2*-WT mice. B, Immunoblots for the indicated proteins in homogenates and isolated lysosomes from livers of *Nrf2*-WT or *Nrf2*-KO mice. C, Densitometric quantification of lysosomal proteins in B relative to LAMP1 levels. Data are mean ± SEM (n=3 livers per mouse genotype). Statistical analysis was performed using Student's t test. *p<0.05 vs. *Nrf2*-WT mice. (GBA, β-glucocerebrosidase).

To directly measure CMA in isolated lysosomes, we incubated them with purified recombinant RNAse A, a bona fide substrate of CMA [116], in the absence or presence of proteasome inhibitors (PI). The amount of RNAse A recovered in untreated lysosomes represents the fraction bound at the lysosomal membrane, because the protein internalized during the incubation time is rapidly degraded. Pretreatment with PI allows recovering lysosomes with both the RNAse A bound and the one internalized for degradation (see Fig. 9 in 'Materials and Methods'). Thus, uptake was calculated as the difference in RNAse A levels between non-treated and PI-treated conditions. As shown in Fig. 44A and 44B, lysosomes from *Nrf2*-KO mice showed a trend toward reduced RNAse A uptake in comparison with *Nrf2*-WT littermates, although it did not reach statistical significance. We confirmed that the observed differences were not due to differences in lysosomal membrane integrity (Fig. 44C) or reduced proteolytic activity, which was in fact higher in the absence of NRF2 (Fig. 44D).

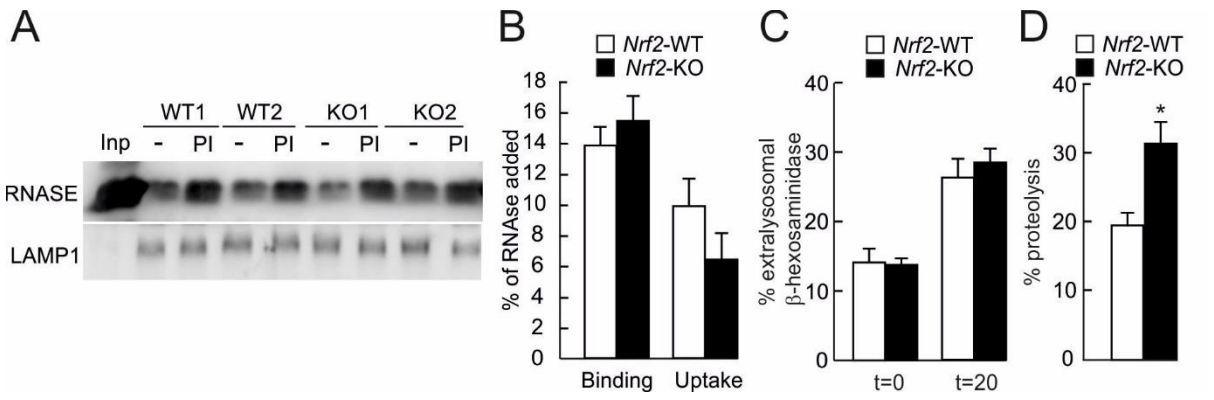

Figure 44. RNAse A uptake in lysosomes extracted from livers of *Nrf2*-WT and *Nrf2*-KO mice. A, Lysosomes isolated from livers of *Nrf2*-WT and *Nrf2*-KO mice were pretreated or not with protease inhibitors (PI) to inhibit lysosomal proteolysis and incubated with purified RNAse A for 20 min at 37ºC. At the end of the incubation, lysosomes were recovered by centrifugation and subjected to SDS-PAGE and immunoblot for the indicated proteins. LAMP1 is shown as control of similar lysosomal recovery after the incubation. B, Densitometric quantification of RNAse A binding and uptake in *Nrf2*-WT or *Nrf2*-KO isolated lysosomes. Data are mean ± SEM (n=3 livers per mouse genotype). Statistical analysis was performed using Student's t test. C, Lysosomes isolated from livers of *Nrf2*-WT and *Nrf2*-KO mice were collected by centrifugation right after isolation or after 20 min incubation at 37ºC, and β-hesoxaminidase activity was measured in pellets and supernatant. Broken lysosomes were calculated as the percentage of total lysosomal β-hesoxaminidase activity detected in the media. Data are mean ± SEM (n = 3 livers per mouse genotype). D, Lysosomes isolated from livers of *Nrf2*-WT and *Nrf2*-KO mice were treated with 0.1% Triton X-100 to disrupt the lysosomal membrane (broken lysosomes) and incubated with a pool of 3H-labeled cytosolic proteins for 20 min at 37ºC. At the end of the incubation samples were precipitated in acid and filtered to calculate the amount of proteolysis as the percentage of initial radioactivity in protein (precipitable) detected in free amino acids and small peptides (soluble) at the end of the incubation. Data are mean ± SEM (n = 3 livers per mouse genotype). Statistical analysis was performed using Student's t test. *p<0.05 vs. *Nrf2*-WT mice.

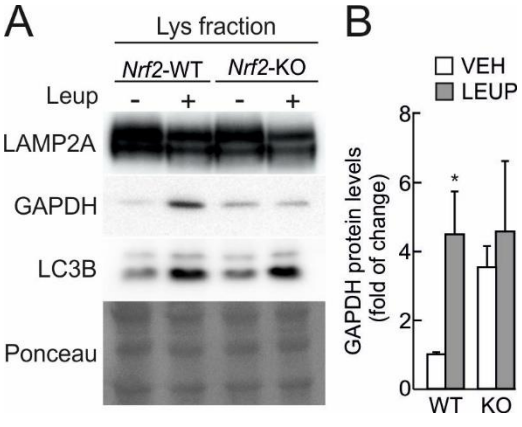

Figure 45. Impaired degradation of endogenous GAPDH in lysosomes from *Nrf2*-KO mice. A, *Nrf2*-WT and *Nrf2*-KO mice were starved for 24 h. Lysosomal proteolysis was inhibited *in vivo* with 2 intraperitoneal injections of leupeptin (Leup, 2 mg/100g body weight) 16 and 2 h before sacrifice. Representative immunoblots of the indicated endogenous proteins in lysosomal-enriched fractions from livers of *Nrf2*-WT (WT) and *Nrf2*-KO (KO) mice. B, Densitometric quantification of representative immunoblots from A relative to total protein levels stained with Ponceau Red. Data are mean ± SEM (n=3). Statistical analysis was performed using Student's t test. *p<0.05 vs. *Nrf2*-WT vehicle-treated mice.

We also measured the degradation of the endogenous CMA substrate GAPDH [116] in lysosomes from *Nrf2*-WT and *Nrf2*-KO mice. Mice were starved for 24 h to maximally induce CMA, and then injected intraperitoneally with vehicle or leupeptin to block proteolysis inside lysosomes. Because LAMP2A and LAMP1 levels may oscillate with leupeptin due to changes in the ratio between cargo and lysosomal components, we normalized lysosomal GAPDH levels with total lysosomal protein as stained with Ponceau Red. As shown in Fig. 45A and 45B, GAPDH accumulated in lysosomes from leupeptin-treated *Nrf2*-WT mice but not *Nrf2*-KO mice, which already exhibited higher basal levels of lysosomal GAPDH in the absence of NRF2. Altogether, these results suggest that NRF2 deficiency impairs basal CMA at the level of substrate internalization.

11. Pathophysiological significance of the new NRF2/LAMP2A axis in cancer.

Because both NRF2 and CMA activity have been reported to be up-regulated in multiple cancers, we analyzed the correlation between *NFE2L2* and *LAMP2* expression in 30 cohorts of The Cancer Genome Atlas (TCGA) from different tumors with the available RNAseq data from the Xena Browser database (https://xenabrowser.net/). Table 10 summarizes the 15 TCGA datasets with the best correlation coefficients (R) between *NFE2L2* and *LAMP2*.

The best correlation coefficient with the available datasets showed up for large B cell lymphomas (DLBC). However, the number of samples analyzed in this dataset was low (48). Therefore, the most significant correlation between *NFE2L2* and *LAMP2* was found in cohorts from low grade glioma and glioblastomas (GBMLGG). As shown in Fig. 46A, the expression of both *NFE2L2* and *LAMP2* shows a positive correlation in these datasets. Kaplan-Meier curves reflected reduced mean survival in patients from the GBMLGG cohort

which exhibited higher *NFE2L2* expression compared to the ones with lower expression, and a similar tendency was also observed with *LAMP2* expression (Fig. 46B).

Of note, this approach compares transcriptional changes of these two genes (and not specifically the *LAMP2A* isoform), and up-regulation of both NRF2 and LAMP2A could also occur at the protein level. To gain a more precise insight in the connection between NRF2 and LAMP2A in glioblastomas, we next knocked-down NRF2 in glioblastoma explants from four independent patients with lentivirally-transduced shRNA against *NFE2L2* for 7 days. As observed in Fig. 47A and 47B, all primary cultures exhibited a drastic decrease in NRF2 expression to just the 10-20% of the original levels. In parallel, a significant down-regulation of *LAMP2A* mRNA levels and, to a lesser extent, protein levels was observed when silencing NRF2.

Type of cancer (cohort)	Number of samples	p-value	R
Large B cell lymphoma (DLBC)	48	1,61752E-07	0.69
Low grade glioma and glioblastoma (GBMLGG)	702	7,99519E-56	0.54
Testicular cancer (TGCT)	156	1,18752E-12	0.52
Thymoma (THYM)	122	1,47967E-09	0.51
Endometrioid cancer (UCEC)	201	8,77315E-13	0.47
Acute myeloid leukemia (LAML)	173	4,31053E-07	0.37
Kidney clear cell carcinoma (KIRC)	606	9,69561E-19	0.34
Esophageal cancer (ESCA)	196	1,01965E-06	0.34
Melanoma (SKCM)	474	4,74664E-12	0.3
Cervical cancer (CESC)	308	3,93214E-08	0,3
Pancreatic cancer (PAAD)	183	2,43098E-05	0.3
Liver cancer (LIHC)	423	1,61692E-08	0.27
Breast cancer (BRCA)	1218	1,67128E-21	0.26
Lung cancer (LUNG)	1129	7,00284E-18	0.25
Prostate cancer (PRAD)	550	7,42241E-08	0.22

Table 10. Correlation analysis between *NFE2L2* and *LAMP2* expression in human cancers. The table summarizes the analysis of the 15 datasets of The Cancer Genome Atlas (TCGA) with the most significant correlation between *NFE2L2* and *LAMP2* expression according to the Pearson's correlation coefficient (R). The number of samples included in each dataset is also provided.

Altogether, our *in silico* and *in vitro* results support the functionality of the novel NRF2/LAMP2A axis in gliomas and glioblastomas, unveiling a new pathway to be further explored for therapeutic applications.

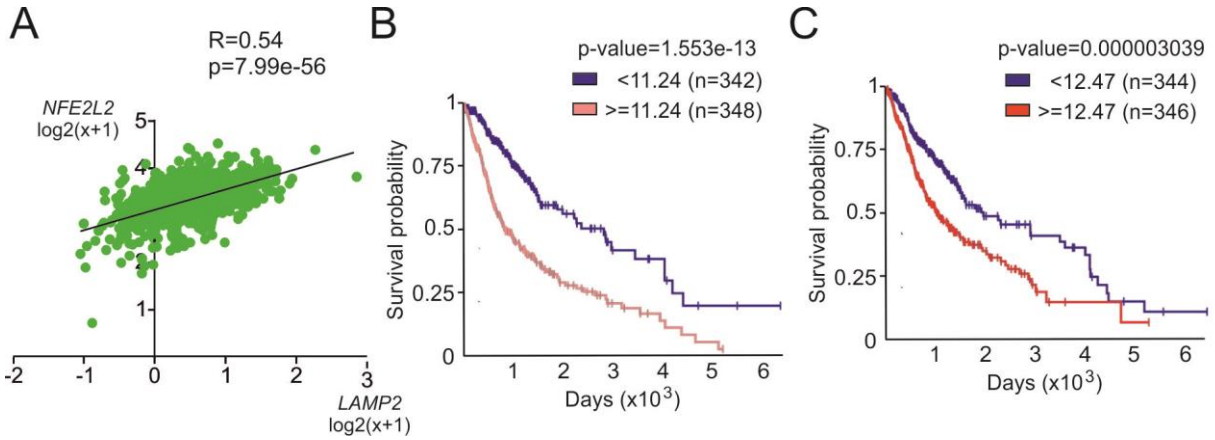

Figure 46. *NFE2L2* and *LAMP2* expression positively correlate in human gliomas and glioblastomas. A, Graphs showing positive correlation between *NFE2L2* and *LAMP2* expression in the TCGA datasets from low grade glioma and glioblastoma (GBMLGG). Expression levels, expressed as log2(x+1) transformed RSEM normalized counts, were directly obtained from the Xena Browser database. Pearson's correlation coefficient (R) and p-value calculated as a function of the t distribution are also shown. B, Kaplan-Meier curves obtained from the dataset in A from the Xena Browser database. The p-value resulting from the logrank analysis is depicted.

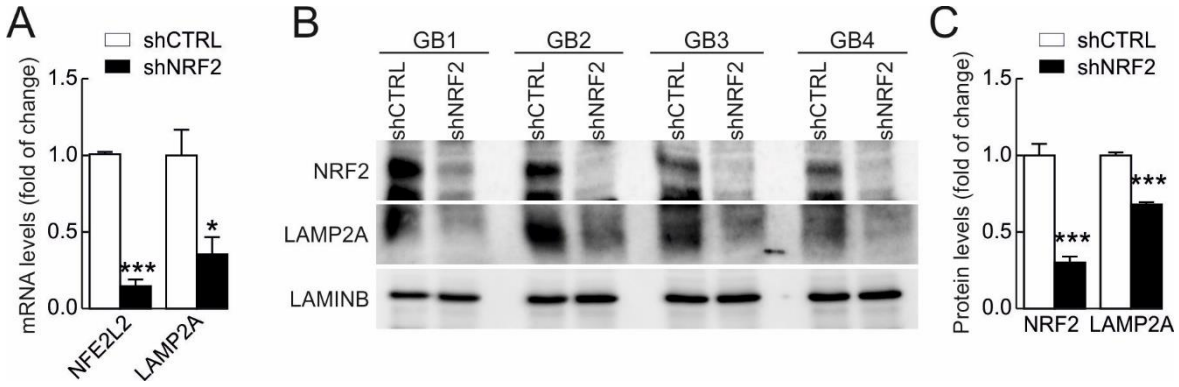

Figure 47. Genetic manipulation of NRF2 modifies LAMP2A levels in glioblastoma explants. A-C, Four human glioblastoma explants (GB1-4) were transduced with a lentivirus encoding control shRNA (shCTRL) or against *NFE2L2* (shNRF2). A, Expression levels of *NFE2L2* and *LAMP2A* were determined by qRT-PCR and normalized to *GAPDH* levels. Data are mean ± SEM (n=4). Statistical analysis was performed using Student's t test. *p<0.05 and ***p<0.001 vs. shCTRL levels. B, Immunoblot analysis of the indicated proteins from lysates as in A. C, Densitometric quantification of immunoblots in B relative to LAMIN B protein levels. Data are mean ± SEM (n=4). Statistical analysis was performed using Student's t test. ***p<0.001 vs. shCTRL cells.

Discussion

1. NRF2 is a regulator of macroautophagy gene expression

Transcription factor NRF2 and autophagy are essential elements to maintain cellular homeostasis, especially under stressful conditions. It had been reported that electrophiles, ROS or nitric oxide, all of which activate NRF2, can also can induce autophagy [91, 205, 206]. Here we report a mechanistic link based on NRF2 dependent regulation of at least 8 macroautophagy related genes that participate in autophagy initiation (*ULK1*), cargo recognition (*SQSTM1* and *CALCOCO2*), autophagosome formation and elongation (*ATG4D*, *ATG2B*, *ATG5*, *ATG7* and *GABARAPL1*) and autolysosome clearance (*ATG4D*). Previous studies had described that the cargo recognition proteins p62 [67] and NDP52 [68] encompass in their promoter regulatory regions one and three AREs, respectively. We have confirmed and extended these observations by finding three additional functional AREs in the p62 encoding gene. The upregulation of p62 is particularly relevant as phosphorylated p62 competes with NRF2 for KEAP1 binding and sequesters this E3 ligase adapter in protein inclusions [99] or takes it to degradation by autophagy [207], thus relieving NRF2 from this constrain. By doing so, we suggest that p62 can act as a molecular switch that, through NRF2 activation, leads to global up-regulation of autophagy genes.

Few studies have performed direct ChIP analysis of NRF2, because of the low or even misleading specificity of available antibodies [208]. Therefore, we undertook a different approach based on the analysis of other proteins that bind AREs, specifically MAFF, MAFK and BACH1, for which ChIP sequencing data are available in the ENCODE database, because at the time that these experiments were performed the ENCODE did not have an online resource to analyze NRF2 binding. The fact that MAFF, MAFK or BACH1 proteins might bind these sequences does not necessarily mean that NRF2 does, as sequence variations determine preference for different binding partners [209]. For this reason, we generated a PSSM and a script in order to compare each of the sequences from the ENCODE database with the consensus human ARE for NRF2 according to the JASPAR database (http://jaspar.genereg.net/). The script can be applied to the analysis of any gene of the ENCODE and, because this database in based on empirical data, it should provide more reliable information than theory-based softwares. Of note, this script identified with a high *relative score* the already known AREs in the *HMOX1* and *NQO1* promoters.

In previous studies, the effect of SFN on autophagy was attributed to the modulation of signaling events of the mTOR pathway through RPS6KB1/pS6K1 (Ribosomal protein S6 kinase beta-1) [210], activation of AMPK [211] or the MAPK/ERK pathways [205] rather than to

targeting NRF2 itself. However, we show in this work that the induction of macroautophagy genes by SFN is impaired in *Nrf2*-KO MEFs, therefore indicating that NRF2 is, at least, partially involved. In fact, these observations might be also extrapolated to invertebrates where loss of the homologue of KEAP1 in *D. melanogaster* (DmKEAP1) results in Atg8 (homologue to mammalian LC3) and macroautophagy induction dependent on CncC/NRF2 and independent on MITF/TFEB [212]. Interestingly, slight differences may be found in the response to NRF2 depending on species, cell type or the mechanism of NRF2 activation or inhibition. For instance, although we found binding of NRF2 to an ARE in *ATG7* and reduced mRNA and protein levels of this gene in *Nrf2*-KO MEFs, SFN treatment did not significantly increase its expression in HEK293T or HT22 under the experimental conditions used in this work. This may reflect cell-specific and stimulus-dependent regulation of macroautophagy [90, 213].

The proteins involved in macroautophagy are thought to be expressed in sufficient amounts to sustain basal activity, making post-translational modifications and protein-protein interactions critical for its regulation [214]. However, mild changes in gene expression combined with other signaling pathways, may account for large variations in autophagy activity. Thus, we have observed that NRF2 deficiency by itself did not significantly alter either basal autophagy flux under non-stressing conditions or autophagy induction by serum deprivation, as determined by LC3B-II levels. However, impaired autophagosome formation was detected in *Nrf2*-KO MEFs in response to stressful conditions elicited by H_2O_2 treatment. More importantly, NRF2 deficiency also aggravated proteinopathy in our mouse model of AD. These results support that NRF2 is necessary to achieve an optimal autophagic response upon stressful conditions.

2. Functional relevance of NRF2 in a new mouse model of AD

In spite of the efforts made over the last decades, the etiology of AD remains largely unknown. This is in part caused by incomplete reproduction of the human pathology in animal models merely exhibiting proteinopathy associated to Aβ and TAU. Current AD models do not completely recapitulate molecular mechanisms that correlate with the general decline of homeostatic capacity during ageing and may contribute significantly to the disease process. These mechanisms include oxidative, inflammatory and metabolic stress, which may precede the accumulation of protein aggregates in prodromal and early phases of sporadic AD [144, 215]. NRF2 activity has been shown to decrease with age [43, 165, 166, 216], probably resulting in

homeostatic disturbances related to AD. Based on this rationale and to address the impact of NRF2 on proteinopathy *in vivo*, especially in regard to macroautophagy, we generated a new mouse model based on the expression of human APP(V717I) and TAU(P301L) in a wild type (AT-*Nrf2*-WT mice) or *Nrf2*-knockout (AT-*Nrf2*-KO mice) genetic background.

Previous studies have addressed the impact of NRF2 loss in mouse models of AD with either amyloidopathy [217, 218] or tauopathy [53, 219] alone, but not in combination as presented here. Although we did not detect significant differences in the hippocampus of *Nrf2*-KO vs. *Nrf2*-WT mice, AT-*Nrf2*-KO mice exhibited a modest increase in oxidative and pro-inflammatory markers compared to AT-*Nrf2*-WT mice, suggesting that the proteotoxic challenge represented by human mutant APP and TAU expression rendered them more sensitive to oxidative and inflammatory stress. It must be born in mind that the slight increase in oxidative and inflammatory markers is persistent over the life span of the animals and mimics the low-grade but chronic oxidative and inflammatory stress characteristic of human pathology [220]. Memory and learning were severely impaired in the AT-*Nrf2*-KO mice as early as 6 months, preceding the presence of amyloid plaques and TAU fibrillary aggregates. These findings suggest that the lack of NRF2 replicates a prodromal condition of human AD and is in line with other findings in other animal models [221-223].

Although a reduced expression of *bona fide* NRF2-target genes was detected in cultured primary neurons derived from NRF2-WT vs. *Nrf2*-KO mice, we found minimal changes of ARE-gene expression in the hippocampus of 13-month-old animals. This is in line with a previous study [201] and our own transcriptomic data [224] showing no significant changes in the expression levels of well-known NRF2 targets in brains of NRF2-deficient mice, and also consistent with the lack of oxidative stress in the hippocampus of *Nrf2*-KO vs. *Nrf2*-WT mice. In fact, disruption of the gene coding for NRF2 in mice causes no overt phenotype if they are cared for under the optimal unstressed conditions of some animal facilities [225]. This fact suggests that NRF2 is not required under unstressed conditions or that there are compensatory mechanisms with other bZIP transcription factors. Indeed, NRF3 was reported to partially compensate for the lack of NRF2 in skin of NRF2-null mice [62, 226]. However, NRF2-deficient mice are extremely vulnerable to various toxic insults, such as cigarette smoke [227, 228], hepatotoxic chemicals [229, 230], traumatic brain injury [231] or neurotoxic chemicals [232, 233]. Our results support that the lack of NRF2 makes mice more sensitive to proteotoxic insults as well.

Reduced clearance of aggregation-prone proteins is a hallmark of many diseases, including AD [234]. In fact, macroautophagy deficiency has been shown to produce

neurodegeneration in mice [155, 235]. In accordance with a previous study in the APP/PS1 mice [201], our results show modest or no changes in macroautophagy gene expression in the whole hippocampus of AT-*Nrf2*-KO vs. AT-*Nrf2*-WT mice. However, in double-immunofluorescence assays, we did find differences in the levels of macroautophagy proteins when we compared APP- and TAU-expressing neurons from AT-*Nrf2*-WT vs the AT-*Nrf2*-KO brains. Therefore, the effect of NRF2 was detected specifically in the neurons under proteotoxic attack.

Impaired autophagy in neurons from the AT-*Nrf2*-KO mice correlated with altered APP processing, stalled in multiple swollen vacuoles with reduced levels of p62. It was surprising to find lower total levels of Aβ as well as an apparent reduction in amyloid plaques in AT-*Nrf2*-KO compared to AT-*Nrf2*-WT, as this observation implies a reduction of the amyolidogenic processing of APP. However, similar results have been reported for neuronal ATG7-deficient mice, which show impaired secretion, reduced total Aβ levels and fewer amyloid plaques [157]. Several studies have found that autophagosomes are a place for generation of Aβ [236, 237] and β-secretase and γ-secretase appear to be localized at least in part in autophagosomes [238, 239]. Thus, a reduction of autophagosomes might lead to lower Aβ load. In support of this hypothesis, we found reduced levels of the autophagy markers p62, NDP52, ULK1, AGT5, GABARAPL1 and LC3B in the AT-*Nrf2*-KO mice.

Our results are also consistent with a recent study in which the amyloidogenic mouse model APP/PS1 lacking NRF2 exhibits enhanced accumulation of APP in multivesicular bodies, endosomes, and lysosomes and shows an altered production of amyloid proteins due to impaired autophagic flux [201]. In these mice, NRF2-deficiency leads to increased amyloid plaque accumulation, whereas our AT-*Nrf2*-KO mice exhibited a tendency to develop fewer amyloid plaques compared to the wild type counterparts despite presenting worse cognitive performance and reduced LTP. These findings may be reconciled considering that the APP/PS1 mice exhibit a very strong amyloidogenic processing of APP (due to combined APP and PS1 mutations), while our model exhibits mild amyloidogenic processing (APP-mutated only), suggesting reduced availability of extracellular Aβ peptides for plaque formation similar to what is observed in the "APP-only" transgenic mice with ATG7-deficiency [157]. Moreover, we also observed increased levels of the soluble Aβ*56 oligomer in AT-*Nrf2*-KO mice. This oligomer results in memory impairment, is associated with pathological forms of TAU [240-242] and, very importantly, negatively correlates with plaque deposition [243, 244].

Although TAU can be degraded through several proteolytic pathways, it is increasingly being recognized that impaired autophagy also plays a central role in tauopathy

[245]. For instance, macroautophagy activation in the brain led to a reduction in the number of neurons containing TAU inclusions as well as decreased amount of insoluble TAU, together with diminished p62 levels [246]. Our results are fully consistent with at least partial NRF2-dependent autophagic degradation of TAU, given its co-localization with p62 in autophagic vacuoles. Consistently, we found more insoluble and hyperphosphorylated TAU in AT-*Nrf2*-KO mice. These observations also fit with a previous report showing that TAU is a cargo for NDP52, regulated by NRF2. Our study supports, therefore, that lack of the transcription factor NRF2 aggravates tauopathy in mice [245].

Altogether, the generation and characterization of our new mouse model of AD point to a critical role of NRF2 in modulating oxidative, inflammatory and proteostatic events, at least in part, through the regulation of macroautophagy.

3. NRF2 regulates CMA through the transcriptional control of *Lamp2a*

We have also described a molecular link between NRF2 and CMA, which occurs through the control of *LAMP2A* transcription. Knockout of *Lamp2a* or *Nrf2* results in increased susceptibility to different stressors [132, 247], indicating a crucial role of these pathways in the maintenance of cellular homeostasis under different circumstances. In fact, the redox status controls CMA activity, presumably to eliminate oxidized proteins during mild oxidative damage [124]. Interestingly, Kiffin and co-workers showed that CMA induction upon oxidative stress occurred through increased *Lamp2a* transcription [124]. Our results indicate that LAMP2A induction and consequent CMA activation after H_2O_2 or PQ treatment were severely impaired in *Nrf2*-KO cells. Therefore, NRF2 is an essential transcriptional regulator of CMA upon oxidative challenge.

In this work, we have identified two functional AREs in the *LAMP2* gene. Chemical and genetic manipulation of NRF2 results in modest changes in cellular *Lamp2a* mRNA and protein levels, albeit similar to those observed for the NRF2 target p62. LAMP2A has a slow turnover, with a half-life of approximately 46 h for total LAMP2A and 57 h for lysosomal LAMP2A [118]. Hence, small changes in mRNA *Lamp2a* levels may have a marked impact on protein levels and CMA activity. Other studies show similar oscillations, further supporting this notion [117, 126, 139, 248]. In contrast with the discrete changes in total cellular LAMP2A levels, the effects of NRF2-deficiency are much more evident in isolated lysosomes, the place where LAMP2A is required for CMA. In fact, the lysosomal levels of LAMP2A correlate with changes in the rate of CMA [127]. Thus, CMA was barely detectable in *Nrf2*-KO

hepatocytes, suggesting a crucial role for NRF2 in the modulation of CMA also under basal conditions.

The *LAMP2* gene encodes three splice variants, *LAMP2A*, *LAMP2B* and *LAMP2C* that possess different transmembrane and cytosolic regions and enable specific functions. Although several roles have been proposed for LAMP2B and LAMP2C [130, 249-251], only LAMP2A is involved in CMA [117, 132, 162]. Somewhat intriguingly, we could not detect consistent differences in the expression levels of *LAMP2B* or *LAMP2C* upon genetic manipulation of NRF2 despite being coded by the same gene. An explanation may stem from the fact that the three spliced variants exhibit differential regulation [127, 130, 252] and tissue-specific patterns [130, 131]. While LAMP2A and LAMP2B are highly expressed in most tissues, LAMP2C appears to be very restricted [130], supporting a differential splicing regulation of the *LAMP2* gene. Importantly, a previous study showed that paraquat transcriptionally induced *Lamp2a* expression without affecting the other two isoforms [253]. Altogether, these data suggest the existence of additional post-transcriptional regulatory mechanisms of the *Lamp2* gene that still need to be unveiled.

While we have described the transcriptional regulation of *Lamp2a* by NRF2, other layers of CMA regulation are still possible. For example, lysosomes from *Nrf2*-KO livers exhibited higher levels of HSC70 compared to *Nrf2*-WT livers. Although it is plausible that higher levels of HSC70 are a result of the relative decrease in lysosomal cargoes, we cannot discard that this increase represents a compensatory mechanism to counteract impaired CMA. In fact, increased HSC70 levels have been previously reported in other conditions with reduced lysosomal levels of LAMP2A, such as livers from old mice and in *Lamp2a*-KO mice [162, 203].

The impairment of CMA in *Nrf2*-KO mice was evidenced by a deficient uptake in an *in vitro* reconstituted system with RNase A but, more importantly, by the reduced degradation *in vivo* of the endogenous *bona fide* CMA substrate GAPDH. The fact that the differences in the uptake *in vivo* for the endogenous substrate are more pronounced than for the exogenously added protein in the isolated *in vitro* system could be attributed to the lack of other competing substrates in this last one. Interestingly, a previous report showed that astrocyte-specific NRF2 overexpression reduced the levels of another CMA substrate, MEF2D (myocyte enhancer factor 2D) [254]. However, this study was just correlative and ours is the first one to show that changes in CMA substrates are at the level of lysosomal degradation by CMA.

The crosstalk between both autophagic pathways has been extensively reported both *in vivo* and *in vitro*, whereby one reacts compensatorily to the loss of activity in the other [132, 137,

[203]. However, in this work we show that the functional connection between NRF2 and CMA is independent of macroautophagy. Therefore, NRF2 might act as a regulatory node in the proteolytic network represented by macroautophagy and CMA (Fig. 48).

4. Complex transcriptional networks assure cell proteostasis

In higher eukaryotes, the family of FOXO (Forkhead box protein O) transcription factors, GATA1 (Erythroid transcription factor) and TFEB (Transcription factor EB), activate macroautophagy [107, 255, 256] while ZKSCAN3 (Zinc finger protein with KRAB and SCAN domains 3) and GATA4 (Transcription factor GATA-4) are involved in the repression [257, 258]. Our study has added NRF2, suggesting different roles of these factors in the adaptation to specific autophagic needs.

The transcriptional inducers TFEB and FOXO3/FOXO3A participate in multiple scenarios and nutrient-deprivation is the best characterized [259, 260]. Nonetheless, NRF2 may be more relevant in tissues that support highly oxidative metabolism. By this mechanism, oxidative stress-induced NRF2 may function under nutrient-rich conditions to upregulate transcription of genes encoding proteins required for autophagy, similar to what has been found for the transcription factors TFEB and FOXO3 under starvation conditions. As the brain is not allowed to starve and must function under all nutritional conditions, NRF2 may be particularly a relevant to activate autophagy in neurons.

Different transcription factors might also regulate *LAMP2* expression. AP-1 and SP-1 binding sites were found in the *LAMP2* promoter [261], although were not confirmed to be functional enhancers. MAF proteins, binding partners of NRF2, also heterodimerize with NFAT (nuclear factor of activated T-cells), which has been shown to modulate *Lamp2a* transcription upon activation of T lymphocytes [139]. We have identified two functional AREs in the *LAMP2* gene that lose activity when a highly conserved G is replaced to A. This conserved G constitutes the binding site for MAFs in the heterodimer [262] and consequently we suggest that MAFs participate in a dual regulation of *LAMP2* by binding to both NFAT and NRF2. Of note, NRF2 would control not only inducible but also *Lamp2a* basal expression, as *Nrf2*-deficient cells exhibited reduced *Lamp2a* mRNA and protein levels.

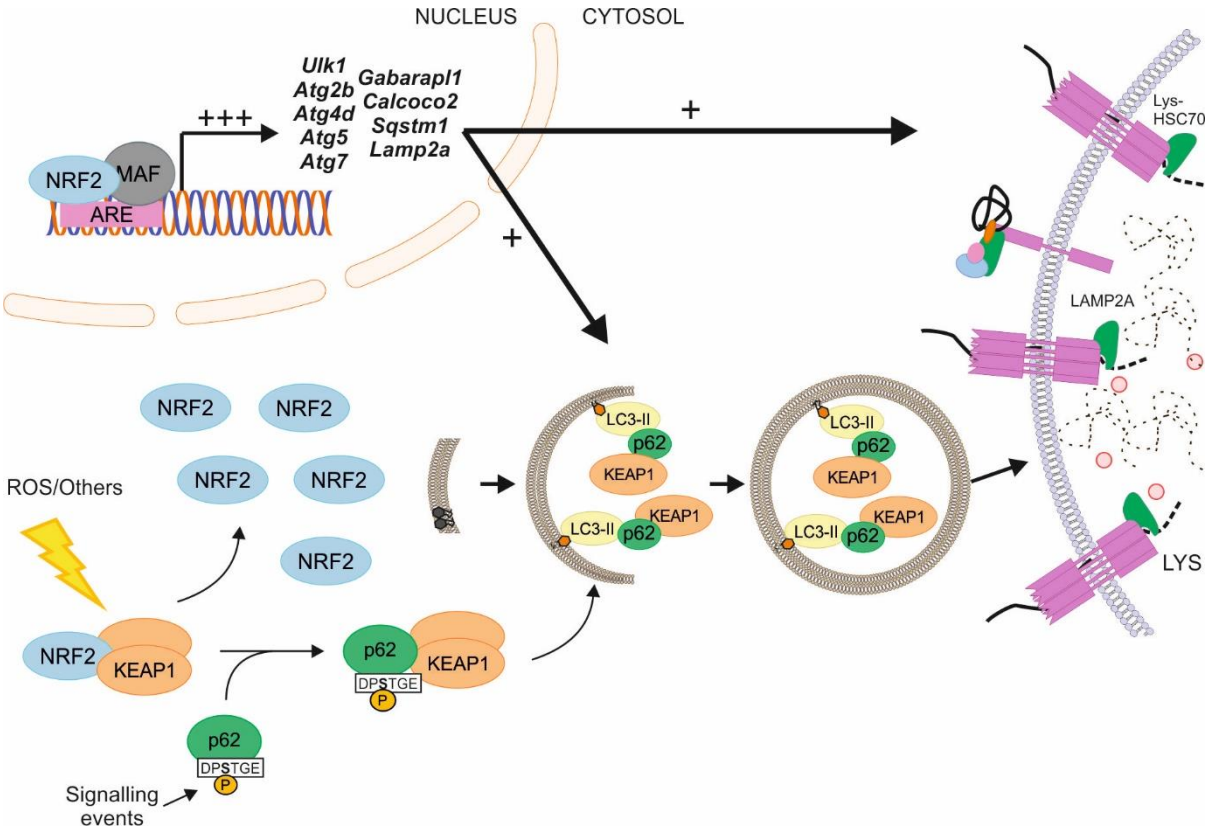

Figure 48. NRF2 controls autophagy through the regulation of macroautophagy and CMA related genes. Different mechanisms, including reactive oxygen species (ROS) or signaling events leading to p62 phosphorylation, result in NRF2 induction and subsequent induction of autophagy- related genes, with a functional impact in macroautophagy and chaperone mediated autophagy. P62 creates a positive feedback loop in which autophagosomal degradation of KEAP1 results in induction of autophagy related genes through upregulation of NRF2.

Therefore, different transcription factors may co-exist to assure proteostasis under several circumstances and in distinct cell types. In fact, levels of basal macroautophagy and CMA activity and the amplitude of the induction are highly variable [122, 134, 139, 173]. The existence of transcriptional networks would allow compensation when the activity of a certain transcription factor is impaired, at least under certain conditions. Similar to what has been discussed here for NRF2, no significant reduction of well-known TFEB target genes is observed in *Tfeb*-KO mice unless mTOR is inhibited [106].

All things considered, while post-translational modifications and protein-protein interactions represent quick adaptations to the cellular needs, transcriptional regulation of autophagy might to be critical for long term adaptation to specific stressful conditions.

5. Therapeutic potential of NRF2 and autophagy in chronic diseases

Chronic diseases demonstrate a high degree of connectivity and a need for more precise, mechanism-based disease rather than the current organ- and symptom-based definitions [263]. In fact, several chronic diseases share common molecular mechanisms, including oxidative stress, chronic inflammation and metabolic unbalance. Based on a network medicine approach, NRF2 was proposed as a key molecular node within a particular cluster of diseases, including AD or cancer [60]. In this work, we have analyzed the impact of NRF2 in the context of a disease with impaired macroautophagy (AD) and a disease usually characterized by over-activation of CMA (cancer).

a. Relevance of NRF2 and autophagy in AD

While there is overwhelming evidence of impaired autophagy in AD [264-267], the role of NRF2 is still controversial. A highly cited study showed by immunohistochemistry with anti-NRF2 polyclonal antibodies available at that time that NRF2 is predominantly localized in the cytoplasm of AD hippocampal neurons, suggesting reduced NRF2 transcriptional activity in the brain [268]. However, other studies have reported increased ARE-regulated proteins in AD brains, such as HMOX1, NQO1, or p62 [269-272]. Interestingly, the rodent *Octodon degus* naturally develops proteinopathic hallmarks of AD with aging that correlate with increased *Nfe2l2* mRNA levels [273], suggesting upregulation of NRF2 to combat proteinopathy. Our results with hippocampal lysates and immunohistochemistry are in line with these latter reports, as we observed increased nuclear NRF2 expression in proteinopathic AD neurons. Aside from technical reasons, one possible explanation for this discrepancy is that NRF2 levels might change during disease progression and in different brain regions.

In this regard, a corollary of our study is that NRF2 might be a therapeutic target for proteinopathies such as AD. On the one hand, we found that NRF2-deficiency impairs macroautophagy in AT-*Nrf2*-KO mice. We interpret these data as a need of NRF2 for an optimal response to proteinopathy. On the other hand, NRF2 and at least HMOX1, p62, NDP52 and ATG7 are upregulated in the hippocampus of AD patients as determined by immunoblot, and NRF2 and p62 proteins are increased in APP- and TAU-injured neurons as determined by immunohistochemistry. Interestingly, *Atg7*-KO mice display p62 and KEAP1 accumulation in ubiquitin-positive inclusion bodies, which leads to NRF2 stabilization and induction of target genes [98]. The excessive accumulation of p62 together with ubiquitinated

proteins has been identified in neurodegenerative diseases, including AD, PD and ALS [164]. Our work supports the observation that phosphorylated p62 is increased in AD samples [272]. This modified form of p62 has higher binding affinity for KEAP1 and drives this NRF2 repressor to autophagosomes [102]. It is then plausible that impairment of autophagy in AD leads to p62-mediated removal of KEAP1 and NRF2 accumulation, which in turn would induce the expression of p62 as well as other autophagy genes providing a feed-forward loop. In fact, Lipinski and co-workers found that AD brains showed increased transcription of autophagy related genes, in contrast to normal aging individuals [159].

In addition to the proposed mechanism of p62-mediated activation of NRF2 in proteinopathies, other mechanisms regulating proteostasis may impact NRF2 activity. Thus, accumulation of unfolded/misfolded proteins will induce the unfolded protein response (UPR) in the ER and, therefore, the activation of PERK (double-stranded RNA-activated protein kinase-like ER kinase) and MAPK (mitogen activated protein kinases) that may result in NRF2 activation [35, 36]. Moreover, protein oligomers and aggregates have been shown to inhibit proteasomal activity [274], probably avoiding NRF2 degradation.

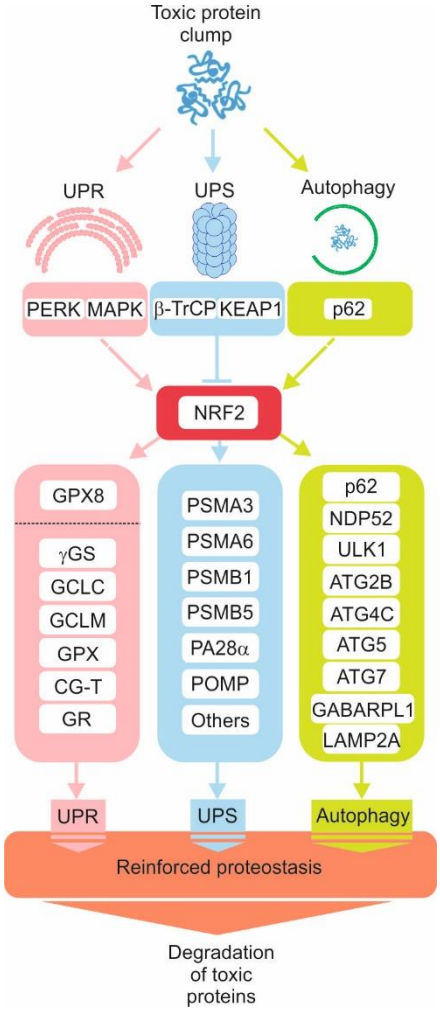

Figure 49. NRF2 as a hub connecting emergency signals derived from proteotoxic insults to a protective transcriptional response. The accumulation of unfolded/misfolded proteins will lead to the activation of the unfolded protein response (UPR) in the ER. Activation of PERK or MAPK may result in the transcriptional induction of the ER resident *Gpx8* and several enzymes regulating GSH levels, critical to ensure correct protein folding. Protein aggregates inhibit proteasome activity (UPS), probably avoiding NRF2 degradation. Although regulation of proteasome genes appears to be related to the paralogue NRF1, NRF2 has been reported to modulate the transcription of proteasome genes such as *Psma3*, *Psma6*, *Psmb1*, *Psmb5* and *Pomp* genes and others. Autophagy is the main pathway for the degradation of protein aggregates. Autophagy also regulates NRF2, connecting this degradation pathway with NRF2 transcriptional induction of *p62*, *Ndp52*, *Ulk1*, *Atg2b*, *Atg4c*, *Atg5*, *Atg7*, *Gabarapl1* and *Lamp2a*.

As a result, NRF2 can be envisioned as a hub connecting proteotoxicity-derived emergency signals to a protective transcriptional response (Fig. 49), controlling the expression of different enzymes critical to ensure correct protein folding [66, 275]; modulating the transcription of several proteasomal subunits [64, 65]; and, as shown in this work, several autophagy-related genes, therefore re-inforcing proteostasis.

However, a key remaining question is whether it will be useful or deleterious to increase NRF2 levels in the brain. As discussed by Hayes and colleagues [276], NRF2 effect might have an U-shaped response, meaning that too low NRF2 levels may result in a loss of cytoprotection and increased susceptibility to stressors, while too much NRF2 might disturb homeostatic balance towards a reductive scenario, which would favor protein misfolding and aggregation. Interestingly, analysis of epidemiological data indicates that the *NFE2L2* gene is highly polymorphic, and some haplotypes are associated with decreased risk and/or delayed onset of AD [167]. Similar observations have been done in regard to other proteinopathies [277, 278]. This physiological variability in *NFE2L2* expression at the population level and low NRF2 levels in the brain [279] support the idea that a slight up-regulation in NRF2 activity may be sufficient to reinforce proteostasis and achieve a benefit under pathological conditions. In fact, the protective role of pharmacological NRF2-mediated protein clearance has been shown in different cell culture and *in vivo* models of neurodegeneration (reviewed in [66]). For instance, autophagy-mediated degradation of phospho- and insoluble-TAU was reported with the organic flavonoid fisetin. This compound was able to induce autophagy by simultaneously promoting the activation and nuclear translocation of both TFEB and NRF2, along with some of its target genes. This response was prevented by TFEB or NRF2 silencing [280]. Interestingly, Jo and colleagues demonstrated that SFN reduced the levels of phosphorylated TAU and increased BECLIN1 and LC3-II, suggesting NRF2 activation may facilitate degradation of this toxic protein through autophagy [68].

Although we have not specifically analyzed here the role of NRF2/LAMP2A axis in AD, the fact that a) CMA activity declines in old rodents and humans [162, 203], favoring the accumulation of oxidized substrates and contributing to the general decline in proteostasis with age; and b) TAU has been shown to be a CMA substrate [281, 282], make it conceivable that CMA activation could be beneficial in this context. We have shown that both macroautophagy related genes and *Lamp2a* can be up-regulated by pharmacological activation of NRF2 with SFN, but future work will be needed to definitely determine if pharmacological activation of NRF2 may be a valid strategy to facilitate degradation of toxic proteins in the brain.

b. Potential implications of the novel NRF2/autophagy axis in cancer

Although the role of autophagy and NRF2 in cancer is complex, the general view is that these homeostatic processes are necessary in order to prevent tumor initiation, but once the tumor has been established, they promote survival of transformed cells, tumor development and resistance to chemotherapeutic agents.

In this study, we have analyzed a potential connection between NRF2 and CMA in glioblastomas. NRF2 activity is generally increased in glioblastoma cell lines [283, 284] and glioblastoma patients [279, 285] and, very importantly, ablation of NRF2 expression was shown to inhibit the proliferation and self-renewal of glioma stem cells (GSCs) [286]. Therefore, we have analyzed the correlation between *NFE2L2* and *LAMP2* expression levels in different cancers, finding a positive correlation in gliomas and glioblastomas. The correlation coefficient in mRNA expression between both genes was roughly 0,5 but this value is quite significant if we consider a) that it integrates all-type of gliomas independently of their classification and source of collection; b) this type of analysis does not differentiate between *LAMP2* isoforms, otherwise it may result in better correlations with *LAMP2A*; and c) NRF2 levels are probably increased at the protein level, so that a mild effect at the mRNA level is observed as a consequence of a subtle induction of the *NFE2L2* gene through its own AREs [195].

In line with previous studies [279, 285] the Kaplan-Meier curves reflect that higher *NFE2L2* expression levels correlate with reduced mean survival in low grade glioma and glioblastoma patients, and *vice versa*. We observed a parallel association between *LAMP2* expression and survival, indicating that individuals with high *LAMP2* expression have worse prognosis than those with low *LAMP2* expression. These results point to the fact that increased CMA may represent an advantage in this type of tumors. For instance, degradation of tumor-suppressor mammalian STE20-like kinase 1 (MST1) by CMA was shown to promote tumorigenesis [175]. Moreover, augmented CMA may also make cancer cells more resistant to different stressors such as oxidative stress [174]. By contrast, blockage of CMA reduced tumorigenicity in cancer cell lines and reduced tumor size and metastasis in mouse xenografts [173].

Although further research is needed to directly confirm increased CMA activity and its precise consequences in specific types of cancers, current evidence is consistent with the hypothesis that reducing the activity of NRF2 and, consequently, CMA, would constitute an interesting therapeutic strategy. In fact, NRF2 inhibition has been proposed as a mechanism to sensitize cancer cells to chemotherapeutic drugs or radiotherapy [287]. For instance, ascorbic acid (vitamin C), a well-known ROS scavenger, was found to sensitize imatinib-resistant

cancer cells by decreasing the levels of the NRF2/ARE complex, reducing the expression of *GCLC* and dropping GSH levels [288]. NRF2 inhibition with the natural compound trigonelline was also shown to render pancreatic cancer cells more susceptible to apoptosis [55]. Interestingly, we observed reduced expression of macroautophagy related genes after trigonelline treatment in HT22 cells. All-transretinoic acid (ATRA) is another example of NRF2 inhibitor that significantly decreases NRF2 activation *in vitro* and *in vivo*. ATRA activates the RARα (retinoic acid receptor α), which forms a complex with NRF2, hence impeding the binding of the transcription factor to ARE genes [289]. ATRA was also shown to decrease CMA through inhibition of *LAMP2A* transcription [290]. Although these inhibitors may have many unspecific effects, we report here that NRF2 silencing with shRNA in explants obtained from different glioblastoma patients resulted in reduced *LAMP2A* mRNA and protein levels. This NRF2/LAMP2A may also be exploited in other types of tumors. Adenocarcinoma A549 cells have been shown to display increased NRF2 [178, 179] and CMA [173] activities. Of note, reduction of NRF2 levels in A549 with a specific shRNA resulted in reduced LAMP2A levels.

Proteolytic networks show a great degree of crosstalk, and one pathway can act compensatorily to the failure of another [132, 137, 203]. It is plausible to think, then, that specifically inhibiting CMA in cancer would result in macroautophagy induction. If this is indeed demonstrated, inhibiting NRF2 may be of greater interest as it can transcriptionally regulate both pathways.

Therefore, until more selective NRF2 small-molecule inhibitors are developed, our results may serve, at least, as a proof-of-concept for reduced autophagy gene expression when inhibiting NRF2. All in all, we believe that the new regulation of macroautophagy and CMA related genes by NRF2 described in this work constitutes a very interesting targetable pathway to be considered for future research for chronic diseases such as cancer.

6. Concluding remarks and future perspectives

As demonstrated in the last years, NRF2 transcriptional signature is not only essential for orchestrating an adequate antioxidant response, but to maintain general homeostasis. In this work, we have described the role of NRF2 in the transcriptional regulation of macroautophagy and CMA, and re-inforced the view of this transcription factor as a regulatory node in the proteolytic network. Therefore, therapeutic possibilities may arise based on the exploitation of NRF2 as a crucial regulator of autophagy in chronic diseases.

Conclusions/ Conclusiones

1. NRF2 regulates macroautophagy through the transcriptional control of several genes involved in this process.

2. NRF2 modulates CMA through the transcriptional control of *Lamp2a*.

3. NRF2 regulates proteostasis, especially under stressful conditions.

4. Modulation of macroautophagy and CMA via NRF2 pharmacological intervention points to a new potential therapeutic target for chronic diseases.

---

1. NRF2 regula la macroautofagia a través del control transcripcional de varios genes implicados en este proceso.

2. NRF2 modula la CMA a través del control transcripcional de *Lamp2a*.

3. El factor de transcripción NRF2 regula la proteostasis, especialmente frente a condiciones de estrés.

4. La modulación de la macroautofagia y la CMA a través de la regulación farmacológica de NRF2 sugiere una posible nueva diana terapéutica para enfermedades crónicas.

References

1. Moi P, Chan K, Asunis I, Cao A, Kan YW. Isolation of NF-E2-related factor 2 (Nrf2), a NF-E2-like basic leucine zipper transcriptional activator that binds to the tandem NF-E2/AP1 repeat of the beta-globin locus control region. Proceedings of the National Academy of Sciences of the United States of America 1994; 91:9926-30.
2. Friling RS, Bensimon A, Tichauer Y, Daniel V. Xenobiotic-inducible expression of murine glutathione S-transferase Ya subunit gene is controlled by an electrophile-responsive element. Proceedings of the National Academy of Sciences of the United States of America 1990; 87:6258-62.
3. Favreau LV, Pickett CB. Transcriptional regulation of the rat NAD(P)H:quinone reductase gene. Identification of regulatory elements controlling basal level expression and inducible expression by planar aromatic compounds and phenolic antioxidants. The Journal of biological chemistry 1991; 266:4556-61.
4. Wasserman WW, Fahl WE. Functional antioxidant responsive elements. Proceedings of the National Academy of Sciences of the United States of America 1997; 94:5361-6.
5. Venugopal R, Jaiswal AK. Nrf1 and Nrf2 positively and c-Fos and Fra1 negatively regulate the human antioxidant response element-mediated expression of NAD(P)H:quinone oxidoreductase1 gene. Proceedings of the National Academy of Sciences of the United States of America 1996; 93:14960-5.
6. Itoh K, Chiba T, Takahashi S, Ishii T, Igarashi K, Katoh Y, et al. An Nrf2/small Maf heterodimer mediates the induction of phase II detoxifying enzyme genes through antioxidant response elements. Biochemical and biophysical research communications 1997; 236:313-22.
7. Chanas SA, Jiang Q, McMahon M, McWalter GK, McLellan LI, Elcombe CR, et al. Loss of the Nrf2 transcription factor causes a marked reduction in constitutive and inducible expression of the glutathione S-transferase Gsta1, Gsta2, Gstm1, Gstm2, Gstm3 and Gstm4 genes in the livers of male and female mice. The Biochemical journal 2002; 365:405-16.
8. McMahon M, Itoh K, Yamamoto M, Chanas SA, Henderson CJ, McLellan LI, et al. The Cap'n'Collar basic leucine zipper transcription factor Nrf2 (NF-E2 p45-related factor 2) controls both constitutive and inducible expression of intestinal detoxification and glutathione biosynthetic enzymes. Cancer research 2001; 61:3299-307.
9. Blank V. Small Maf proteins in mammalian gene control: mere dimerization partners or dynamic transcriptional regulators? Journal of molecular biology 2008; 376:913-25.
10. Kataoka K, Noda M, Nishizawa M. Maf nuclear oncoprotein recognizes sequences related to an AP-1 site and forms heterodimers with both Fos and Jun. Molecular and cellular biology 1994; 14:700-12.
11. Kurokawa H, Motohashi H, Sueno S, Kimura M, Takagawa H, Kanno Y, et al. Structural basis of alternative DNA recognition by Maf transcription factors. Molecular and cellular biology 2009; 29:6232-44.
12. Kerppola TK, Curran T. A conserved region adjacent to the basic domain is required for recognition of an extended DNA binding site by Maf/Nrl family proteins. Oncogene 1994; 9:3149-58.
13. Sun J, Hoshino H, Takaku K, Nakajima O, Muto A, Suzuki H, et al. Hemoprotein Bach1 regulates enhancer availability of heme oxygenase-1 gene. The EMBO journal 2002; 21:5216-24.
14. Hirotsu Y, Katsuoka F, Funayama R, Nagashima T, Nishida Y, Nakayama K, et al. Nrf2-MafG heterodimers contribute globally to antioxidant and metabolic networks. Nucleic acids research 2012; 40:10228-39.
15. Tong KI, Katoh Y, Kusunoki H, Itoh K, Tanaka T, Yamamoto M. Keap1 recruits Neh2 through binding to ETGE and DLG motifs: characterization of the two-site molecular recognition model. Molecular and cellular biology 2006; 26:2887-900.
16. McMahon M, Thomas N, Itoh K, Yamamoto M, Hayes JD. Dimerization of substrate adaptors can facilitate cullin-mediated ubiquitylation of proteins by a "tethering" mechanism:

a two-site interaction model for the Nrf2-Keap1 complex. The Journal of biological chemistry 2006; 281:24756-68.
17. Nioi P, Nguyen T, Sherratt PJ, Pickett CB. The carboxy-terminal Neh3 domain of Nrf2 is required for transcriptional activation. Molecular and cellular biology 2005; 25:10895-906.
18. Katoh Y, Itoh K, Yoshida E, Miyagishi M, Fukamizu A, Yamamoto M. Two domains of Nrf2 cooperatively bind CBP, a CREB binding protein, and synergistically activate transcription. Genes to cells : devoted to molecular & cellular mechanisms 2001; 6:857-68.
19. Kim JH, Yu S, Chen JD, Kong AN. The nuclear cofactor RAC3/AIB1/SRC-3 enhances Nrf2 signaling by interacting with transactivation domains. Oncogene 2013; 32:514-27.
20. Rada P, Rojo AI, Chowdhry S, McMahon M, Hayes JD, Cuadrado A. SCF/{beta}-TrCP promotes glycogen synthase kinase 3-dependent degradation of the Nrf2 transcription factor in a Keap1-independent manner. Molecular and cellular biology 2011; 31:1121-33.
21. Rada P, Rojo AI, Evrard-Todeschi N, Innamorato NG, Cotte A, Jaworski T, et al. Structural and functional characterization of Nrf2 degradation by the glycogen synthase kinase 3/beta-TrCP axis. Molecular and cellular biology 2012; 32:3486-99.
22. Chowdhry S, Zhang Y, McMahon M, Sutherland C, Cuadrado A, Hayes JD. Nrf2 is controlled by two distinct beta-TrCP recognition motifs in its Neh6 domain, one of which can be modulated by GSK-3 activity. Oncogene 2013; 32:3765-81.
23. Wang H, Liu K, Geng M, Gao P, Wu X, Hai Y, et al. RXRalpha inhibits the NRF2-ARE signaling pathway through a direct interaction with the Neh7 domain of NRF2. Cancer research 2013; 73:3097-108.
24. Wakabayashi N, Itoh K, Wakabayashi J, Motohashi H, Noda S, Takahashi S, et al. Keap1-null mutation leads to postnatal lethality due to constitutive Nrf2 activation. Nature genetics 2003; 35:238-45.
25. Devling TW, Lindsay CD, McLellan LI, McMahon M, Hayes JD. Utility of siRNA against Keap1 as a strategy to stimulate a cancer chemopreventive phenotype. Proceedings of the National Academy of Sciences of the United States of America 2005; 102:7280-5A.
26. Tong KI, Padmanabhan B, Kobayashi A, Shang C, Hirotsu Y, Yokoyama S, et al. Different electrostatic potentials define ETGE and DLG motifs as hinge and latch in oxidative stress response. Molecular and cellular biology 2007; 27:7511-21.
27. Baird L, Lleres D, Swift S, Dinkova-Kostova AT. Regulatory flexibility in the Nrf2-mediated stress response is conferred by conformational cycling of the Keap1-Nrf2 protein complex. Proceedings of the National Academy of Sciences of the United States of America 2013; 110:15259-64.
28. Dinkova-Kostova AT, Holtzclaw WD, Cole RN, Itoh K, Wakabayashi N, Katoh Y, et al. Direct evidence that sulfhydryl groups of Keap1 are the sensors regulating induction of phase 2 enzymes that protect against carcinogens and oxidants. Proceedings of the National Academy of Sciences of the United States of America 2002; 99:11908-13.
29. Zhang DD, Hannink M. Distinct cysteine residues in Keap1 are required for Keap1-dependent ubiquitination of Nrf2 and for stabilization of Nrf2 by chemopreventive agents and oxidative stress. Molecular and cellular biology 2003; 23:8137-51.
30. Fukutomi T, Takagi K, Mizushima T, Ohuchi N, Yamamoto M. Kinetic, thermodynamic, and structural characterizations of the association between Nrf2-DLGex degron and Keap1. Molecular and cellular biology 2014; 34:832-46.
31. Sun Z, Huang Z, Zhang DD. Phosphorylation of Nrf2 at multiple sites by MAP kinases has a limited contribution in modulating the Nrf2-dependent antioxidant response. PloS one 2009; 4:e6588.
32. Xu C, Yuan X, Pan Z, Shen G, Kim JH, Yu S, et al. Mechanism of action of isothiocyanates: the induction of ARE-regulated genes is associated with activation of ERK

and JNK and the phosphorylation and nuclear translocation of Nrf2. Molecular cancer therapeutics 2006; 5:1918-26.
33. Shen G, Hebbar V, Nair S, Xu C, Li W, Lin W, et al. Regulation of Nrf2 transactivation domain activity. The differential effects of mitogen-activated protein kinase cascades and synergistic stimulatory effect of Raf and CREB-binding protein. The Journal of biological chemistry 2004; 279:23052-60.
34. Zipper LM, Mulcahy RT. Inhibition of ERK and p38 MAP kinases inhibits binding of Nrf2 and induction of GCS genes. Biochemical and biophysical research communications 2000; 278:484-92.
35. Yu R, Chen C, Mo YY, Hebbar V, Owuor ED, Tan TH, et al. Activation of mitogen-activated protein kinase pathways induces antioxidant response element-mediated gene expression via a Nrf2-dependent mechanism. The Journal of biological chemistry 2000; 275:39907-13.
36. Cullinan SB, Zhang D, Hannink M, Arvisais E, Kaufman RJ, Diehl JA. Nrf2 is a direct PERK substrate and effector of PERK-dependent cell survival. Molecular and cellular biology 2003; 23:7198-209.
37. Huang HC, Nguyen T, Pickett CB. Phosphorylation of Nrf2 at Ser-40 by protein kinase C regulates antioxidant response element-mediated transcription. The Journal of biological chemistry 2002; 277:42769-74.
38. Apopa PL, He X, Ma Q. Phosphorylation of Nrf2 in the transcription activation domain by casein kinase 2 (CK2) is critical for the nuclear translocation and transcription activation function of Nrf2 in IMR-32 neuroblastoma cells. Journal of biochemical and molecular toxicology 2008; 22:63-76.
39. Jain AK, Jaiswal AK. GSK-3beta acts upstream of Fyn kinase in regulation of nuclear export and degradation of NF-E2 related factor 2. The Journal of biological chemistry 2007; 282:16502-10.
40. Torrente L, Sanchez C, Moreno R, Chowdhry S, Cabello P, Isono K, et al. Crosstalk between NRF2 and HIPK2 shapes cytoprotective responses. Oncogene 2017; 36:6204-12.
41. Niture SK, Jain AK, Shelton PM, Jaiswal AK. Src subfamily kinases regulate nuclear export and degradation of transcription factor Nrf2 to switch off Nrf2-mediated antioxidant activation of cytoprotective gene expression. The Journal of biological chemistry 2011; 286:28821-32.
42. Narasimhan M, Patel D, Vedpathak D, Rathinam M, Henderson G, Mahimainathan L. Identification of novel microRNAs in post-transcriptional control of Nrf2 expression and redox homeostasis in neuronal, SH-SY5Y cells. PloS one 2012; 7:e51111.
43. Kuosmanen SM, Sihvola V, Kansanen E, Kaikkonen MU, Levonen AL. MicroRNAs mediate the senescence-associated decline of NRF2 in endothelial cells. Redox biology 2018; 18:77-83.
44. Sun Z, Chin YE, Zhang DD. Acetylation of Nrf2 by p300/CBP augments promoter-specific DNA binding of Nrf2 during the antioxidant response. Molecular and cellular biology 2009; 29:2658-72.
45. Su ZY, Khor TO, Shu L, Lee JH, Saw CL, Wu TY, et al. Epigenetic reactivation of Nrf2 in murine prostate cancer TRAMP C1 cells by natural phytochemicals Z-ligustilide and Radix angelica sinensis via promoter CpG demethylation. Chemical research in toxicology 2013; 26:477-85.
46. Hur W, Gray NS. Small molecule modulators of antioxidant response pathway. Current opinion in chemical biology 2011; 15:162-73.
47. Satoh T, McKercher SR, Lipton SA. Nrf2/ARE-mediated antioxidant actions of pro-electrophilic drugs. Free radical biology & medicine 2013; 65:645-57.
48. Blanco-Ayala T, Anderica-Romero AC, Pedraza-Chaverri J. New insights into antioxidant strategies against paraquat toxicity. Free radical research 2014; 48:623-40.

49. Fourquet S, Guerois R, Biard D, Toledano MB. Activation of NRF2 by nitrosative agents and H2O2 involves KEAP1 disulfide formation. The Journal of biological chemistry 2010; 285:8463-71.
50. McMahon M, Lamont DJ, Beattie KA, Hayes JD. Keap1 perceives stress via three sensors for the endogenous signaling molecules nitric oxide, zinc, and alkenals. Proceedings of the National Academy of Sciences of the United States of America 2010; 107:18838-43.
51. Takaya K, Suzuki T, Motohashi H, Onodera K, Satomi S, Kensler TW, et al. Validation of the multiple sensor mechanism of the Keap1-Nrf2 system. Free radical biology & medicine 2012; 53:817-27.
52. Lin SX, Lisi L, Dello Russo C, Polak PE, Sharp A, Weinberg G, et al. The anti-inflammatory effects of dimethyl fumarate in astrocytes involve glutathione and haem oxygenase-1. ASN neuro 2011; 3.
53. Cuadrado A, Kugler S, Lastres-Becker I. Pharmacological targeting of GSK-3 and NRF2 provides neuroprotection in a preclinical model of tauopathy. Redox biology 2018; 14:522-34.
54. Zhou J, Chan L, Zhou S. Trigonelline: a plant alkaloid with therapeutic potential for diabetes and central nervous system disease. Current medicinal chemistry 2012; 19:3523-31.
55. Arlt A, Sebens S, Krebs S, Geismann C, Grossmann M, Kruse ML, et al. Inhibition of the Nrf2 transcription factor by the alkaloid trigonelline renders pancreatic cancer cells more susceptible to apoptosis through decreased proteasomal gene expression and proteasome activity. Oncogene 2013; 32:4825-35.
56. Sun X, Ou Z, Chen R, Niu X, Chen D, Kang R, et al. Activation of the p62-Keap1-NRF2 pathway protects against ferroptosis in hepatocellular carcinoma cells. Hepatology 2016; 63:173-84.
57. Roh JL, Kim EH, Jang H, Shin D. Nrf2 inhibition reverses the resistance of cisplatin-resistant head and neck cancer cells to artesunate-induced ferroptosis. Redox biology 2017; 11:254-62.
58. Sirota R, Gibson D, Kohen R. The role of the catecholic and the electrophilic moieties of caffeic acid in Nrf2/Keap1 pathway activation in ovarian carcinoma cell lines. Redox biology 2015; 4:48-59.
59. Hayes JD, Dinkova-Kostova AT. The Nrf2 regulatory network provides an interface between redox and intermediary metabolism. Trends in biochemical sciences 2014; 39:199-218.
60. Cuadrado A, Manda G, Hassan A, Alcaraz MJ, Barbas C, Daiber A, et al. Transcription Factor NRF2 as a Therapeutic Target for Chronic Diseases: A Systems Medicine Approach. Pharmacological reviews 2018; 70:348-83.
61. Dick RA, Kwak MK, Sutter TR, Kensler TW. Antioxidative function and substrate specificity of NAD(P)H-dependent alkenal/one oxidoreductase. A new role for leukotriene B4 12-hydroxydehydrogenase/15-oxoprostaglandin 13-reductase. The Journal of biological chemistry 2001; 276:40803-10.
62. Knatko EV, Ibbotson SH, Zhang Y, Higgins M, Fahey JW, Talalay P, et al. Nrf2 Activation Protects against Solar-Simulated Ultraviolet Radiation in Mice and Humans. Cancer prevention research 2015; 8:475-86.
63. Kobayashi EH, Suzuki T, Funayama R, Nagashima T, Hayashi M, Sekine H, et al. Nrf2 suppresses macrophage inflammatory response by blocking proinflammatory cytokine transcription. Nature communications 2016; 7:11624.
64. Kwak MK, Kensler TW. Induction of 26S proteasome subunit PSMB5 by the bifunctional inducer 3-methylcholanthrene through the Nrf2-ARE, but not the AhR/Arnt-XRE, pathway. Biochemical and biophysical research communications 2006; 345:1350-7.
65. Kwak MK, Wakabayashi N, Itoh K, Motohashi H, Yamamoto M, Kensler TW. Modulation of gene expression by cancer chemopreventive dithiolethiones through the

Keap1-Nrf2 pathway. Identification of novel gene clusters for cell survival. The Journal of biological chemistry 2003; 278:8135-45.
66. Pajares M, Cuadrado A, Rojo AI. Modulation of proteostasis by transcription factor NRF2 and impact in neurodegenerative diseases. Redox biology 2017; 11:543-53.
67. Jain A, Lamark T, Sjottem E, Larsen KB, Awuh JA, Overvatn A, et al. p62/SQSTM1 is a target gene for transcription factor NRF2 and creates a positive feedback loop by inducing antioxidant response element-driven gene transcription. The Journal of biological chemistry 2010; 285:22576-91.
68. Jo C, Gundemir S, Pritchard S, Jin YN, Rahman I, Johnson GV. Nrf2 reduces levels of phosphorylated tau protein by inducing autophagy adaptor protein NDP52. Nature communications 2014; 5:3496.
69. Korovila I, Hugo M, Castro JP, Weber D, Hohn A, Grune T, et al. Proteostasis, oxidative stress and aging. Redox biology 2017; 13:550-67.
70. Sleat DE, Della Valle MC, Zheng H, Moore DF, Lobel P. The mannose 6-phosphate glycoprotein proteome. Journal of proteome research 2008; 7:3010-21.
71. Ohsumi Y, Anraku Y. Active transport of basic amino acids driven by a proton motive force in vacuolar membrane vesicles of Saccharomyces cerevisiae. The Journal of biological chemistry 1981; 256:2079-82.
72. Yang Z, Klionsky DJ. Mammalian autophagy: core molecular machinery and signaling regulation. Current opinion in cell biology 2010; 22:124-31.
73. De Duve C, Wattiaux R. Functions of lysosomes. Annual review of physiology 1966; 28:435-92.
74. Mizushima N, Levine B, Cuervo AM, Klionsky DJ. Autophagy fights disease through cellular self-digestion. Nature 2008; 451:1069-75.
75. Reggiori F, Klionsky DJ. Autophagy in the eukaryotic cell. Eukaryotic cell 2002; 1:11-21.
76. Meijer WH, van der Klei IJ, Veenhuis M, Kiel JA. ATG genes involved in non-selective autophagy are conserved from yeast to man, but the selective Cvt and pexophagy pathways also require organism-specific genes. Autophagy 2007; 3:106-16.
77. Lamb CA, Yoshimori T, Tooze SA. The autophagosome: origins unknown, biogenesis complex. Nature reviews Molecular cell biology 2013; 14:759-74.
78. Ariosa AR, Klionsky DJ. Autophagy core machinery: overcoming spatial barriers in neurons. Journal of molecular medicine 2016; 94:1217-27.
79. Boya P, Reggiori F, Codogno P. Emerging regulation and functions of autophagy. Nature cell biology 2013; 15:713-20.
80. Mizushima N. Physiological functions of autophagy. Current topics in microbiology and immunology 2009; 335:71-84.
81. Singh R, Cuervo AM. Autophagy in the cellular energetic balance. Cell metabolism 2011; 13:495-504.
82. Kaur J, Debnath J. Autophagy at the crossroads of catabolism and anabolism. Nature reviews Molecular cell biology 2015; 16:461-72.
83. Wong PM, Puente C, Ganley IG, Jiang X. The ULK1 complex: sensing nutrient signals for autophagy activation. Autophagy 2013; 9:124-37.
84. Ganley IG, Lam du H, Wang J, Ding X, Chen S, Jiang X. ULK1.ATG13.FIP200 complex mediates mTOR signaling and is essential for autophagy. The Journal of biological chemistry 2009; 284:12297-305.
85. Kim J, Kundu M, Viollet B, Guan KL. AMPK and mTOR regulate autophagy through direct phosphorylation of Ulk1. Nature cell biology 2011; 13:132-41.
86. Inoki K, Zhu T, Guan KL. TSC2 mediates cellular energy response to control cell growth and survival. Cell 2003; 115:577-90.

87. Gwinn DM, Shackelford DB, Egan DF, Mihaylova MM, Mery A, Vasquez DS, et al. AMPK phosphorylation of raptor mediates a metabolic checkpoint. Molecular cell 2008; 30:214-26.
88. Kim J, Kim YC, Fang C, Russell RC, Kim JH, Fan W, et al. Differential regulation of distinct Vps34 complexes by AMPK in nutrient stress and autophagy. Cell 2013; 152:290-303.
89. Russell RC, Yuan HX, Guan KL. Autophagy regulation by nutrient signaling. Cell research 2014; 24:42-57.
90. Kroemer G, Marino G, Levine B. Autophagy and the integrated stress response. Molecular cell 2010; 40:280-93.
91. Pajares M, Jimenez-Moreno N, Dias IH, Debelec B, Vucetic M, Fladmark KE, et al. Redox control of protein degradation. Redox biology 2015; 6:409-20.
92. Pajares M, Cuadrado A, Engedal N, Jirsova Z, Cahova M. The Role of Free Radicals in Autophagy Regulation: Implications for Ageing. Oxidative medicine and cellular longevity 2018; 2018:2450748.
93. Zmijewski JW, Banerjee S, Bae H, Friggeri A, Lazarowski ER, Abraham E. Exposure to hydrogen peroxide induces oxidation and activation of AMP-activated protein kinase. The Journal of biological chemistry 2010; 285:33154-64.
94. Cardaci S, Filomeni G, Ciriolo MR. Redox implications of AMPK-mediated signal transduction beyond energetic clues. Journal of cell science 2012; 125:2115-25.
95. Li L, Chen Y, Gibson SB. Starvation-induced autophagy is regulated by mitochondrial reactive oxygen species leading to AMPK activation. Cellular signalling 2013; 25:50-65.
96. Scherz-Shouval R, Shvets E, Fass E, Shorer H, Gil L, Elazar Z. Reactive oxygen species are essential for autophagy and specifically regulate the activity of Atg4. The EMBO journal 2007; 26:1749-60.
97. Frudd K, Burgoyne T, Burgoyne JR. Oxidation of Atg3 and Atg7 mediates inhibition of autophagy. Nature communications 2018; 9:95.
98. Komatsu M, Kurokawa H, Waguri S, Taguchi K, Kobayashi A, Ichimura Y, et al. The selective autophagy substrate p62 activates the stress responsive transcription factor Nrf2 through inactivation of Keap1. Nature cell biology 2010; 12:213-23.
99. Lau A, Wang XJ, Zhao F, Villeneuve NF, Wu T, Jiang T, et al. A noncanonical mechanism of Nrf2 activation by autophagy deficiency: direct interaction between Keap1 and p62. Molecular and cellular biology 2010; 30:3275-85.
100. Fan W, Tang Z, Chen D, Moughon D, Ding X, Chen S, et al. Keap1 facilitates p62-mediated ubiquitin aggregate clearance via autophagy. Autophagy 2010; 6:614-21.
101. Copple IM, Lister A, Obeng AD, Kitteringham NR, Jenkins RE, Layfield R, et al. Physical and functional interaction of sequestosome 1 with Keap1 regulates the Keap1-Nrf2 cell defense pathway. The Journal of biological chemistry 2010; 285:16782-8.
102. Ichimura Y, Waguri S, Sou YS, Kageyama S, Hasegawa J, Ishimura R, et al. Phosphorylation of p62 activates the Keap1-Nrf2 pathway during selective autophagy. Molecular cell 2013; 51:618-31.
103. Hashimoto K, Simmons AN, Kajino-Sakamoto R, Tsuji Y, Ninomiya-Tsuji J. TAK1 Regulates the Nrf2 Antioxidant System Through Modulating p62/SQSTM1. Antioxidants & redox signaling 2016; 25:953-64.
104. Adelman SH. The word for the future is data. Michigan medicine 1990; 89:74.
105. Palmieri M, Impey S, Kang H, di Ronza A, Pelz C, Sardiello M, et al. Characterization of the CLEAR network reveals an integrated control of cellular clearance pathways. Human molecular genetics 2011; 20:3852-66.
106. Settembre C, Zoncu R, Medina DL, Vetrini F, Erdin S, Erdin S, et al. A lysosome-to-nucleus signalling mechanism senses and regulates the lysosome via mTOR and TFEB. The EMBO journal 2012; 31:1095-108.

107. Settembre C, Di Malta C, Polito VA, Garcia Arencibia M, Vetrini F, Erdin S, et al. TFEB links autophagy to lysosomal biogenesis. Science 2011; 332:1429-33.
108. Sardiello M, Palmieri M, di Ronza A, Medina DL, Valenza M, Gennarino VA, et al. A gene network regulating lysosomal biogenesis and function. Science 2009; 325:473-7.
109. Mammucari C, Milan G, Romanello V, Masiero E, Rudolf R, Del Piccolo P, et al. FoxO3 controls autophagy in skeletal muscle in vivo. Cell metabolism 2007; 6:458-71.
110. Zhao J, Brault JJ, Schild A, Cao P, Sandri M, Schiaffino S, et al. FoxO3 coordinately activates protein degradation by the autophagic/lysosomal and proteasomal pathways in atrophying muscle cells. Cell metabolism 2007; 6:472-83.
111. Sanchez AM, Csibi A, Raibon A, Cornille K, Gay S, Bernardi H, et al. AMPK promotes skeletal muscle autophagy through activation of forkhead FoxO3a and interaction with Ulk1. Journal of cellular biochemistry 2012; 113:695-710.
112. Backer JM, Bourret L, Dice JF. Regulation of catabolism of microinjected ribonuclease A requires the amino-terminal 20 amino acids. Proceedings of the National Academy of Sciences of the United States of America 1983; 80:2166-70.
113. Wing SS, Chiang HL, Goldberg AL, Dice JF. Proteins containing peptide sequences related to Lys-Phe-Glu-Arg-Gln are selectively depleted in liver and heart, but not skeletal muscle, of fasted rats. The Biochemical journal 1991; 275 (Pt 1):165-9.
114. Chiang HL, Terlecky SR, Plant CP, Dice JF. A role for a 70-kilodalton heat shock protein in lysosomal degradation of intracellular proteins. Science 1989; 246:382-5.
115. Dice JF, Chiang HL. Peptide signals for protein degradation within lysosomes. Biochemical Society symposium 1989; 55:45-55.
116. Cuervo AM, Terlecky SR, Dice JF, Knecht E. Selective binding and uptake of ribonuclease A and glyceraldehyde-3-phosphate dehydrogenase by isolated rat liver lysosomes. The Journal of biological chemistry 1994; 269:26374-80.
117. Cuervo AM, Dice JF. A receptor for the selective uptake and degradation of proteins by lysosomes. Science 1996; 273:501-3.
118. Cuervo AM, Dice JF. Regulation of lamp2a levels in the lysosomal membrane. Traffic 2000; 1:570-83.
119. Bandyopadhyay U, Kaushik S, Varticovski L, Cuervo AM. The chaperone-mediated autophagy receptor organizes in dynamic protein complexes at the lysosomal membrane. Molecular and cellular biology 2008; 28:5747-63.
120. Salvador N, Aguado C, Horst M, Knecht E. Import of a cytosolic protein into lysosomes by chaperone-mediated autophagy depends on its folding state. The Journal of biological chemistry 2000; 275:27447-56.
121. Agarraberes FA, Terlecky SR, Dice JF. An intralysosomal hsp70 is required for a selective pathway of lysosomal protein degradation. The Journal of cell biology 1997; 137:825-34.
122. Massey A, Kiffin R, Cuervo AM. Pathophysiology of chaperone-mediated autophagy. The international journal of biochemistry & cell biology 2004; 36:2420-34.
123. Cuervo AM, Knecht E, Terlecky SR, Dice JF. Activation of a selective pathway of lysosomal proteolysis in rat liver by prolonged starvation. The American journal of physiology 1995; 269:C1200-8.
124. Kiffin R, Christian C, Knecht E, Cuervo AM. Activation of chaperone-mediated autophagy during oxidative stress. Molecular biology of the cell 2004; 15:4829-40.
125. Hubbi ME, Hu H, Kshitiz, Ahmed I, Levchenko A, Semenza GL. Chaperone-mediated autophagy targets hypoxia-inducible factor-1alpha (HIF-1alpha) for lysosomal degradation. The Journal of biological chemistry 2013; 288:10703-14.
126. Park C, Suh Y, Cuervo AM. Regulated degradation of Chk1 by chaperone-mediated autophagy in response to DNA damage. Nature communications 2015; 6:6823.

127. Cuervo AM, Dice JF. Unique properties of lamp2a compared to other lamp2 isoforms. Journal of cell science 2000; 113 Pt 24:4441-50.
128. Eskelinen EL, Cuervo AM, Taylor MR, Nishino I, Blum JS, Dice JF, et al. Unifying nomenclature for the isoforms of the lysosomal membrane protein LAMP-2. Traffic 2005; 6:1058-61.
129. Gough NR, Hatem CL, Fambrough DM. The family of LAMP-2 proteins arises by alternative splicing from a single gene: characterization of the avian LAMP-2 gene and identification of mammalian homologs of LAMP-2b and LAMP-2c. DNA and cell biology 1995; 14:863-7.
130. Perez L, McLetchie S, Gardiner GJ, Deffit SN, Zhou D, Blum JS. LAMP-2C Inhibits MHC Class II Presentation of Cytoplasmic Antigens by Disrupting Chaperone-Mediated Autophagy. Journal of immunology 2016; 196:2457-65.
131. Konecki DS, Foetisch K, Zimmer KP, Schlotter M, Lichter-Konecki U. An alternatively spliced form of the human lysosome-associated membrane protein-2 gene is expressed in a tissue-specific manner. Biochemical and biophysical research communications 1995; 215:757-67.
132. Massey AC, Kaushik S, Sovak G, Kiffin R, Cuervo AM. Consequences of the selective blockage of chaperone-mediated autophagy. Proceedings of the National Academy of Sciences of the United States of America 2006; 103:5805-10.
133. Kaushik S, Massey AC, Cuervo AM. Lysosome membrane lipid microdomains: novel regulators of chaperone-mediated autophagy. The EMBO journal 2006; 25:3921-33.
134. Arias E, Koga H, Diaz A, Mocholi E, Patel B, Cuervo AM. Lysosomal mTORC2/PHLPP1/Akt Regulate Chaperone-Mediated Autophagy. Molecular cell 2015; 59:270-84.
135. Schneider JL, Suh Y, Cuervo AM. Deficient chaperone-mediated autophagy in liver leads to metabolic dysregulation. Cell metabolism 2014; 20:417-32.
136. Cuervo AM, Palmer A, Rivett AJ, Knecht E. Degradation of proteasomes by lysosomes in rat liver. European journal of biochemistry / FEBS 1995; 227:792-800.
137. Kaushik S, Massey AC, Mizushima N, Cuervo AM. Constitutive activation of chaperone-mediated autophagy in cells with impaired macroautophagy. Molecular biology of the cell 2008; 19:2179-92.
138. Cuervo AM. Chaperone-mediated autophagy: selectivity pays off. Trends in endocrinology and metabolism: TEM 2010; 21:142-50.
139. Valdor R, Mocholi E, Botbol Y, Guerrero-Ros I, Chandra D, Koga H, et al. Chaperone-mediated autophagy regulates T cell responses through targeted degradation of negative regulators of T cell activation. Nature immunology 2014; 15:1046-54.
140. Halliwell B. Reactive oxygen species and the central nervous system. Journal of neurochemistry 1992; 59:1609-23.
141. Markesbery WR. Oxidative stress hypothesis in Alzheimer's disease. Free radical biology & medicine 1997; 23:134-47.
142. Butterfield DA, Swomley AM, Sultana R. Amyloid beta-peptide (1-42)-induced oxidative stress in Alzheimer disease: importance in disease pathogenesis and progression. Antioxidants & redox signaling 2013; 19:823-35.
143. Pratico D, Uryu K, Leight S, Trojanoswki JQ, Lee VM. Increased lipid peroxidation precedes amyloid plaque formation in an animal model of Alzheimer amyloidosis. The Journal of neuroscience : the official journal of the Society for Neuroscience 2001; 21:4183-7.
144. Nunomura A, Perry G, Aliev G, Hirai K, Takeda A, Balraj EK, et al. Oxidative damage is the earliest event in Alzheimer disease. Journal of neuropathology and experimental neurology 2001; 60:759-67.
145. Calabrese V, Scapagnini G, Ravagna A, Colombrita C, Spadaro F, Butterfield DA, et al. Increased expression of heat shock proteins in rat brain during aging: relationship with

mitochondrial function and glutathione redox state. Mechanisms of ageing and development 2004; 125:325-35.
146. Tonnies E, Trushina E. Oxidative Stress, Synaptic Dysfunction, and Alzheimer's Disease. Journal of Alzheimer's disease : JAD 2017; 57:1105-21.
147. Mhatre M, Floyd RA, Hensley K. Oxidative stress and neuroinflammation in Alzheimer's disease and amyotrophic lateral sclerosis: common links and potential therapeutic targets. Journal of Alzheimer's disease : JAD 2004; 6:147-57.
148. Ko SY, Lin YP, Lin YS, Chang SS. Advanced glycation end products enhance amyloid precursor protein expression by inducing reactive oxygen species. Free radical biology & medicine 2010; 49:474-80.
149. Lovell MA, Xiong S, Xie C, Davies P, Markesbery WR. Induction of hyperphosphorylated tau in primary rat cortical neuron cultures mediated by oxidative stress and glycogen synthase kinase-3. Journal of Alzheimer's disease : JAD 2004; 6:659-71; discussion 73-81.
150. Horiguchi T, Uryu K, Giasson BI, Ischiropoulos H, LightFoot R, Bellmann C, et al. Nitration of tau protein is linked to neurodegeneration in tauopathies. The American journal of pathology 2003; 163:1021-31.
151. Zheng H, Koo EH. The amyloid precursor protein: beyond amyloid. Molecular neurodegeneration 2006; 1:5.
152. Zhang YW, Thompson R, Zhang H, Xu H. APP processing in Alzheimer's disease. Molecular brain 2011; 4:3.
153. Feinstein SC, Wilson L. Inability of tau to properly regulate neuronal microtubule dynamics: a loss-of-function mechanism by which tau might mediate neuronal cell death. Biochimica et biophysica acta 2005; 1739:268-79.
154. Mietelska-Porowska A, Wasik U, Goras M, Filipek A, Niewiadomska G. Tau protein modifications and interactions: their role in function and dysfunction. International journal of molecular sciences 2014; 15:4671-713.
155. Komatsu M, Waguri S, Chiba T, Murata S, Iwata J, Tanida I, et al. Loss of autophagy in the central nervous system causes neurodegeneration in mice. Nature 2006; 441:880-4.
156. Friedman LG, Lachenmayer ML, Wang J, He L, Poulose SM, Komatsu M, et al. Disrupted autophagy leads to dopaminergic axon and dendrite degeneration and promotes presynaptic accumulation of alpha-synuclein and LRRK2 in the brain. The Journal of neuroscience : the official journal of the Society for Neuroscience 2012; 32:7585-93.
157. Nilsson P, Loganathan K, Sekiguchi M, Matsuba Y, Hui K, Tsubuki S, et al. Abeta secretion and plaque formation depend on autophagy. Cell reports 2013; 5:61-9.
158. Dice JF. Altered degradation of proteins microinjected into senescent human fibroblasts. The Journal of biological chemistry 1982; 257:14624-7.
159. Lipinski MM, Zheng B, Lu T, Yan Z, Py BF, Ng A, et al. Genome-wide analysis reveals mechanisms modulating autophagy in normal brain aging and in Alzheimer's disease. Proceedings of the National Academy of Sciences of the United States of America 2010; 107:14164-9.
160. Carnio S, LoVerso F, Baraibar MA, Longa E, Khan MM, Maffei M, et al. Autophagy impairment in muscle induces neuromuscular junction degeneration and precocious aging. Cell reports 2014; 8:1509-21.
161. Ott C, Konig J, Hohn A, Jung T, Grune T. Macroautophagy is impaired in old murine brain tissue as well as in senescent human fibroblasts. Redox biology 2016; 10:266-73.
162. Cuervo AM, Dice JF. Age-related decline in chaperone-mediated autophagy. The Journal of biological chemistry 2000; 275:31505-13.
163. Nixon RA, Wegiel J, Kumar A, Yu WH, Peterhoff C, Cataldo A, et al. Extensive involvement of autophagy in Alzheimer disease: an immuno-electron microscopy study. Journal of neuropathology and experimental neurology 2005; 64:113-22.

164. Kuusisto E, Kauppinen T, Alafuzoff I. Use of p62/SQSTM1 antibodies for neuropathological diagnosis. Neuropathology and applied neurobiology 2008; 34:169-80.
165. Suh JH, Shenvi SV, Dixon BM, Liu H, Jaiswal AK, Liu RM, et al. Decline in transcriptional activity of Nrf2 causes age-related loss of glutathione synthesis, which is reversible with lipoic acid. Proceedings of the National Academy of Sciences of the United States of America 2004; 101:3381-6.
166. Rahman MM, Sykiotis GP, Nishimura M, Bodmer R, Bohmann D. Declining signal dependence of Nrf2-MafS-regulated gene expression correlates with aging phenotypes. Aging cell 2013; 12:554-62.
167. von Otter M, Landgren S, Nilsson S, Zetterberg M, Celojevic D, Bergstrom P, et al. Nrf2-encoding NFE2L2 haplotypes influence disease progression but not risk in Alzheimer's disease and age-related cataract. Mechanisms of ageing and development 2010; 131:105-10.
168. Hayes JD, McMahon M. NRF2 and KEAP1 mutations: permanent activation of an adaptive response in cancer. Trends in biochemical sciences 2009; 34:176-88.
169. Shibata T, Ohta T, Tong KI, Kokubu A, Odogawa R, Tsuta K, et al. Cancer related mutations in NRF2 impair its recognition by Keap1-Cul3 E3 ligase and promote malignancy. Proceedings of the National Academy of Sciences of the United States of America 2008; 105:13568-73.
170. Kensler TW, Wakabayashi N. Nrf2: friend or foe for chemoprevention? Carcinogenesis 2010; 31:90-9.
171. White E. The role for autophagy in cancer. The Journal of clinical investigation 2015; 125:42-6.
172. Tasset I, Cuervo AM. Role of chaperone-mediated autophagy in metabolism. The FEBS journal 2016; 283:2403-13.
173. Kon M, Kiffin R, Koga H, Chapochnick J, Macian F, Varticovski L, et al. Chaperone-mediated autophagy is required for tumor growth. Science translational medicine 2011; 3:109ra17.
174. Saha T. LAMP2A overexpression in breast tumors promotes cancer cell survival via chaperone-mediated autophagy. Autophagy 2012; 8:1643-56.
175. Li L, Fang R, Liu B, Shi H, Wang Y, Zhang W, et al. Deacetylation of tumor-suppressor MST1 in Hippo pathway induces its degradation through HBXIP-elevated HDAC6 in promotion of breast cancer growth. Oncogene 2016; 35:4048-57.
176. Jovcevska I, Kocevar N, Komel R. Glioma and glioblastoma - how much do we (not) know? Molecular and clinical oncology 2013; 1:935-41.
177. Rojo AI, Salinas M, Martin D, Perona R, Cuadrado A. Regulation of Cu/Zn-superoxide dismutase expression via the phosphatidylinositol 3 kinase/Akt pathway and nuclear factor-kappaB. The Journal of neuroscience : the official journal of the Society for Neuroscience 2004; 24:7324-34.
178. Singh A, Misra V, Thimmulappa RK, Lee H, Ames S, Hoque MO, et al. Dysfunctional KEAP1-NRF2 interaction in non-small-cell lung cancer. PLoS medicine 2006; 3:e420.
179. Wang R, An J, Ji F, Jiao H, Sun H, Zhou D. Hypermethylation of the Keap1 gene in human lung cancer cell lines and lung cancer tissues. Biochemical and biophysical research communications 2008; 373:151-4.
180. Vidal M, Morris R, Grosveld F, Spanopoulou E. Tissue-specific control elements of the Thy-1 gene. The EMBO journal 1990; 9:833-40.
181. Terwel D, Muyllaert D, Dewachter I, Borghgraef P, Croes S, Devijver H, et al. Amyloid activates GSK-3beta to aggravate neuronal tauopathy in bigenic mice. The American journal of pathology 2008; 172:786-98.
182. Terwel D, Lasrado R, Snauwaert J, Vandeweert E, Van Haesendonck C, Borghgraef P, et al. Changed conformation of mutant Tau-P301L underlies the moribund tauopathy, absent

in progressive, nonlethal axonopathy of Tau-4R/2N transgenic mice. The Journal of biological chemistry 2005; 280:3963-73.
183. Moechars D, Dewachter I, Lorent K, Reverse D, Baekelandt V, Naidu A, et al. Early phenotypic changes in transgenic mice that overexpress different mutants of amyloid precursor protein in brain. The Journal of biological chemistry 1999; 274:6483-92.
184. Laemmli UK. Cleavage of structural proteins during the assembly of the head of bacteriophage T4. Nature 1970; 227:680-5.
185. Navarrete M, Perea G, Fernandez de Sevilla D, Gomez-Gonzalo M, Nunez A, Martin ED, et al. Astrocytes mediate in vivo cholinergic-induced synaptic plasticity. PLoS biology 2012; 10:e1001259.
186. Sherman MA, Lesne SE. Detecting abeta*56 oligomers in brain tissues. Methods in molecular biology 2011; 670:45-56.
187. Kaushik S, Cuervo AM. Methods to monitor chaperone-mediated autophagy. Methods in enzymology 2009; 452:297-324.
188. Storrie B, Madden EA. Isolation of subcellular organelles. Methods in enzymology 1990; 182:203-25.
189. Koga H, Martinez-Vicente M, Macian F, Verkhusha VV, Cuervo AM. A photoconvertible fluorescent reporter to track chaperone-mediated autophagy. Nature communications 2011; 2:386.
190. Arias E. Methods to Study Chaperone-Mediated Autophagy. Methods in enzymology 2017; 588:283-305.
191. Keene MA, Elgin SC. Micrococcal nuclease as a probe of DNA sequence organization and chromatin structure. Cell 1981; 27:57-64.
192. McGhee JD, Wood WI, Dolan M, Engel JD, Felsenfeld G. A 200 base pair region at the 5' end of the chicken adult beta-globin gene is accessible to nuclease digestion. Cell 1981; 27:45-55.
193. Creyghton MP, Cheng AW, Welstead GG, Kooistra T, Carey BW, Steine EJ, et al. Histone H3K27ac separates active from poised enhancers and predicts developmental state. Proceedings of the National Academy of Sciences of the United States of America 2010; 107:21931-6.
194. Potteti HR, Reddy NM, Hei TK, Kalvakolanu DV, Reddy SP. The NRF2 activation and antioxidative response are not impaired overall during hyperoxia-induced lung epithelial cell death. Oxidative medicine and cellular longevity 2013; 2013:798401.
195. Kwak MK, Itoh K, Yamamoto M, Kensler TW. Enhanced expression of the transcription factor Nrf2 by cancer chemopreventive agents: role of antioxidant response element-like sequences in the nrf2 promoter. Molecular and cellular biology 2002; 22:2883-92.
196. Klionsky DJ, Abdelmohsen K, Abe A, Abedin MJ, Abeliovich H, Acevedo Arozena A, et al. Guidelines for the use and interpretation of assays for monitoring autophagy (3rd edition). Autophagy 2016; 12:1-222.
197. Herl L, Thomas AV, Lill CM, Banks M, Deng A, Jones PB, et al. Mutations in amyloid precursor protein affect its interactions with presenilin/gamma-secretase. Molecular and cellular neurosciences 2009; 41:166-74.
198. Muratore CR, Rice HC, Srikanth P, Callahan DG, Shin T, Benjamin LN, et al. The familial Alzheimer's disease APPV717I mutation alters APP processing and Tau expression in iPSC-derived neurons. Human molecular genetics 2014; 23:3523-36.
199. Barghorn S, Zheng-Fischhofer Q, Ackmann M, Biernat J, von Bergen M, Mandelkow EM, et al. Structure, microtubule interactions, and paired helical filament aggregation by tau mutants of frontotemporal dementias. Biochemistry 2000; 39:11714-21.
200. Lynch MA. Long-term potentiation and memory. Physiological reviews 2004; 84:87-136.

201. Joshi G, Gan KA, Johnson DA, Johnson JA. Increased Alzheimer's disease-like pathology in the APP/ PS1DeltaE9 mouse model lacking Nrf2 through modulation of autophagy. Neurobiology of aging 2015; 36:664-79.
202. Larson ME, Lesne SE. Soluble Abeta oligomer production and toxicity. Journal of neurochemistry 2012; 120 Suppl 1:125-39.
203. Schneider JL, Villarroya J, Diaz-Carretero A, Patel B, Urbanska AM, Thi MM, et al. Loss of hepatic chaperone-mediated autophagy accelerates proteostasis failure in aging. Aging cell 2015; 14:249-64.
204. Kishi-Itakura C, Koyama-Honda I, Itakura E, Mizushima N. Ultrastructural analysis of autophagosome organization using mammalian autophagy-deficient cells. Journal of cell science 2014; 127:4089-102.
205. Jo C, Kim S, Cho SJ, Choi KJ, Yun SM, Koh YH, et al. Sulforaphane induces autophagy through ERK activation in neuronal cells. FEBS letters 2014; 588:3081-8.
206. Zhang L, Cardinal JS, Bahar R, Evankovich J, Huang H, Nace G, et al. Interferon regulatory factor-1 regulates the autophagic response in LPS-stimulated macrophages through nitric oxide. Molecular medicine 2012; 18:201-8.
207. Taguchi K, Fujikawa N, Komatsu M, Ishii T, Unno M, Akaike T, et al. Keap1 degradation by autophagy for the maintenance of redox homeostasis. Proceedings of the National Academy of Sciences of the United States of America 2012; 109:13561-6.
208. Lau A, Tian W, Whitman SA, Zhang DD. The predicted molecular weight of Nrf2: it is what it is not. Antioxidants & redox signaling 2013; 18:91-3.
209. Yamamoto T, Kyo M, Kamiya T, Tanaka T, Engel JD, Motohashi H, et al. Predictive base substitution rules that determine the binding and transcriptional specificity of Maf recognition elements. Genes to cells : devoted to molecular & cellular mechanisms 2006; 11:575-91.
210. Hac A, Domachowska A, Narajczyk M, Cyske K, Pawlik A, Herman-Antosiewicz A. S6K1 controls autophagosome maturation in autophagy induced by sulforaphane or serum deprivation. European journal of cell biology 2015; 94:470-81.
211. Lee JH, Jeong JK, Park SY. Sulforaphane-induced autophagy flux prevents prion protein-mediated neurotoxicity through AMPK pathway. Neuroscience 2014; 278:31-9.
212. Jain A, Rusten TE, Katheder N, Elvenes J, Bruun JA, Sjottem E, et al. p62/Sequestosome-1, Autophagy-related Gene 8, and Autophagy in Drosophila Are Regulated by Nuclear Factor Erythroid 2-related Factor 2 (NRF2), Independent of Transcription Factor TFEB. The Journal of biological chemistry 2015; 290:14945-62.
213. Mizushima N, Yamamoto A, Matsui M, Yoshimori T, Ohsumi Y. In vivo analysis of autophagy in response to nutrient starvation using transgenic mice expressing a fluorescent autophagosome marker. Molecular biology of the cell 2004; 15:1101-11.
214. Mizushima N, Yoshimori T, Levine B. Methods in mammalian autophagy research. Cell 2010; 140:313-26.
215. Cuello AC. Early and Late CNS Inflammation in Alzheimer's Disease: Two Extremes of a Continuum? Trends in pharmacological sciences 2017; 38:956-66.
216. Zhou L, Zhang H, Davies KJA, Forman HJ. Aging-related decline in the induction of Nrf2-regulated antioxidant genes in human bronchial epithelial cells. Redox biology 2018; 14:35-40.
217. Kanninen K, Heikkinen R, Malm T, Rolova T, Kuhmonen S, Leinonen H, et al. Intrahippocampal injection of a lentiviral vector expressing Nrf2 improves spatial learning in a mouse model of Alzheimer's disease. Proceedings of the National Academy of Sciences of the United States of America 2009; 106:16505-10.
218. Branca C, Ferreira E, Nguyen TV, Doyle K, Caccamo A, Oddo S. Genetic reduction of Nrf2 exacerbates cognitive deficits in a mouse model of Alzheimer's disease. Human molecular genetics 2017; 26:4823-35.

219. Lastres-Becker I, Innamorato NG, Jaworski T, Rabano A, Kugler S, Van Leuven F, et al. Fractalkine activates NRF2/NFE2L2 and heme oxygenase 1 to restrain tauopathy-induced microgliosis. Brain : a journal of neurology 2014; 137:78-91.
220. Di Bona D, Scapagnini G, Candore G, Castiglia L, Colonna-Romano G, Duro G, et al. Immune-inflammatory responses and oxidative stress in Alzheimer's disease: therapeutic implications. Current pharmaceutical design 2010; 16:684-91.
221. Hooper C, Markevich V, Plattner F, Killick R, Schofield E, Engel T, et al. Glycogen synthase kinase-3 inhibition is integral to long-term potentiation. The European journal of neuroscience 2007; 25:81-6.
222. Mudher A, Shepherd D, Newman TA, Mildren P, Jukes JP, Squire A, et al. GSK-3beta inhibition reverses axonal transport defects and behavioural phenotypes in Drosophila. Molecular psychiatry 2004; 9:522-30.
223. Wilson RS, Leurgans SE, Boyle PA, Bennett DA. Cognitive decline in prodromal Alzheimer disease and mild cognitive impairment. Archives of neurology 2011; 68:351-6.
224. Rojo AI, Pajares M, Rada P, Nunez A, Nevado-Holgado AJ, Killik R, et al. NRF2 deficiency replicates transcriptomic changes in Alzheimer's patients and worsens APP and TAU pathology. Redox biology 2017; 13:444-51.
225. Chan K, Lu R, Chang JC, Kan YW. NRF2, a member of the NFE2 family of transcription factors, is not essential for murine erythropoiesis, growth, and development. Proceedings of the National Academy of Sciences of the United States of America 1996; 93:13943-8.
226. Braun S, Hanselmann C, Gassmann MG, auf dem Keller U, Born-Berclaz C, Chan K, et al. Nrf2 transcription factor, a novel target of keratinocyte growth factor action which regulates gene expression and inflammation in the healing skin wound. Molecular and cellular biology 2002; 22:5492-505.
227. Iizuka T, Ishii Y, Itoh K, Kiwamoto T, Kimura T, Matsuno Y, et al. Nrf2-deficient mice are highly susceptible to cigarette smoke-induced emphysema. Genes to cells : devoted to molecular & cellular mechanisms 2005; 10:1113-25.
228. Gebel S, Diehl S, Pype J, Friedrichs B, Weiler H, Schuller J, et al. The transcriptome of Nrf2-/- mice provides evidence for impaired cell cycle progression in the development of cigarette smoke-induced emphysematous changes. Toxicological sciences : an official journal of the Society of Toxicology 2010; 115:238-52.
229. Chan K, Han XD, Kan YW. An important function of Nrf2 in combating oxidative stress: detoxification of acetaminophen. Proceedings of the National Academy of Sciences of the United States of America 2001; 98:4611-6.
230. Enomoto A, Itoh K, Nagayoshi E, Haruta J, Kimura T, O'Connor T, et al. High sensitivity of Nrf2 knockout mice to acetaminophen hepatotoxicity associated with decreased expression of ARE-regulated drug metabolizing enzymes and antioxidant genes. Toxicological sciences : an official journal of the Society of Toxicology 2001; 59:169-77.
231. Jin W, Wang H, Yan W, Zhu L, Hu Z, Ding Y, et al. Role of Nrf2 in protection against traumatic brain injury in mice. Journal of neurotrauma 2009; 26:131-9.
232. Innamorato NG, Jazwa A, Rojo AI, Garcia C, Fernandez-Ruiz J, Grochot-Przeczek A, et al. Different susceptibility to the Parkinson's toxin MPTP in mice lacking the redox master regulator Nrf2 or its target gene heme oxygenase-1. PloS one 2010; 5:e11838.
233. Rojo AI, Innamorato NG, Martin-Moreno AM, De Ceballos ML, Yamamoto M, Cuadrado A. Nrf2 regulates microglial dynamics and neuroinflammation in experimental Parkinson's disease. Glia 2010; 58:588-98.
234. Rubinsztein DC, Codogno P, Levine B. Autophagy modulation as a potential therapeutic target for diverse diseases. Nature reviews Drug discovery 2012; 11:709-30.

235. Hara T, Nakamura K, Matsui M, Yamamoto A, Nakahara Y, Suzuki-Migishima R, et al. Suppression of basal autophagy in neural cells causes neurodegenerative disease in mice. Nature 2006; 441:885-9.
236. Agholme L, Hallbeck M, Benedikz E, Marcusson J, Kagedal K. Amyloid-beta secretion, generation, and lysosomal sequestration in response to proteasome inhibition: involvement of autophagy. Journal of Alzheimer's disease : JAD 2012; 31:343-58.
237. Zheng L, Terman A, Hallbeck M, Dehvari N, Cowburn RF, Benedikz E, et al. Macroautophagy-generated increase of lysosomal amyloid beta-protein mediates oxidant-induced apoptosis of cultured neuroblastoma cells. Autophagy 2011; 7:1528-45.
238. Yu WH, Cuervo AM, Kumar A, Peterhoff CM, Schmidt SD, Lee JH, et al. Macroautophagy--a novel Beta-amyloid peptide-generating pathway activated in Alzheimer's disease. The Journal of cell biology 2005; 171:87-98.
239. Yu WH, Kumar A, Peterhoff C, Shapiro Kulnane L, Uchiyama Y, Lamb BT, et al. Autophagic vacuoles are enriched in amyloid precursor protein-secretase activities: implications for beta-amyloid peptide over-production and localization in Alzheimer's disease. The international journal of biochemistry & cell biology 2004; 36:2531-40.
240. Lesne S, Koh MT, Kotilinek L, Kayed R, Glabe CG, Yang A, et al. A specific amyloid-beta protein assembly in the brain impairs memory. Nature 2006; 440:352-7.
241. Lesne SE, Sherman MA, Grant M, Kuskowski M, Schneider JA, Bennett DA, et al. Brain amyloid-beta oligomers in ageing and Alzheimer's disease. Brain : a journal of neurology 2013; 136:1383-98.
242. Handoko M, Grant M, Kuskowski M, Zahs KR, Wallin A, Blennow K, et al. Correlation of specific amyloid-beta oligomers with tau in cerebrospinal fluid from cognitively normal older adults. JAMA neurology 2013; 70:594-9.
243. Cheng IH, Scearce-Levie K, Legleiter J, Palop JJ, Gerstein H, Bien-Ly N, et al. Accelerating amyloid-beta fibrillization reduces oligomer levels and functional deficits in Alzheimer disease mouse models. The Journal of biological chemistry 2007; 282:23818-28.
244. Lesne S, Kotilinek L, Ashe KH. Plaque-bearing mice with reduced levels of oligomeric amyloid-beta assemblies have intact memory function. Neuroscience 2008; 151:745-9.
245. Wang Y, Mandelkow E. Degradation of tau protein by autophagy and proteasomal pathways. Biochemical Society transactions 2012; 40:644-52.
246. Schaeffer V, Lavenir I, Ozcelik S, Tolnay M, Winkler DT, Goedert M. Stimulation of autophagy reduces neurodegeneration in a mouse model of human tauopathy. Brain : a journal of neurology 2012; 135:2169-77.
247. Ma Q. Role of nrf2 in oxidative stress and toxicity. Annual review of pharmacology and toxicology 2013; 53:401-26.
248. Zhang C, Cuervo AM. Restoration of chaperone-mediated autophagy in aging liver improves cellular maintenance and hepatic function. Nature medicine 2008; 14:959-65.
249. Nishino I, Fu J, Tanji K, Yamada T, Shimojo S, Koori T, et al. Primary LAMP-2 deficiency causes X-linked vacuolar cardiomyopathy and myopathy (Danon disease). Nature 2000; 406:906-10.
250. Tanaka Y, Guhde G, Suter A, Eskelinen EL, Hartmann D, Lullmann-Rauch R, et al. Accumulation of autophagic vacuoles and cardiomyopathy in LAMP-2-deficient mice. Nature 2000; 406:902-6.
251. Fujiwara Y, Kikuchi H, Aizawa S, Furuta A, Hatanaka Y, Konya C, et al. Direct uptake and degradation of DNA by lysosomes. Autophagy 2013; 9:1167-71.
252. Murphy KE, Gysbers AM, Abbott SK, Spiro AS, Furuta A, Cooper A, et al. Lysosomal-associated membrane protein 2 isoforms are differentially affected in early Parkinson's disease. Movement disorders : official journal of the Movement Disorder Society 2015; 30:1639-47.

253. Kiffin R, Kaushik S, Zeng M, Bandyopadhyay U, Zhang C, Massey AC, et al. Altered dynamics of the lysosomal receptor for chaperone-mediated autophagy with age. Journal of cell science 2007; 120:782-91.
254. Gan L, Vargas MR, Johnson DA, Johnson JA. Astrocyte-specific overexpression of Nrf2 delays motor pathology and synuclein aggregation throughout the CNS in the alpha-synuclein mutant (A53T) mouse model. The Journal of neuroscience : the official journal of the Society for Neuroscience 2012; 32:17775-87.
255. Webb AE, Brunet A. FOXO transcription factors: key regulators of cellular quality control. Trends in biochemical sciences 2014; 39:159-69.
256. Kang YA, Sanalkumar R, O'Geen H, Linnemann AK, Chang CJ, Bouhassira EE, et al. Autophagy driven by a master regulator of hematopoiesis. Molecular and cellular biology 2012; 32:226-39.
257. Chauhan S, Goodwin JG, Chauhan S, Manyam G, Wang J, Kamat AM, et al. ZKSCAN3 is a master transcriptional repressor of autophagy. Molecular cell 2013; 50:16-28.
258. Kobayashi S, Volden P, Timm D, Mao K, Xu X, Liang Q. Transcription factor GATA4 inhibits doxorubicin-induced autophagy and cardiomyocyte death. The Journal of biological chemistry 2010; 285:793-804.
259. Settembre C, Ballabio A. TFEB regulates autophagy: an integrated coordination of cellular degradation and recycling processes. Autophagy 2011; 7:1379-81.
260. Zhao Y, Yang J, Liao W, Liu X, Zhang H, Wang S, et al. Cytosolic FoxO1 is essential for the induction of autophagy and tumour suppressor activity. Nature cell biology 2010; 12:665-75.
261. Sawada R, Jardine KA, Fukuda M. The genes of major lysosomal membrane glycoproteins, lamp-1 and lamp-2. 5'-flanking sequence of lamp-2 gene and comparison of exon organization in two genes. The Journal of biological chemistry 1993; 268:9014-22.
262. Kimura M, Yamamoto T, Zhang J, Itoh K, Kyo M, Kamiya T, et al. Molecular basis distinguishing the DNA binding profile of Nrf2-Maf heterodimer from that of Maf homodimer. The Journal of biological chemistry 2007; 282:33681-90.
263. Goh KI, Cusick ME, Valle D, Childs B, Vidal M, Barabasi AL. The human disease network. Proceedings of the National Academy of Sciences of the United States of America 2007; 104:8685-90.
264. Rubinsztein DC, DiFiglia M, Heintz N, Nixon RA, Qin ZH, Ravikumar B, et al. Autophagy and its possible roles in nervous system diseases, damage and repair. Autophagy 2005; 1:11-22.
265. Martinez-Vicente M. Autophagy in neurodegenerative diseases: From pathogenic dysfunction to therapeutic modulation. Seminars in cell & developmental biology 2015; 40:115-26.
266. Wong YC, Holzbaur EL. Autophagosome dynamics in neurodegeneration at a glance. Journal of cell science 2015; 128:1259-67.
267. Goetzl EJ, Boxer A, Schwartz JB, Abner EL, Petersen RC, Miller BL, et al. Altered lysosomal proteins in neural-derived plasma exosomes in preclinical Alzheimer disease. Neurology 2015; 85:40-7.
268. Ramsey CP, Glass CA, Montgomery MB, Lindl KA, Ritson GP, Chia LA, et al. Expression of Nrf2 in neurodegenerative diseases. Journal of neuropathology and experimental neurology 2007; 66:75-85.
269. Raina AK, Templeton DJ, Deak JC, Perry G, Smith MA. Quinone reductase (NQO1), a sensitive redox indicator, is increased in Alzheimer's disease. Redox report : communications in free radical research 1999; 4:23-7.
270. Wang Y, Santa-Cruz K, DeCarli C, Johnson JA. NAD(P)H:quinone oxidoreductase activity is increased in hippocampal pyramidal neurons of patients with Aalzheimer's disease. Neurobiology of aging 2000; 21:525-31.

271. Schipper HM, Bennett DA, Liberman A, Bienias JL, Schneider JA, Kelly J, et al. Glial heme oxygenase-1 expression in Alzheimer disease and mild cognitive impairment. Neurobiology of aging 2006; 27:252-61.
272. Tanji K, Miki Y, Ozaki T, Maruyama A, Yoshida H, Mimura J, et al. Phosphorylation of serine 349 of p62 in Alzheimer's disease brain. Acta neuropathologica communications 2014; 2:50.
273. Inestrosa NC, Reyes AE, Chacon MA, Cerpa W, Villalon A, Montiel J, et al. Human-like rodent amyloid-beta-peptide determines Alzheimer pathology in aged wild-type Octodon degu. Neurobiology of aging 2005; 26:1023-8.
274. Thibaudeau TA, Anderson RT, Smith DM. A common mechanism of proteasome impairment by neurodegenerative disease-associated oligomers. Nature communications 2018; 9:1097.
275. He X, Ma Q. Redox regulation by nuclear factor erythroid 2-related factor 2: gatekeeping for the basal and diabetes-induced expression of thioredoxin-interacting protein. Molecular pharmacology 2012; 82:887-97.
276. Tebay LE, Robertson H, Durant ST, Vitale SR, Penning TM, Dinkova-Kostova AT, et al. Mechanisms of activation of the transcription factor Nrf2 by redox stressors, nutrient cues, and energy status and the pathways through which it attenuates degenerative disease. Free radical biology & medicine 2015; 88:108-46.
277. von Otter M, Bergstrom P, Quattrone A, De Marco EV, Annesi G, Soderkvist P, et al. Genetic associations of Nrf2-encoding NFE2L2 variants with Parkinson's disease - a multicenter study. BMC medical genetics 2014; 15:131.
278. Bergstrom P, von Otter M, Nilsson S, Nilsson AC, Nilsson M, Andersen PM, et al. Association of NFE2L2 and KEAP1 haplotypes with amyotrophic lateral sclerosis. Amyotrophic lateral sclerosis & frontotemporal degeneration 2014; 15:130-7.
279. Fan Z, Wirth AK, Chen D, Wruck CJ, Rauh M, Buchfelder M, et al. Nrf2-Keap1 pathway promotes cell proliferation and diminishes ferroptosis. Oncogenesis 2017; 6:e371.
280. Kim S, Choi KJ, Cho SJ, Yun SM, Jeon JP, Koh YH, et al. Fisetin stimulates autophagic degradation of phosphorylated tau via the activation of TFEB and Nrf2 transcription factors. Scientific reports 2016; 6:24933.
281. Wang Y, Martinez-Vicente M, Kruger U, Kaushik S, Wong E, Mandelkow EM, et al. Tau fragmentation, aggregation and clearance: the dual role of lysosomal processing. Human molecular genetics 2009; 18:4153-70.
282. Caballero B, Wang Y, Diaz A, Tasset I, Juste YR, Stiller B, et al. Interplay of pathogenic forms of human tau with different autophagic pathways. Aging cell 2018; 17.
283. Cong ZX, Wang HD, Wang JW, Zhou Y, Pan H, Zhang DD, et al. ERK and PI3K signaling cascades induce Nrf2 activation and regulate cell viability partly through Nrf2 in human glioblastoma cells. Oncology reports 2013; 30:715-22.
284. Ji XJ, Chen SH, Zhu L, Pan H, Zhou Y, Li W, et al. Knockdown of NF-E2-related factor 2 inhibits the proliferation and growth of U251MG human glioma cells in a mouse xenograft model. Oncology reports 2013; 30:157-64.
285. Kanamori M, Higa T, Sonoda Y, Murakami S, Dodo M, Kitamura H, et al. Activation of the NRF2 pathway and its impact on the prognosis of anaplastic glioma patients. Neuro-oncology 2015; 17:555-65.
286. Zhu J, Wang H, Sun Q, Ji X, Zhu L, Cong Z, et al. Nrf2 is required to maintain the self-renewal of glioma stem cells. BMC cancer 2013; 13:380.
287. Taguchi K, Yamamoto M. The KEAP1-NRF2 System in Cancer. Frontiers in oncology 2017; 7:85.
288. Tarumoto T, Nagai T, Ohmine K, Miyoshi T, Nakamura M, Kondo T, et al. Ascorbic acid restores sensitivity to imatinib via suppression of Nrf2-dependent gene expression in the imatinib-resistant cell line. Experimental hematology 2004; 32:375-81.

289. Wang XJ, Hayes JD, Henderson CJ, Wolf CR. Identification of retinoic acid as an inhibitor of transcription factor Nrf2 through activation of retinoic acid receptor alpha. Proceedings of the National Academy of Sciences of the United States of America 2007; 104:19589-94.
290. Anguiano J, Garner TP, Mahalingam M, Das BC, Gavathiotis E, Cuervo AM. Chemical modulation of chaperone-mediated autophagy by retinoic acid derivatives. Nature chemical biology 2013; 9:374-82.

Appendices

Appendix I

Appendix I. Script created with Python 3.4 to compare in human genes the putative AREs with the PSSM and calculate their relative score.

```
import sys
import re

def Get_PSSM(FileName):
   tmp={}
   MyFile=open(FileName,'r')
   for Nt in ["A","C","G","T"]:
      pos=MyFile.readline()
      tmp[Nt]=pos.strip().split("\t")
   MyFile.close()
   return(tmp)

def Get_Coordin(Coord):
   MyRE=r'(\w*)(chr[0-9XY]{1,2}):(\d+)-(\d+)'
   MyReg=re.compile(MyRE)
   Res=MyReg.search(Coord)
   return(Res.groups())

def Get_MaxScore(Seq,PSSM):
   MaxSc=-100000
   book={}
   for idx in range(len(Seq)-len(PSSM["A"])+1):
      tmpSc=0
      sseq=""
      sequence=[]
      sequence2=[]
      for pos in range(len(PSSM["A"])):
         tmpSc=tmpSc+float(PSSM[Seq[idx+pos]][pos])
         sseq=sseq + Seq[idx+pos]
      if MaxSc<tmpSc:
         MaxSc=tmpSc
         sequence.append(str(tmpSc))
         sequence2.append(sseq)
         book=dict(list(book.items()) + list((dict(zip(sequence,sequence2))).items()))
   return(MaxSc)

def Get_Seq(Seq,PSSM):
   MaxSc=-100000
   book={}
   for idx in range(len(Seq)-len(PSSM["A"])+1):
      tmpSc=0
      sseq=""
      sequence=[]
      sequence2=[]
      for pos in range(len(PSSM["A"])):
         tmpSc=tmpSc+float(PSSM[Seq[idx+pos]][pos])
         sseq=sseq + Seq[idx+pos]
      if MaxSc<tmpSc:
         MaxSc=tmpSc
         sequence.append(str(tmpSc))
         sequence2.append(sseq)
         book=dict(list(book.items()) + list((dict(zip(sequence,sequence2))).items()))
   return(book[str(MaxSc)]))

def Main(Args):
   PSSM={}
   PSSM=Get_PSSM(Args[1])
   MyFile=open(Args[2],'r')
   for Line in MyFile:
      Fields=Line.strip().split("\t")
      (Name,Chr,Str,End)=Get_Coordin(Fields[0])
      directseq=Fields[1]
      basecomplement={"A":"T":"C":"G","T":"A":"G":"C"}
      rDNAsense=directseq[::-1]
      antisenseDNA=""
      for base in rDNAsense:
         antisenseDNA = antisenseDNA+basecomplement[base]
      MaxScore=Get_MaxScore(Fields[1].upper(),PSSM)
      MaxScore2=Get_MaxScore(antisenseDNA.upper(),PSSM)
      Sequence=Get_Seq(Fields[1].upper(),PSSM)
      Sequence2=Get_Seq(antisenseDNA.upper(),PSSM)
      finded= Fields[1].find(Sequence)
      finded2= antisenseDNA.find(Sequence2)
      if int(Str)>int(End):
         print(Name,"\t",Chr,"\t",str(int(Str)-finded),"\t",str(int(Str)-finded-15),"\t",
```

```
            round(MaxScore,2),"\t",round(MaxScore+22.54)/(19.111+22.54),3),"\t",
            Sequence,"\t", str(finded2+int(End)),"\t", str(finded2+int(End)+11),"\t",
            round(MaxScore2,2),"\t",round(MaxScore2+22.54)/(19.111+22.54),3),"\t",Sequence2)
      else:
         print(Name,"\t",Chr,"\t",str(finded+int(Str)),"\t",str(finded+int(Str)+11),"\t",
            round(MaxScore,2),"\t",round(MaxScore+22.54)/(19.111+22.54),3),"\t",
            Sequence,"\t",str(int(End)-finded2),"\t",str(int(End)-finded2-11),"\t",
            round(MaxScore2,2),"\t",round(MaxScore2+22.54)/(19.111+22.54),3),"\t",Sequence2)
   MyFile.close()

if__name__=='__main__':
   if len(sys.argv)<2:
      print("You must provide the name of the files containing the sequences and PSSM")
   else:
      Main(sys.argv)
   sys.exit()
```